MODELLING THE ION EXCHANGE PROCESS IN PRESSURISED WATER REACTORS

By

Nathan Lee

A thesis submitted to the University of Birmingham for the degree of

ENGINEERING DOCTORATE IN FORMULATION ENGINEERING

UNIVERSITY OF BIRMINGHAM

School of Chemical Engineering

College of Engineering and Physical Sciences

University of Birmingham

September 2020

ABSTRACT

The process of ion exchange is one of the most common ways of removing unwanted or damaging ions from an effluent stream and is used in coolant treatment. Ion exchange is used within the treatment systems for coolant streams in nuclear power plants; specifically for the removal of radioactive ions such as cobalt-60 to minimise exposure risks to people in the immediate environment and those required to undertake maintenance. Other ions, such as nickel, iron and zinc are also present in the primary circuit and can form various other radionuclides contributing to increased levels of activity in the plant.

This work encompasses determining parameters such as rate constants and selectivity coefficients of the mentioned species in order to input them into a custom-built model. In addition, this work looks at determining temperature dependent equations for ion exchange resin degradation, as well as for the rate constants and selectivity coefficients.

The model will be able to predict the behaviour of ion exchange resins and the primary coolant flowing through taking into consideration typical PWR chemistry, activation products and various interactions with the resins in an ion exchange column. This work has only considered the use of cations and cationic ion exchange resins.

It was found that the model was able to accurately predict plant chemistry using a range of different input concentrations species. Validating the model predictions against experimental data showed discrepancies, however it was able to show correct trends of species removal via ion exchange. Finally, the model was able to show similar trends with regards to plant activity removal and demonstrated the capability of being able to predict an ion exchange resins' lifetime.

ACKNOWLEDGEMENTS

I will be forever grateful to the University of Birmingham and EPSRC for granting me the opportunity to conduct research as an EngD researcher in a field I have grown to love. This gratitude extends to Richard Greenwood as without him this opportunity would not be possible.

I would like to thank my supervisor, Andy Ingram for his continued support throughout the project and for his guidance.

From our sponsors Rolls-Royce, I would like to extend my gratitude to all who have supported me during the program: Andrew Powell, Lara-Jane Pegg, Danni Eklid, Jon Morrison, Nick Jones, and Fred Lord.

Also, from Rolls-Royce I would like to give special thanks to Andy Banks for not just his continued support but also for sharing his plethora of knowledge regarding systems modelling.

Further to those already mentioned, I would like to extend my thanks to the following people for their support in a multitude of areas: from the University of Birmingham, Lynn Draper, Joseph Hriljac, Anastasios Papadiamantis, John Hooper, Kathleen Hynes and all of my peers on the Formulation Engineering doctoral program.

Finally, I would like to thank my family and friends for the love and support throughout this project. I would not have been able to do this without you all.

CONTENTS

1 INTRODUCTION **1**

1.1 BACKGROUND 1

1.1.1 Pressurised Water Reactors *1*

1.1.2 Coolant Treatment System *3*

1.1.3 Ion Exchange Resins *5*

1.2 BUSINESS CASE 7

2 LITERATURE REVIEW **9**

2.1 GENERAL INTRODUCTION 9

2.2 PRIMARY CIRCUIT PROPERTIES 10

2.2.1 Coolant Chemistry *10*

2.2.1.1 Boron *10*

2.2.1.2 Lithium Hydroxide *11*

2.2.1.3 Hydrogen *12*

2.2.2 Primary Circuit Materials *13*

2.2.2.1 Nickel-Based Alloys *14*

2.2.2.2 Stainless Steels *15*

2.2.2.3 Zircaloy *15*

2.2.2.4 Cobalt-Based Alloys *16*

2.2.3 Reactor Core Properties *17*

2.2.3.1 Neutron Flux *17*

2.2.3.2 Radioactive Fission Products *19*

2.2.3.3 Radionuclide Inventory *21*

2.3 ION EXCHANGE PROCESS 25

2.3.1 Ion Exchange Resins *26*

2.3.2 Ion Exchange Kinetics *28*

2.3.3 Selectivity Coefficients *30*

2.4 Ion Exchange Modelling 31
2.4.1 Mass Action Models 31
2.4.1.1 Law of Mass Action 31
2.4.1.2 Homogenous Mass Action Model 34
2.4.1.3 Heterogeneous Mass Action Model 35
2.4.1.4 Ion Association 35
2.4.2 Multicomponent Adsorption Models 37
2.4.3 Sorption Isotherms 37
2.5 Summary of Critical Literature 40
2.5.1 Ion Exchange Equilibrium Constants 40
2.5.2 Ion Exchange Kinetics 41
2.5.3 Research Gap 42
3 ION EXCHANGE EQUILIBRIUM 43
3.1 Introduction 43
3.2 Materials and Methods 43
3.3 Results & Discussion 47
3.3.1 Effect of competing ions on cobalt adsorption 47
3.3.2 Sorption Isotherms 54
3.3.3 Selectivity Coefficients 59
3.4 Summary 65
4 ION EXCHANGE KINETICS 67
4.1 Introduction 67
4.2 Materials and Methods 67
4.3 Results & Discussion 71
4.3.1 Rate constants 71
4.3.2 Effect of flow rate on cobalt adsorption 77
4.3.3 Mass Transfer Coefficients 79
4.3.4 Resin Temperature Degradation 82

4.4 SUMMARY 88

5 PWR ION EXCHANGE MODELLING 90

5.1 INTRODUCTION 90

5.2 SOFTWARE 90

5.2.1 FACSIMILE 90

5.2.2 MATLAB 91

5.2.3 MULTEQ 91

5.3 MODEL DESCRIPTION 91

5.4 FACSIMILE MODEL DESCRIPTION 93

5.4.1 Model Transport 94

5.4.2 Thermal Effects 95

5.4.3 Chemical Reactions 96

5.4.4 Radio-activation and Decay 100

5.4.5 Metal Release (Corrosion) 101

5.4.6 Ion Exchange Reactions. 102

5.5 RUNNING THE MODEL 105

5.5.1 Input Data 106

5.5.2 Output Data 107

5.6 MODEL VALIDATION 108

5.6.1 Validation Set 1 Test Results 108

5.6.2 Validation Set 2 Test Results 111

5.6.3 Validation Set 3 Test Results 124

5.7 SUMMARY 127

6 CONCLUSIONS & FURTHER WORK 129

6.1 ION EXCHANGE EQUILIBRIUM 129

6.2 ION EXCHANGE KINETICS 130

6.3 ION EXCHANGE MODELLING 130

6.4 FURTHER WORK 131

7 REFERENCES **132**

8 APPENDIX **144**

8.1 CHAPTER 3 SUPPLEMENTARY 144

8.1.1 Metal Salt Comparison Graphs *144*

8.1.2 ICP-OES Calibration Plots *145*

8.2 CHAPTER 4 SUPPLEMENTARY 149

8.2.1 Linear Plots from Second Order Rate Equation *149*

8.2.2 Transient Experiments Results (Concentration vs Time) *153*

8.2.3 Transient Experiments Results (Flow Rate) *156*

8.3 CHAPTER 5 SUPPLEMENTARY 158

8.3.1 Ion Exchange Model Walkthrough. *158*

8.3.2 Effect of Time Steps on the Model. *169*

8.3.3 FACSIMILE Ion Exchange Code.* *171*

List of Tables

Table 2.1 Composition of nickel-based alloys. [32] 14

Table 2.2 Composition of Stainless Steels. [34] 15

Table 2.3 Composition of zirconium-based alloys. [32] 16

Table 2.4 Composition of Cobalt-based alloys. [36] 17

Table 2.5 Table of predominant radionuclides from fission of uranium-235. [42] 20

Table 2.6 Table of activation products formed from the coolant [43] 22

Table 2.7 Table of activation products formed from plant materials [25] 23

Table 3.1 Source of metal ions used. 44

Table 3.2. Equilibrium Experiment Parameters 47

Table 3.3 Isotherm parameters for cobalt sorption onto Purolite NRW-160 resin. 58

Table 3.4. Experimentally Determined Selecitivy Coeffecients for Cations 59

Table 3.5 Selecitivy Coeffecients for Cations from Literature [96] 60

Table 3.6. Experientally Determined Temperature Dependent Selectivity Coeffecients for Cations. 62

Table 3.7. Experimentally Derived Van't Hoff Equation Parameter 64

Table 4.1 Source of metal ions used. 68

Table 4.2 Second order rate constants at 25, 35, 45, 55 and 65°C for Cobalt, Copper, Zinc, Nickel and Iron. 73

Table 4.2 Second order rate constants at 25, 35, 45, 55 and 65°C for Cobalt, Copper, Zinc, Nickel and Iron. 75

Table 4.3 Mass transfer coefficients for cobalt ions with varying flow rates 80

Table 4.4 Results of Resin Autoclave experiments. 85

Table 4.5 Temperature degradation rate constants. 86

Table 4.6 Arrhenius Parameters for resin tempererature degradation 87

Table 5.1. Table of user chemical inputs vs model chemical input. 97

Table 5.2. Table of acid-base chemical reactions used in the model (not including their isotopic variants).[97] 99

Table 5.3. Table of Main Ion Exchange Reactions [1 2] 104

TABLE 5.4. TABLE OF PREDICTED pH_T VALUES FROM THE MODEL AT A RANGE OF LITHIUM AND BORON CONCENTRATIONS. 110

TABLE 5.5. LIST OF MODEL GEOMETRY PARAMETERS USED FOR VALIDATION SET 2. 111

TABLE 5.6. TABLE OF INITIAL CATION CONENTRATIONS USED FOR VALIDATION SET 2. 112

TABLE 5.7. EXPERIMENTAL RESULTS FROM CHAPTER 4. 113

TABLE 5.8. MODEL PREDICTED RESULTS FROM VALIDATION SET 2. 114

LIST OF FIGURES

FIGURE 1.1 DIAGRAM OF A PWR PLANT. [11] 2

FIGURE 1.2- DIAGRAM OF THE CTS (COOLANT TREATMENT SYSTEM) IN A PWR [11] 4

FIGURE 1.3 CHEMICAL STRUCTURE OF AN ION EXCHANGE RESIN SHOWING THE POLYSTYRENE BACKBONE CROSS-LINKED WITH DIVINYLBENZENE.[11] 5

FIGURE 2.1 REACTION SCHEME FOR THE FISSION OF URANIUM – 235. [38] 18

FIGURE 2.2 YIELD % OF ELEMENTS VIA FISSION OF URANIUM-235. [41] 20

FIGURE 2.3 ION EXCHANGE RESIN WITH A POLYSTYRENE BACKBONE CROSSLINKED WITH DIVINYLBENZENE AND A SULPHONIC ACID FUNCTIONAL GROUP. [95] 27

FIGURE 2.4 ION EXCHANGE RESIN WITH A POLYSTYRENE BACKBONE CROSSLINKED WITH DIVINYLBENZENE AND A QUATERNARY AMMONIUM FUNCTIONAL GROUP. 27

FIGURE 2.5. IMAGE OF CATION ION EXCHANGE RESIN BEADS. 28

FIGURE 3.1. EFFECT OF COBALT ION ADSORPTION CAPACITY IN THE PRESENCE OF COMPETING METAL IONS. 48

FIGURE 3.2. RECOVERY DEGREE (%) OF TOTAL METAL IONS 50

FIGURE 3.3 - SEPARATION FACTOR OF COBALT WITH OTHER DIVALENT AND TRIVALENT COMPETING IONS. 52

FIGURE 3.4 - SEPARATION FACTOR OF COBALT WITH OTHER COMPETING IONS INCLUDING MONOVALENT IONS. 53

FIGURE 3.5 – LAGMUIR PLOT OF C_E/Q_E VS C_E, SHOWING THE GRADIENT AND INTERCEPTS USED FOR CALCULATION OF Q_{MAX} AND K_L. ALSO SHOWING A VALUE FOR R^2. 54

FIGURE 3.6 – LAGMUIR PLOT SHOWING THE FIT OF EXPERIMENTAL AND THEORETICAL DATA USING VALUES CALCULATED FOR Q_{MAX} AND K_L. 55

FIGURE 3.7 – FREUNDLICH PLOT OF QE) VS LOG (CE), SHOWING THE GRADIENT AND INTERCEPTS USED FOR CALCULATION OF N AND KF 56

FIGURE 3.8 - FREUNDLICH PLOT SHOWING THE FIT OF EXPERIMENTAL AND THEORETICAL DATA USING VALUES CALCULATED FOR N AND K_F. 56

FIGURE 3.9 – DUBININ-RADUSHKEVICH PLOT OF LOG (Q_E) VS $\boldsymbol{\varepsilon}^2$, SHOWING THE GRADIENT AND INTERCEPTS USED FOR CALCULATION OF $\boldsymbol{\beta}$ AND E. ALSO SHOWING A VALUE FOR R^2. 57

FIGURE 3.10 – DUBININ-RADUSHKEVICH PLOT SHOWING THE FIT OF EXPERIMENTAL AND THEORETICAL DATA USING VALUES CALCULATED FOR $\boldsymbol{\beta}$ AND $\boldsymbol{\varepsilon}$. 57

Figure 4.1 Simplified schematic of custom-built rig for variable flow rate experiments. 71
Figure 4.2 Linear Plots of Eq 4.1 to determine second order rate constant, k for (A)Cobalt, (B)Nickel, (C)Zinc, (D)Iron and (E)Copper at 25°C. 76
Figure 4.3 Linear Plots of Eq 4.7 to determine Activation Energies and Arhenius Prefactors for Cobalt, Nickel, Zinc, Iron and Copper 77
Figure 4.4 Cobalt effluent concentration against effluent volume at different flow rates. (Starting Concentration = 1000ppb) 78
Figure 4.5 Mass Transfer Coefficients against Flow Rate at different influent concentrations 81
Figure 4.6 Results from TGA on ion exchange resin (NRW-160) 83
Figure 4.7 Results from Eq 4.9 determining degradation rate constants at various temperatures 86
Figure 4.8 Arhenius plot of ln (k) avs 1/T for resin degradation 87
Figure 5.1 Graphical User Interface showing parameter inputs for the Ion Exchange Model 92
Figure 5.2 Schematic of the Model Design 94
Figure 5.3 Radionuclide GUI inputs 101
Figure 5.4 Metal Release GUI inputs 102
Figure 5.5 Schematic of the Model Design 105
Figure 5.6 Developed coolant chemistry lithium/pH_T regimes [109][110]. 110
Figure 5.7 Experimental vs Model Concentration vs Time Results for cations; (A)Cobalt; (B)Copper; (C)Nickel; (D)Zinc; and (E)Iron 117
Figure 5.8 Model predicted pH values from Figure 5.7 results. 118
Figure 5.9 pH dependent speciation for (A)Cobalt[113]; (B)Nickel[112]; (C)Zinc[111] and (D)Copper[114]. 119
Figure 5.10 Experimental vs Model Concentration vs Time Results for cations with added Boric Acid; (A)Cobalt; (B)Copper; (C)Nickel; (D)Zinc; and (E)Iron 122
Figure 5.11 Model predicted pH values from Figure 5.10 results. 122
Figure 5.12 The corrosion product activity in the primary coolant of a typical PWR with different removal rates [18] 125
Figure 5.13 GUI output for Validation Set 3 - demonstrating primary circuit activity reaching saturation. 126

Figure 5.14 Model output for Validation Set 3 - demonstrating effect of flow rate changes on primary circuit activity saturation 126
Figure 5.15 GUI output for Validation Set 3 - demonstrating the eventual decline in IXC efficiency. 127
Figure 8.1.1 Effect of Metal Salts on Adsorption (1) 144
Figure 8.1.2 Effect of Metal Salts on Adsorption (2) 144
Figure 8.1.3 ICP-OES Calibration Plot for Cobalt 145
Figure 8.1.4 ICP-OES Calibration Plot for Zinc 145
Figure 8.1.5 ICP-OES Calibration Plot for Nickel 146
Figure 8.1.6 ICP-OES Calibration Plot for Iron 146
Figure 8.1.7 ICP-OES Calibration Plot for Sodium 147
Figure 8.1.8 ICP-OES Calibration Plot for Lithium 147
Figure 8.1.9 ICP-OES Calibration Plot for Copper 148
Figure 8.1.10 ICP-OES Calibration Plot for Aluminum 148
Figure 8.2.1 Linear Plots of Eq 4.1 to determine second order rate constant, k for (A)Cobalt, (B)Nickel, (C)Zinc, (D)Iron and (E)Copper at 35°C. 149
Figure 8.2.2 Linear Plots of Eq 4.1 to determine second order rate constant, k for (A)Cobalt, (B)Nickel, (C)Zinc, (D)Iron and (E)Copper at 45°C. 150
Figure 8.2.3 Linear Plots of Eq 4.1 to determine second order rate constant, k for (A)Cobalt, (B)Nickel, (C)Zinc, (D)Iron and (E)Copper at 55°C. 151
Figure 8.2.4 Linear Plots of Eq 4.1 to determine second order rate constant, k for (A)Cobalt, (B)Nickel, (C)Zinc, (D)Iron and (E)Copper at 65°C. 152
Figure 8.2.5 Cobalt Concentration against Time at 25°C, 35°C, 45°C, 55°C and 65°C. 153
Figure 8.2.6 Copper Concentration against Time at 25°C, 35°C, 45°C, 55°C and 65°C. 153
Figure 8.2.7 Zinc Concentration against Time at 25°C, 35°C, 45°C, 55°C and 65°C. 154
Figure 8.2.8 Nickel Concentration against Time at 25°C, 35°C, 45°C, 55°C and 65°C. 154
Figure 8.2.9 Iron Concentration against Time at 25°C, 35°C, 45°C, 55°C and 65°C 155
Figure 8.2.10 Cobalt effluent concentration against effluent volume at different flow rates. (Starting Concentration = 750ppb) 156

FIGURE 8.2.11 COBALT EFFLUENT CONCENTRATION AGAINST EFFLUENT VOLUME AT DIFFERENT FLOW RATES. (STARTING CONCENTRATION = 500PPB) 156
FIGURE 8.2.12 COBALT EFFLUENT CONCENTRATION AGAINST EFFLUENT VOLUME AT DIFFERENT FLOW RATES. (STARTING CONCENTRATION = 250PPB) 157
FIGURE 8.3.1 OPEN ION EXCHANGE MODEL 158
FIGURE 8.3.2 ION EXCHANGE MODEL GRAPHICAL USER INTERFACE DROP DOWN MENU 159
FIGURE 8.3.3 GUI INPUT DESCRIPTION EXAMPLE 159
FIGURE 8.3.4 MODEL RUN PREREQUISITE 160
FIGURE 8.3.5 GUI INPUTS DESCRIPTION 161
FIGURE 8.3.6 IXM MODEL RUN DISPLAY 162
FIGURE 8.3.7 IXM MODEL ERROR TEXT DISPLAY 162
FIGURE 8.3.8 ION EXCHANGE MODEL GRAPHICAL USER INTERFACE DROP DOWN MENU 163
FIGURE 8.3.9 GRAPH DISPLAY OPTIONS 164
FIGURE 8.3.10 BASIC MODEL RUN WITH LOW TIME STEPS 169
FIGURE 8.3.11 BASIC MODEL RUN WITH HIGH TIME STEPS 170

1 INTRODUCTION

1.1 Background

Around one tenth (10.2%) of the world's electricity is generated by about 450 nuclear reactors [13]. France currently uses nuclear power to generate three quarters of its electricity. Countries such as Belgium, Slovenia, Switzerland, and Sweden generate one third or more, with countries such as the USA, Spain and Russia generating about one fifth. Currently, nuclear power within the UK generates approximately one quarter (25%) of the entire country's electricity, with the projection to raise this to almost a third (33.15%) by 2035 [12]. From the 15 reactors operating in the UK, the reactor Sizewell B located on the Suffolk coast is the only pressurised water reactor (PWR). Sizewell B was commissioned in 1995 and is operated by EDF Energy, with the aim for the plant to remain in operation until 2055. A new PWR, Hinkley Point C, is currently in build and expected to be commissioned by 2025 at a £20.3bn cost with a 60-year life expectancy [14] [15].

1.1.1 Pressurised Water Reactors

The basic function of a PWR is to convert energy of nuclear fission to electricity whilst maintaining low carbon emissions. They are immensely complicated thermodynamic heat engines, which consist of a primary and secondary circuit separated by a heat exchanger. This separation is needed as to protect the turbine in the secondary circuit from activated species produced by the reactor core, as seen in Figure 1.1.

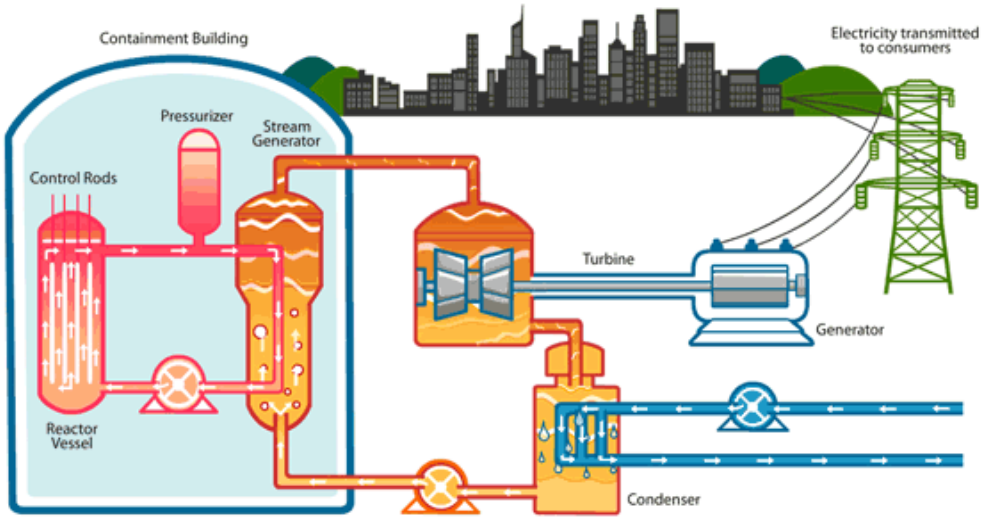

Figure 1.1 Diagram of a PWR plant. [11]

Nuclear fission of uranium-235 fuel in the reactor core enclosed in the reactor vessel produces neutrons with large kinetic energies, which are moderated into thermal neutrons by the coolant, water. Thermal neutrons are necessary for successful fission of uranium-235 and are also responsible for heating the coolant up to 300°C [1] , which is held under high pressure, approximately 155 bar [1] , by the pressurizer in order to maintain a liquid state. Control rods are in use within the reactor vessel to control the fission rate of the uranium fuel. In civil plants the control rods are typically made of boron as they are good neutron absorbers, so the lowering or raising of these rods greatly controls the fission rate preventing runaway reactions. The heat produced in the primary coolant due to the fission reactions is transferred to a secondary coolant loop, in the steam generator, where steam is produced, due to the vastly lower pressure. This superheated steam then drives a conventional steam turbine and produces electricity.

Due to the extreme conditions within a PWR, the inner components are manufactured from a number of alloys, formulated to withstand such conditions and minimise damage done to them. Corrosion of the various metal parts in the primary circuit of the reactor consisting mainly of nickel-base alloys, stainless steels and zircalloy, results in the release of corrosion products in the form of metal oxides and ionic species [2] . Several corrosion products arise from the corrosion of nickel based alloys, such as nickel ferrite, which is the most abundant and also cobalt ferrite which appears in a much smaller quantity [3] [4] . These products circulate through the primary circuit and when passing by the core these elements can become activated under neutron flux. The deposition of the activated corrosion products in areas out of neutron flux is the main cause of radioactive contamination [5] . The main activated species responsible for this contamination and high dose rates are ^{60}Co and ^{58}Co, the others are ^{54}Mn and ^{59}Fe [6] [7] [8] . These activated particles can transport around the primary circuit and deposit onto surfaces [9] , therefore presenting the risk of high radiation doses to workers during maintenance of the primary circuit, even when remote from the core. Other radioactive species responsible for high dose rates include ^{131}I - ^{135}I, ^{131}Cs – ^{135}Cs, typically formed from fission products.

1.1.2 Coolant Treatment System

The coolant treatment systems, CTS, within PWRs employ the use of particle filters and demineralizers/ion exchange resins connected to the primary circuit to remove unwanted radioactive ions and particles, as well as species which may harm the system. The CTS is also known as the Chemical and Volume Control System (CVCS) as seen in Figure 1.2, with the added functionality of being able to alter concentration affecting the pH and to maintain the level of the pressurizer at a desired point.

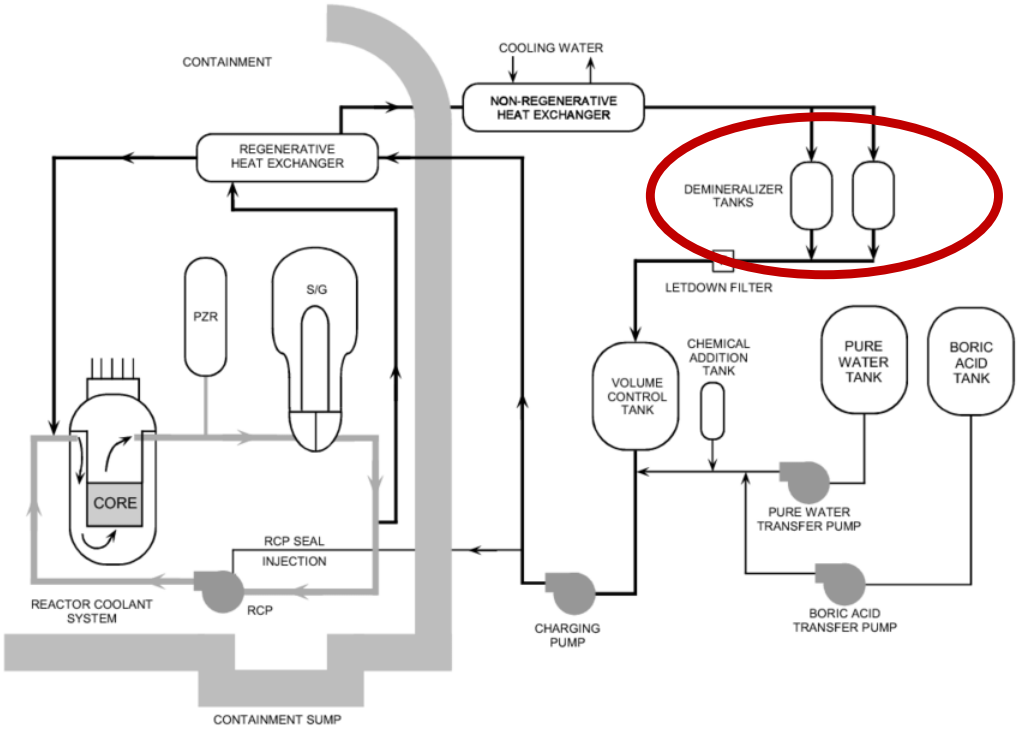

Figure 1.2- Diagram of the CTS (Coolant Treatment System) in a PWR [11]

The main function of the CTS is to remove both suspended and dissolved radioactive corrosion and fission products, which may be released into the primary coolant during the operation of the reactor plant. In this way the primary circuit activity is kept to a minimum and dose rates to personnel are minimised. The process of ion exchange is used because it is one of the most common ways of removing unwanted ions from an effluent stream and is the most commonly used method in water treatment [10] .The process of ion exchange utilises ion exchange resins held in ion exchange columns which is highlighted by the red circle in Figure 1.2. The CTS operates in a pressurized environment at a much lower temperature than the primary circuit, ~50°C, which is due to the limitations of the ion exchange resins. Typically, 1% of the entire primary circuit volume is diverted and

cooled at any one time before being passed through the CTS and returned to the main circuit.

The resin beads in the Ion Exchange Column (IXC) act both as a filter for the removal of solid particulates and as an ion exchange resin for the removal of dissolved species. Before entering the IXC the coolant must be cooled to prevent deterioration of the resin. This is done via the use of a regenerative, non-regenerative cooler system cooling from ~300°C to 50°C. The regenerative cooler works by minimising heat loss by exchange between the leaving (hot) and returning (cool) coolant. The exchange is not 100% efficient, requiring the use of a further cooling step using the non-regenerative cooler.

1.1.3 Ion Exchange Resins

Most Ion exchange (IX) resins used in industry are spherical beads composed of a polystyrene backbone cross linked with DiVinylBenzene (DVB) as seen in Figure 1.3.

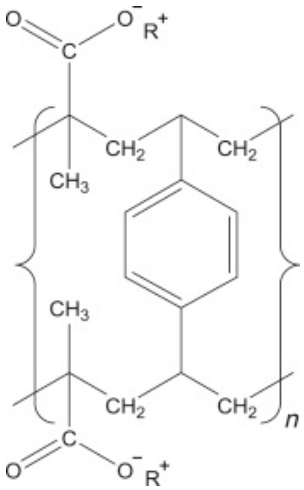

Figure 1.3 Chemical Structure of an Ion Exchange Resin showing the polystyrene backbone cross-linked with DiVinylBenzene.[11]

They are used to remove ionic species from primary coolant by binding them onto active sites on the resin surface and exchanging an alternative ion, such as H^+ or OH^-. The IX resin is initially loaded with ions with a low affinity for the resin (such as H^+ or OH^-). This ensures that these ions preferentially exchange with contaminant ions that have a higher affinity for the IX resin.

Two different forms of IX resin exist; cationic and anionic, to allow for exchange with cations and anions. Cationic resins have positive ions as the functional group to exchange, such as H^+, Li^+ or NH_4^+, whereas anionic resins have negatively charges ions as the functional group to exchange such as OH^-. It is common practice to use a mixture of the two resins, in what is known as a mixed bed IX resin in an ion exchange column. The cationic resin is usually in a lower proportion to the anionic resin to compensate for the lower capacity of the anionic resin.

Ion-exchange capacity represents the total of active sites or functional groups responsible for ion exchange in a polymer membrane [18]. IX resins will gradually lose their capacity when subjected to temperatures exceeding approximately 60°C, as the limits of thermal stability are imposed by the bonds in the functional groups. The 60°C limit more applies to the anionic resin as carbon-nitrogen bonds, typically used in ammonium functional groups begin to lose their strength. Cationic resins have a temperature limit of approximately 100°C due to greater thermal stability of the bonds (commonly carbon-sulfur) used in the functional groups, but this temperature limit can vary depending on the chemical make-up of the resin.

The use of the regenerative, non-regenerative cooler system is used to reduce the temperature of the coolant to below 60°C, due to the anionic resin temperature limitation, then back to normal operating temperature (NOT).

1.2 Business Case

The understanding of ion-exchange behaviour is a fundamental cornerstone of reactor chemistry, and the optimisation of the CTS offers the potential for cost, space-saving and plant simplification benefits. The work scope involves understanding the ion-exchange process in terms of selectivity and its kinetics. In literature this is well understood, however there are gaps in the understanding when the ion exchange process is applied to a pressurised water reactor. There is a lack of knowledge of the impact the processes in a PWR primary circuit have on the CTS, and more specifically the ion exchange resins. The harsh conditions and complex chemistry in the primary circuit is a stark contrast to how ion exchange resins are conventionally used.

thermal degradation mechanisms, column exhaustion and breakthrough, selectivity behaviour and activity removal.

Due to the limited number of exchange sites available and the role of heat with regards to resin degradation, IX resin only has a finite lifetime. IX resin suppliers provide a resin lifetime for each of their resins and after this time, it is recommended that a resin is replaced in order for the IXC to continue to operate efficiently. Therefore, the work scope also involves investigating the thermal degradation mechanisms associated with IX resins at high temperatures. Thermal degradation of anion resins has been investigated thoroughly in both academia and industry. There are major gaps when cation resins are regarded, which will be a focus for this part of the work scope.

Finally, the work scope also includes the development of a modelling tool, taking into consideration kinetics, equilibrium behaviour and thermal degradation, to predict IX behaviour in a PWR and aid in the process of resin life optimisation.

2 LITERATURE REVIEW

2.1 General Introduction

This review seeks to cover the current state of the knowledge in these areas, with specific interest in the methods used to study the phenomena. The chemical environment of a PWRs primary coolant circuit is of great importance to this thesis, and a brief explanation of guideline chemistry conditions for the primary coolant can be found in section 2.2. In addition to the chemical environment, the plant materials and processes occurring in and out of the reactor core are fundamental to this thesis and an explanation of what these processes are, and the type of materials used are also explain in section 2.2.

This review also seeks to cover literature surrounding ion exchange equilibrium and kinetics. Understanding ion exchange equilibrium and kinetic behaviour is crucial to the development of any form of ion exchange modelling system, as determining the parameters discussed in section 2.3 and 2.4 are fundamental towards the work this thesis has done. These parameters include selectivity coefficients, rate constants, mass transfer coefficients and also degradation rates.

The different approaches to modelling ion exchange are also discussed in section 2.4 of this review, including the homogenous and heterogenous mass action models, multicomponent adsorption models and isotherm models.

2.2 Primary Circuit Properties

2.2.1 Coolant Chemistry

The coolant in the primary circuit has two main functions: to act as a medium for heat transfer between the primary and secondary circuits from the fission reactions in the reactor core; and to act as a neutron moderator to reduce the energy of fast high energy neutrons to enable fission reactions to take place. Reducing the energy of the fast high energy neutrons is also known as thermalizing, producing the thermal neutrons necessary for successful fission reactions. The chemistry and operating conditions of the coolant is carefully maintained in order to ensure safe operation of the reactor. These controls include maintaining the pH of the coolant within a specific band of minimum solubility, thus reducing the formation of corrosion products and deposition within the reactor core; and minimising levels of oxygen in order to retain structural integrity by minimising the rate of corrosion and dissolution of plant structural materials [19][20].

2.2.1.1 Boron

Boron is typically added to PWRs to control the reactivity of the core. Commonly as boric acid (H_3BO_3), it is added to the primary circuit to act as a neutron poison; absorbing thermal neutrons which could have been used for fission reactions. Naturally boron consists primarily of two stable isotopes ^{11}B (80.1%) and ^{10}B (19.9%). The isotope ^{10}B has an exceptionally high neutron capture cross section of 3840 barns, whereas ^{11}B has a relatively low neutron capture cross section of 0.005 barns [21]. The neutron capture cross section can also be interpreted as the probability for an atom to capture a neutron. With

^{10}B more likely to capture a neutron it will undergo the following reaction under high neutron flux in the reactor core:

$$^{10}_{5}\boldsymbol{B} + {}^{1}_{0}\boldsymbol{n} \rightarrow {}^{7}_{3}\boldsymbol{Li} + {}^{4}_{2}\boldsymbol{He}\ (\boldsymbol{\alpha}) \qquad \text{(Eq. 2.1)}$$

As the proportion of ^{10}B to ^{11}B is so low, an enrichment process is therefore necessary before use in a PWR [22]. Using enriched boric acid allows for smaller quantities of the acid to be used, therefore requiring a lower concentration of pH raiser to reach a desired pH.

2.2.1.2 Lithium Hydroxide

LiOH is used as the primary pH raiser in the primary circuit due to it being a strong base and having a relatively high solubility. Once in solution LiOH release hydroxyl (OH^-) ions which in turn increases the pH. It is used to maintain the pH and the amount added depends on the amount of Boron present in the primary circuit. Boron concentrations can vary between 0 and 2000 mg kg^{-1} over the time between refuelling, also known as a cycle which can be from 18 – 24 months, so the amount of LiOH required constantly changes and needs to be continuously monitored. Maintaining the pH of the system helps to maintain the structural integrity of plant materials, with many of the components having their lowest solubility point within a certain pH region, minimising corrosion. The pH of the primary circuit in a PWR depends on the plant and the materials it uses, but the typical pH range is between 10 and 11 which requires a lithium concentration of around 2 mg kg^{-1} and little or no boric acid. However, it has been reported that with elevated concentrations of lithium in the region of 3.5 mg kg^{-1} ($pH_{300°C}$ 7.4) the effects of a phenomenon known as pressurised water stress corrosion cracking (PWSCC) is more

prevalent. In the case of alloy 600, a 20 % decrease in material lifetime is observed when using in excess of 3.5 mg kg^{-1} of lithium [23-26].

Lithium occurs naturally in two isotopic forms: lithium-7 (^{7}Li) and lithium-6 (^{6}Li) with the abundancies of 92.4 % and 7.6 % respectively. ^{6}Li has a neutron capture cross section of 940 barns [27] compared with 45 mbarns for ^{7}Li. ^{6}Li will react with neutrons under neutron flux within the reactor core to give tritium via the reaction:

$$^{6}_{3}Li + {}^{1}_{0}n \rightarrow {}^{3}_{1}H + {}^{4}_{2}He\ (\alpha) \qquad \text{(Eq. 2.2)}$$

Tritium (^{3}H) is a radioactive isotope of hydrogen that emits low-energy beta particles and has a half-life of 12.6 years [28]. This long-lived isotope is not desirable in the primary circuit, which is why LiOH is isotopically enriched with the ^{7}Li isotope up to 99.95%, drastically minimising tritium production [29].

2.2.1.3 Hydrogen

Hydrogen (H_2) is added to the primary circuit to supress the formation of oxidising species, generated via water hydrolysis, by reacting with them as they are formed in the reactor core [30]. The production of oxidising species such as hydrogen peroxide (H_2O_2) and hydroxyl radicals (OH·) occur via the reactions Eq 2.3 – 2.5:

$$H_2O + \gamma \rightarrow H_2O^+ + e^- \qquad \text{(Eq. 2.3)}$$

$$H_2O^+ + H_2O \rightarrow H_3O^+ + OH\cdot \qquad \text{(Eq. 2.4)}$$

$$OH\cdot + OH\cdot \rightarrow H_2O_2 \qquad \text{(Eq. 2.5)}$$

With the addition of H_2 the competing reaction (Eq 2.6) following by (Eq 2.7) can take place, thus reducing the concentration of H_2O_2, lowering the corrosion rates of plant materials.

$$\boldsymbol{OH\cdot + H_2 \rightarrow H_2O + H\cdot} \qquad \text{(Eq. 2.6)}$$

$$\boldsymbol{H\cdot + OH\cdot \rightarrow H_2O} \qquad \text{(Eq. 2.7)}$$

It has been reported that a concentration of between 10 -15 $g.kg^{-1}$ of H_2 is sufficient to completely scavenge the oxidants from the radiolysis of water, however for PWR operations the suggested concentration is between $25 - 50$ g kg^{-1} [31].

2.2.2 Primary Circuit Materials

PWRs consist of a number of coolant facing materials which are meticulously selected due their different mechanical and physical properties. The plant materials are also selected based on their varying degrees of corrosion resistance and ability to remain structurally intact which under the harsh conditions of a PWR for extended periods of time.

Table 2.1 Composition of nickel-based alloys. [32]

Chemical Element %											
Alloy	Ni	Cr	Fe	Mo	Co	Mn	Cu	Si	C	S	P
Alloy 600	>72.0	14	6			1	<0.5	<0.5	<0.15	<0.015	
Alloy 690	>58.0	27	7	8	<1.0	<0.5	<0.05	<0.5	<0.05	<0.015	<0.015

2.2.2.1 Nickel-Based Alloys

Nickel-based alloys are commonly used in tubing within the steam generator (SG), mainly due to their excellent resistance to PWSCC, compared to other materials, coupled with good mechanical properties. The high resistance to PWSCC is primarily due to the high chromium content in the alloy and with the high percentage of nickel in the alloy supports a face centred cubic (FCC) crystal structure, which aids in ductility and toughness.

There are many nickel-based alloys which all have varying compositions. Universally used alloys in PWRs are Alloy 600, Alloy 690, where Inconel® is a registered trademark referring to a family of austenitic nickel-chromium superalloys including Alloy 600 and 690. The composition of these alloys is displayed in Table 2.1, with the choice of alloy typically being chosen due to purpose and cost.

Nuclear plants are built with long term operation in mind, and one of the issues with Alloy 600 in particular is the stress corrosion cracking (SCC) which occurs over time [61]. They were first selected for used during the 1960s and they have proven to be very susceptible to cracking [32][33]. Due to the higher chromium content in Alloy 690 and less susceptibility

to SCC, it has become more of an industry standard. Due to the higher chromium content in Alloy 690 it is also more expensive than Alloy 600.

2.2.2.2 Stainless Steels

Stainless steels in PWRs are used for the primary circuit pipework, cladding of components and for welds. They have high resistance to corrosion in high temperature water due to the enrichment of chromium on the surface, which is able to react with oxygen to form a passivating layer of chromium oxide (Cr_2O_3), hindering corrosion. The two most common austenitic stainless steels (SS) used in PWRs are SS-304 and SS-316 where the composition of each is displayed in Table 2.2. The mechanical properties of the two materials are comparable, SS-316 possesses more nickel and molybdenum which gives the material greater chemical resistance. This does however also increase the price of SS-316 compared with SS-304.

Table 2.2 Composition of Stainless Steels. [34]

Chemical Element %							
Alloy	C	N	Cr	Ni	Mo	S	Fe
SS - 304	0.04	0.06	18	8.7	-	<0.002	Balanced
SS - 316	0.04	0.04	17	11	2.1	<0.002	Balanced

2.2.2.3 Zircaloy

The uranium-235 fuel is encased in a cladding that consists of variant of Zircaloy, a zirconium-based alloy. The composition of the alloys is displayed in Table 2.3, where zirconium is balanced. These alloys and are selected for cladding the fuel plates due to

their low neutron capture cross section of 0.2 barns [35], high thermal conductivity, high corrosion resistance and resistance to radiation damage [32].

Table 2.3 Composition of zirconium-based alloys. [32]

Chemical Element %					Chemical Element (mg.kg^{-1})			
Alloy	Sn	Fe	Cr	Ni	O	Co	Hf	U
Zircaloy - 2	1.2-1.7	0.07-0.20	0.05-0.15	0.03-0.08	1200-1400	20	100	3.5
Zircaloy - 4	1.2-1.7	0.18-0.24	0.07-0.13	-	1200-1400	20	100	3.5

When sourcing, the amount of hafnium (Hf) in these zirconium alloys requires monitoring and minimising, as most of the isotopes of Hf have high neutron capture cross sections [36], which could lower reactivity by capturing the thermal neutrons required by the uranium-235 for fission.

2.2.2.4 Cobalt-Based Alloys

Cobalt-based alloys, also known as Stellite®(registered trade name of Delero Stellite) are used in PWRs for parts which require excellent resistance to most forms of wear and are required to maintain its integrity over a range of temperatures, such as valve seats [32]. Stellite-6 whose composition is displayed in Table 2.4, is a commonly used cobalt-based alloy in PWRs as it has demonstrated outstanding resistance to corrosion and erosion.

Table 2.4 Composition of Cobalt-based alloys. [36]

Chemical Element %								
Alloy	Co	Cr	W	C	Fe	Ni	Si	Mo
Stellite - 6	Balanced	28.5	4.7	1.1	2.3	2.3	1.2	0

2.2.3 Reactor Core Properties

The reactor core is an integral component for the function of a PWR as it is where the uranium-235 fuel is held and the necessary fission reactions occur. It is where the harshest of conditions are experienced, such as high temperatures, high pressures, and large areas of irradiation. For the reactor to work efficiently, there should be a steady balanced rate of neutron generation and consumption; in this instance the reactor is said to be critical. When fewer neutrons are produced the reactor is said to be sub critical and when more neutrons are the produced the reactor is said to be super critical. Sub critical reactors will not be able to maintain a steady power output and fission reactions will eventually cease, stalling the reactor, and when super critical, the fission reactions will be uncontrollable, leading towards a meltdown of the core.

2.2.3.1 Neutron Flux

Figure 2.1 shows the reaction scheme for fission of uranium-235 illustrating the production of high energy neutrons. These high energy neutrons, also referred to as fast neutrons, are what the coolant moderates to lower energy neutrons, thermal neutrons, used for fission of the fuel. Whilst the reactor is in critical operation, there are countless fission reactions occurring at the same time producing numerous fast neutrons and

eventually thermal neutrons. The area, where neutrons are generated and consumed is also known as an area of neutron flux, where any species passing though can be subject to activation by capturing a neutron and changing their atomic structure and in some cases changing into a radioactive species known as radionuclides.

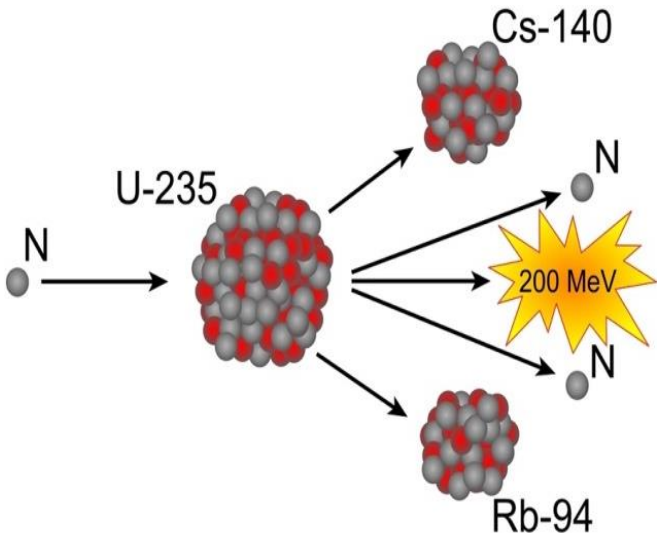

Figure 2.1 Reaction scheme for the fission of uranium – 235. [38]

The neutron flux (Φ), is defined as the number of neutrons crossing an area per unit of time, with units of neutrons (n) m^2.s. As neutrons can have different energies, such as being fast or thermal, values of neutron flux are only given for groups of neutrons with the same or similar energies. Values for neutron flux vary from reactor to reactor, taking into consideration the amount of fuel, the type of moderator and design of the reactor core. Neutron fluence is defined as the number of neutrons accumulated during an irradiation period within a unit area, with units of (n m^2), and can be used to determine a value for the parameter, neutron flux. As there is no direct method to count the number of neutrons of certain energies, neutron fluence is determined indirectly by use of

dosimeters located within the area. The dosimeter contains an isotope which changes into a radioisotope upon interaction with a neutron, with the consequent radioactivity being measured and a value for neutron fluence being inferred [40].

2.2.3.2 Radioactive Fission Products

As seen in Figure 2-1, the fission of uranium-235 produces elements of smaller mass. It does this by capturing the neutron and transforming into uranium-236 which is unstable, resulting in the nucleus splitting apart releasing energy, neutrons and the fragments of intermediate mass. After fission it is common that the splitting is not symmetric, in fact a lighter atom and heavy one are typically seen from fission in what is known as asymmetric splitting [41]. Figure 2.2 shows the yield from fission of uranium-235 against the mass number of an atom. In most cases the fission products produced are neutron rich and therefore unstable, causing the atom to undergo beta (β^-) decay to reach a stable form, where a neutron is converted into a proton with the emission of a positron and subsequently gamma photons. The radionuclides unstable nature causes it to be radioactive, and continually decays into a stable nuclide governed by the half-life ($t_{1/2}$) of the specific radionuclide. Table 2.5 shows the predominant radionuclides formed, along with their half-lives, decay mechanism and daughter nuclide. [Note. Some radionuclides may have multiple decays routes to reach a stable daughter nuclide.

Table 2.5 Table of predominant radionuclides from fission of uranium-235. [42]

Radionuclide	Radiation Produced	Half-Life ($t_{1/2}$)	Stable Daughter Nuclide
Iodine-131	β−, γ	8.05 d	Xenon-131
Xenon-133	β−, γ	5.24 d	Cesium-133
Caesium-137	β−, γ	30 y	Barium -137
Rubidium-94	β−	2.70 s	Strontium-94
Strontium-90	β−	28.7 y	Yttrium-90 -> Zirconium-90
Krypton-85	β−, γ	10.8 y	Rubidium-85

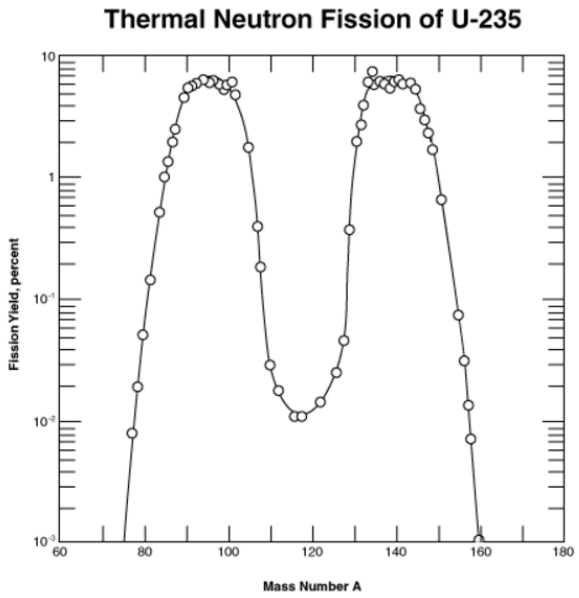

Figure 2.2 Yield % of elements via fission of uranium-235. [41]

2.2.3.3 Radionuclide Inventory

During operation of a PWR, large inventories of radionuclides are produced. The distinguishable radiation given off by the decaying isotopes are a cause for concern from a radiation protection perspective. Easily shielded radiation such as alpha (α) and beta (β) have a minimal effect on personnel radiation exposure, but gamma (γ) radiation, with its low linear energy transfer, has a major effect on personnel radiation exposure due to it being highly penetrating, requiring more extensive shielding.

Both the primary coolant and plant materials can form unstable radionuclides when under neutron flux in the reactor core. During normal plant operation, out-of-core radiation is dominated by coolant activation products (Table 2.6), which predominantly arise from the coolant elements coming under neutron flux. The radiation produced is from the decay of the radionuclides, meaning a longer half-life would produce more radiation overall.

Table 2.6 Table of activation products formed from the coolant [43]

Radionuclide	Production Pathway	Half-Life ($t_{1/2}$)	Radiation Produced
^{3}H	^{6}Li (n, α) ^{3}H	12.3 years	β^-
^{13}N	^{17}O (p, α) ^{13}N	10.0 minutes	β^+
^{16}N	^{16}O (n, p) ^{16}N	7.1 seconds	β^-, γ
^{17}N	^{17}O (n, p) ^{17}N	4.0 seconds	β^-, γ
^{19}O	^{18}O (n, γ) ^{19}N	29.0 seconds	β^-, γ
^{18}F	^{18}O (p, n) ^{18}F	1.8 hours	β^+

The primary coolant is predominately made up of H_2O, and once fully dissociated, the individual elements can interact with neutrons under neutron flux to form radioisotopes. The formation of ^{16}N gives rise to the dominant source of radiation during normal operating conditions, due to its large abundance in the coolant and high energetic γ-rays it gives off whilst it decays. Fast neutrons can be captured by ^{16}O to form an unstable isotope which will decay into ^{16}N, but they may also induce recoil protons from the water molecules, which in turn can be captured by ^{17}O and ^{18}O to subsequently decay into ^{13}N and ^{18}F respectively as shown in Table 2.6. Access to the reactor is confined during normal operation because of the enormous activity from ^{16}N, however the short half-lives of most of these species make them inconsequential once the reactor is shut down as within a few minutes after reactor shutdown the concentration of the radioisotopes will be negligible. When plant materials interact with neutrons in the reactor core, they produce radioisotopes, which have much more significant radioactivity even after the reactor is

shut down. This is due to the long half-lives of these radioisotopes, which typically are within the range of days to years.

Table 2.7 Table of activation products formed from plant materials [25]

Radionuclide	Production Pathway	Half-Life ($t_{1/2}$)	Radiation Produced
^{60}Co	^{59}Co (n, γ) ^{59}Co	5.27 years	β^-, γ
^{58}Co	^{58}Ni (n, p) ^{58}Co	71.4 days	β^-, γ
^{59}Fe	^{58}Fe (n, γ) ^{59}Fe	45.1 days	β^-, γ
^{55}Fe	^{54}Fe (n, γ) ^{55}Fe	2.6 years	γ
^{54}Mn	^{54}Fe (n, p) ^{54}Mn	300 days	γ
^{56}Mn	^{55}Mn (n, γ) ^{56}Mn	2.6 hours	β^-, γ

Table 2.7 contains a list of some the most common corrosion-based activation products. The majority of the radioisotopes formed are of somewhat small concern as they either; have relatively short half-life; emit a comparatively low energy γ radiation; or have a parent isotope with a low natural abundancy. For example, the parent isotope to ^{59}Fe, ^{58}Fe has a rather low natural abundance (0.282%) [44], which means there is a low probability of formation. This along with the short half-life of ^{59}Fe makes this radioisotope and so many others a small cause for concern.

The two radioisotopes which have the most significant cause for concern are ^{58}Co and ^{60}Co.

^{60}Co is formed via the activation of ^{59}Co with a thermal neutron, whereas ^{58}Co however is formed via the activation of ^{58}Ni with a fast neutron as seen in Table 2.7.

The natural abundancy of cobalt is 100 % ^{59}Co and the isotope has a relatively large neutron capture cross section (37.1 barns) [45], which makes ^{60}Co one of the most commonly seen radioisotope in the primary circuit. Both cobalt and nickel come from corrosion of plant structural materials, more specifically cobalt comes from stellite and nickel comes from the majority of materials used, although more prevalent in nickel based alloys. ^{60}Co has an exceptionally long half-life of 5.27 years and also emits 2 highly energetic γ-rays with energies of 1.17 and 1.3 MeV [46], which means ^{60}Co is the most significant contributor to radiation seen outside the reactor core due to transport and deposition of the radioisotope. As of late, due to the large contribution of out of core radiation from ^{60}Co, huge strides have been made to decrease or remove completely the cobalt inventory in PWRs to move away from the formation of ^{60}Co [47-49].

The natural abundancy of nickel only contains ~68% of the ^{58}Ni isotope and the activation process includes fast neutrons, which has a much smaller interaction probability compared with thermal neutrons, so the activation of ^{58}Ni is not as likely to occur resulting in ^{58}Co not being as commonly seen in the primary circuit as ^{60}Co. ^{58}Co has a much shorter half-life of 71.4 days and also emits comparatively weaker γ-ray with an energy of 811keV, which means ^{58}Co is not as much as a contributor to radiation seen outside the reactor core compared with ^{60}Co. These radioisotopes of cobalt are the cause for 80-90 % of the total radioactivity during normal operations and during shutdowns [50], (roughly 30% and 50% for ^{58}Co and ^{60}Co, respectively) [51].

2.3 Ion Exchange Process

Ion exchange is a phenomenon that occurs naturally in nature. Materials such as wool, silk, selected minerals and cell membranes all exhibit a form of ion exchange. Studies conducted during the last century [52-55] have shown that the ion exchange process has major benefits in a wide range of industrial applications.

Ion exchange is a simple chemical reaction, where undesired ions are exchanged for other ions of a similar charge. This stoichiometric chemical reaction must maintain a charge balance between the solution and the resin phases.

$$\overline{\mathrm{A}} + \mathrm{B}^{z} \leftrightarrow \overline{\mathrm{B}} + \mathrm{A}^{z} \qquad Eq.\,2.8$$

Eq 2.8 shows the reversible reaction between counterions A and B of charge z, where the top bar denotes ions in the resin phase.

Cation resins and anion resins are the two most common resins used in the ion exchange process, where cation resins attract positively charge ions and anion resins attract negatively charge ions. There are four main types of ion exchange resins which differ in their functional groups:

- Strongly acidic cation resins which feature sulphonic acid functional groups.
- Weakly acidic cation resins which feature carboxylic acid functional groups.
- Strongly basic anion resins which feature quaternary amine functional groups; and
- Weakly basic anion resins which feature primary, secondary, or tertiary amine functional groups.

2.3.1 Ion Exchange Resins

Ion exchange resins were developed in 1935 by Adam and Holmes [56], also discovering that a water insoluble resin consisting of polyhydric phenols containing amino groups could be used to exchange acids from aqueous solutions. Results from further experiments [57] concluded that ion exchange resins with a sulphonic acid group possessed a superior resin capacity; meaning a larger number of exchange sites available for ion exchange to take place.

Advancements in ion exchange manufacturing in the 1940s [58-59) found that cross-linked polystyrene resins with attached sulphonic acid groups possessed higher ion exchange capacities than any resin made previously. Today, in the industry of wastewater treatment where ion exchange resins are used, the industry standard is for the resin to have a polystyrene backbone crosslinked with divinylbenzene. For cation resins, sulphonic acid functional groups are often used (Figure 2.3), and for anion resins, quaternary ammonium groups are commonly used (Figure 2.4).

Purolite, a well know ion exchange resin manufacturer, supplies the nuclear industry with resins for water treatment. As nuclear water contains highly radioactive ions, the need for a high-capacity resin is paramount, hence why the resins supplied consist of a polystyrene backbone crosslinked with divinylbenzene, with sulphonic acid functional group for cation resins and quaternary ammonium functional group for anion resins. Figure 2.5 shows what the suppled resins typically looks like.

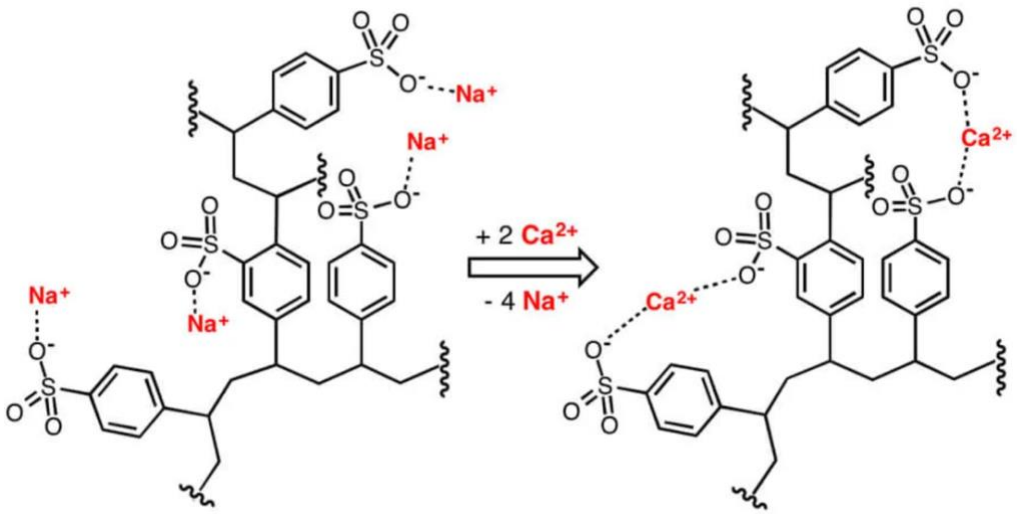

Figure 2.3 Ion exchange resin with a polystyrene backbone crosslinked with divinylbenzene and a sulphonic acid functional group. [95]

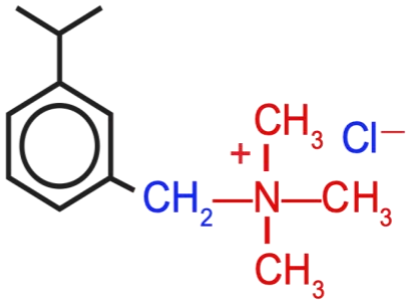

Figure 2.4 Ion exchange resin with a polystyrene backbone crosslinked with divinylbenzene and a quaternary ammonium functional group.

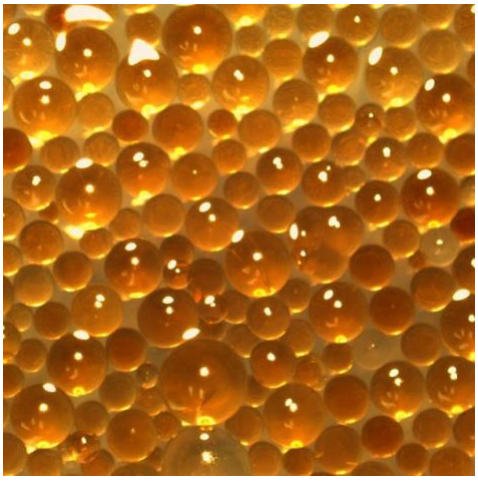

Figure 2.5. Image of cation ion exchange resin beads.

2.3.2 Ion Exchange Kinetics

It is essential that electroneutrality is maintained during the ion exchange process [62]. As the charged species attached to the resin is considered fixed and not able to cross the polymer – solution interface, a Donnan-type equilibrium begins to develop. Once at equilibrium there is an uneven distribution of ions between the polymer and solution phases resulting in the Donnan potential. This potential inhibits the further diffusion of counter-ions and co-ions if electroneutrality is not adhered to, where counter ions in an ion exchanger are the mobile exchangeable ions and the co-ions are the mobile ionic species in an ion exchanger with a charge of the same sign as the fixed ions. A given Donnan potential also excludes multivalent co-ions more efficiently than monovalent ions, which means ions of higher charges will exchange preferentially over those of lower charge [60]. A feature of the processes and materials that utilize the Donnan equilibrium principle is that the physical existence of a semi-permeable membrane is not essential. It is the immobility of ions (cation or anion) to diffuse out from one phase to the other that

leads to the phenomenon of 'semi-permeability', where a "fictitious" membrane can exist. Thus, a cation exchange resin with covalently attached fixed negative charges or an anion exchange resin with fixed positive charges exhibit semi-permeable behaviours [122].

The reversible ion exchange reaction between counterions A and B, in Eq 2.8 can be regarded as a multistep mechanism:

1. Diffusion of ion B from the bulk solution to the resin surface through the liquid film or boundary layer. (This step is known as film diffusion)

2. Diffusion of ion B through the internal structure of the resin. (This step is known as particle diffusion)

3. The chemical ion exchange reaction between ions A and B.

4. Diffusion of ion A through the internal structure of the resin back to the resins surface. (This step is known as particle diffusion)

5. Diffusion of ion A from the resin surface to the bulk solution through the liquid film or boundary layer. (This step is known as film diffusion)

Steps 1 and 5 are often referred to as film diffusion and steps 2 and 4 are referred to as particle diffusion. The rate determining step is generally either one of these diffusion

steps, with the concentration of solution being the deciding factor. This can be estimated by using the Helfferich coefficient, ϕ:

$$\phi = \frac{X\breve{D}\delta}{CDr_0}(5 + 2\alpha_B^A) \qquad Eq.2.9$$

Where X is the concentration of ions on the resin (fixed), C is the concentration of the solution, Ď and D are the interdiffusion coefficients in the exchanger and solution phases respectively; δ is the film thickness; r_o is the resin bead radius; and α_B^A is the separation factor. If ϕ >> 1, then the rate determining step is considered to be the film diffusion step. If ϕ << 1, then the rate determining step is considered to be the particle diffusion step.

2.3.3 Selectivity Coefficients

Cations and anions demonstrate an order of preferred affinity towards species uptake by conventional ion exchange resins. Generally, for all cation and anion exchangers the resin affinities follow the order [42]:

Ion $^{|z+1|}$ > Ion $^{|z|}$

Where z is the electrovalency of the ion (±).

Experimentally observed selectivity coefficients are often represented by the value of the separation factor, α_B^A which is defined by:

$$\alpha_B^A = \frac{(C_B)_r(C_A)_s}{(C_A)_r(C_B)_s} \qquad Eq.2.10$$

Where $C_A$is the concentration of species A and $C_B$is the concentration of species B. The r and s denote the resin and solution phase respectively.

For theoretical treatments of ion exchange it is preferred to define equilibrium in terms of the selectivity coefficient K_B^A [60] defined by:

$$K_B^A = \frac{(C_B)_r{}^{zA}(C_A)_s{}^{zB}}{(C_A)_r{}^{zB}(C_B)_s{}^{zA}} \qquad Eq.2.11$$

Where zA and zB are the ionic charges of the species.

2.4 Ion Exchange Modelling

Ion exchange isotherms characterise equilibrium conditions by representing concentrations of counter ions in the exchanger as a function of their concentrations in solution at constant temperature.

It is necessary for a model incorporating such conditions that it covers all possible experimental conditions with great accuracy in order to be used in the design and optimisation of ion exchange processes [122]. In the application of water waste treatments, it is important to concentrate on the ion exchange equilibrium as its accurate representation is vital for computer aided design.

2.4.1 Mass Action Models

2.4.1.1 Law of Mass Action

The ion exchange of counter ions A^{z_A} and B^{z_B} with general valences z_A and z_B can be represented by the general law of mass action equation:

$$z_B A^{z_A} + z_A \overline{B^{z_B}} \rightleftharpoons z_B \overline{A^{z_A}} + z_A B^{z_B} \qquad Eq.2.12$$

Where the top bar denotes the resin phase.

The corresponding thermodynamic equilibrium constant is expressed in terms of the activities a_i and $\overline{a}_i$ of the two ions by:

$$K_B^A(T) = \frac{\overline{a}_A^{z_B}\, a_B^{z_A}}{a_A^{z_B}\, \overline{a}_B^{z_A}} \qquad Eq.\,2.13$$

The activities of both species are calculated from the product of their concentrations with the corresponding activity coefficients, γ_i on the same concentration scale. Mole fractions y_i are adopted for the solid phase and molalities, m_i for the solution phase resulting in Eq 2.14 and Eq 2.15.

$$\overline{a}_i = \overline{\gamma}_i * y_i \qquad Eq.\,2.14$$

$$a_i = \gamma_i * m_i \qquad Eq.\,2.15$$

When the exchanger is considered to be ideal, $\overline{\gamma}_i = 1$. This therefore reduces equation 2 to the corrected selectivity coefficient, K_{aB}^A:

$$K_{aB}^A\,(T,\, y_i) = K_B^A * \frac{\overline{\gamma}_B^{z_A}}{\overline{\gamma}_A^{z_B}} = \frac{y_A^{z_B}\, a_B^{z_A}}{a_A^{z_B}\, y_B^{z_A}} \qquad Eq.\,2.16$$

Whereas in systems where both phases are considered ideal (both γ_i & $\overline{\gamma}_i = 1$), the quantity to represent equilibrium is known as the selectivity coefficient calculated by:

$$K_c(T,\ y_i, m_i) = \frac{y_A^{z_B}\ m_B^{z_A}}{m_A^{z_B}\ y_B^{z_A}} \qquad Eq.2.17$$

In the case of multicomponent systems, the previous equations are easily extended to n_C exchangeable counter-ions. For example, for the ternary system $A^{z_A}/B^{z_B}/C^{z_C}$ the following equilibria are now implied:

$$z_B A^{z_A} + z_A \overline{B^{z_B}} \rightleftharpoons z_B \overline{A^{z_A}} + z_A B^{z_B} \qquad Eq.2.18$$

$$z_B C^{z_C} + z_C \overline{B^{z_B}} \rightleftharpoons z_B \overline{C^{z_C}} + z_C B^{z_B} \qquad Eq.2.19$$

$$z_C A^{z_A} + z_A \overline{C^{z_C}} \rightleftharpoons z_C \overline{A^{z_A}} + z_A C^{z_C} \qquad Eq.2.20$$

Whose equilibrium constants are:

$$K_B^A = \frac{\overline{a_A}^{z_B}\ a_B^{z_A}}{a_A^{z_B}\ \overline{a_B}^{z_A}} \quad Eq.2.21 \qquad K_B^C = \frac{\overline{a_C}^{z_B}\ a_B^{z_C}}{a_C^{z_B}\ \overline{a_B}^{z_C}} \quad Eq.2.22 \qquad K_C^A = \frac{\overline{a_A}^{z_C}\ a_C^{z_A}}{a_A^{z_C}\ \overline{a_C}^{z_A}} \quad Eq.2.23$$

Only two equations are independent, since the three equilibrium constants satisfy the 'triangle rule', $(K_C^B)^{z_A}\ (K_C^A)^{-z_B}\ (K_B^A)^{z_C} = 1$. Once more, these results may be extended to any ion exchange system involving $n_c > 3$ counter-ions, $A_i^{z_i}$.

In a multicomponent ideal system, when the selectivity coefficients are known, the mole fraction of any counter-ion y_i in exchanger may be expressed in terms of x_i by:

$$y_i + \sum_{\substack{j=1 \\ j \neq 1}}^{n} \frac{x_j}{K_{c,i/j}^{1/z_i} m_t^{z_j/z_i - 1}} \left(\frac{y_i}{x_i}\right)^{z_j/z_i} = 1 \qquad Eq.\,2.24$$

Where x_i is the mole fraction of counter-ion A^{z_i} in solution and m_t the total molality of ionic species.

2.4.1.2 Homogenous Mass Action Model

Ion exchange equilibrium is commonly represented or predicted by homogeneous mass action models, which treats the process as a chemical reaction [123]. In homogenous mass action models, as well as treating the ion exchange process as a chemical reaction, the exchanger is assumed homogenous and the non-idealities can be taken into account by introducing the activity coefficients of ions in solution and solid phases.

In early works, which belong to the first group Dranoff and Lapidus (1957) [124] it was assumed that the ion exchange equilibrium is ideal, i.e., the activity coefficients of all components equal unity both in solution and in the solid phase. This model corresponds to assuming that the presence of other counter-ions does not affect the equilibrium exchange between two particular ions, which implies constant selectivity coefficients. Of course the behaviour of systems where the selectivity coefficients change with the resin composition cannot be described on the basis of these models, see Helfferich, (1962) [125]. For this we need to introduce non-idealities in the mixture behaviour resulting from the interaction among the counter-ions in the liquid and in the solid phase.

2.4.1.3 Heterogeneous Mass Action Model

There are a number of other models which can be used which treats the ion exchange reactions as different processes. The heterogeneous mass action model is also based on the law of mass action in which ideal behaviour for both the solution and the solid phase and the heterogeneity of ion exchange sites has been assumed. This differs to the homogeneous model, as that model, also based on the same law of mass action, takes into account non-ideal behaviour for both the solution and the solid phase.

Valverde, de Lucas and Rodríguez, (1999) [126] performed a study comparing the performance of heterogeneous and homogenous mass action models to predict multicomponent ion exchange equilibria. For the heterogeneous mass action model, the adjustable parameters were used in the prediction of the ternary equilibrium data. In all cases the prediction of the heterogeneous model was in good agreement with experimental data. They reported that the homogeneous model was superior to the heterogeneous model in the prediction of ternary systems, however, it should be noted that the results demonstrate the potential of the heterogeneous model in predicting the equilibrium ion exchange data for binary and ternary systems.

2.4.1.4 Ion Association

Due to incomplete dissociation of the ions not all the ions are available for ion exchange. As well as it being necessary to model the equilibrium between the ions in the solution and exchanger phases, it is also necessary to model the equilibrium between the ions and the ion pairs. Both sets of equilibria are dependent on temperature. Equilibrium will be established between the associated and dissociated forms corresponding to the equation:

$$M_x X_m \rightleftharpoons x M^{m+} + m X^{x-} \qquad Eq.\,2.25$$

Kester and Pykowicz (1975) [127] developed a method for this purpose. In this method the stability constant K_S^{MX} is defined as:

$$K_S^{MX} = \frac{[M_x X_m]}{[M^{m+}]_f^x [X^{x-}]_f^m} \qquad Eq. 2.26$$

where, $[M]_f$ is the free ion concentration of species M, and m and x are the valence of cation M and X. There is literature where formation constants of various ion pairs at different temperatures have been calculated and all values of α_m, degree of dissociation, are fitted for each metal ion by the following equation:

$$\alpha_m = 1 - [\, a_1 + \, b_1(T - 25)]C^{\frac{1}{2}} - [a_2 + \, b_2(T - 25)]C + \, a_3 C^{\frac{3}{2}} \qquad Eq. 2.27$$

The stability constant is defined in terms of α_m as

$$K_S^{MX} = \frac{(1 - \alpha_m)}{(C_m \alpha_m (\alpha_m + (z_m - 1)))} \qquad Eq. 2.28$$

The values of K_S^{MX} and α_m stability constant and degree of dissociation are then used to solve Eq 2.26 and determine the concentrations of free ions available for the ion exchange for the M^{m+} - N^{n+} binary system with X^{x-}.

The activity for free ion M^{m+} is related to the free ion concentration by:

$$a^{M^{m+}} = \, \gamma_{M^{m+}} [M^{m+}]_f \qquad Eq. 2.29$$

2.4.2 Multicomponent Adsorption Models

Various isotherm models like Freundlich, Langmuir, Redlich–Peterson and Sips are used to discuss the equilibrium behaviour of single-component adsorption. The Freundlich model assumes that adsorption occurs on a heterogeneous surface and the heat of adsorption is distributed in a non-uniform manner. While the Langmuir model assumes that adsorption happens at homogeneous active sites on the adsorbent surface. Models used for single component systems are not applied to multicomponent systems, because multicomponent adsorption involves a more complicated mechanism. Therefore, the single component isotherm models are modified to multicomponent system to be able to determine the equilibrium behaviour.

2.4.3 Sorption Isotherms

Sorption Isotherms describe the equilibrium for the adsorption of an adsorbent under constant temperature. Three isotherm models were used to fit cation resin adsorption data: Langmuir, Freundlich and Dubinin-Radushkevich isotherm. The sorption of Co (II) by Purolite NRW 160 resin was quantitatively evaluated by amount of Co (II) retained on resin, q_i .

Eq 2.30

$$q_e = \frac{(C_{0-} C_e)V}{m}$$

The Langmuir isotherm assumes that there is no interaction between adsorbate molecules and that adsorption is localised in a monolayer on the resin surface [93] and is represented in its linear form in Eq.2.31.

$$\frac{C_e}{q_e} = \frac{1}{q_{max}} C_e + \frac{1}{K_L q_{max}}$$

Eq 2.31

Where: V = volume of solution (dm^3), m = mass of resin used (g), q_e = Mass of solute adsorbed at equilibrium ($mg\ g^{-1}$), C_e = equilibrium concentration of adsorbate in solution ($mg\ dm^{-3}$), q_{max} = maximum adsorption capacity ($mg\ g^{-1}$), K_L= Langmuir constant ($dm^3\ mg^{-1}$)

Variables q_{max} and K_L are evaluated from the slope and intercept of $\frac{C_e}{q_e}$ versus C_e, respectively. An important feature of the Langmuir isotherm is the dimensionless parameter of the equilibrium R_L. Values for R_L are determined by Eq.2.32.

$$R_L = \frac{1}{1 + K_L C_0}$$

Eq.2.32

Where: R_L = The dimensionless parameter of the equilibrium can have following values: $R_L = 0$ for irreversible sorption isotherm, $0 < R_L < 1$ for favourable sorption isotherm, $R_L = 1$ for linear sorption isotherm and $R_L > 1$ for unfavourable sorption , C_0 = initial concentration of adsorbate in solution.

The Freundlich isotherm equation describes the empirical relationship between heterogeneous surfaces [93]. An example of the Freundlich equation in its linear form is represented in Eq.2.33 [93].

$$\log(q_e) = \log K_F + \frac{1}{n} \log C_e$$

Eq 2.33

Where C_e = equilibrium concentration of adsorbate in solution [mg dm-3], K_F = adsorbate constant, n = adsorbent constant, q_e = Mass of solute adsorbed at equilibrium ($mg\ g^{-1}$)

A value of n between 1 and 10 indicates a favourable sorption and the larger the n, the greater the heterogeneity. A value of n above 1 indicates normal adsorption, whereas a value of n below 1 indicates cooperative adsorption [93].

The Dubinin-Radushkevich isotherm allows the identification of the mechanism of adsorption, either physical or chemical, from the systems mean free energy, E (kJ mol^{-1}) and is described by Eq 2.34 - Eq. 2.36, having initially been linearised:

$$ln(q_e) = ln(q_m) - \beta\varepsilon^2 \quad \text{Eq.2.34}$$

$$\varepsilon = RT\ln\left(1 + \frac{1}{C_e}\right) \quad \text{Eq.2.35}$$

$$E = \frac{1}{\sqrt{2\beta}} \quad \text{Eq.2.36}$$

where β (mol^2 kJ^{-2}) is the activity coefficient related to mean adsorption energy, ε is the Polanyi potential, R (8.314 J mol^{-1} K^{-1}) and T (K) are the universal gas constant and absolute temperature respectively and E is the mean free energy per molecule of adsorbate (kJ mol^{-1}).

A plot of $ln(q_e)$ vs. ε^2 yields a straight line from which the DRK constants and mean free energy can be calculated. Chemisorption is considered to be the dominant process if $8<E<16$ kJ mol^{-1} with a value of $E<8$ kJ mol^{-1} indicating a physisorption process [102].

2.5 Summary of Critical Literature

2.5.1 Ion Exchange Equilibrium Constants

Many authors have written about the calculation of equilibrium constants (Argersinger et al., 1950; Hogfeldt, 1990). The ions in the solution phase are assumed to be ideal in many applications, and the resin phase activity coefficients are interlinked with the equilibrium constant to yield the selectivity coefficient.

(Allen et al., 1989) stated that selectivity coefficients are a function of solution concentration because selectivity coefficient values increase by an order of magnitude when solution concentrations were increased from 0.1eq L^{-1} to 1.0eq L^{-1}.

Mehablia (1994) used Gaines and Thomas' (1953) method, which successfully separated the equilibrium constant from the resin and solution ionic concentrations, yielding a thermodynamically consistent mass action equilibrium constant coupled with an activity coefficient model.

Kunin (1960) made several observations about ion exchange equilibria that are useful in qualitatively predicting the selectivity of an exchanging species. At low concentrations and normal temperatures (15-40 °C), the selectivity of the exchanging species increases with increasing ion valency:

i. $Na^{+} < Ca^{2+} < Al^{3+} < Th^{4+}$.

He also determined that assuming ions have the same valence, with standard temperatures and low concentrations, then the selectivity of an exchanging species increases with atomic number:

i. Li < Na < K < Rb < Cs,

ii. Mg < Ca < Sr < Ba.

It was also established that ions with high activity have greater ion exchange potential. Furthermore, increasing degree of crosslinking of the resin polymer bead also increased the selectivity of the ion and reversely, decreasing the amount of cross linking reduces the selectivity.

De Bokx et al. (1989) studied the ion-exchange equilibria of alkali-metal and alkaline-earth-metal ions by using surface-sulfonated polystyrene-divinylbenzene resins. This work used a chromatographic method in which one of the exchanging ions is present in trace quantities only. It was found that the selectivity coefficient is independent of the concentration of the liquid phase, and therefore selectivity in ion exchange is due solely to interactions in the resin phase. It was shown that selectivity is determined by the interaction between adsorbed ions and not by the interaction of separate adsorbed ions within the resin

2.5.2 Ion Exchange Kinetics

Kinetic analysis of ion exchange resins is especially important in designing ion exchange columns and determining the usability state of resins for a specific operation. The main objective of the kinetic study of the ion exchange process is to determine the exchange mechanism for theoretical purposes as well as to obtain the mass transfer coefficient for design purposes (Liberti, 1983). A mass-transfer coefficient across a liquid-solid interface is used to investigate the packed-bed kinetics of ion exchange. The Mass transfer coefficient effectively compares the rate at which ions can be removed by the resin to the rate at which water flows through the exchange bed (Foutch & Hussey, 2004).

Work conducted by Frisch & kunin and Helfferich determined that the kinetics of an ion exchange bed, at low influent concentrations, is controlled by external mass-transfer resistance (i.e. film diffusion).

Kitchener (1954) investigated ion exchange kinetics in detail, taking into considering a number of conditions where high rates of exchange are generally favoured. A more simplified treatment is to adopt the Nernst film diffusion theory, which states that the ion exchange reaction is controlled by two simultaneous diffusion steps – diffusion through the boundary layer (Nernst film) and diffusion through the actual resin particle. The solution is considered perfectly mixed and transport through the boundary layer (Nernst film) is equated by Fick's law with a certain equivalent thickness.

2.5.3 Research Gap

In literature, most of ion exchange modelling has been limited to mathematical modelling of ion exchange equilibria on ion exchange media, or diffusion models, where the transport parameters depend on the species concentration. Most of these methods are described in Section 2.4, and they are typically implemented for water treatment processes where conditions are tame and manageable. Using a combination of these techniques it would be beneficial for industry and academia to explore modelling where conditions are harsh, such as in a PWR. Integrating other factors such as thermal resin degradation into an ion exchange model will be hugely beneficial. In addition, the use of a model which can predict resin lifetime based of off activity removal efficiency would be a huge benefit for entire nuclear industry.

3 ION EXCHANGE EQUILIBRIUM

3.1 Introduction

To be able to model the ion exchange process in a PWR, understanding ion exchange equilibrium is fundamental. This section covers the equilibrium behaviour specifically with cobalt metal ions and other competing monovalent, divalent and trivalent metal ions. Cobalt was the main focus of research for this section as it is the most important species PWRs wish to remove from the primary circuit via ion exchange, due to the high levels of activity from the radionuclides ^{60}Co and ^{58}Co.

This section also explores the adsorption characteristics of cobalt on ion exchange resins using isotherm models, namely Langmuir, Freundlich and Dubinin-Radushkevich. These isotherm models provide a quantitative analysis into the equilibrium behaviour of cobalt and explain the type of adsorption that happens in this process.

Finally, this section also details calculated selectivity coefficients cobalt and a range of divalent metal ions. Furthermore, the temperature dependency of selectivity coefficients is explored, and a temperature dependent equation is derived using the Van't Hoff equation. The experimentally obtained parameters and equations will be essential in modelling the ion exchange process, more of which is detailed in Chapter 5.

3.2 Materials and Methods

All reagents used in these experiments were purchased from Sigma Aldrich, Fisher Scientific and Acros Organics (analytical grade and of minimum 95% purity), see Table

3.1, and used in solution form after dissolving in water. Ultrapure Type I water (18.2 MΩcm) was used for all solution preparations.

Table 3.1 Source of metal ions used.

Metal Ion	**Metal Salt**	**Supplier (Purity)**
Sodium	Sodium Sulphate Anhydrous	Fisher Scientific (99+%)
Cobalt	Cobalt Sulphate Heptahydrate	Acros Organics (99+%)
Copper	Copper Sulphate Pentahydrate	Sigma-Aldrich (≥98%)
Zinc	Zinc Sulphate Heptahydrate	Fisher Scientific (98%)
Nickel	Nickel Sulphate Hexahydrate	Fisher Scientific (99+%)
Iron (II)	Iron (II) Sulphate Heptahydrate	Acros Organics (99+%)
Iron (III)	Iron (III) Sulphate Pentahydrate	Acros Organics (97%)
Aluminium	Aluminium Sulphate Hexadecahydrate	Sigma-Aldrich (95%)

The ion exchange resins (NRW-160) were provided by Purolite in form of spherical beads ranging from 425 to 1200 microns. The molecular structure is described as macroporous polystyrene crosslinked with divinylbenzene with a sulphonic acid functional group (-SO_3H) which provides the active site for ion exchange.

Preparation of solutions were carried out by dissolving metal salts into the ultrapure Type I water in 2L batches and the subsequent solutions were decanted into 150ml polyethylene bottles. For ion exchange equilibrium experiments specified masses of ion exchange resins were weighed and added to the polyethylene bottles of solution and were then agitated using a revolving apparatus for 24 hours.

For temperature dependant experiments ion exchange resins were weighed and added to conical flasks filled with the metal ion solutions. These solutions were then agitated in a temperature controlled incubated MaxQ6000 shaker at a range of temperatures until equilibrium was reached. The metal ion concentration was analysed before and after the solutions were deemed to of reached equilibrium (24 hours). Literature has shown that typically equilibrium for these type of experiments is reached somewhere between 4 and 5 hours [10][98], however there is other literature which states equilibrium is assured to of been reached at the 24 hour mark[100]. For this reason, 24 hours was taken as the benchmark for when equilibrium has been reached.

At the end of the experiments the final metal ion concentrations were analysed using Inductively Coupled Plasma Optical Emissions Spectroscopy (ICP-OES) using a Perkin Elmer Optical Emission Spectrometer (model Optima 8000). Prior to analysis the samples were acidified with 0.2 ml 2% Nitric acid in preparation for analysis. The standards used for calibration were prepared using 2% Nitric acid. At the start of an ICP-OES analysis, a blank of only 2% nitric acid is taken, which is why the samples have to be prepared with 2% nitric acid as to know what to measure against the blank. The linear correlation coefficient R value of the calibration graph was higher than 0.9995 before proceeding with

the analysis. ICP-OES calibration graphs for all metals used in this thesis are shown in Figures 8.1.3 – 8.1.10 in the appendix under Chapter 3 Supplementary.

Preliminary equilibrium experiments were carried out to ascertain an appropriate concentration range, resin mass range, and metal ion salt. For the metal ion salt the equilibrium concentration of cobalt using cobalt sulphate, cobalt nitrate and cobalt chloride were measured using ICP-OES. The initial cobalt ion concentrations were 1000 mg L^{-1} and 500 mg L^{-1} (ppm) and the resin masses used were 0.2 g, 0.4 g, 0.6 g, 0.8 g and 1.0 g. The results from this experiment are illustrated in the appendix under Chapter 3 Supplementary. From Figures 8.1.1 and 8.1.2 there is no discernible difference with regards to cobalt adsorption between the different salts. With this, it was decided to move forward with using only one salt and sulphates were chosen.

With regards to the concentration range and resin masses used, they remain consistent with other experimental work in literature where equilibrium concentrations were examined.[10][98][99]. The values used for the concentration range and resin masses were scaled in line with what was presented in previous literature. These ranges allow for a final equilibrium concentration high enough to be detected via ICP-OES.

Table 3.2. Equilibrium Experiment Parameters

	Parameters
Sample Volume	100 ml
Revolver speed	5 rpm
Analysis Sample Size	10 ml
Duration	24 hrs
Metal Ion Concentration range	10 mg L^{-1} - 250 mg L^{-1}
Temperature Range	20 °C – 70 °C
Resin mass range	0.03 to 0.15 grams

3.3 Results & Discussion

3.3.1 Effect of competing ions on cobalt adsorption

The investigation on the ion adsorption capacity (mol g^{-1}) was carried out using initial concentration of 1mmol L^{-1} of cobalt ion with 1 mmol L^{-1} competing ion in 100ml batches. The resin loading was 0.03 g, 0.06 g, 0.09 g, 0.12 g and 0.15g per batch. The equilibrium method described in Section 3.2 was used here.

$$q_e = \frac{(C_o - C_e)V}{m} \qquad \text{Eq 3.1.}$$

q_e Amount of adsorbed metal per unit of ion exchange material ($mol_{ion}\ g_{resin}^{-1}$)

C_o Initial ion concentration ($mg_{ion}\ L^{-1}$ or $mol_{ion}\ L^{-1}$)

C_e Equilibrium ion concentration ($mg_{ion}^{-1}\ L$ or $mol_{ion}\ L^{-1}$)

V Volume of solution (L)

m Mass of ion exchange resin (g_{resin}).

Eq 3.1 was used to calculate the amount of adsorbed metal per unit of ion exchange material, where the results can be seen in Figure 3.1.

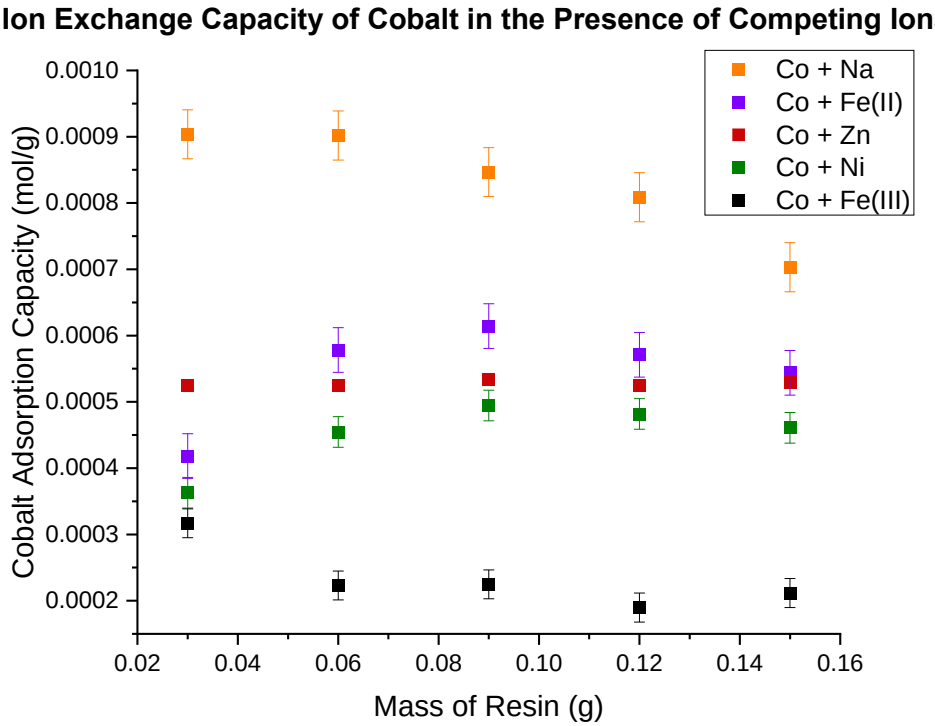

Figure 3.1. Effect of cobalt ion adsorption capacity in the presence of competing metal ions.

The trivalent metal ion Fe^{3+} generally has a lower cobalt ion exchange capacity for any total equilibrium ion concentration as shown in Figure 3.1. It is likely that multivalent

competing ion altered the surface morphology of ion exchange resin and reducing the availability of vacant active sites for cobalt adsorption. The monovalent metal ion, Na has a much higher cobalt ion exchange capacity for any total equilibrium ion concentration. This is most likely due to the increase in available vacant sites for cobalt adsorption due to its mono-valency. The divalent ions all behaved similarly in terms of cobalt ion exchange capacity and the reason is likely to be due to the cobalt ions having the same valency so competition for adsorption is less distinguishable. As multivalent ion adsorption requires adjacent available sites therefore the adsorption process alters the physical configurations of active sites available for subsequent adsorption of multivalent metal ions onto the surface of the ion exchange resin. These results are also supported by (Inglezakis, Zorpas, Loizidou and Grigoropoulou, 2005) [101] who found that the presence of other cations in heavy metal solutions reduced removal, via ion exchange, of the latter due to simultaneous exchange of positively charge cations which occupy available exchange sites. It was also found that heavy metals in the presence of multivalent cations, uptake is considerably lowered compared with monovalent species.

3.3.1.1 Recovery Degree

Recovery degree is percentage removal of ions from the solution by the ion exchange resin. The recovery degree is described by the following equation:

$$R = \frac{C_o - C_{eq}}{C_o} \times 100 \qquad \text{Eq 3.2}$$

R Recovery Degree (%)

C_o Initial molar concentration of ions (mol L^{-1})

C_{eq} Equilibrium molar concentration of ions (mol L^{-1})

Figure 3.2 shows that the recovery degree, calculated using Equation 3.2 increases with the mass of resin used, explained by the increase in available capacity as more resin is used. The recovery degree is lower with trivalent Iron Fe^{3+} at higher masses illustrating that overall ion adsorption is lower with higher valency ions and higher with low valency ions. This observation further supports the theory that the presence of multivalent competing ions alters the locations of the available active sites and effectively blocking adsorption.

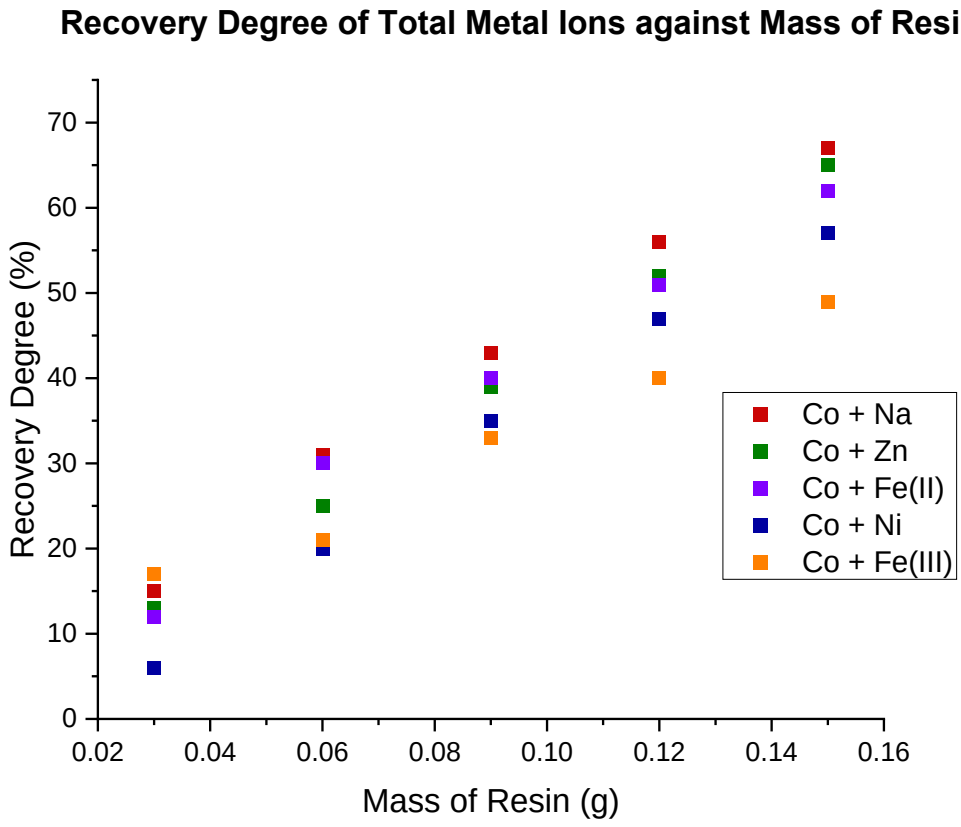

Figure 3.2. Recovery Degree (%) of Total Metal Ions

3.3.1.2 Separation Factor

The Separation factor is a relative measure of ion affinity to resin between two different metal ions. In this case, cobalt affinity is measured against the competing metal ions used for these experiment sets.

The Separation factor is described by the following equation:

$$\alpha_{Co/M} = \frac{D_{Co}}{D_M} \qquad \text{Eq 3.3}$$

$\alpha_{Co/M}$ Separation factor. Ratio of distribution coefficient of cobalt ions Co^{2+} to competing metal ion M.

D_{Co} Distribution coefficient of cobalt ions

D_M Distribution coefficient of competing metal ions

Where the Distribution coefficient is described by the following equation:

$$D = \frac{qe}{C_{eq}} \qquad \text{Eq 3.4}$$

D Distribution coefficient ($L\ g^{-1}$)

q_e Ion adsorption capacity ($mol\ g^{-1}$)

C_{eq} Equilibrium concentration of ions ($mol\ L^{-1}$)

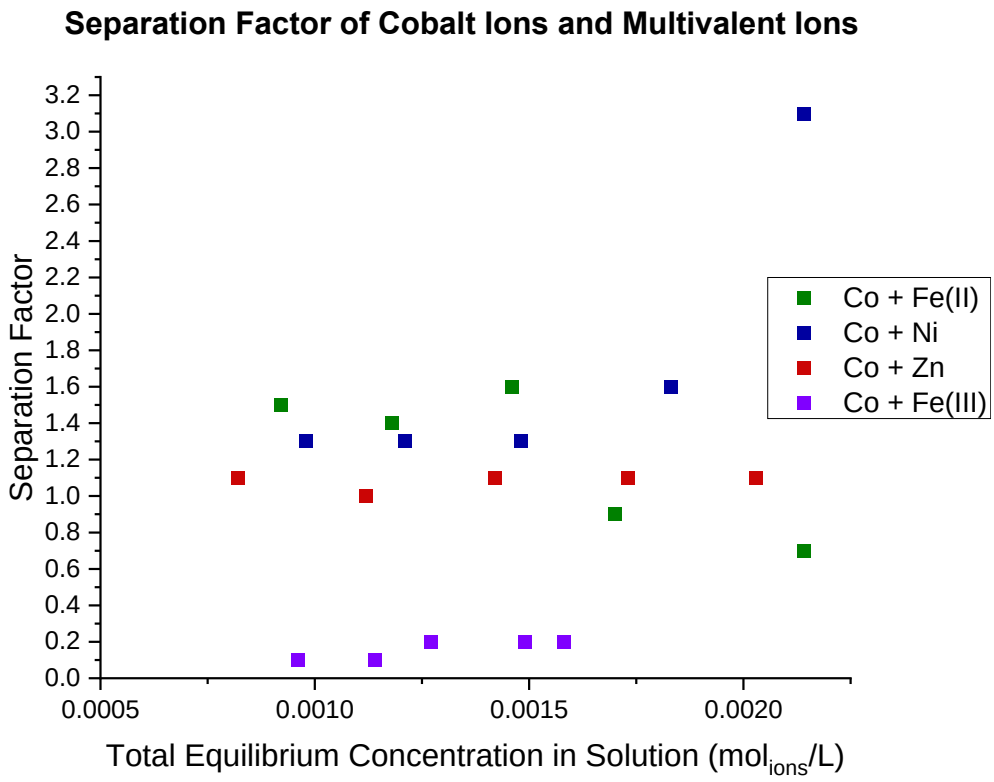

Figure 3.3 - Separation factor of cobalt with other divalent and trivalent competing ions.

The results show that the trivalent competing ions have higher affinity than divalent cobalt ions therefore suppressing the adsorption of cobalt ions onto the ion exchange resin. The divalent competing ions have similar adsorption affinity to divalent cobalt. The larger separation factor shows that adsorption affinity of cobalt ion is much higher than the monovalent sodium as shown in Figure 3.4. Oppositely, the smaller separation factor shows that with trivalent ions cobalt has a much lower affinity for the ion exchange resin as shown in Figure 3.3. This means that there is a clear trend in different magnitudes of separation factor according to the valency on the competing ion.

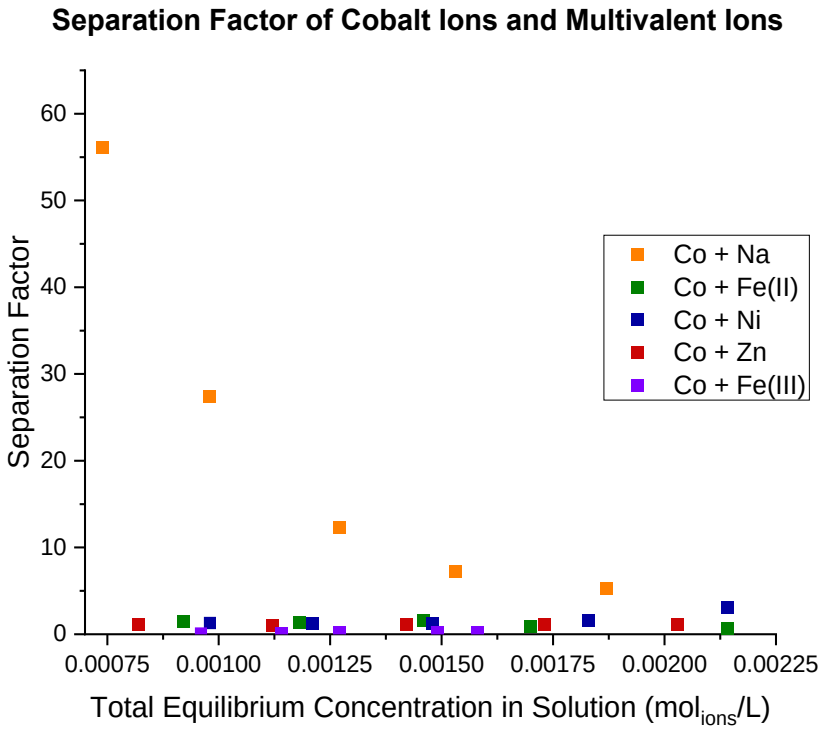

Figure 3.4 - Separation factor of cobalt with other competing ions including monovalent ions.

Cobalt adsorption affinity relative to the competing ion is as follows:

- Cobalt >> Monovalent metal ion (Na^{+})
- Cobalt ~ Divalent metal ions (Fe^{2+}, Ni^{2+}, Zn^{2+})
- Cobalt < Trivalent metal ions (Fe^{3+})

These correlates with the work done by Helffrerich [63], who claimed this is due to the phenomena 'electroselectivity'. Electroselectivity is where the ion of highest charge is preferred by the exchanger, and this becomes more pronounced with increasing dilution of the external solution.

3.3.2 Sorption Isotherms

Equilibrium experiments were conducted to provide data for isotherm models. This was done by varying the initial concentration in contact with the resin and allowing the system to reach equilibrium, all in order to obtain a number of data points to achieve a fit.

The equilibrium data obtained from sorption experiments of Co (II) onto Purolite NRW-160 resin form were fitted to linear Langmuir equation (Eq. 2.31). The values of Langmuir parameters (K_L and q_{max}) were determined from plots of $\frac{C_e}{q_e}$ Vs C_e and corresponding R^2 values are displayed on Figure 3.5. The determined values were then used produce theoretical data points for every C_e and compared with the experimental data as shown in Figure 3.6.

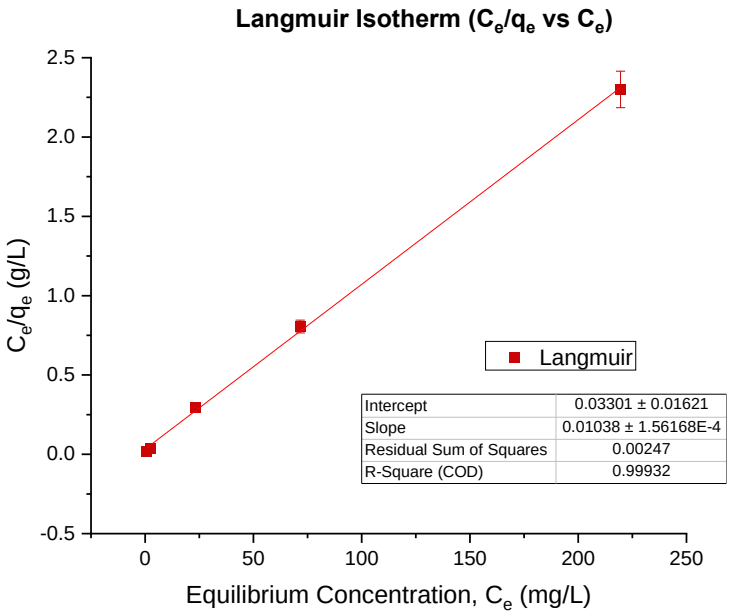

Figure 3.5 – Lagmuir plot of C_e/q_e vs C_e, showing the gradient and intercepts used for calculation of q_{max} and K_L. Also showing a value for R^2.

Using Eq.2.32, values of R_L for each concentration used were calculated and these values are highlighted in Table 3.3. With values between 0 and 1, it indicates that it is a favourable isotherm simply meaning that this adsorption process easily and preferentially occurs. The values of Freundlich parameters (K_F and n) were determined from plots of log(q_e)Vs log (C_e) and corresponding R^2 values are displayed on Figure 3.7. The value of n shown in Table 3.3 has been calculated using Eq.2.33 and its value indicates that the process is normal adsorption as opposed to cooperative adsorption, meaning that the adsorption process is not affected by the already adsorbed metal ions.

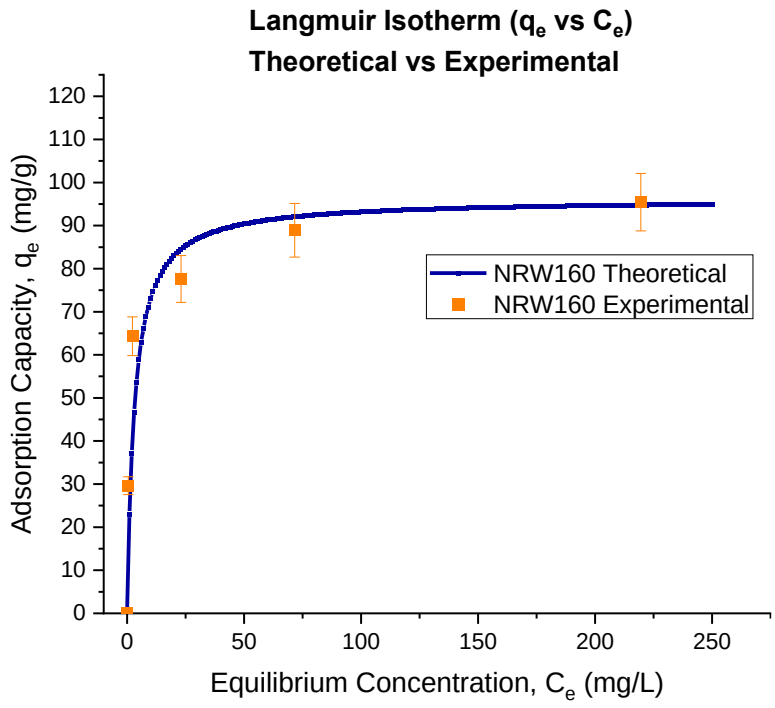

Figure 3.6 – Lagmuir plot showing the fit of experimental and theoretical data using values calculated for q_{max} and K_L.

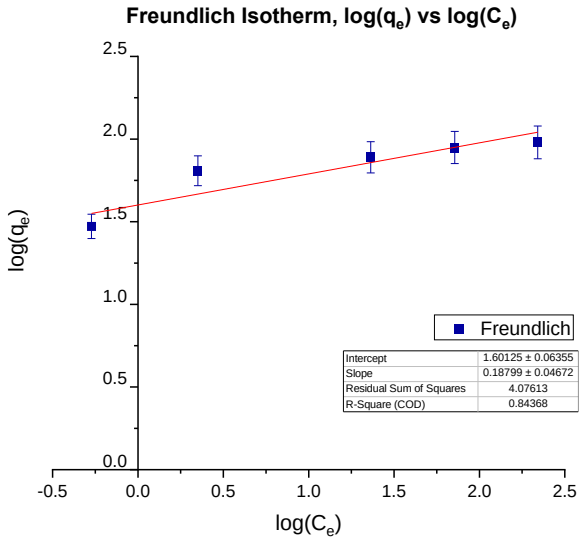

Figure 3.7 – Freundlich plot of qe) vs log (ce), showing the gradient and intercepts used for calculation of n and KF

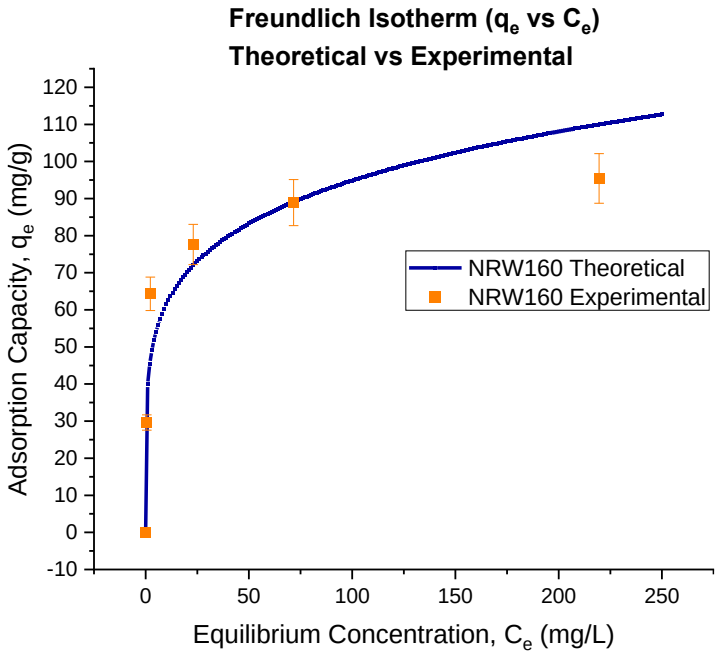

Figure 3.8 - Freundlich plot showing the fit of experimental and theoretical data using values calculated for n and K_F.

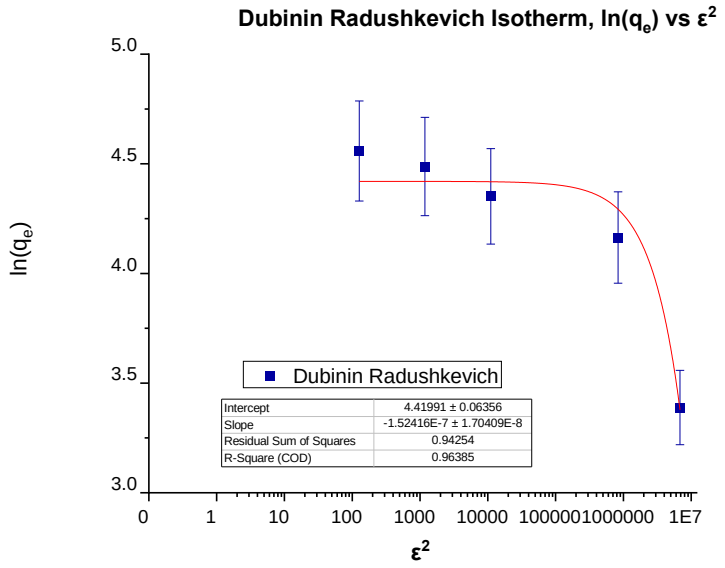

Figure 3.9 – Dubinin-Radushkevich plot of log (q_e) Vs ε^2, showing the gradient and intercepts used for calculation of β and E. Also showing a value for R^2.

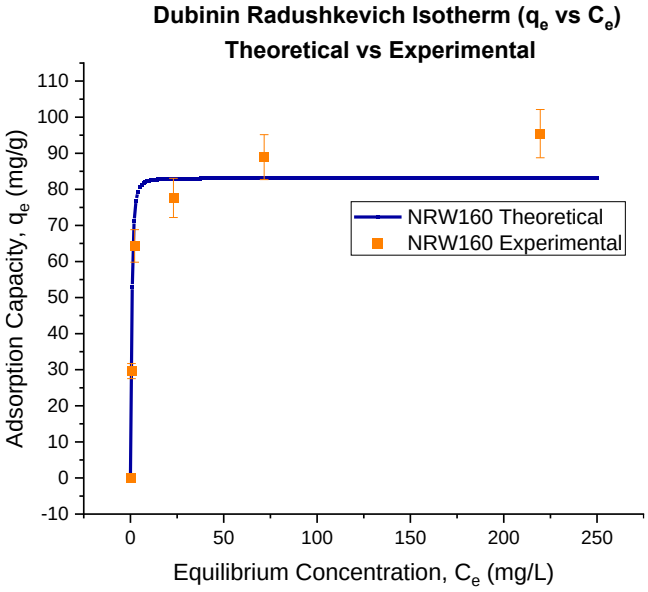

Figure 3.10 – Dubinin-Radushkevich plot showing the fit of experimental and theoretical data using values calculated for β and ε.

The values of Dubinin-Radushkevich parameters (β and ε) were determined from plots of log (q_e) Vs ε^2 and corresponding R^2 values are displayed on Figure 3.9. The value of the mean free energy of sorption E calculated with Eq.2.36 was 1.81 kJ mol^{-1} indicating a physisorption process. The value of correlation coefficients in Table 3.3 shows that the experimental data is more suited to the Langmuir model of monolayer coverage of the resin.

Table 3.3 Isotherm parameters for cobalt sorption onto Purolite NRW-160 resin.

Type of isotherm model	**Parameters**	**Value**
Freundlich	n	5.32
	K_F, mg g^{-1}	39.93
	R^2	0.844
Langmuir	q_{max}, mg g^{-1}	96.2
	K_L, L mg^{-1}	0.315
	R_L	0.012 – 0.222
	R^2	0.999
Dubinin-Radushkevich	β, mol^2 J^{-2}	$-1.52x10^{-7}$
	q_{max}, mg g^{-1}	83.7
	R^2	0.964
	E, kJ mol^{-1}	1.81

3.3.3 Selectivity Coefficients

Equilibrium experiments were conducted to provide data to determine selectivity coefficients using Eq 2.11 for various metal ions. These experiments were conducted using the same equilibrium method described in Section 3.2. However, the only discernible difference was that the MAXQ600 Shaker was used for the agitation. The determined values at 25˚C are shown in Table 3.4 and preference series is as follows:

$Fe^{2+} > Cu^{2+} > Ni^{2+} > Co^{2+} > Zn^{2+}$

Table 3.4. Experimentally Determined Selecitivy Coeffecients for Cations

Cation	**Selectivity Coefficients (Exchange with H^+)**
Fe^{2+}	78.5
Zn^{2+}	48.2
Co^{2+}	70.9
Ni^{2+}	74.1
Cu^{2+}	75.3

Selectivity coefficients are notoriously difficult determine as they rarely remain constant and will vary with experimental conditions such as temperature, concentration, and the presence of other species in solution. Typically, selectivity coefficients are extracted from manufacturers' data of research literature.

For strong acid resins, like the one used in these experiments, the values of selectivity coefficients from a resin manufacturer are shown in Table 3.5 and the preference series is as follows:

$Cu^{2+} > Ni^{2+} > Co^{2+} > Zn^{2+} > Na^{+} > H^{+} > Li^{+}$

Table 3.5 Selecitivy Coeffecients for Cations from Literature [96]

Cation	Relative Selectivity Coefficients	(Relative Selectivity Coefficients)^2
Li^{+}	0.68	0.46
H^{+}	1.00	1
Zn^{2+}	2.57	6.60
Co^{2+}	2.59	6.71
Ni^{2+}	2.76	7.62
Cu^{2+}	3.03	10.0

The experimentally determined selectivity coefficients follow the same preference series as the values from literature; however, the values from literature [96] used a different stoichiometry of reaction for hetero-valent exchange. This is the reason why literature values were also squared, as to allow for a direct comparison with the experimental results which showed experimental selectivity coefficients are an order of magnitude out. Selectivity coefficients are difficult to determine and depend on a range of conditions such as total solution concentration, resin concentration and type of resin used. As it is unknown of the experimental conditions used to determine these literature values it can be attributed to the order of magnitude difference. However, similar work conducted by (Lee, Kuan and Chern, 2007) [100] yielded selectivity coefficients for copper and zinc of

40.43 and 37.48 respectively at 298K, and also matched the selectivity series seen in Table 3.4 and 3.5. These values are on the same order of magnitude as the values determined experimentally in this chapter and were also determined based on a heavy metal and Hydrogen.

3.3.3.1 Temperature Dependent Selectivity Coefficients

These experiments were conducted using the temperature dependent method described in section 3.2. The standard enthalpy change associated with ion exchange reactions in resins is generally small and shows a small dependence on temperature given by the Van't Hoff equation:

$$lnK_{MH} = -\left(\frac{\Delta H}{R}\right)\frac{1}{T} + \left(\frac{\Delta S}{R}\right) \qquad \text{Eq 3.12}$$

Where K_{MH} is the selectivity coefficient of metal ion M against H^+, T is the absolute temperature (K), R is the molar gas constant (J mol^{-1} K^{-1}), ΔS is the standard entropy change (J mol^{-1}) and ΔH is the standard enthalpy change (kJ mol^{-1}). The standard free energy change ΔG (kJ mol^{-1}) can be derived from the relationship:

$$\Delta G = \Delta H - T\Delta S \qquad \text{Eq 3.13}$$

Table 6 shows the selectivity coefficients determined for cobalt, copper, zinc, nickel, and iron at 298K, 308K, 318K, 328K and 338K. Figure 3.11 shows the plot of Eq 3.12 in order to determine the gradient $\left(\frac{\Delta S}{R}\right)$ and intercept $\left(\frac{\Delta H}{R}\right)$.

The values for the derived parameters are shown in Table 3.7 and can be used to input back into the Van't Hoff equation to determine selectivity coefficients for the metal ions used. Work conducted by Boyd reported thermochemical data for ion exchange resins

with a range of ions, however his work was done using organic ion exchange resins and the ions used would be of minimal interest for the use in PWRs.

Table 3.6. Experientally Determined Temperature Dependent Selectivity Coeffecients for Cations.

Cation	**Selectivity Coefficients**				
	298K	308K	318K	328K	338K
Co^{2+}	70.9	73.7	78.0	80.0	84.0
Cu^{2+}	75.38	81.4	86.7	94.3	97.1
Zn^{2+}	48.2	49.4	51.5	55.5	58.5
Ni^{2+}	74.0	76.4	79.5	81.0	85.7
Fe^{2+}	78.5	81.3	83.6	84.8	87.3

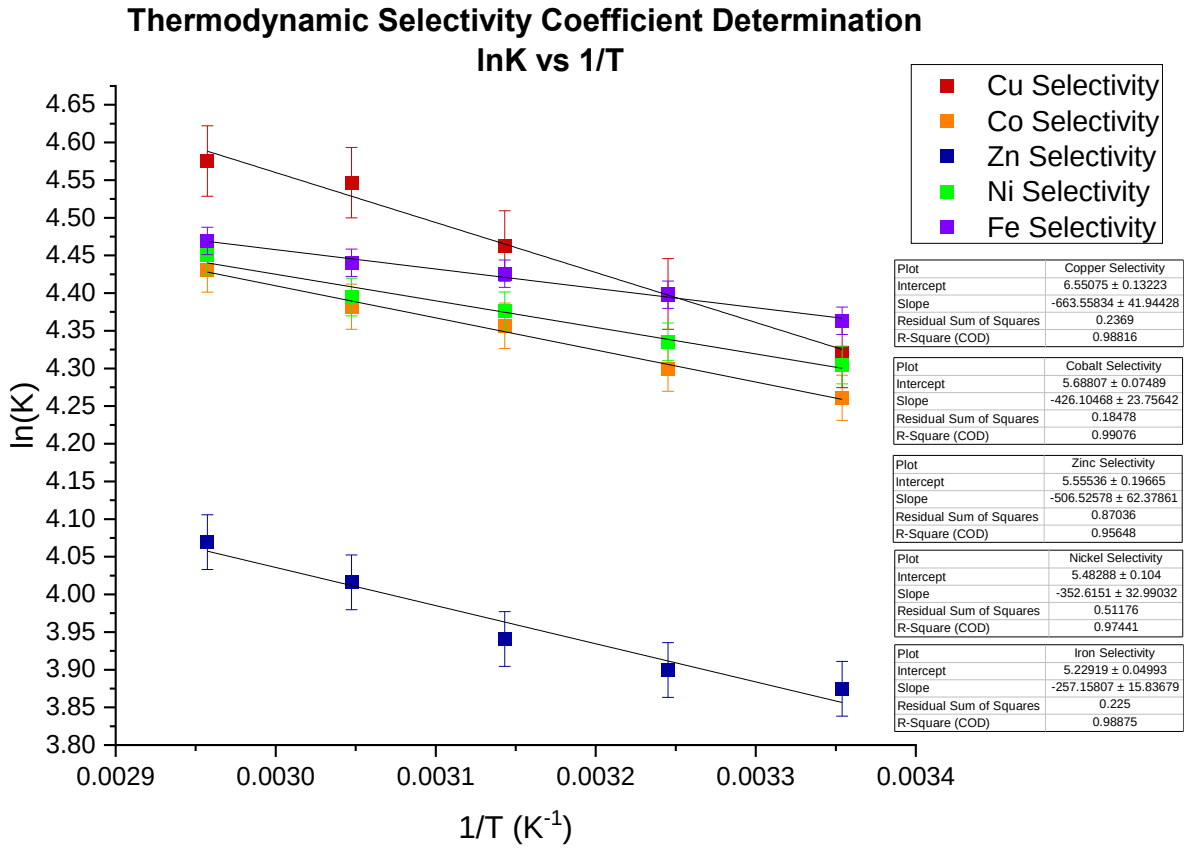

Figure 3.11. Thermodynamic selectivity coeffeicient determination. lnK v 1/T.

The ΔG values in Table 3.7 are all negative which is indicative of a spontaneous process mean there is little to no energy needed to overcome for this reaction to happen. This is indicative of a physisorption process which is further supported by the value of the Dubinin-Radushkevich isotherm parameter, mean free energy. The values in Table 3.7 are also consistent with similar work conducted by (Lee, Kuan and Chern, 2007). There is also a link between the value of ΔG and the mass number of metal ions, with a higher mass number resulting in a lower ΔG value, which is also consistent with the literature.

Table 3.7. Experimentally Derived Van't Hoff Equation Parameter

Metal ion	ΔH (kJ mol^{-1})	ΔS (J mol^{-1} K^{-1})	ΔG (kJ mol^{-1})				
			298 K	308 K	318 K	328 K	338 K
Cobalt	3.54	47.29	-10.55	-11.02	-11.50	-11.97	-12.44
Copper	5.52	54.46	-10.71	-11.26	-11.80	-12.35	-12.89
Zinc	4.21	46.19	-9.55	-10.01	-10.48	-10.94	-11.40
Nickel	2.93	45.58	-10.65	-11.11	-11.56	-12.02	-12.48
Iron	2.14	43.48	-10.82	-11.25	-11.69	-12.12	-12.56

3.4 Summary

This section explored the effect of competing ions against cobalt resin adsorption. The relative affinity series was found to follow Monovalent << Divalent << Trivalent, which is further supported by literature. In addition, separation factors for cobalt ions against other monovalent, divalent and trivalent ions were obtained and illustrated showing the magnitude differences between valences. It is postulated that for ions of a higher valence, multiple sites are used for adsorption which is preferred over an ion of a lower valence which uses less sites for adsorption.

This section also investigated equilibrium data for the sorption of cobalt ions onto Purolite NRW-160, to be analysed using Freundlich, Langmuir and Dubinin–Radushkevich isotherm models; sorption was best fitted by the Langmuir model. The values of sorption intensity ($0 < R_L < 1$) indicates that Co (II) sorption onto Purolite NRW-160 resin has a favourable sorption isotherm. The value of the mean free energy of sorption, *E,* was of 1.81 kJ mol^{-1}, indicating that the sorption process follows a physical ion-exchange mechanism (Jain, Garg and Kadirvelu, 2009) [102]. This is also referred to as non-specific adsorption, which occur as a result of long range weak Van der Waals forces between the adsorbate and adsorbents, hence a low value for the mean free energy of sorption results in physisorption. Chemisorption is when a covalent bond is formed between the adsorbate and adsorbent and requires significant activation energies to occur.

Furthermore, the value of n from the Freundlich isotherm showed that the process follows a normal adsorption process.

Finally, this section presented experimentally determined selectivity coefficients for a range of metal ions. Compared with literature values, the values are an order of magnitude out, however they do follow the same affinity series. The difference could be attributed to a number of things involving experimental parameters, and as the literature values do not explain how they were determined the order of magnitude difference is likely to be due to that. Furthermore, using the Van't Hoff equation, temperature dependant selectivity coefficient equations were determined using experimentally derived values for ΔG, ΔH and ΔS.

4 Ion Exchange Kinetics

4.1 Introduction

To be able to model the ion exchange process in a PWR, understanding ion exchange kinetics is of great importance. This section covers the kinetic behaviour of ion exchange reactions between ion exchange resins and cobalt, iron, nickel, zinc, and copper metal ions. These metal ions were of focus as they are species which are commonly found in the PWR primary circuit coolant.

This section explores the determination of rate constants and their temperature dependency, deriving an Arrhenius type equation using activation energies for implementation into the ion exchange model described in Chapter 3.

This section also explores the effect of flow rate on adsorption of cobalt onto the ion exchange resin as well as determination of mass transfer coefficients to gain a better understanding of the kinetic behaviour during the ion exchange process.

Finally, this section explores the effect of temperature on the ion exchange resins themselves. It is well known that resins have an operational temperature limit as they begin to undergo a degradation mechanism above this limit. This section attempts to derive a time and temperature dependent equation to predict ion exchange behaviour and a range of temperatures.

4.2 Materials and Methods

This experimental set up for these experiments were similar to those in Chapter 3. The reagents used in these experiments are found in Table 4.1 with the suppliers and purities provided. When preparing solutions, ultrapure Type I water (18.2 MΩcm) was used. The

ion exchange resin used in these experiments was the same resin used in Chapter 3, NRW 160, provided by Purolite.

Table 4.1 Source of metal ions used.

Metal Ion	**Metal Salt**	**Supplier (Purity)**
Cobalt	Cobalt Sulphate Heptahydrate	Acros Organics (99+%)
Copper	Copper Sulphate Pentahydrate	Sigma-Aldrich (≥98%)
Zinc	Zinc Sulphate Heptahydrate	Fisher Scientific (98%)
Nickel	Nickel Sulphate Hexahydrate	Fisher Scientific (99+%)
Iron (II)	Iron (II) Sulphate Heptahydrate	Acros Organics (99+%)

For the temperature dependent experiments in Section 4.3.1 0.08g of ion exchange resin were weighed and added to conical flasks filled with 100ml of a metal ion solution with concentrations of 1mmol L^{-1}. These solutions were then agitated in a temperature controlled incubated MaxQ6000 shaker at a range of temperatures (298K, 308K, 318K, 328K and 338K) with samples being taken periodically at 5, 10, 15, 20, 30, 45, 60 and 120 minutes. The sample's metal ion concentration was then analysed using ICP-OES. The concentration of the samples was also analysed prior to any resin addition to obtain the true starting concentration. Preliminary experiments were carried out to ascertain an appropriate resin mass and solution volume to use for the selected 1mmol L^{-1} concentration of metal ions. Limited by the size of the MaxQ6000 no more than 100ml

conical flasks could be used for these experiments for all metal ions. A resin mass of 0.08g was found to be optimal for these experiments in order to see the initial concentration loss in the early stages of the ion exchange process. Obtaining sufficient data points in the early stages of these experiments are crucial to the analysis of the kinetics. The preliminary experiments were conducted a sufficient number of times in order to be confident about any variance that may occur due to the low resin loading.

For the flow rate dependent experiments in Section 4.3.2 and 4.3.3 a custom flow rig was built and used to obtain results. The rig as seen in Figure 4.1, consisted of a 5L reservoir which contained the metal ion solutions and a HPLC pump with a manometric module to pump the solution through stainless steel/titanium tubing. The tubing also housed a cell which contained 3g of the ion exchange resin held in place by a custom piece of Bekipor, a highly porous filter membrane. The cell had a cross sectional area of 1.27cm^2, a bed length of 4.4cm and the bed porosity/voidage was calculated to be 0.53.

Experiments were carried out at room temperature (25°C), and with flow rates of 0.1, 0.3, 0.75, 1.5 and 3.0 ml s^{-1}, which translates into residence times of 44s, 14.67s, 5.86s, 2.93s and 1.47s respectively. These flow rates and residence times are much faster and quicker than what it is seen in industry. The reason these values were chosen was so that the solution would never be in total equilibrium with the column. The allows for the effect of a change in flow rate to be observed, for if the solution were flowing slow enough to be in equilibrium the effluent concentration would remain the same, as long as the column was not saturated.

Samples were collected in test tubes from the solution exiting the rig, which would then be analysed using ICP-OES.

For the ion exchange resin temperature degradation experiments in Section 4.3.4, 10g of resin was added to a 45ml acid digestion vessel filled with ultrapure type I water. The acid digestion vessel is a pressure vessel that completely encapsulates a sample within a PTFE environment and is rated for use up to 250°C.

The acid digestion vessel was then placed in an oven at temperatures ranging from 60 - 200°C, for periods ranging 3 hours to 7 days. The resin's capacity before and after the experiments was then measured using a titration method provided by Purolite [103]. The titration method involved:

- Transfer ~10g of sample to a capacity funnel.
- Regenerate resin with 1000ml of 4% Hydrochloric acid solution at a flow rate of 25ml min^{-1}.
- Rinse the resin with mixed bed water until effluent is free of chloride ion when tested in 0.1N Silver Nitrate.
- Pass sufficient 5% Sodium Chloride solution at 25ml min^{-1} through the resin sample to fill a clean, dry 1000ml volumetric flask to calibration mark. Mix contents of flask well be inverting several times.
- Remove a 100ml aliquot to each of two clean, dry Erlenmeyer flasks, covering each flask after transfer is complete.
- Titrate each aliquot with standardised 0.1N sodium hydroxide solution to the phenolphthalein endpoint. The titration should agree within 0.1. If they do not, titrate a third aliquot and record the average as T.

- Calculate the weight capacity (meq g^{-1}) $= \frac{T(ml)\ x\ N\ NaOH\ x\ 10}{W,(wet\ grams)\ x\ Solids}$
- Calculate volume capacity (meq ml^{-1}) = $\frac{weight\ capacity\ x\ Solids\ x\ D}{62.4}$
- Where Solids $= 1 - (\frac{\%MHC}{100})$,where MHC is moisture holding capacity and D is density in lbs cu^{-1}.

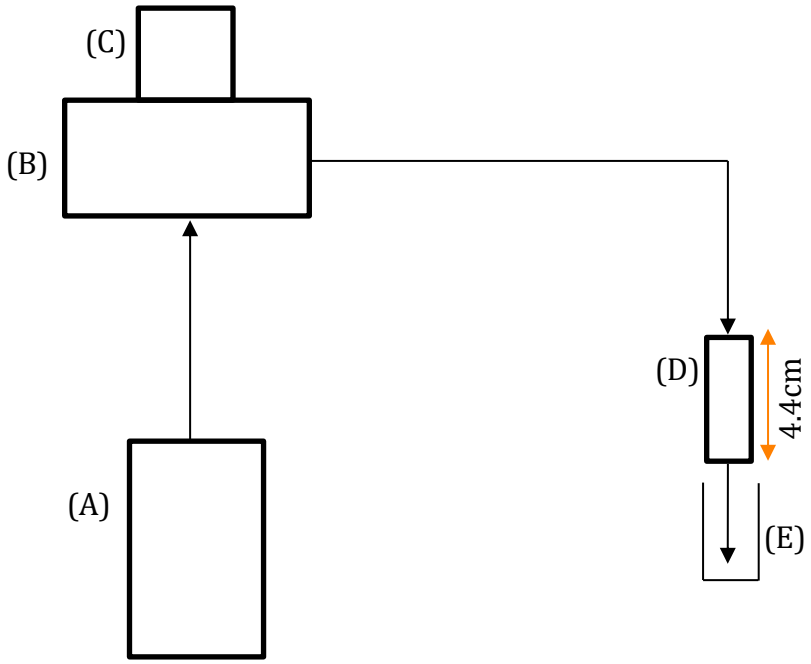

A. Reservoir.
B. HPLC Pump. (5L)
C. Manometric Module.
D. Cell with 3g of Ion Exchange Resin.
E. Sampling tube.

Figure 4.1 Simplified schematic of custom-built rig for variable flow rate experiments.

4.3 Results & Discussion

4.3.1 Rate constants

Transient experiments were conducted at room temperature (25°C) to provide data to determine rate constants using Eq 4.1 [64] for various metal ions. 0.08g of ion exchange resin were weighed and added to conical flasks filled with 100ml of a metal ion solution

with concentrations of 1mmol L^{-1}. These solutions were then agitated in a temperature controlled incubated MaxQ6000 shaker at a range of temperatures (298 K, 308 K, 318 K, 328 K and 338 K) with samples being taken periodically at 5, 10, 15, 20, 30, 45, 60 and 120 minutes. The sample's metal ion concentration was then analysed using ICP-OES.

This equation is for a second order reaction that is first order in each of the two reactants A and B with the equation A + B → P, where P is the products formed.

$$ln\left(\frac{[B]/[B]_0}{[A]/[A]_0}\right) = ([B]_0 - [A]_0)kt \qquad \text{Eq. 4.1}$$

Where [A] and [B] are the concentrations of species at time t, [A] and [B] are the initial concentrations of species and k is the second order rate constant. From the above equation [A] is the concentration of the resin species (R-H) and [B] is the concentration of the metal species to be exchanged.

The plot for the above expression for cobalt, nickel, zinc, iron, and copper ions from the results of the experiment can be seen in Figure 4.1.

The same transient experiments were repeated at 35, 45, 55 and 65°C with graphs similar to Figure 4.2 being produced. The gradients were used to determine values of k from Eq 4.1 with units of L mol^{-1} min^{-1}, which were then converted to a value with units of L mol^{-1} s^{-1}, shown in Table 4.2.

Results show that the rate of uptake onto the resin increases as temperature increases. This is expected as diffusivity increases as temperature increases, which results in faster reaction rates, as described by the Stokes-Einstein equation:

$$D = \frac{k_B T}{6\pi\mu r} \qquad \text{Eq. 4.2}$$

Table 4.2 Second order rate constants at 25, 35, 45, 55 and 65°C for Cobalt, Copper, Zinc, Nickel and Iron.

	k (L mol^{-1} min^{-1})					k (L mol^{-1} s^{-1})				
	25°C	35°C	45°C	55°C	65°C	25°C	35°C	45°C	55°C	65°C
Cobalt	2.034	2.137	2.812	2.819	2.804	0.034	0.036	0.047	0.047	0.047
Copper	0.613	0.816	0.956	0.989	1.146	0.010	0.014	0.016	0.016	0.019
Zinc	0.911	1.097	1.202	1.500	1.831	0.015	0.018	0.020	0.025	0.031
Nickel	0.991	1.254	1.550	1.885	2.109	0.017	0.021	0.026	0.031	0.035
Iron	1.567	2.623	2.709	4.225	5.290	0.026	0.044	0.045	0.070	0.088

Where D is the diffusion constant, k_B is Boltzmann's constant, T is temperature (K), μ is the dynamic viscosity and r is the radius of the diffusing ions.

The surface film thickness, δ is also affected by temperature and demonstrates a correlation with Schmidt and Reynolds numbers. Although this correlation was established for a packed bed of resin, it holds true for results in Chapter 4. [65] [66]:

$$\frac{d_p}{\delta} = 2 + \left(1.1\ Sc^{\frac{1}{3}}\right)(Re^{0.6}) \qquad \text{Eq. 4.3}$$

Where d_p is the diameter of the resin bead and Sc and Re are the Schmidt and Reynolds numbers respectively described as:

$$Sc = \frac{\mu}{\rho D} \qquad \text{Eq. 4.4}$$

And;

$$\mathrm{Re} = \frac{DV}{\upsilon} \qquad \text{Eq. 4.5}$$

Where ρ is the density of solution, V is the superficial fluid velocity and υ is the kinematic viscosity defined as $\frac{\mu}{\rho}$. The equations demonstrate that changes in temperature have an effect on film thickness resulting in a change in reaction rates. It also demonstrates that the effect on film thickness with temperature depends on a balance of the Schmidt and Reynolds numbers.

Using the second order rate constants, activation energies and Arrhenius pre factors were calculated using the Arrhenius equation:

$$\mathrm{k} = \mathrm{A_0 e}^{\frac{-E_A}{RT}} \qquad \text{Eq. 4.6}$$

Figure 4.3 shows the plot of data using the Eq 4.7, which is the linearised form of Eq. 4.6:

$$\ln\mathrm{k} = \ln\mathrm{A} - \frac{E_A}{R}\left(\frac{1}{T}\right) \qquad \text{Eq. 4.7}$$

The gradients and intercepts were then used to determine values for activation energy and Arrhenius pre factors shown in Table 4.2 which appears to be consistent with similar work done in literature [67] [68]. (Abdelwahab et al.,2013) explored the removal of zinc from aqueous solutions using cation resins and calculated the activation energy of Zinc ions onto the resin to be 19.8 kJ mol^{-1} compared with the value of 14.266kJ mol^{-1} seen in Table 4.2. (Jones et al.,2019) explored the removal of cobalt ions from aqueous solutions using cation resins. An activation energy of 15.49 kJ mol^{-1} was calculated for cobalt compared with the value of 7.762 kJ mol^{-1} as seen in Table 4.2.

Table 4.2 Second order rate constants at 25, 35, 45, 55 and 65°C for Cobalt, Copper, Zinc, Nickel and Iron.

Arrhenius Parameters for metal ion exchange					
Metal	Co^{2+}	Cu^{2+}	Zn^{2+}	Ni^{2+}	Fe^{2+}
E_a (kJ mol^{-1})	7.762	12.211	14.266	16.141	24.423
A (L mol^{-1} s^{-1})	0.787	1.505	4.705	11.325	523.512
R^2	0.796	0.935	0.978	0.993	0.955

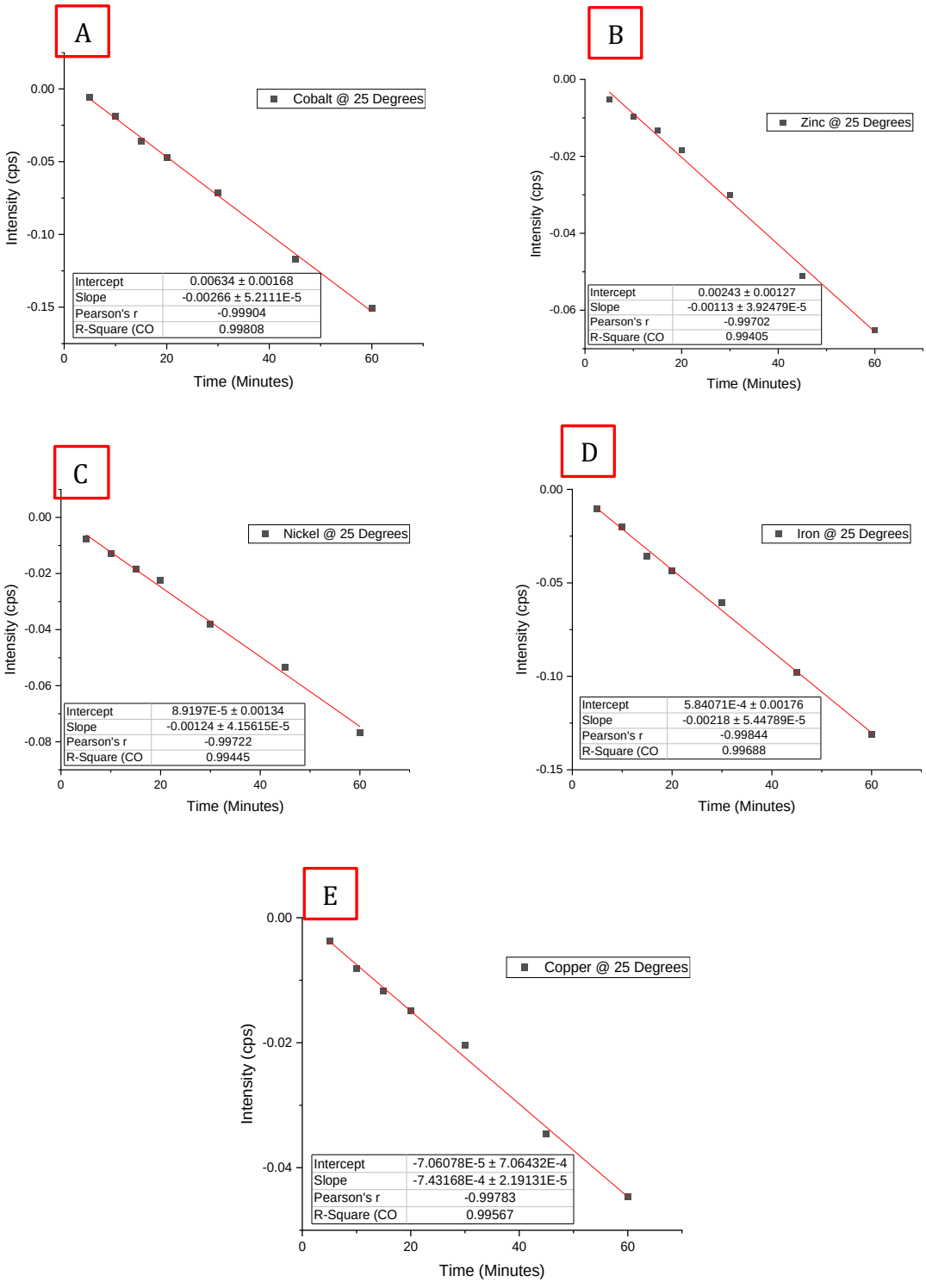

Figure 4.2 Linear Plots of Eq 4.1 to determine second order rate constant, k for (A)Cobalt, (B)Nickel, (C)Zinc, (D)Iron and (E)Copper at 25°C.

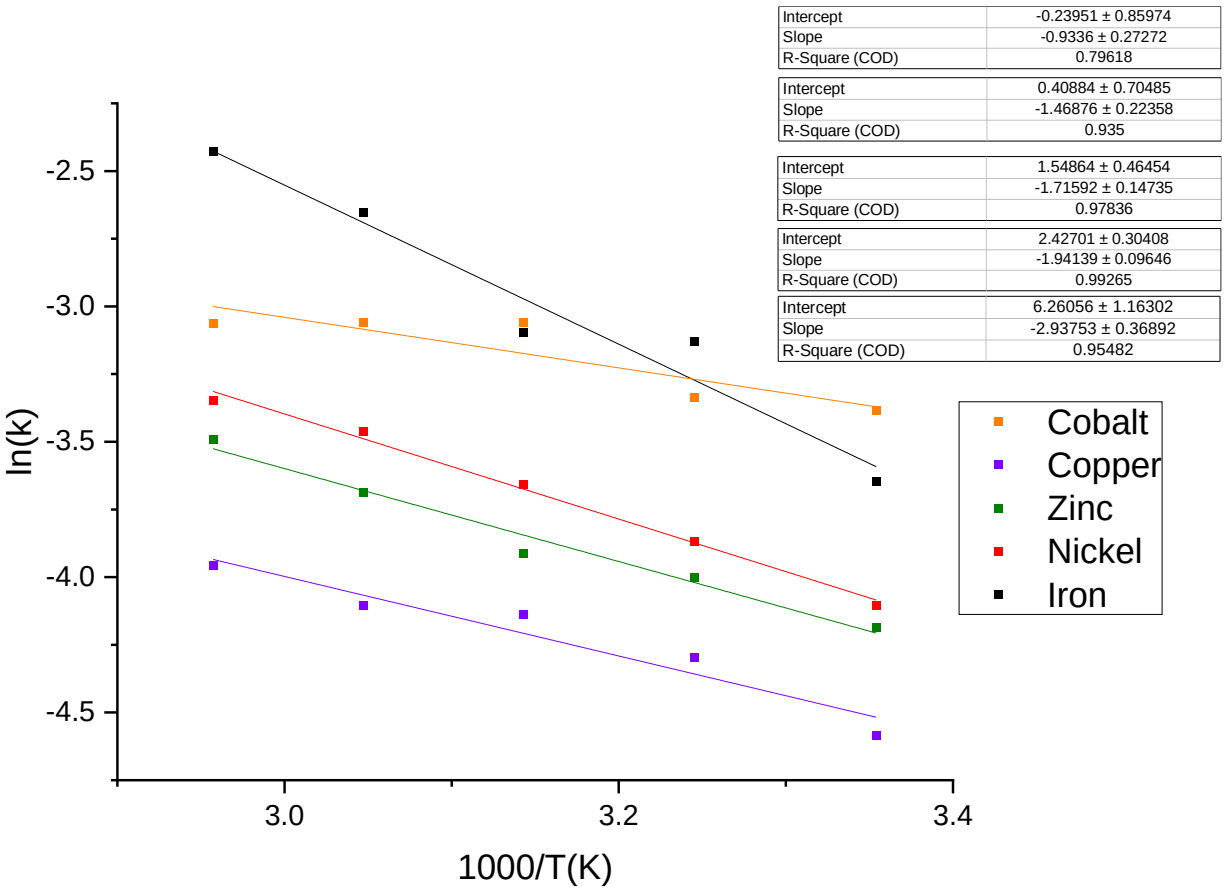

Figure 4.3 Linear Plots of Eq 4.7 to determine Activation Energies and Arhenius Prefactors for Cobalt, Nickel, Zinc, Iron and Copper.

4.3.2 Effect of flow rate on cobalt adsorption

Using the custom-built rig, transient experiments were conducted to explore the effect of flow rate on cobalt uptake onto the resin. The starting concentration of cobalt solution was 1000 ppb, and the results are shown in Figure 4.4.

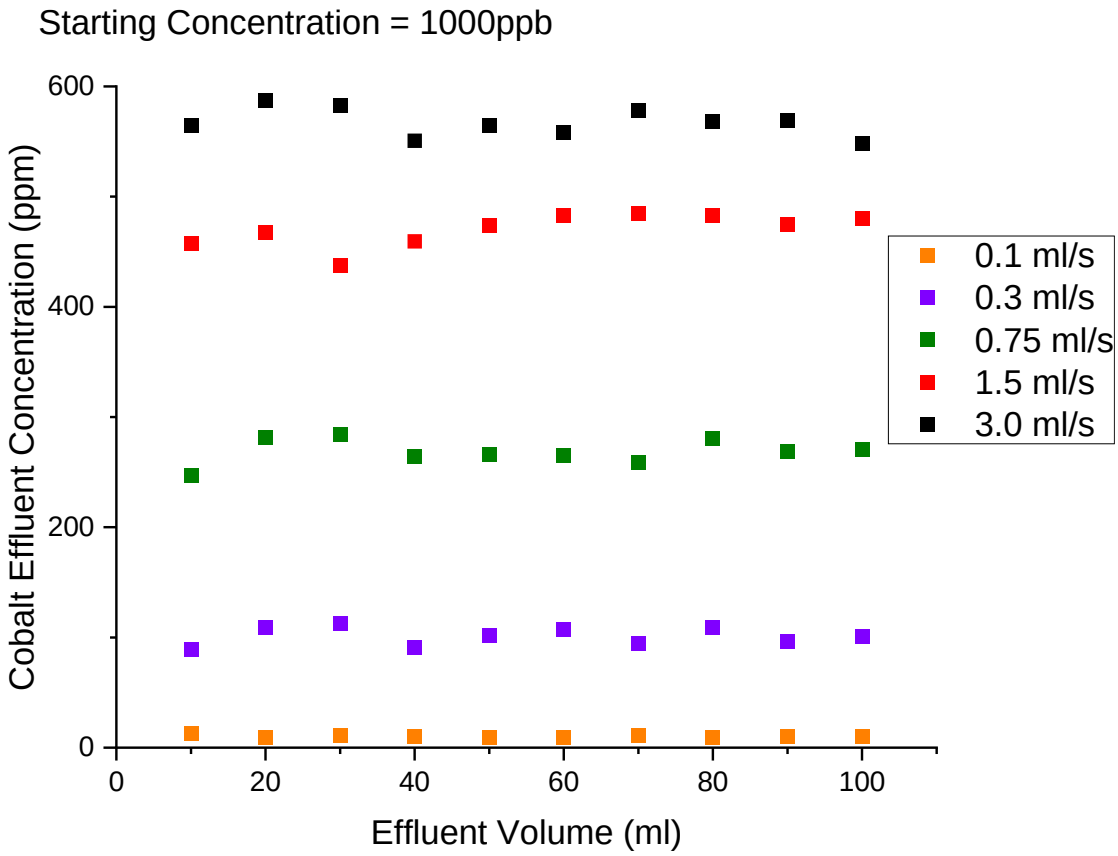

Figure 4.4 Cobalt effluent concentration against effluent volume at different flow rates. (Starting Concentration = 1000ppb)

The flow rates were set much faster than industrial practice to ensure that the resin remained unsaturated and data points would occur within the mass transfer zone (MTZ), where the mass transfer zone is described as the zone of a packed column where the active adsorption occurs [69].

The short residence times of 44 s, 14.67 s, 5.86 s, 2.93 s and 1.47 s for the flow rates of 0.1, 0.3, 0.75, 1.5 and 3.0 ml s^{-1} respectively, coupled with low influent concentration allows saturation to not be reached, however it is also important to ensure that the effluent is not in equilibrium with the resin. Increasing the flow rate also increases the width of the mass transfer zone so this means that the MTZ expands beyond the sample point and beyond

the end of the resin bed, so the concentration seen at the sampling point is going to be much higher. This is also known as the MTZ not being fully developed and is due to a low residence time not allowing adsorption equilibrium to be reached [70],[71]. Figure 4.4 had an initial concentration of 1000 ppb, however there were repeats using an initial concentration of 750 ppb, 500 ppb and 250 ppb. These graphs are illustrated in Chapter 4 Supplementary in the Appendix. Figures 8.11 – 8.13 follow the same trend as seen in Figure 4.4. There appears to be more variation in the results as the flow rate becomes faster, but this can be attributed to the speed at which the sample had to be swapped out at was too great.

4.3.3 Mass Transfer Coefficients

Flowrate is known to affect resin performance through residence time. Flowrate is often set to optimise heat exchange between primary and secondary loops. An increase in flowrate was found to have an adverse effect on cation ion uptake [72], which can be related to the reduction in residence time between the cation ion solution and the fixed resin bed. Mass Transfer Coefficients (MTC) are diffusion rate constants that relate the mass transfer rate over a transfer area with the concentration change as a driving force [73]. The following equation equates for MTCs but is only valid for circumstances of fast flow or low residence time:

$$MTC(k_i) = -\frac{V}{SZAR_i}\ln\left(\frac{C_i^{eff}}{C_i^{f}}\right) \qquad Eq.4.7$$

Where S the specific surface area of resin withing the column (cm^2cm^{-3}), described as:

$$S = a_s(1 - \varepsilon) \qquad Eq.4.8$$

Where k_i is the Mass Transfer Coefficient (cm s^{-1}), V is the volumetric flowrate (ml s^{-1}), a_s is the specific surface area of resin bead, ε is the column void fraction, Z is the resin bed height (cm), A is the cross sectional area of bed (cm^2), R_i is the Resin volume fraction of cationic to anionic, C_i^{eff} is the ion effluent concentration and C_i^f is the initial ion concentration in solution.

Table 4.3 Mass transfer coefficients for cobalt ions with varying flow rates.

	k_i (m s^{-1}) x 10^{-5}				
	Flow rate (ml s^{-1})				
C_i^f (ppb) (↓)	0.1	0.3	0.75	1.5	3.0
250	Not Detectable	6.07	7.65	9.72	13.61
500	Not Detectable	6.91	8.19	10.61	13.89
750	Not Detectable	5.01	7.07	9.51	13.37
1000	2.45	4.02	6.18	8.47	11.69

The experiments from Section 4.3.2 were repeated with a range of different starting concentrations allowing mass transfer coefficients to be calculated using Eq.4.7. It can be concluded that increasing flow rate resulted in an increase in mass transfer coefficient

where the mass transfer coefficient values begin to plateau at the higher range of flow rates, as illustrated by Figure 4.5. The increase in flow rates results in a decrease in the thickness of the boundary layer around the resin. This therefore suggests that kinetics is controlled by film diffusion (diffusion across the boundary layer).

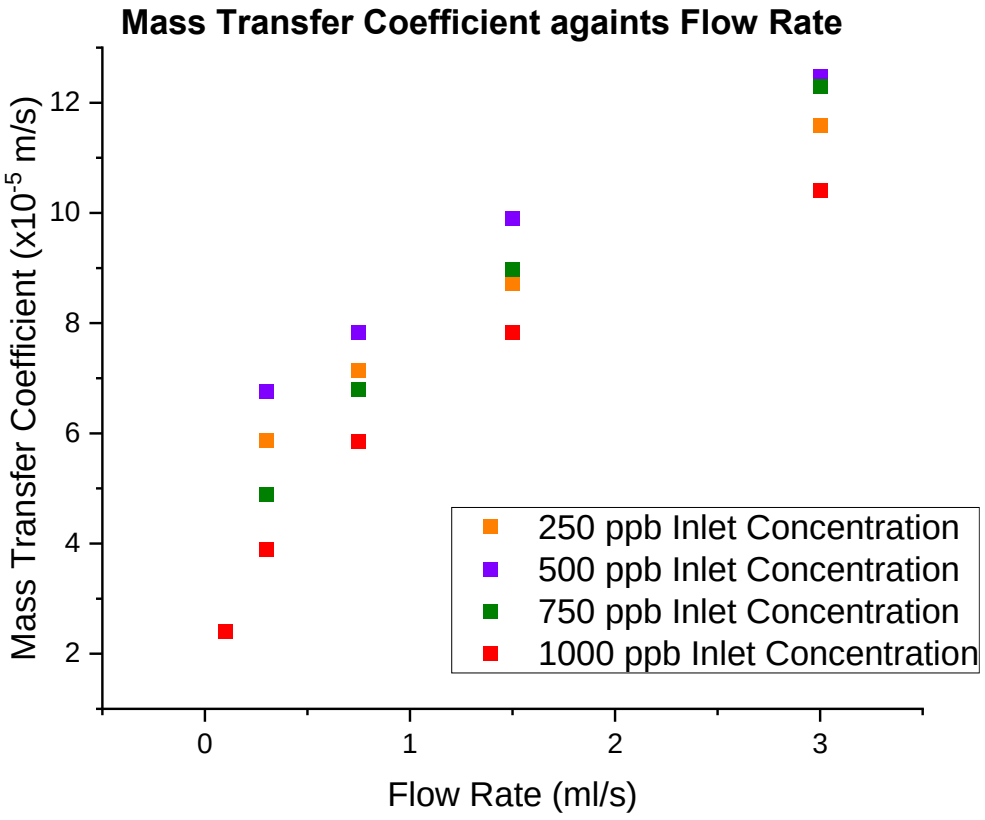

Figure 4.5 Mass Transfer Coefficients against Flow Rate at different influent concentrations

4.3.4 Resin Temperature Degradation

Ion exchange resins are known to have an operational temperature limit, with cation resins being graded up to 120°C and anion resins up to 60°C. Above these temperatures the resin beings to degrade and lose its capacity.

A thermogravimetric analysis (TGA) was performed on the NRW-160 resin to characterise it and observe as it degrades. The TGA was set up to ramp up the temperature to 100°C at a rate of 20°C min^{-1}, then held for 10 minutes before ramping up to 500°C at the same rate. The results are shown in Figure 4.6.

The number of peaks refer to the number of degradation stages. The first large peak can be attributed to dehydration of the hydrophilic resin surface. The second smaller peak between 100°C and 150°C can be attributed to further dehydration after the restart.

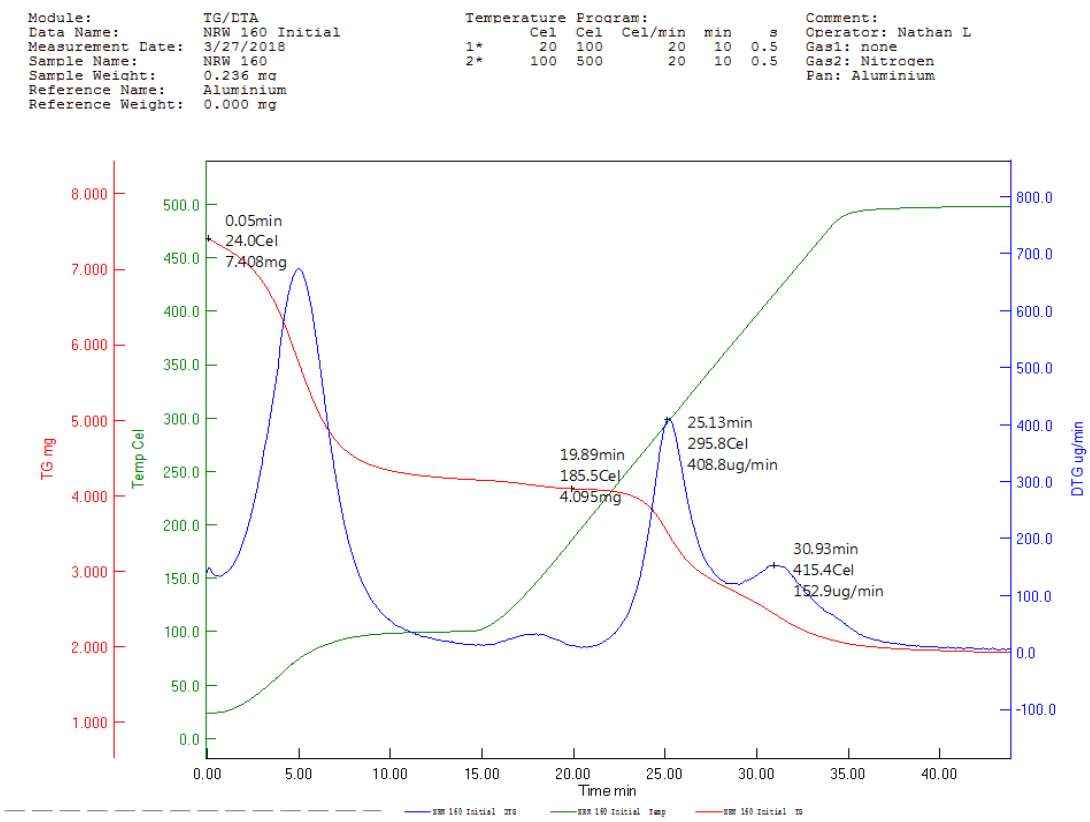

Figure 4.6 Results from TGA on ion exchange resin (NRW-160)

Third Peak between 250°C and 400°C is attributed to the scission of the sulphonic acid functional Group and the final peak is then attributed to scission of bonds and decomposition of the polymer matrix [74][75][76]. These results indicate that the resin doesn't suffer sever capacity loss until the temperature approaches 300°C showing that if the ion exchange resin were to suffer a thermal transient of temperatures sub-250°C, the capacity loss may be minimal.

Eq 4.9 was used to obtain second order rate constant for the degradation of the resin at various temperatures.

$$\frac{1}{C} = \frac{1}{C_0} - kt \qquad Eq.\,4.9$$

Where C is the capacity of the resin (eq L^{-1}), and k is the rate constant. The results are tabulated in Table 4.4 and 4.5, with the results are illustrated on Figure 4.7.

The data sheet for the ion exchange resin NRW-160 states that it has a maximum operating temperature of 120˚C. The results appear to agree with this maximum operating temperature as capacity reductions up to this temperature are negligible, however above this temperature the capacity changes are more evident. The results also suggest that the resin is able to withstand short bursts of higher temperatures with little to no change on the resultant capacity, but when subjected to higher temperatures for an extended period of the time, the detrimental effect on capacity is more pronounced.

Table 4.4 Results of Resin Autoclave experiments.

60°C			**100°C**			**120°C**			**150°C**			**200°C**		
Time (hrs)	Capacity, C (eq L^{-1})	1/C	Time (hrs)	Capacity, C (eq L^{-1})	1/C	Time (hrs)	Capacity, C (eq L^{-1})	1/C	Time (hrs)	Capacity, C (eq L^{-1})	1/C	Time (hrs)	Capacity, C (eq L^{-1})	1/C
0	2.27	0.44	0	2.27	0.44	0	2.27	0.44	0	2.27	0.44	0	2.27	0.44
3	2.27	0.44	3	2.27	0.44	3	2.27	0.44	3	2.25	0.44	3	2.20	0.45
6	2.27	0.44	6	2.27	0.44	6	2.27	0.44	6	2.22	0.45	6	2.14	0.47
24	2.27	0.44	24	2.27	0.44	24	2.25	0.44	24	2.20	0.45	24	2.00	0.50
168	2.27	0.44	168	2.26	0.44	168	2.24	0.45	168	1.91	0.52	168	1.11	0.90

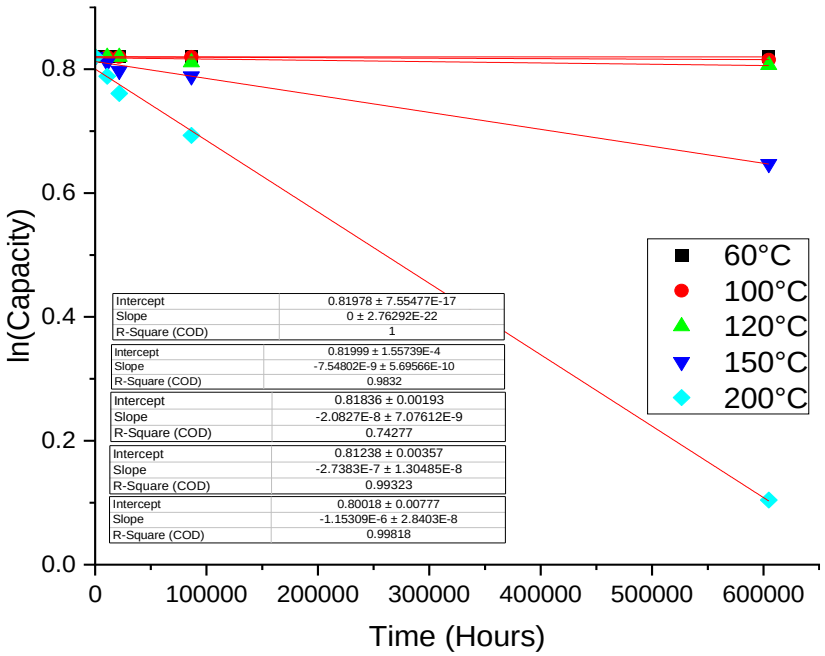

Figure 4.7 Results from Eq 4.9 determining degradation rate constants at various temperatures

Table 4.5 Temperature degradation rate constants.

Temperature (°C)	**k (L eq^{-1} s^{-1})**
60	3.33×10^{-9}
100	3.33×10^{-9}
120	9.24×10^{-9}
150	1.32×10^{-7}
200	7.55×10^{-7}

Using the second order rate constants in Table 4.5, activation energies and Arrhenius pre factors were calculated using Eq 4.5 and 4.6. Figure 4.8 shows the plot of Eq 4.6, where the gradients and intercepts were then used to determine the value for the activation energy and Arrhenius pre factor shown in Table 4.6

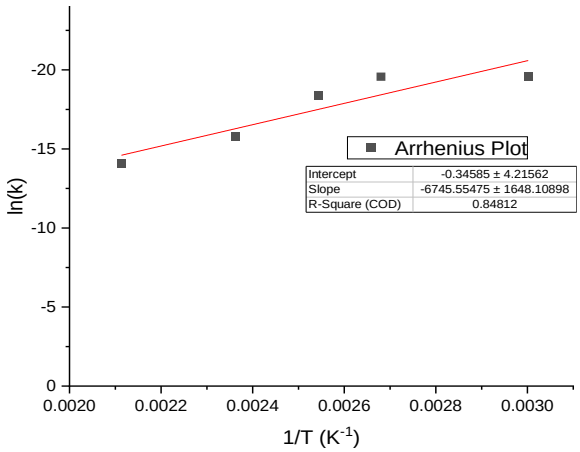

Figure 4.8 Arhenius plot of ln (k) avs 1/T for resin degradation

Table 4.6 Arrhenius Parameters for resin tempererature degradation.

Arrhenius Parameters	NRW-160 Resin
E_a (kJ mol^{-1})	56.08
A (L eq^{-1} s^{-1})	0.71

The determined activation energy and Arrhenius pre factor also appears to be relatively consistent with values determined for similar ion exchange resins in literature [94]. These values can now be implemented into an ion exchange model to calculate the capacity of ion exchange resins at any input temperature. (Simister et al., 2004) investigated the thermal degradation rate of polystyrene-divinyl benzene ion exchange resins in ultra-

pure water at ambient and service temperature. The ion exchange resin was subjected to multiple temperatures (25.2 °C, 30.1 °C, 41.5 °C, 50.0 °C, 61.3 °C and 72.3 °C) and degradation was measured by the amount of total organic carbon (TOC) being released in the effluent. An average activation energy of 41.5 kJ mol^{-1} was calculated for cation resins compared with a figure of 56.08 kJ mol^{-1} calculated in Table 4.6.

4.4 Summary

This section explored the kinetic behaviour of ion exchange. Using the Arrhenius equation, temperature dependent rate constants were derived, producing parameters which would be implemented into the ion exchange model which is discussed in Chapter 3.

This section also explored the effect of flow rate on adsorption, and it was found that as the flowrate increases, the values for mass transfer coefficients and effluent cobalt ion concentration also increased. It was determined that this is due to the effects of residence time, where if the flow rate increases the residence time would decreases resulting in reduced uptake of ions. In addition, it was determined that an increase in flow rate also increased the width of the mass transfer zone extending beyond the sampling point, which further explains the reduced ion uptake with increased flow rate.

Finally, this section explored the effect of temperature on the ion exchange resin's capacity. It was found that short bursts of high temperature exposure had little to no effect on the resin's capacity, but when subjected for a longer period of time the capacity reduction in the resin is more prevalent. Once again using the Arrhenius equation and using the determined values for activation energy and Arrhenius pre-factor, a

temperature dependant capacity equation can be implemented into the model described in Chapter 3.

5 PWR ION EXCHANGE MODELLING

5.1 Introduction

This section details the construction of a FACSIMILE model of the coolant in a PWR primary circuit interacting with an ion exchange column. The model utilises a graphical user interface to use as a front end for the FACSIMILE model. The previous chapters provided parameters which has been used within the model although it is important to note that these parameters are not fixed; the user of the model can edit them within the FACSIMILE code to best suit the system they are trying to model.

The model aims to provide accurate details about plant chemistry for a range of chemical inputs whilst interacting with the ion exchange column. Furthermore, the model also aims to be able to predict trends in species removal from the coolant with respect to changes in temperature and flow rates. Finally, the model aims to provide information on ion exchange lifetime and provide insight as to when a column may need to be replaced.

This section details the equations used within the model, an overview of how the model works and model validation efforts.

5.2 Software

5.2.1 FACSIMILE

FACSIMILE is a program used to solve differential equations for a Windows operating system. The benefit of using FACSIMILE over other differential equation solvers is the programs' ability to understand physical and chemical systems, with unique notation for inputting chemical equilibrium data. As this model requires a large amount of

thermodynamic data, FACSIMILE easily allows it to be inputted without sacrificing solving speed.

FACSIMILE solves differential equations by using the predictor-solver method [15], where a value for the solution is predicted and then checked using a different method. The program also uses Newton iterations to provide solutions [14].

5.2.2 MATLAB

MATLAB (Matrix Laboratory) is a proprietary multi-paradigm programming language and numerical computing environment developed by MathWorks [17]. In the context of this thesis MATLAB was used to produce a Graphical User Interface (GUI) to use as a front end for the FACSIMILE code. MATLAB was chosen due to the ease of communication between programs and the ability not to sacrificing model run times.

5.2.3 MULTEQ

In order to model the chemistry of the primary circuit coolant, a large amount of thermodynamic data is required for numerous chemical species. MULTEQ contains a database with various equations used to determine temperature dependent equilibrium constants for a range of chemical species. These equations are integrated into the model and are also used for calculations by the MULTEQ equation solver, a piece of software by Electric Power Research Institute (EPRI) [16]. The MULTEQ database has been used in previous research involving modelling PWR phenomena [20] [21] [22].

5.3 Model Description

The model is comprised of two main files. The first is a FACSIMILE model file that contains over 3000 lines of code with the underlying equations described in the remainder of this

section. The FACSIMILE code can be seen in APPENDIX 8.1. The second is a MATLAB file, also containing over 3000 lines of code, which generates the Graphical User Interface (GUI) used to call the FACSIMILE file with a specific set of inputs. The MATLAB file has a number of dependent sub files which allows communication between the two programs. The GUI, as seen in Figure 5.1, allows the user to edit the values of a large number of input parameters including those that describe the geometry of the PWR being modelled, the water chemistry, as well as the values of a number of physical parameters that underlie the model. The values of the parameters are an integral part of the model as if certain parameters are left blank or set to 0; the model will fail to run. A check of all parameters for the system being modelled should always be performed.

The validation described in Section 5.3 was performed with parameters similar to a typical PWR and also with parameters imitating the experimental set up seen in Sections 3 and 4.

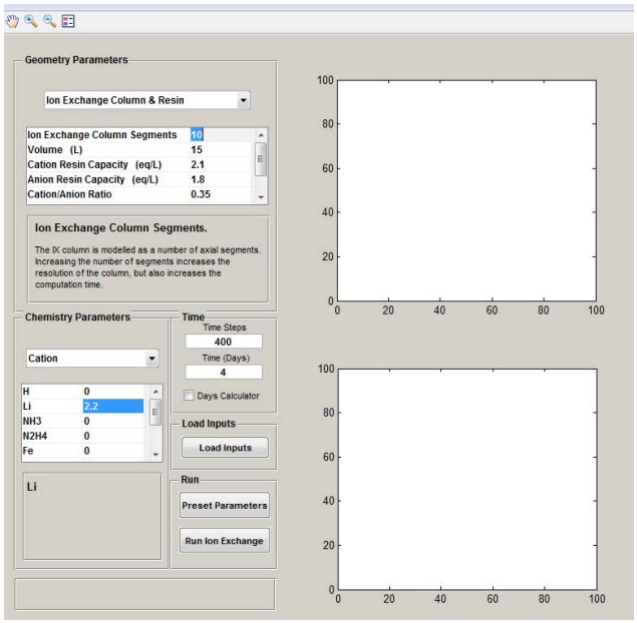

Figure 5.1 Graphical User Interface showing parameter inputs for the Ion Exchange Model

5.4 Facsimile Model Description

The model only considers the primary circuit of a PWR as it is only the primary circuit coolant which passes through the ion exchange column. The model treats the primary circuit as two discrete sections with a 'bulk' section, which is to simulate the primary coolant, and an 'Ion eXchange Column' (IXC) section, which is to simulate the PWR ion exchange column. The model is set up to continuously recirculate the coolant in the bulk through the IXC as shown in Figure 5.2.

The FACSIMILE model describes the changes in chemistry of the coolant as it moves from the bulk through the IXC and back to the bulk.

The main processes that are modelled are:

- The transport around the sections based on user inputted flow rates.
- Primary circuit chemistry including hydrolysis reactions of chemical species also see in Table 5.2.
- Ion exchange reactions for a range of cations and anions on cationic and anionic resins as seen in Table 5.3
- Radiation chemical reactions in the coolant resulting in the formation of radioisotopes such as ^{60}Co and ^{58}Co.
- Temperature dependent degradation of chemical species and ion exchange resins.

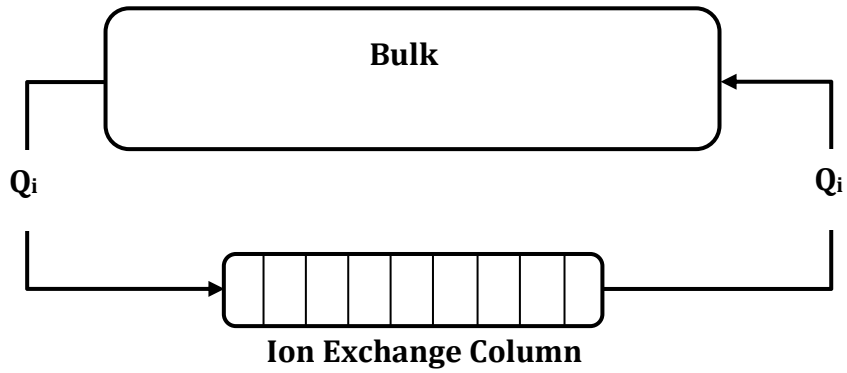

Figure 5.2 Schematic of the Model Design

The ion exchange column can be broken up into a number of segments in order to observe how the concentration changes as coolant is flowed through the cell. If one segment was chosen only one concentration will be outputted following total exchange with all the resin. However, if ten segments were chosen, for example, then the column would consist of 10 sections each with 1/10 of the resin capacity. The coolant will then individually exchange with each section while passing through, taking into consideration the reaction in the previous section.

5.4.1 Model Transport

The transport between the sections is described by:

$$\frac{dC_i}{dt} = \frac{Q_i}{V_i}(C_{i-1} - C_i) + \left(\frac{\partial C_i}{\partial t}\right) \qquad Eq\ 5.1$$

Where C_i is the species concentration in mol kg^{-1}, Q_i is the mass flow rate of coolant from i-1 into i in units of kg s^{-1} and V_i is the mass of coolant in kg. The final term describes the changes in chemical species due to chemical reactions involving interactions with the ion exchange column. $\left(\frac{\partial C_i}{\partial t}\right)$ is a partial derivative, which stands for changes in concentration

other than from the species leaving and entering the cell. These other changes in concentration stem from the change in concentration due to ion exchange with the resin, as well as any decay mechanisms that may happen to the species.

5.4.2 Thermal Effects

The temperature of each section is user input and if this is to change, the coolant in the primary circuit will either expand or contract. To avoid this volume change the model uses the mass of coolant as opposed to the volume; however the temperature of the water would affect the dissociation constant [104], K_w.

$$K_w = [H^+][OH^-] \qquad Eq\ 5.2$$

With the change due to temperature, this would in turn affect the pH observed via the equation:

$$pK_w = -log_{10}K_w = pH + pOH \qquad Eq\ 5.3$$

The expression used in the model for the temperature dependent ionic product of water is given by the expression [104]:

$$pK_w = -4.098 - \frac{3245.2}{T} + \frac{2.2362 \times 10^5}{T^2} - \frac{3.984 \times 10^7}{T^3} + \left(13.957 - \frac{1262.3}{T} + \frac{8.5641 \times 10^5}{T^2}\right) log_{10}\rho_w \qquad Eq\ 5.4$$

Where T is the temperature in K and ρ_w is the density of water given by the equation:

$$pK_w = \frac{1 + 0.1342489\theta^{\frac{1}{3}} - 3.946263 \times 10^{-3}\theta}{3.1975 - 0.3151548\theta^{\frac{1}{3}} - 1.203374 \times 10^{-3}\theta + 7.489081 \times 10^{-13}\theta^4} \qquad Eq\ 5.5$$

Where θ is a temperature correction equal to the subtraction of temperature in kelvin from 647.26.

5.4.3 Chemical Reactions

The basis of this model is a set of numerical equations which represent the chemical system to be modelled. The model comprises of over 40 reactions whose forward rate constants k_f is assumed to be high as to simulate instant equilibrium. The model includes a number of reversible reactions, mostly acid-base equilibria where the temperature dependant equilibrium constant is given by one of the following the expressions:

$$log\ _{10}K_q = A + BT_c + CT_c^2 + DT_c^3 + ET_c^4 \qquad Eq\ 5.6$$

or

$$log\ _{10}K_q = \frac{A}{T} + B + CT + Dlog_{10}T + \frac{E}{T^2} + nlog_{10}K_w \qquad Eq\ 5.7$$

Where K_q is the equilibrium constant for a given reaction, T is the temperature in K, T_c is the temperature in °C and letters A, B, C, D, E, and n are constants specific to each chemical species, seen in Table 5.2. The MULTEQ database was used to obtain thermodynamic data leading to these equilibrium constants of species commonly found in the primary circuit coolant, where they are expressed in molal units.

The model assumes ideal interactions between species in solution and does not take into consideration activity coefficients of specific species. The user is able to input a value for concentration in ppm for a number of chemical species, however in an attempt to maintain electro-neutrality the model will use a neutral form of the species to input instead, as seen in Table 5.1.

Table 5.1. Table of user chemical inputs vs model chemical input.

User Input Chemical	**Model Input Chemical**
Lithium (Li)	Lithium Hydroxide (LiOH)
Boron (B)	Boric Acid (H_3BO_3)
Cobalt (Co)	Cobalt (II) Hydroxide ($Co(OH)_2$)
Ammonia (NH_3)	Ammonia (NH_3)
Iron (Fe)	Iron (II) Hydroxide ($Fe(OH)_2$)
Nickel (Ni)	Nickel (II) Hydroxide ($Ni(OH)_2$)
Copper (Cu)	Copper (II) Hydroxide ($Cu(OH)_2$)

Aqueous Chemical Reactions	**A**	**B**	**C**	**D**	**E**	**n**
$H_2O \rightleftharpoons H^+ + OH^-$ [1]						
$LiOH \rightleftharpoons Li^+ + OH^-$	$1.67x10^5$	$-2.57\ x10^3$	$-3.08\ x10^{-1}$	$9.00x10^2$	$-1.26x10^7$	1.00
$NH_3 + H^+ \rightleftharpoons NH_4^+$ [2]	$1.00x10^1$	$-3.30x10^{-2}$	$7.86x10^{-5}$	$-9.69x10^{-8}$		
$H_3BO_3 + OH^- \rightleftharpoons BO_4^-$	$3.82x10^3$	$-3.59x10^1$		$1.12x10^1$		
$2H_3BO_3 + OH^- \rightleftharpoons B_2O(OH)_5^- + H_2O$	$2.53x10^3$	-3.13				
$3H_3BO_3 + OH^- \rightleftharpoons B_3O_3(OH)_4^- + 3H_2O$	$2.67x10^3$	-2.79				
$4H_3BO_3 \rightleftharpoons B_4O_2(OH)_8 + 2H_2O$	$-4.99x10^3$	4.07				
$Fx10^{2+} + H_2O \rightleftharpoons FeOH^+ + H^+$	$-1.83x10^3$	-2.99				
$Fe^{2+} + 2H_2O \rightleftharpoons Fe(OH)_2 + 2H^+$	$-6.18\ x10^3$	$-1.63x10^{-1}$				
$Fe^{2+} + 2H_2O + OH^- \rightleftharpoons Fe(OH)_3^- + 2H^+$	$-7.19\ x10^3$	3.11				
$Co^{2+} + H_2O \rightleftharpoons CoOH^+ + H^+$	$-2.65\ x10^3$	-1.08				
$Co^{2+} + 2H_2O \rightleftharpoons Co(OH)_2 + 2H^+$	$-5.61\ x10^3$	-1.99				
$Ni^{2+} + H_2O \rightleftharpoons NiOH^+ + H^+$	$-2.63\ x10^3$	-1.09				
$Ni^{2+} + 2H_2O \rightleftharpoons Ni(OH)_2 + 2H^+$	$-3.80\ x10^3$	-5.29				
$Ni^{2+} + 2H_2O + OH^- \rightleftharpoons Ni(OH)_3^- + 2H^+$	$-2.75\ x10^3$	-6.79				1.00
$Cu^{2+} + H_2O \rightleftharpoons CuOH^+ + H^+$	$4.58\ x10^3$	$-2.99\ x10^2$	$-7.99\ x10^2$	$1.21\ x10^2$		
$CuOH^+ + 2H_2O \rightleftharpoons 2\ Cu(OH)_2 + 2H^+$	$-5.69\ x10^3$	$2.18\ x10^2$	$6.99\ x10^{-2}$	$-9.12\ x10^1$		1.00

$CuOH^+ + 2H_2O \rightleftharpoons Cu(OH)_3^- + 2H^+$	-5.69×10^3	2.18×10^2	6.99×10^{-2}	-9.12×10^1		1.00
$Zn^{2+} + H_2O \rightleftharpoons ZnOH^+ + H^+$	-3.16×10^3	1.73				
$Zn^{2+} + 2H_2O \rightleftharpoons Zn(OH)_2 + 2H^+$	-4.95×10^3	6.40×10^{-1}				
$Zn^{2+} + 3H_2O \rightleftharpoons Zn(OH)_3^- + 3H^+$	-5.02×10^3	2.42				1.00
$Zn^{2+} + 4H_2O \rightleftharpoons Zn(OH)_4^{2-} + 4H^+$	-3.14×10^3	-4.87	7.57×10^{-3}			2.00

Table 5.2. Table of acid-base chemical reactions used in the model (not including their isotopic variants).[97]

[1] This equation is dependent upon the ionic product of water in eq 5.2 and 5.4.

[2] This equation is based on eq 5.6, whereas all other equations are based on eq 5.

The rate coefficients can be modified within the facsimile file to suit user needs, where the reverse rate constant (k_r) for the reactions in Table 5.2 are given by:

$$k_r = \frac{k_f}{K_q} \qquad Eq\ 5.8$$

For the purpose of these experiments a default fast rate was used.

5.4.4 Radio-activation and Decay

The model splits all relevant species into their relative natural abundancies [44], [105], such as ^{59}Co, ^{58}Ni, ^{59}Fe and ^{54}Fe, which may be activated by a neutron flux in the core. The model adopts a relatively simplistic approach to this phenomenon by implementing the activation cross sections of ^{59}Co, ^{58}Ni, ^{59}Fe and ^{54}Fe [106], [107] and values for thermal and fast neutron flux profiles [108]. Neutron fluxes in the core are not a user input in the GUI but can be modified by changing the value in the Facsimile code. The model assumes that the fast and thermal neutron flux is constant through plant life even though this may not be representative of a real plant through life. Only species present in the bulk section can become activated and can become taken up by the ion exchange column.

Decay is modelled for all radionuclides in all sections of the plant. Only direct decay products are included in the model. After this there is no further activation unless the decay product is one of the 4 nuclides modelled.

The equation used to describe the formation and decay of the active species is:

$$\frac{d[A]}{dt} = \sigma\varphi[B] - \lambda[A] \qquad Eq\ 5.9$$

Where [A] is the concentration of the activated species, [B] is the concentration of species being activated, σ is the neutron cross section, φ is the neutron flux and λ is the decay constant for the radio-active species.

The model also takes into account the production of fission products. The user can input specific radionuclide yields, the reactor power, a radionuclide production rate, and a toggle to turn the neutron flux on and off, as see in Figure 5.3.

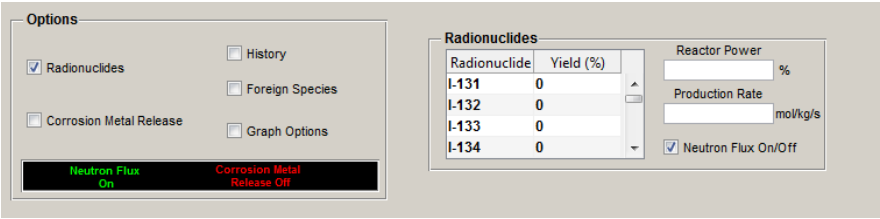

Figure 5.3 Radionuclide GUI inputs

The model also takes into account the activity produced from the decay of radionuclides. It uses the following equation to produce a value for activity in the SI unit of Becquerel (Bq):

$$Activity = N_A \lambda [A] \qquad Eq\ 5.10$$

Where N_A is Avogadro's constant (6.0223×10^{23}), $[A]$ is the concentration of the radioactive species A and λ is the decay constant for species.

5.4.5 Metal Release (Corrosion)

The metal species Co, Ni and Fe are produced in the primary circuit via the corrosion of materials. The model adopts a relatively simplistic approach to this phenomenon by allowing the user to input a value, see Figure 5.4, for the total surface area of a primary circuit and a value for the release rate of metals in units of g m^{-2} $s^{-0.5}$. This is to allow the

rate to be dependent upon the area as whilst a material corrodes the surface area decreases causing the release rate to also decrease.

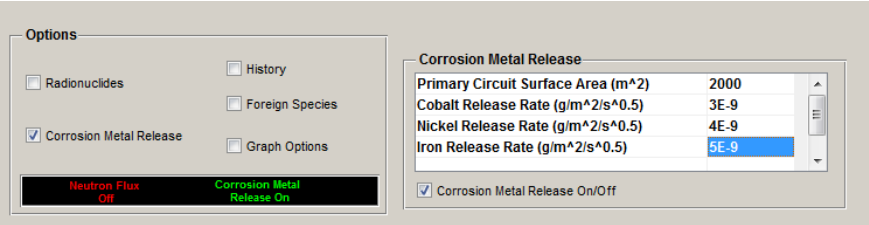

Figure 5.4 Metal Release GUI inputs

5.4.6 Ion Exchange Reactions.

The user can input a value for a volume of the IXC section. This represents the coolant and the resin in equal parts, assuming a 0.5 void fraction for the ion exchange resin. The user can also input values for cation and anion resin capacity, along with the ratio by which the cation and anion resin are split by. The user is also able to input the flow rate at which the primary coolant flows through the ion exchange column. The model will calculate the number of exchangeable species there are on the resin in molal units and then models the exchange process with species in solution via a 1-step process. Literature states that the ion exchange process is 2-stages; mass transfer through the bulk liquid to the resin surface (boundary layer), then an exchange reaction at the surface. The mass transfer step is typically the rate determining step and the exchange step is typically rapid. The reason for using a one step process is due to the model's one step process overall rate being insignificantly different to that of the two-stage process.

The exchange reaction between a species in solution and the resin,

$$xR_H + M^x \rightleftharpoons R_M + xH^+ \qquad Eq\ 5.11$$

Where R_H is the resin with H^+ ions, M is the species to be exchanged and x is the valency of the species to be exchanged, is modelled by defining the forward and reverse rates:

$$k_r = k_{er} \qquad Eq\ 5.12$$

$$k_f = k_{er} K_{i-j} \qquad Eq\ 5.13$$

Where, k_{er} is the exchange rate constant and $K_{i\text{-}j}$ is the selectivity coefficient between ions i and j. The temperature dependant selectivity coefficients determined in Chapter 3 is used in this model; however, the user can overwrite these in the FACSIMILE file. The value for temperature dependant rate constant, k_{er} determined in Chapter 4 is also used in this model although this value can be overwritten by modifying the FACSIMILE file. The polynomial equation for cation resin temperature degradation determined in Chapter 4 is also coded into the model.

As well as cation resin exchange, anion resin exchange is also modelled. Due to the lack of experimental data with regards to anion resin, selectivity coefficients with regards to anion species have been set to 1 by default, although they can be altered within the FACSIMILE code. Furthermore, there is no temperature degradation mechanism modelled for anion resins, so a temperature spike in the IXC would have no effect on the anion resin partition.

Table 5.3. Table of Main Ion Exchange Reactions [1] [2]

Ion Exchange Reactions
$RH + Li^+ \rightleftharpoons RLi + H^+$
$RH + NH4^+ \rightleftharpoons RNH4 + H^+$
$2RH + Fe^{2+} \rightleftharpoons R_2Fe + 2H^+$
$RH + FeOH^+ \rightleftharpoons RFeOH + H^+$
$ROH + Fe(OH)_3^- \rightleftharpoons RFe(OH)_3 + OH^-$
$2RH + Cu^{2+} \rightleftharpoons R_2Cu + 2H^+$
$RH + CuOH^+ \rightleftharpoons RCuOH + H^+$
$ROH + Cu(OH)_3^- \rightleftharpoons RCu(OH)_3 + OH^-$
$2RH + Co^{2+} \rightleftharpoons R_2Co + 2H^+$
$RH + CoOH^+ \rightleftharpoons RCoOH + H^+$
$2RH + Zn^{2+} \rightleftharpoons R_2Zn + 2H^+$
$RH + ZnOH^+ \rightleftharpoons RZnOH + H^+$
$ROH + Zn(OH)_3^- \rightleftharpoons RZn(OH)_3 + OH^-$
$2ROH + Zn(OH)_4^{2-} \rightleftharpoons R_2Zn(OH)_4 + 2OH^-$
$2RH + Ni^{2+} \rightleftharpoons R_2Ni + 2H^+$
$RH + NiOH^+ \rightleftharpoons RNiOH + H^+$
$RH + Ni(OH)_3^- \rightleftharpoons RNi(OH)_3 + OH^-$
$ROH + BOH_4^- \rightleftharpoons RBOH_4 + OH^-$
$ROH + B_2OOH_5^- \rightleftharpoons RB_2OOH_5 + OH^-$
$ROH + B_3O_3OH_4^- \rightleftharpoons RB_3O_3OH_4 + OH^-$

Where 'R' denotes the resin phase.

[1] Ion exchange reactions not listed here include the exchange with produced radionuclides and exchange with specific isotopes of species.

[2] All reactions are repeated in the model with all possible starting resin species such as R-Li, R-NH_4 and R_2Co.

5.5 Running the model

The FACSIMILE model is run from a Matlab GUI which allows the user to define a calculation with changing conditions such as flow rate, chemistry and temperature. Although FACSIMILE is capable of running with these changing variables within its own program, it was considered that using the GUI would make the program more stable and provide a better user experience. The GUI will translate input parameters into a text file, which will be used by FACSIMILE to provide an output as a text file that will return the results to the GUI for the user to interpret (Figure 5.5).

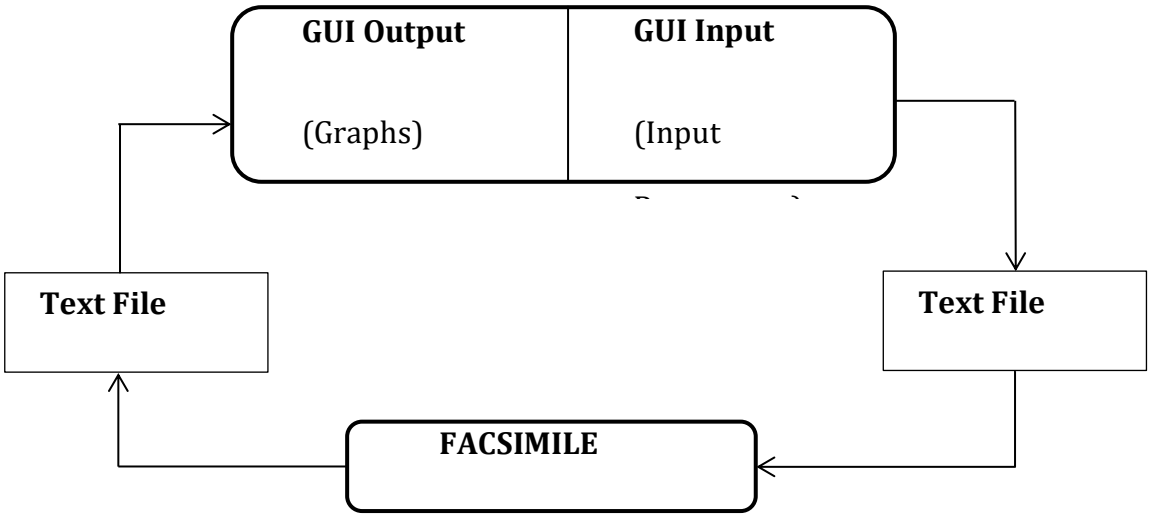

Figure 5.5 Schematic of the Model Design

The model runs in two modes: Batch mode and History mode. Batch mode runs with all parameters defined at the start and allowed to run until equilibrium with the system has been reached. This mode requires three types of user input:

- Chemistry data defined at the beginning of the run but may be changed by the model's calculations.

- Geometry data defined at the beginning of the run which will remain constant throughout the model's calculations.
- Operational parameters, such as temperature and flow rate which will remain constant throughout the model's calculations.

History mode runs with all parameters defined at the start; however, time-dependent parameters are used. The user can change parameters such as the chemistry, temperature, flow rate, neutron flux and metal release as any defined time. This mode has the same user inputs as Batch mode with the latter becoming time-dependent parameters which will change based on user input.

5.5.1 Input Data

The model takes inputs from 2 main input files which are generated by the GUI from the user inputs. Both input files contain time varying parameters such as the time the model is run for, as well as the number of output time steps in the calculation. Time steps is a crucial input parameter as it a higher number provides greater results resolution, but also an increase in model run time. An example of this effect is seen in Chapter 5 Supplementary in the Appendix. The first input file is only used in Batch mode and contains the following data:

Chemistry data:

- Initial concentrations of input species such as Li, B, Co, Ni, Fe and Cu in units of ppm (mg kg^{-1}).

Geometry data:

- The number of segments to split the IXC into. This number is to find a balance between quality of output results and model runtime.

- IXC parameters such as volume (L), capacity (eq L^{-1}) and cation/anion ratio.
- Bulk parameters such as volume. (kg)

Operational data:

- The temperature of both sections. (K)
- The flows rate though both sections. (kg s^{-1})
- The reactor power (%)

History mode utilises both input files, where the second input file contains the following data:

- An array containing the runtime, time steps and the time dependent values for temperature, flow rate and rector power.
- An array containing time dependent flags to toggle neutron flux and metal release on and off.

The change in temperature whilst using History mode will result in values for ρ_w, K_w, K_q, rate constants and selectivity coefficients being recalculated with the new temperature value at every user defined stage.

5.5.2 Output Data

Output files are generated by the model at the user defined time steps containing:

- Concentration of all aqueous species in the bulk.
- The pH of the bulk.
- Concentrations of all aqueous and resin species in the IXC.

The output text files are then used by the Matlab GUI to generate plots of the data against time. Alternatively, the user can export the text file to another program to produce bespoke plots of the data. The GUI has 5 main displays for plots:

- A display for the concentration of the pH raising species (Li, B and NH_3).
- A display for the main metal species (Co, Ni, Fe, Cu and Zn).
- A display for the resin concentrations.
- A display for pH of the bulk; and
- A display the activity from radionuclides in the bulk.

A model walkthrough can be seen in the in Chapter 5 Supplementary in the Appendix.

5.6 Model Validation

In order to class the model as valid, a number of tests have been devised to prove its validity. Ensuring the model is able to predict correct pH_Ts and concentrations of species in solution after interaction with the IXC is paramount.

The tests have been split into 3 sets of tests:

1) Set 1 tests the models' ability to predict the pH of the primary circuit coolant for a range of PWR chemistry Regimes.
2) Set 2 tests the models' ability to accurately predict the concentration of chemical species in solution after passing though the IXC.
3) Set 3 tests the models' ability to accurately predict trends in IXC behaviour with respect to activity removal from the primary circuit.

5.6.1 Validation Set 1 Test Results

Chemistry regimes in PWRs involving Lithium and Boron have been developed from since the 1980s to present. These chemistry regimes are summarised in Figure 5.6.

The model was used to predict the pH for the different chemistry regimes seen in Figure 5.6. The only input parameters of importance in this test were a temperature of 300°C and

the initial Boron and Lithium concentration, as changing any other input parameters would have no effect on the result.

The values in Table 5.4 indicate that the model has accurately predicted pH_T values for multiple chemistry regimes. This gives confidence that the model can predict new chemistry regimes with inputs of Lithium and Boron Concentration.

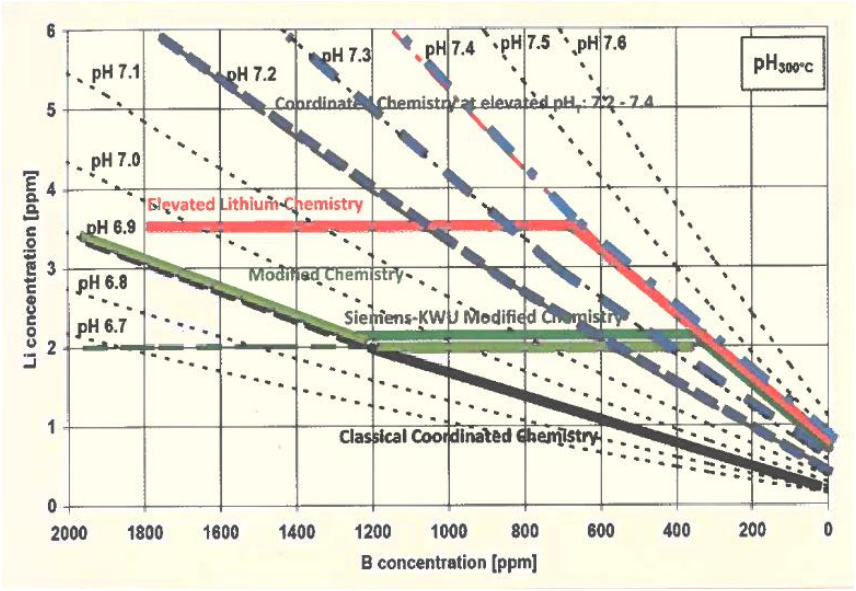

Figure 5.6 Developed coolant chemistry lithium/pH_T regimes [109][110].

Table 5.4. Table of predicted pH_T values from the model at a range of Lithium and Boron Concentrations.

Model calculated pH							
Boron(↓)/Lithium(→) Concentration (ppm)	0	1	2	3	4	5	6
0	-	7.56	-	-	-	-	-
200	-	7.20	7.50	7.68	7.80	-	-
400	-	7.00	7.31	7.48	7.61	7.71	-
600	-	6.87	7.17	7.35	7.47	7.57	-
800	-	6.76	7.06	7.24	7.36	7.46	7.54
1000	-	-	6.98	7.15	7.28	7.37	7.45
1200	-	-	6.90	7.08	7.20	7.30	7.38
1400	-	-	6.84	7.01	7.14	7.23	7.31
1600	-	-	6.78	6.95	7.08	7.18	7.26
1800	-	-	6.72	6.90	7.03	7.12	7.20
2000	-	-	6.68	6.85	6.98	7.07	7.15

5.6.2 Validation Set 2 Test Results

Experimental results from Chapter 4 were used to compare results from the model. The list of geometry parameters and justification for their use are listed in Table 5.5.

Table 5.5. List of model geometry parameters used for Validation Set 2.

Model Parameter	**Value**	**Justification**
IXC Parameters		
IXC Segments	10	Default number to break the IX column up in to and observe how concentration changes through each segment.
Volume (L)	0.000102564	0.08g of resin was used for this experiment. Materials data sheet provided a conversion of 760 – 800 g L^{-1}. An average of 780 was used.
Cation Capacity (Eq L^{-1})	2.38	This was the capacity determined via titration method in Chapter 4.
Cation Anion Ratio	1	Only cation resin was used for these experiments.
Coolant Parameters		
Volume (kg)	0.1	100ml of solution was used for these experiments.
Temperature in Bulk (°C)	25	Experiments performed at 25°C
Temperature in IXC (°C)	25	Experiments performed at 25°C
Flow Rate (kg s^{-1})	4	Fast flow rate chosen to simulate rapid

All other geometry parameters which could be input would have no bearing on the result produced. The initial concentrations were the same as in Chapter 4, Table 5.6 All model runs performed with 100% protonated resin (R-H).

Table 5.6. Table of initial cation conentrations used for Validation Set 2.

Initial Model Concentration	**Value**
Cations	
Iron(ppm)	55.131
Zinc (ppm)	71.164
Nickel (ppm)	63.178
Cobalt (ppm)	60.249
Copper (ppm)	70.872

The results from Chapter 4 and the model predicted results are presented in Tables 5.7 and 5.8. Graphs illustrating the differences between the two results are shown in Figures 5.7.

Table 5.7. Experimental Results from Chapter 4.

Experimental Results									
	Time in Minutes								
	0	5	10	15	20	30	45	60	120
Cation	Concentration (ppm)								
Co	60.25	57.46	52.00	46.36	43.12	37.40	29.76	25.75	14.26
Cu	70.87	65.13	59.40	55.36	52.21	47.57	38.56	33.95	15.64
Zn	71.16	65.92	61.98	58.98	55.31	48.48	39.36	34.95	19.60
Ni	63.18	57.29	53.82	50.70	48.54	41.71	36.59	30.68	18.50
Fe	55.13	52.38	49.99	46.47	44.86	41.79	36.10	32.11	17.15

Table 5.8. Model Predicted Results from Validation Set 2.

Model Predicted Results									
	Time in Minutes								
	0	5	10	15	20	30	45	60	120
Cation	Concentration (ppm)								
Co	60.25	59.10	58.09	57.12	56.16	54.33	51.76	49.36	41.21
Cu	70.87	70.57	70.36	70.13	69.87	69.30	68.37	67.40	63.53
Zn	71.16	71.01	71.01	71.00	70.98	70.96	70.90	70.81	70.27
Ni	63.18	62.55	62.54	62.54	62.54	62.52	62.50	62.46	62.06
Fe	55.13	52.92	51.09	49.40	47.83	44.98	41.28	38.10	28.63

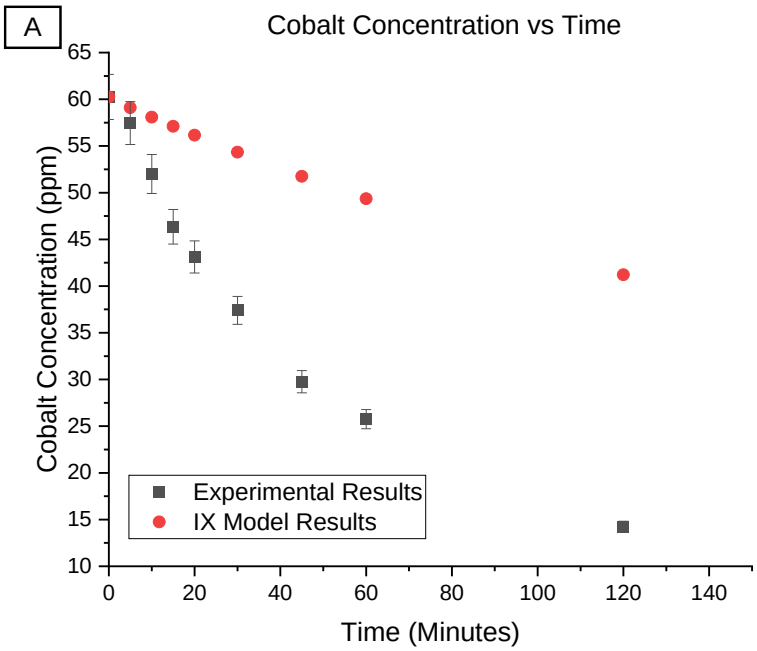
A
Cobalt Concentration vs Time
Cobalt Concentration (ppm)
Time (Minutes)
Experimental Results
IX Model Results

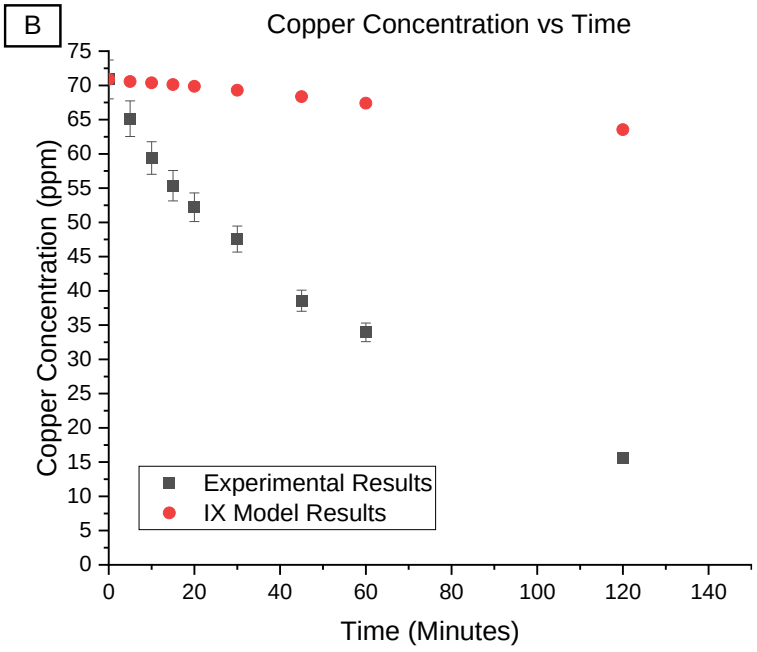
B
Copper Concentration vs Time
Copper Concentration (ppm)
Time (Minutes)
Experimental Results
IX Model Results

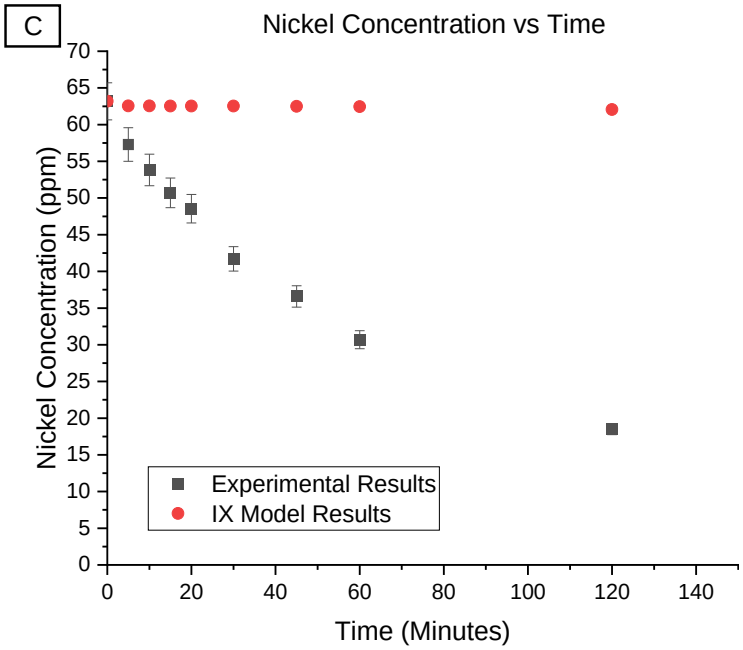
C
Nickel Concentration vs Time
Nickel Concentration (ppm)
Time (Minutes)
Experimental Results
IX Model Results

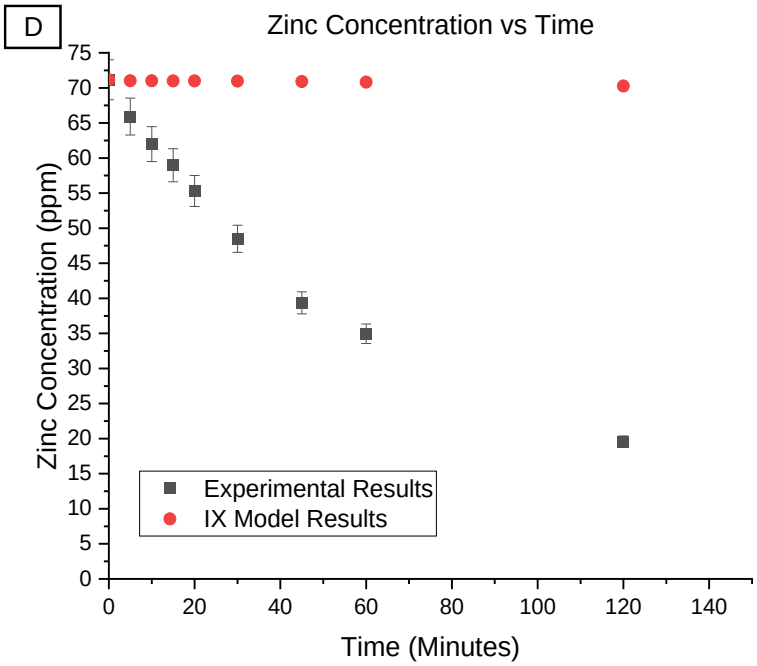
D
Zinc Concentration vs Time
Zinc Concentration (ppm)
Time (Minutes)
Experimental Results
IX Model Results

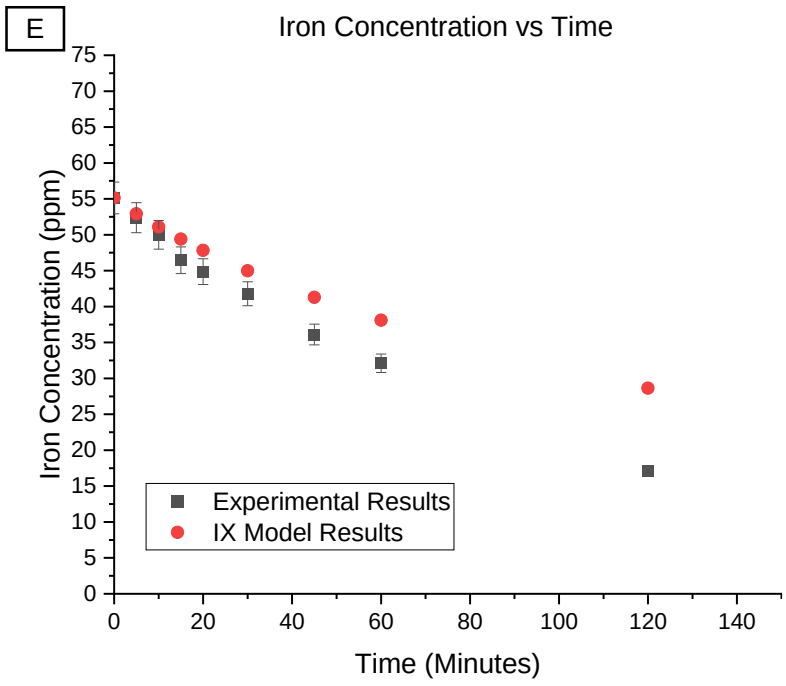

Figure 5.7 Experimental vs Model Concentration vs Time Results for cations; (A)Cobalt; (B)Copper; (C)Nickel; (D)Zinc; and (E)Iron

The results illustrated in Figure 5.7 indicate that the model is under predicting the uptake of the metal cations onto the resin. As there is no anion species present, it appears as though the cation species are being exchanged onto the resin but at a slower rate than what is seen experimentally. For zinc and nickel the rate of uptake appears to slower than others. An analysis of the text files produced by the GUI has indicated that this effect is due to the speciation of the metals at different pH. Figure 5.8 illustrates the pH observed for the model results, with all pH values being relatively high. Although the experimental pH was not measured at the time, it can be assumed that the experimental pH would be acidic due to sulphate salts being used to make the metal ion solution.

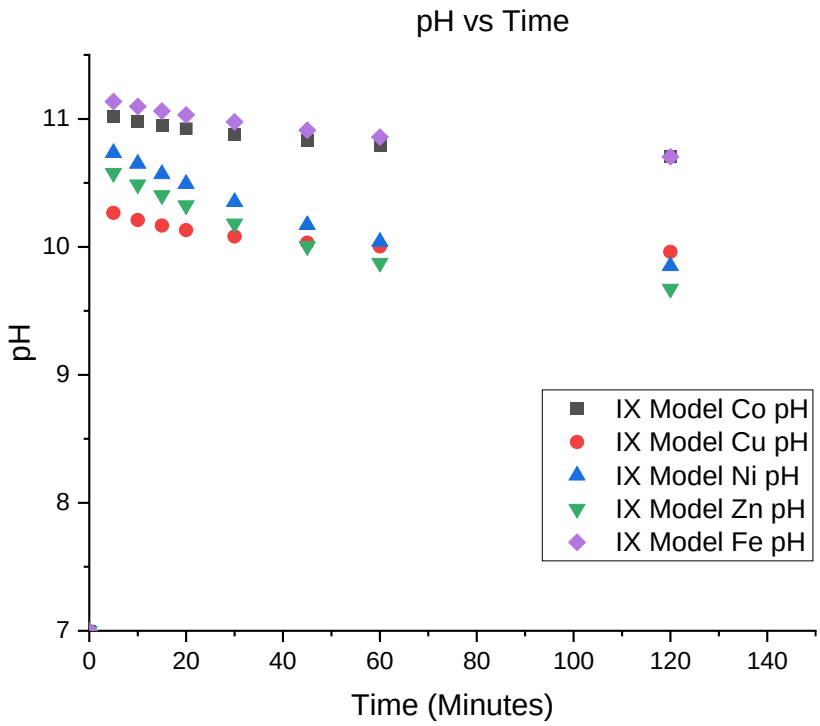

Figure 5.8 Model predicted pH values from Figure 5.7 results.

Figure 5.9 shows the speciation of these metals with changes in pH and indicates that for the models' prediction, the metals have higher concentrations in the $M(OH)_2$ and $M(OH)_3^-$ forms. As the model only used cation resin, the resultant $M(OH)_3^-$ species would still be present in solution as there is no anion resin to exchange with and the neutral species $M(OH)_2$ would also be present in solution as there is no resin type to exchange with, resulting in a higher observed bulk concentration. However, this would apply to the experimental results also, so a possible explanation as to why this phenomenon doesn't appear to be observed experimentally could be due to the uptake of the $M(OH)_2$ species as a neutral electrolyte as opposed to undergoing ion exchange. As the species is neutral it is not hindered by the effects of Donnan exclusion so would be able to enter the resin particle undisturbed. Once inside the resin particle the pH may be vastly different causing

a speciation change back to the M^{2+} or $M(OH)^{+}$ forms, which would then be strongly bound within the resin structure. This postulation is also supported by results from repeating the same model predictions, but with an added boron concentration in the form of boric acid to drastically reduce the pH, as seen in Figure 5.10.

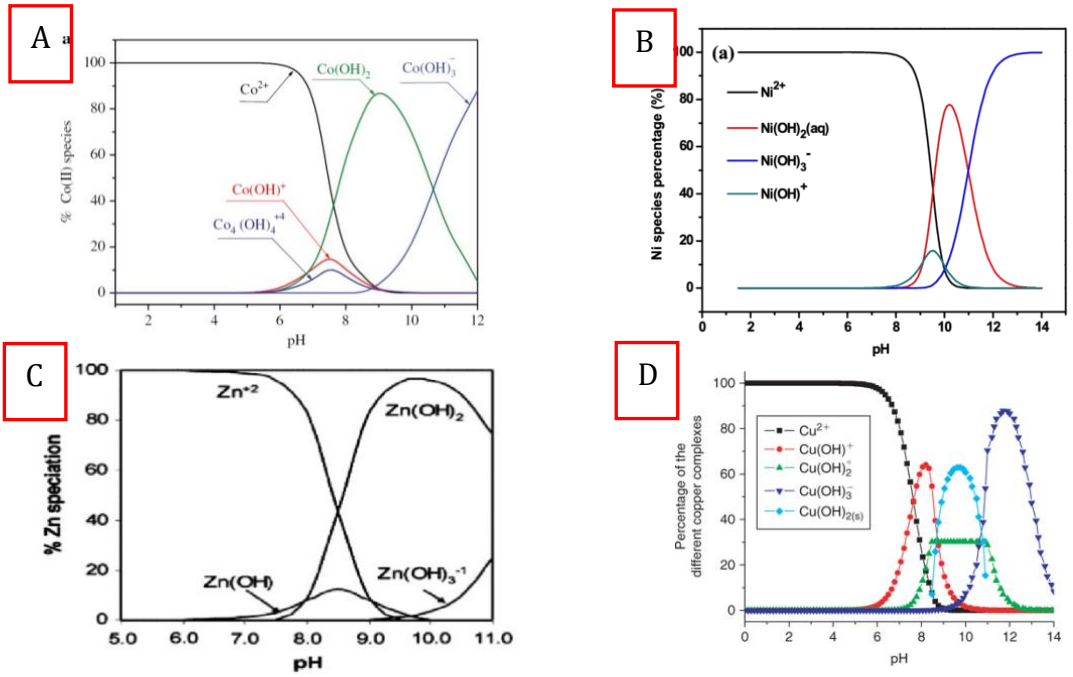

Figure 5.9 pH dependent speciation for (A)Cobalt[113]; (B)Nickel[112]; (C)Zinc[111] and (D)Copper[114].

Figure 5.10 show that as the pH is reduced the rate of uptake for all species increases, which must mean that in acidic conditions the M^{2+} form must be preferred allowing for exchange with the cation resin. Figure 5.11 illustrates the low pH values predicted from the model results shown in Figure 5.10, compared with the high pH values shown in Figure 5.8.

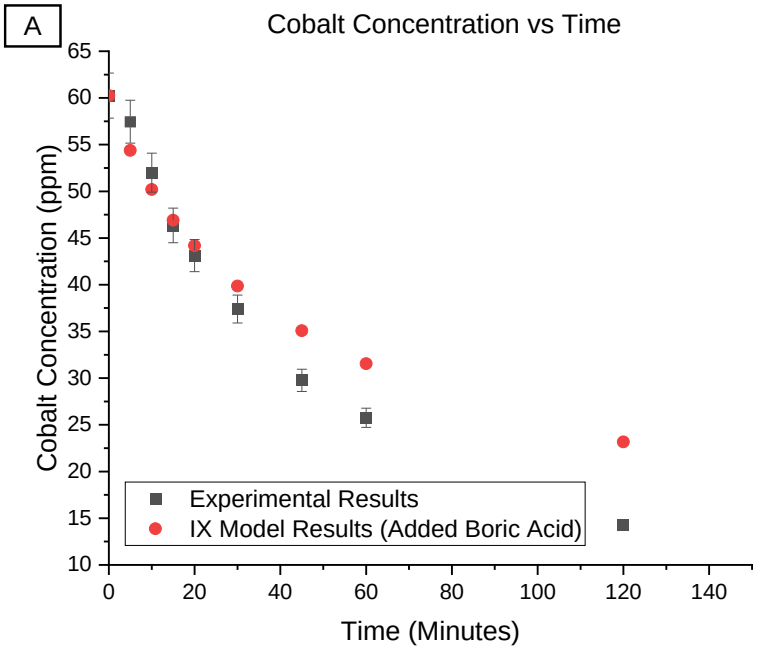
A
Cobalt Concentration vs Time
Cobalt Concentration (ppm)
Time (Minutes)
Experimental Results
IX Model Results (Added Boric Acid)

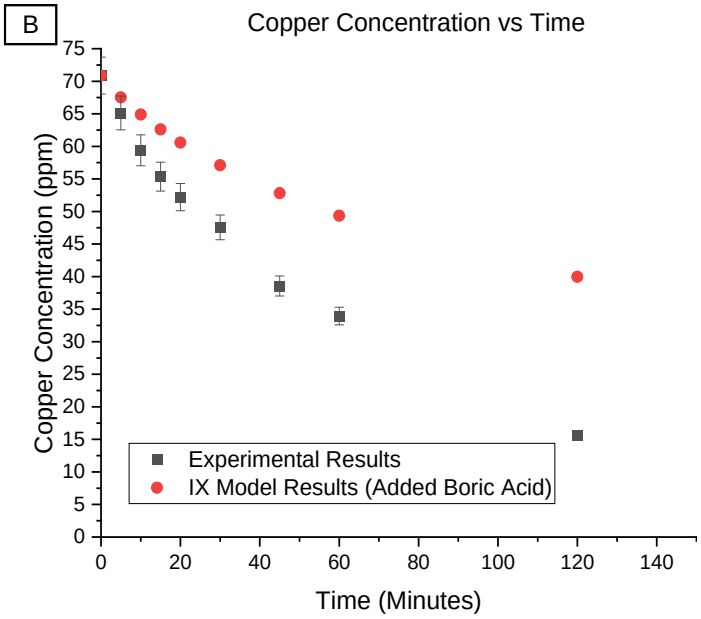
B
Copper Concentration vs Time
Copper Concentration (ppm)
Time (Minutes)
Experimental Results
IX Model Results (Added Boric Acid)

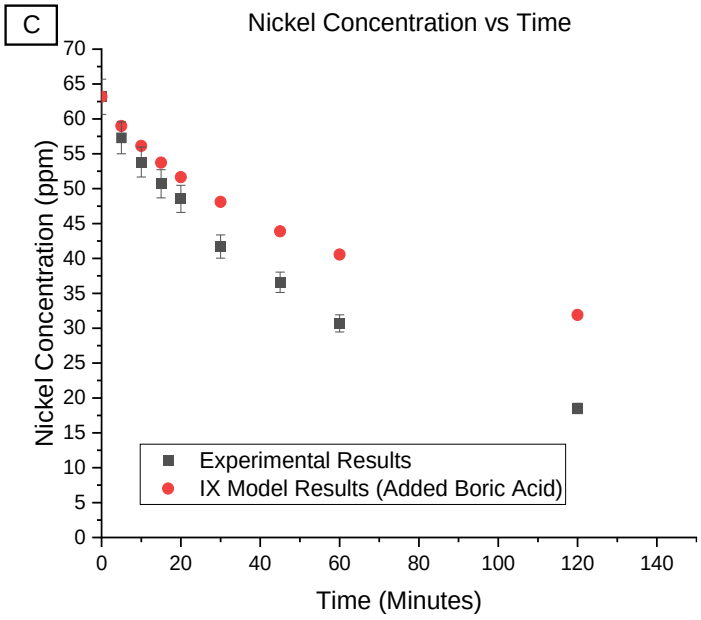
C
Nickel Concentration vs Time
Nickel Concentration (ppm)
Time (Minutes)
Experimental Results
IX Model Results (Added Boric Acid)

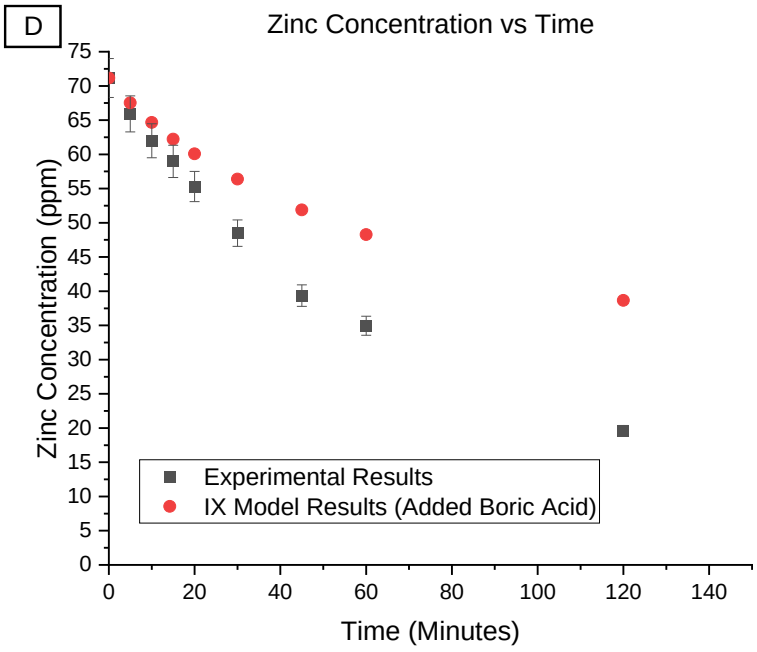
D
Zinc Concentration vs Time
Zinc Concentration (ppm)
Time (Minutes)
Experimental Results
IX Model Results (Added Boric Acid)

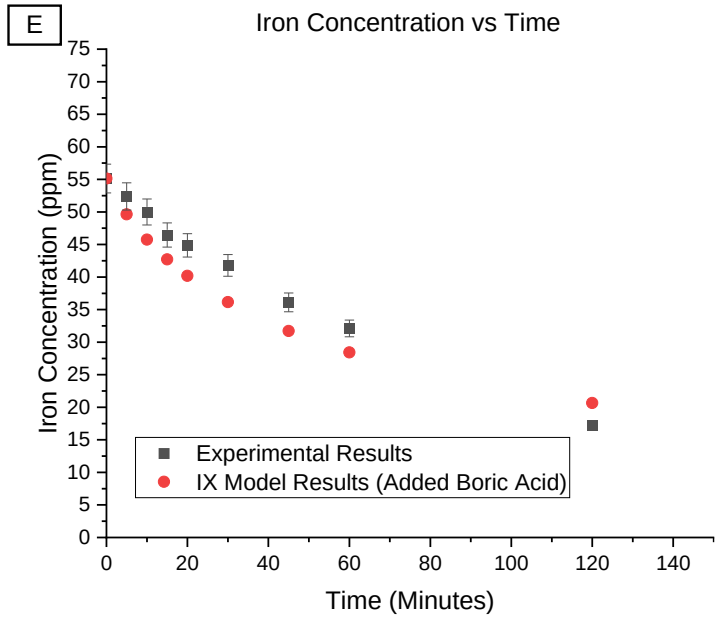

Figure 5.10 Experimental vs Model Concentration vs Time Results for cations with added Boric Acid; (A)Cobalt; (B)Copper; (C)Nickel; (D)Zinc; and (E)Iron

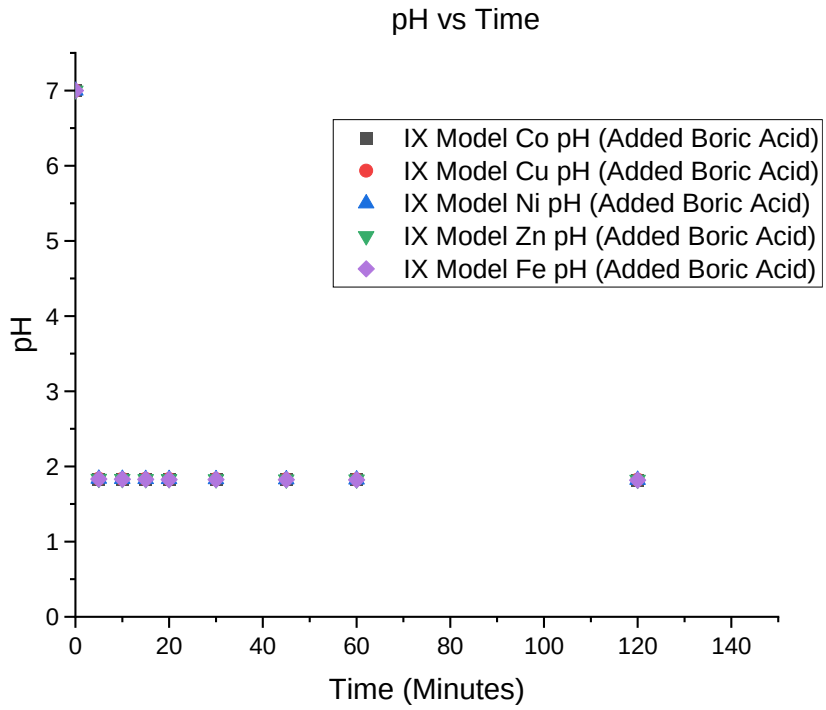

Figure 5.11 Model predicted pH values from Figure 5.10 results.

As previously mentioned, the salts used to obtain the experimental results were sulphates, which when in solution creates acidic conditions, would promote uptake of the M^{2+} form onto the resin. The model does not contain equilibrium data for sulphate salts which could also explain the discrepancy in the experimental and model results; however, the model does demonstrate the exchange process which theoretically would be seen in a PWR, as there would be no sulphates and the main counter ion would be the hydroxyl (OH^-) species with the conditions remaining basic.

5.6.3 Validation Set 3 Test Results

In PWR plants, the concentration of species exiting the IXC are not measured and used as a means for determining the efficiency of the ion exchange resins. It is common for plants to measure the efficiency of their IXC by its ability to remove activity from the primary circuit [8]. As metal ions are being released into the primary circuit coolant from corrosion products, the activity in the primary circuit will build up as the species become active whilst under neutron flux. These species will flow through the IXC thus removing the species and the associated activity from the coolant. This recirculation process will eventually cause the activity in the primary circuit to plateau and reach a saturation value as evidenced by Figure 5.12.

Figure 5.12 also illustrates the effect of flow rate on the activity in the primary circuit coolant. As the flow rate, or rate of removal, increases the saturation point of activity decreases.

By varying the flow rate in the model, it was possible to replicate similar results from (Rafique et al., 2015) [18] and (Rafique et al., 2015) [19]. By ensuring the model's metal release and neutron flux function is on and entering arbitrary values for geometry and release rates, results shown in Figures 5.13 and 5.14 are produced. This demonstrates that the model is capable determining an optimum flow rate, or removal rate, for a PWR system. Furthermore, Figure 5.15 demonstrates that the model is capable of being used as a lifing tool, to determine how long the IXC will be efficient for. By selecting optimum parameters and allowing the model to run for an indefinite period of time the resin will begin to become saturated allowing activity to be leaked back into the primary circuit coolant. Figure 5.15 shows that after a period the resin will start to lose its efficiency as it

begins to become saturated with radionuclides causing the activity in the coolant rise in a parabolic manner. This information could be used in the design phase of a PWR to anticipate how long before the IXC needs to be replaced

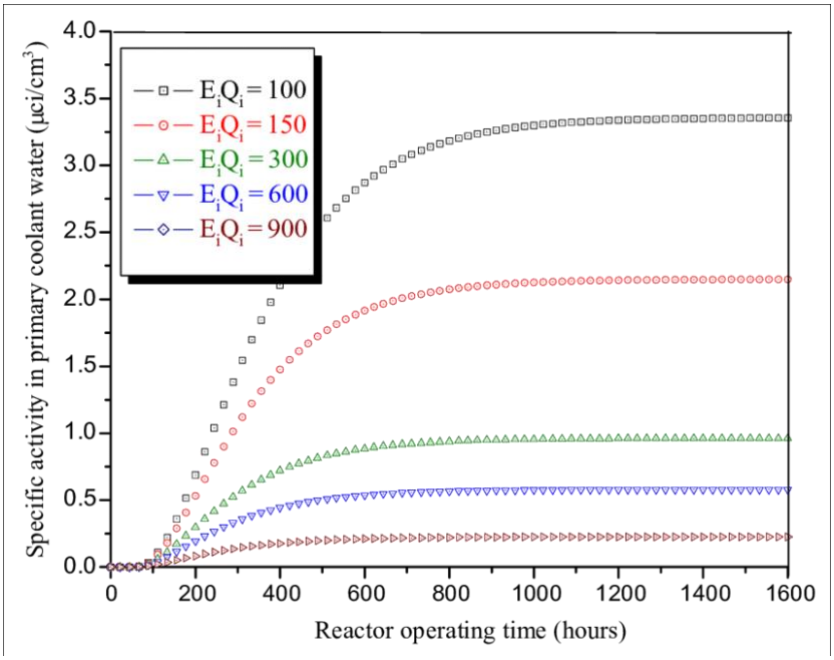

Figure 5.12 The corrosion product activity in the primary coolant of a typical PWR with different removal rates [18].

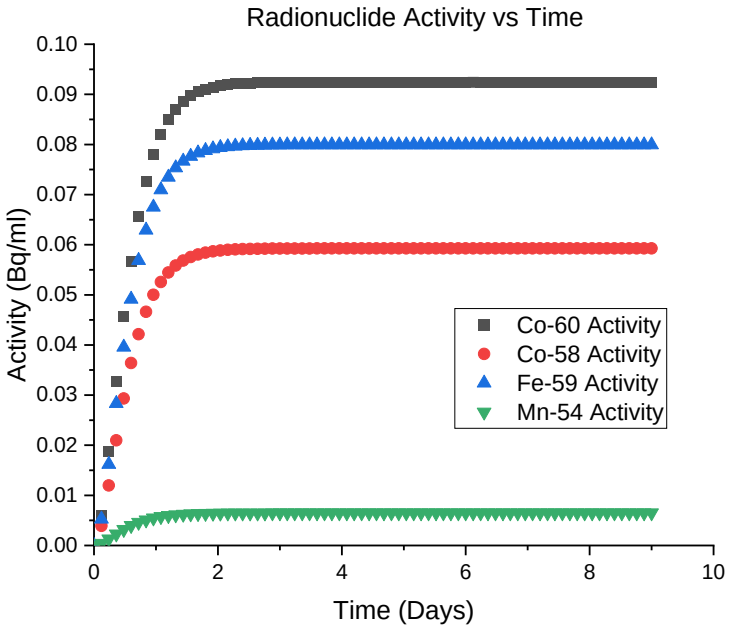

Figure 5.13 GUI output for Validation Set 3 - demonstrating primary circuit activity reaching saturation.

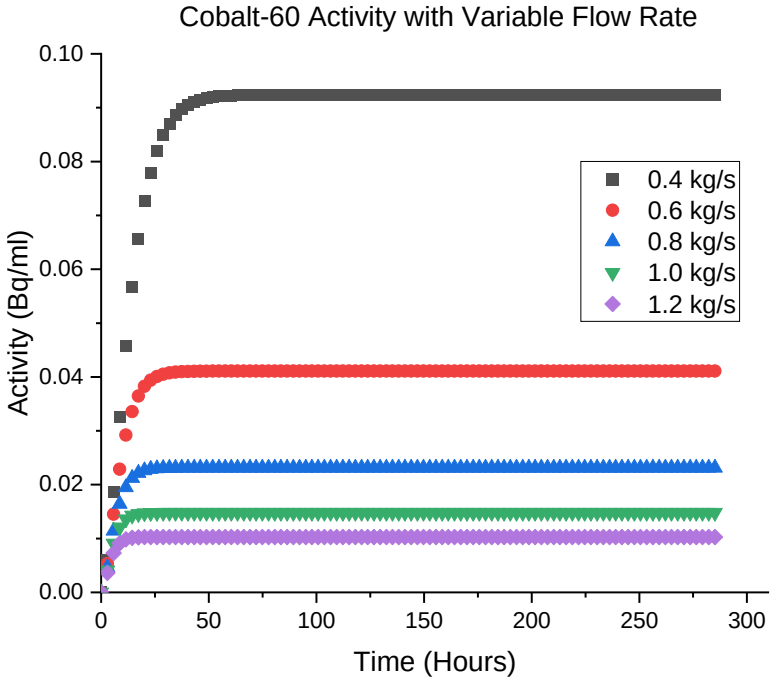

Figure 5.14 Model output for Validation Set 3 - demonstrating effect of flow rate changes on primary circuit activity saturation.

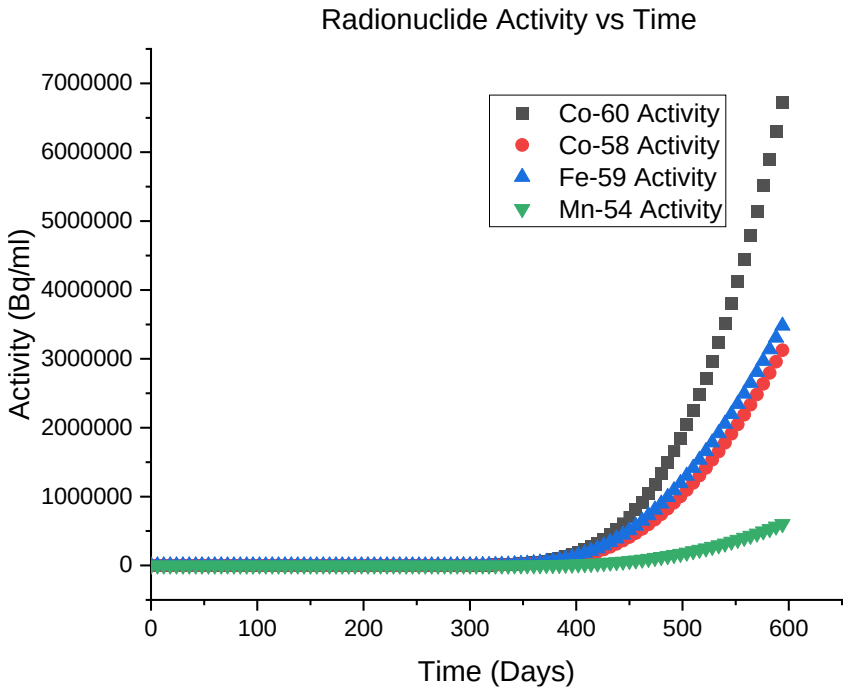

Figure 5.15 GUI output for Validation Set 3 - demonstrating the eventual decline in IXC efficiency.

5.7 Summary

This section has detailed the construction of a model designed to predict ion exchange behaviour with a PWR primary coolant. The model is able to accurately predict plant chemistry parameters such as pH for a range of different chemical inputs.

The model also demonstrates the removal of species from the coolant via ion exchange, although there were discrepancies between the model predictions and experimental results. These discrepancies could be explained due to the speciation at different pHs, however further work would be needed to be able investigate ion exchange rates experimentally with changes in pH and then compare them with the model's predictions.

Finally the model is also able to demonstrate activity removal via the ion exchange column and exhibits trends which have been proven in literature. This gives the model the capability, with the correct set of parameters, to be able to predict the resins lifetime.

6 CONCLUSIONS & FURTHER WORK

This thesis has explored three sections of study into ion exchange behaviour, with outputs from the first two chapters feeding into the final chapter. This section aims to summarise the findings and state future work which could be conducted.

6.1 Ion Exchange Equilibrium

The first section of work looked into the equilibrium behaviour of ion exchange. The relative affinity series for resins was determined to follow Monovalent << Divalent << Trivalent which is supported by literature and explained with the Donnan potential. Ion exchange equilibrium with cobalt ions were also modelled using isotherm models namely, Langmuir, Freundlich and Dubinin-Radushkevich. The Langmuir isotherm displayed the best fit and the values of sorption intensity, $R_{L,}$ indicates that Co (II) sorption onto Purolite NRW-160 resin has a favourable sorption isotherm. The value of the mean free energy of sorption, *E,* was of 1.81 kJ mol^{-1}, indicating that the sorption process follows a physical ion-exchange mechanism. Furthermore, the value of n from the Freundlich isotherm showed that the process follows a normal adsorption process.

This section of work also determined selectivity coefficients for metal ions commonly found in the primary circuit coolant. The Van't Hoff equation was used to experimentally determine values for ΔG, ΔH and ΔS in order to derive a temperature dependent equation for selectivity coefficients.

6.2 Ion Exchange Kinetics

This section of work explored the kinetic behaviour of ion exchange. Temperature dependent second order rate constants using the Arrhenius equation were derived for use in the ion exchange model. This section also looked at the effect of flow rate on adsorption and it was shown that flowrate inversely affected mass transfer coefficients and effluent cobalt ion concentration. The cause of this effect was due to residence time and manipulation of mass transfer zones. As flowrate increases, residence time decreases, and ion uptake is reduced. For optimal resin performance, maximal mass transfer should be achieved through an optimal combination of residence contact time and mass transfer coefficient value. Furthermore, results suggest that kinetics for the system is controlled by film diffusion.

Finally, this section explored the effect of temperature on the resins ability to perform. The ability to perform was determined by the resin's resultant capacity after being subjected to various temperatures for various lengths of time. It was found that short bursts of high temperature exposure had little to no effect on the resin capacity, but when subjected for a longer time the detrimental effect is more established.

6.3 Ion Exchange Modelling

This final section of work detailed the creation of a model designed to predict ion exchange behaviour with PWR primary circuit coolant. The model was proven to be able to accurately predict plant chemistry parameters such as pH for a range of different chemical inputs. In addition, the model was proven to exhibit species removal via ion exchange with resin species obey the laws of mass action. Furthermore, the model has demonstrated the ability to model activity removal, verifying that with correct plant

parameter inputs it can predict resin lifetimes. This is beneficial for being able to anticipate when a resin bed may need to be replaced or determining what type of resin may be required for a desired lifetime.

6.4 Further Work

All further work involved would be to further develop the model. It would be interesting to investigate the effect of modelling the two-step approach to ion exchange; film diffusion across the boundary layer, then particle diffusion into the resin and observe differences from the currently modelled one step approach.

Also investigating the effect of using mass transfer coefficients as the overall rate constant would be of interest to see how the model predicts against experimental results.

Furthermore, repeating the experimental results from Chapter 3, but operating in a much higher pH would be useful to justify the hypothesis regarding the speciation of ions at high and low pHs.

Finally, it has been observed in literature that ion exchange resins can suffer radiation damage and experience loss of capacity. Performing experiments where resin is subject to radiation would provide data which could implemented into the model. This would give a more realistic picture as to what happens to the ion exchange resin through life in a PWR.

7 REFERENCES

[1] Vnsafety.eu. (2016). PWR Fundamentals. [online] Available at: http://www.vnsafety.eu/doc.php?nd=o55&tid=55&lg=1&docid=38&site=1 [Accessed 2 Feb. 2017].

[2] Martin Cabañas, B., Leclercq, S., Barboux, P., Fédoroff, M. and Lefèvre, G. (2011). Sorption of nickel and cobalt ions onto cobalt and nickel ferrites. Journal of Colloid and Interface Science, 360(2), pp.695-700.

[3] F. Dacquait, C. Andrieu, M. Berger, J.L. Bretelle, A. Rocher, in: Proc. 10th Int. Conf. on Water Chemistry of Nuclear Systems, Avignon, France, 2002.

[4] M. Boursier, M. Dupin, P. Gossot, Y. Rouillon, in: Proc. 9th Symp. on Environmental Degradation of Materials in Nuclear Power Systems-water Reactors, New Port Beach, CA, 1999, p. 155.

[5] G.C.W. Comley, Prog. Nucl. Energy 16 (1985) 41.

[6] T.F.J. MARCHL. Occupational radiation exposures in Siemens designed PWRs. SFEN. Chemistry in Water Reactors : Operating experience and new developments. Nice, France. 24-27 April 1994.

[7] B.C. FRIEDRICH. Reduction of Co60 inventory in LWR. Kerntechnik, Vol. 54, n°2. 1989.

[8] T. KITABATA. Occupational dose reduction by water chemistry measures in Fugen.

[9] Dowex Chemicals (2000) Fundamentals of Ion Exchange [Online] available at: http://msdssearch.dow.com/PublishedLiteratureDOWCOM/dh_0032/0901b803800326ca.pdf?filepath=liquidseps/pdfs/noreg/177-01837.pdf&fromPage=GetDoc Accessed: 31/10/2016

[10] Gilca, E. Maicaneanu, A. Ilea, P. (2013) Removal of zinc ions as zinc chloride complexes from strongly acidic aqueous solutions by ionic exchange. Central European Journal of Chemistry, 12(8), 821-828.

[11] Gfycat. (2019). THREE COOLING CIRCUITS OF PRESSURISED WATER REACTOR GIF | Gfycat. [online] Available at: https://gfycat.com/fittingenragedantbear [Accessed 6 Nov. 2019].

[12] The Department of Energy & Climate Change: Nuclear power in the UK, page 19, National Audit Office, published 13 July 2016, accessed 12 December 2019.

[13] World Nuclear Association (2019). World Nuclear Performance Report 2019. [online] Available at: https://www.world-nuclear.org/getmedia/d77ef8a1-b720-44aa-9b87-abf09f474b43/performance-report-2019.pdf.aspx [Accessed 6 Dec. 2019].

[14] "Hinkley Point: EDF raises cost estimate for nuclear plant". BBC News. BBC. 3 July 2017. Retrieved 3 July 2017.

[15] "Cost of Hinkley Point nuclear plant climbs another £1.5bn to over £20bn, as project is again delayed". The Telegraph. 3 July 2017. Retrieved 3 July 2017.

[16] USNRC Technical Training Center. Reactor Concepts Manual - Pressurized Water Reactor systems, 2003. www.nrc.gov/reading-rm/basic-ref/teachers/04.pdf.

[17] Qiu, Y., Chen, Y., Zhang, G., Yu, L. and Mantri, R. (2017). Developing solid oral dosage forms. Academic Press.

[18] Kundu, P. and Dutta, K. (2018). Progress and recent trends in microbial fuel cells. Chapter 4 - Polymer Electrolyte Membranes for Microbial Fuel Cells: Part A. Nafion-Based Membranes. Elsevier, pp.47-72.

[19] Killeen, J., Nordmann, F., Schunk, J. and Vonkova, K., 2010, July. Optimisation of water chemistry to ensure reliable water reactor fuel performance at high burnup and in ageing plant (FUWAC): an International Atomic Energy Agency coordinated research project. In International Conference on Water Chemistry of Nuclear Reactor Systems, NPC (Vol. 2010, pp. 3-7).

[20] Nordmann, F. and Rochester, D., 2014. Key Emerging Issues and Recent Progress Related to Plant Chemistry/Corrosion in PWR/VVER/CANDU Reactors. Advanced Nuclear Technology International.

[21] Nuclear Power. (2019). Boron 10 - Nuclear Power. [online] Available at: https://www.nuclear-power.net/glossary/boron-10/ [Accessed 27 Dec. 2019].

[22] Song, M.C. and Lee, K.J., 2003. The evaluation of radioactive corrosion product at PWR as change of primary coolant chemistry for long-term fuel cycle. Annals of Nuclear Energy, 30(12), pp.1231-1246.

[23] K. Norring, B. Rosborg, J. Engström, J. Svenson, Influence of LiOH and H_2 on primary side IGSCC of alloy 600 steam generator tubes, in: Contribution of Materials Investigation to the Resolution of problems encountered in PWR Plants. Volume 1, 1990.

[24] W.H. Bamford, J. Foster, Crack growth and microstructural characterization of alloy 600 head penetration materials, in, Electric Power Research Inst., 1995.

[25] M.C. Song, K.J. Lee, The evaluation of radioactive corrosion product at PWR as change of primary coolant chemistry for long-term fuel cycle, Annals of Nuclear Energy, 30 (2003) 1231-1246.

[26] P. Millet, E. Rapport, PWR Primary Water Chemistry Guidelines, vol. 2, Revision 5, in, TR Patent 105,714, 1999.

[27] Holden, N.E., 2010. The impact of depleted ^{6}Li on the standard atomic weight of lithium. Chemistry international, 32(1), p.12.

[28] Palomo, M., Penalver, A., Aguilar, C. and Borrull, F., 2007. Tritium activity levels in environmental water samples from different origins. Applied radiation and isotopes, 65(9), pp.1048-1056.

[29] Ault, T., Brozek, K., Fan, L., Folsom, M., Kim, J. and Zeismer, J., 2012. Lithium isotope enrichment: feasible domestic enrichment alternatives. DOE report UCBTH, pp.12-005.

[30] R. Reiss, S. Odar, J. Kysela, and F. Nordmann, “LCC-7 SPECIAL TOPIC REPORT PWR / VVER Primary Side Coolant Chemistry Volume I – Technical Basis and Recent Discussions PWR / VVER Primary Side,” A.N.T. INTERNATIONAL, 2011.

[31] P. Millett, “PWR Primary Water Chemistry Guidelines - Volume 1, Revision 4,” EPRI, 1999.

[32] Féron, D. (2012). Nuclear corrosion science and engineering. Cambridge, UK: Woodhead Publishing.

[33] Féron, D. Staehle, R.W.. (2016). Stress Corrosion Cracking of Nickel-Based Alloys in Water-Cooled Nuclear Reactors - The Coriou Effect (EFC 67) - 2.2 Some Benchmarks.Elsevier. Retrieved

from https://app.knovel.com/hotlink/pdf/id:kt010WKQT1/stress-corrosion-cracking/some-benchmarks

[34] [16] I. Odnevall Wallinder, J. Lu, S. Bertling, C. Leygraf, Release rates of chromium and nickel from 304 and 316 stainless steel during urban atmospheric exposure—a combined field and laboratory study, Corrosion Science, 44 (2002) 2303-2319.

[35] S.F. Mughabghab, Neutron Cross Sections: Neutron Resonance Parameters and Thermal Cross Sections Part B: Z=61-100, Elsevier Science, 2012.

[36] Thermal neutron cross sections for the 1991 table of the isotopes. (1991). Washington, D.C.: United States. Dept. of Energy.

[37] J.-C. Shin, J.-M. Doh, J.-K. Yoon, D.-Y. Lee, J.-S. Kim, Effect of molybdenum on the microstructure and wear resistance of cobalt-base Stellite hardfacing alloys, Surface and Coatings Technology, 166 (2003) 117-126.

[38] Iaea.org. (2020). Tackling the Challenges of Nuclear Data in the Future. [online] Available at: https://www.iaea.org/newscenter/news/tackling-the-challenges-of-nuclear-data-in-the-future [Accessed 7 Jan. 2020].

[39] Odette, G. and Lucas, G. (2001). Embrittlement of nuclear reactor pressure vessels. JOM, 53(7), pp.18-22.

[40] https://www.osti.gov/etdeweb/servlets/purl/20375315

[41] http://uu.diva-portal.org/smash/get/diva2:1108293/FULLTEXT01.pdf

[42] Martin, A., Harbison, S., Beach, K. and Cole, P., 2010. An Introduction To Radiation Protection. Springer-Verlag Berlin Heidelberg, pp.323-324.

[43] K.-H. Neeb, The radiochemistry of nuclear power plants with light water reactors, Walter de Gruyter, 2011.

[44] IUPAC Subcommittee for Isotopic Abundance Measurements by K.J.R. Rosman, P.D.P. Taylor Pure Appl. Chem. 1999, 71, 1593-1607.

[45] Pomerance, H. (1952). Thermal Neutron Capture Cross Sections. Physical Review, 88(2), pp.412-413.

[46] G. Audi, O. Bersillon, J. Blachot, A.H. Wapstra, The Nubase evaluation of nuclear and decay properties, Nuclear Physics A, 729 (2003) 3-128.

[47] H. Ocken, Reducing the cobalt inventory in light water reactors, Nuclear technology, 68 (1985) 18-28.

[48] M. Carnus, X. Confort, Replacement of Cobalt base alloys hardfacing by NOREM alloy; EDF experience and development, some metallurgical considerations. Valves application (CLAMA, RAMA).

[49] G. Airey, S. Bryant, D. Richards, Valve operability testing and stellite replacement, in: Sizewell'B'-the first of the UK PWR power stations, 1989.

[50] Féron, D., 2012. Overview of nuclear materials and nuclear corrosion science and engineering. In Nuclear Corrosion Science and Engineering (pp. 481). Woodhead Publishing.

[51] B.M. Cabanas, Comportement des produits de corrosion dans le circuit primaire des centrales REP-sorption du cobalt et du nickel sur des ferrites représentatifs, in, Université Paris Sud-Paris XI, 2010.

[52] Way, J. T. J. Roy. Agr. Soc. Eng. (1850), 11, 313.

[53] Thomson, H. S. J. Roy. Agr. Soc. Eng. (1850), 11,68.

[54] Gans, R. Brit. Pat. 3494,

[55] Crosfield, Jos. Brit. Pat. 455,374. Liebknecht, 0., Ger. Pat. 763,926; Brit. Pat. 450,574 and 450,575. Octrooien, N. M. Mif. Activit. Brit. Pat. 450,179 and 450,540. Permutit Co., Brit. Pat. 478,134.

[56] Adams, E. A. and HolinGS, Z. L. Adsorptive properties of synthetic resins. J, Soc. Chen. Ind. 54,1 (1935),

[57] Holmes, E. L. Brit. Pat. 474,361; U.S. Pat. 2,191,853. Holmes, E. L. and Holmes, L. E. Brit. Pat. 588,380.

[58] British Thomson-Houston, Co. Ltd. Brit. Pat. 577,707. D'Alelio, G. F. U.S. Pat. 2,366,007.

[59] Dow Chemical Co. Brit. Pat. 677,350. McBurney, C. H. U.S. Pat. 2,329,710. Pepper, K. W., Paisley, H. M.

[60] Harland, C., 1994. Ion Exchange. Cambridge: Royal Society of Chemistry.

[61] [D.J. Kim, H.P. Kim S.S. Hwang, Comparison between Alloy 600 and Alloy 690 ODSCC behaviour, Nuclear Materials Safety Research Division, Korea Atomic Energy Research Institute(KAERI), Yuseong, Daejeon, Korea, 305-353, 2015.

[62] R. Paterson, An introduction to ion exchange, Heyden in cooperation with Sadtler Research Laboratories [Philadelphia], 1970.

[63] F.G. Helfferich, Ion exchange, Courier Corporation, 1995.

[64] Atkins, P. and De Paula, J., 2010. Physical Chemistry. 7th ed. Oxford: Freeman, p.875.

[65] N. Wakao, T. Funazkri, Effect of fluid dispersion coefficients on particle-to- fluid mass transfer coefficients in packed beds: correlation of Sherwood numbers, Chemical Engineering Science, 33 (1978) 1375-1384.

[66] M. Bachet, L. Jauberty, L. De Windt, E. Tevissen, C. De Dieuleveult, H. Schneider, Comparison of mass transfer coefficient approach and Nernst–Planck formulation in the reactive transport modeling of Co, Ni, and Ag removal by mixed- bed ion-exchange resins, Industrial & Engineering Chemistry Research, 53 (2014) 11096-11106.

[67] O. Abdelwahab, N. Amin, E.Z. El-Ashtoukhy, Removal of zinc ions from aqueous solution using a cation exchange resin, Chemical Engineering Research and Design, 91 (2013) 165-173.

[68] Jones, N., 2018. Towards An Improved Understanding Of PWR Coolant Chemistry. Ph.D. University of Manchester.

[69] Qian, W., Song, Q., Ding, H. and Xie, W., 2019. Computational simulations of the mass transfer zone in GS adsorption column packed with Fe3+ type ion exchanger. Chemosphere, 215, pp.507-514.

[70] Mantovaneli, I., Ferretti, E., Simões, M. and Silva, C., 2004. The effect of temperature and flow rate on the clarification of the aqueous stevia-extract in a fixed-bed column with zeolites. Brazilian Journal of Chemical Engineering, 21(3), pp.449-458.

[71] Gableman Process Solutions, 2017. Adsorption Basics Part 1. [online] p.American Institute of Chemical Engineers. Available at: <https://www.aiche.org/sites/default/files/docs/pages/adsorption_basics_part_1.pdf> [Accessed 8 March 2020].

[72] Lawless T, Grime T, J R. Investigation into the interaction of zinc with cation and anion exchange resins under anaerobic, alkaline conditions akin to those in primary circuits.: Nuclear Department.

[73] Bulai, Petru & Balan, Catalin & Scripcariu, Camelia & Macoveanu, Matei. (2009). Equilibrium and Kinetic Studies of Copper (II) Removal on Purolite S930 Resin. 1103-1109.

[74] Rahmatpour, A., Goodarzi, N. and Moazzez, M. (2018). A novel route for synthesis of cross-linked polystyrene copolymer beads with tunable porosity using guar and xanthan gums from bioresources as alternative synthetic suspension stabilizers. Designed Monomers and Polymers, 21(1), pp.116-129.

[75] Fathyz, M., Moghny, A., Awad Allah, A. and A-A El-Bellihi, A. (2013). Preparation of cation-Exchange Resin from Styrene-Divinylbenzene Copolymer Obtained by suspension Polymerization Method. Elixir International Journal, [online] 60 (2013) 16095-16097

[76] Bothe, N., Döscher, F., Klein, J. and Widdecke, H. (1979). Thermal stability of sulphonated styrene-divinylbenzene resins. Polymer, 20(7), pp.850-854.

[77] Martin Cabañas, B., Leclercq, S., Barboux, P., Fédoroff, M. and Lefèvre, G. (2011). Sorption of nickel and cobalt ions onto cobalt and nickel ferrites. Journal of Colloid and Interface Science, 360(2), pp.695-700.

[78] F. Dacquait, C. Andrieu, M. Berger, J.L. Bretelle, A. Rocher, in: Proc. 10th Int. Conf. on Water Chemistry of Nuclear Systems, Avignon, France, 2002.

[79] M. Boursier, M. Dupin, P. Gossot, Y. Rouillon, in: Proc. 9th Symp. on Environmental Degradation of Materials in Nuclear Power Systems-water Reactors, New Port Beach, CA, 1999, p. 155.

[80] G.C.W. Comley, Prog. Nucl. Energy 16 (1985) 41.

[81] T.F.J. Marchl. Occupational radiation exposures in Siemens designed PWRs. SFEN. Chemistry in Water Reactors : Operating experience and new developments. Nice, France. 24-27 April 1994.

[82] B.C. Freidrich. Reduction of Co60 inventory in LWR. Kerntechnik, Vol. 54, n°2. 1989.

[83] T. Kitabata. Occupational dose reduction by water chemistry measures in Fugen.

[84] Dowex Chemicals (2000) Fundamentals of Ion Exchange [Online] available at: http://msdssearch.dow.com/PublishedLiteratureDOWCOM/dh_0032/0901b803800326ca.pdf?filepath=liquidseps/pdfs/noreg/177-01837.pdf&fromPage=GetDoc Accessed: 22/05/2018

[85] Gilca, E. Maicaneanu, A. Ilea, P. (2013) Removal of zinc ions as zinc chloride complexes from strongly acidic aqueous solutions by ionic exchange. Central European Journal of Chemistry, 12(8), 821-828.

[86] IAEA, (2002). Application of Ion Exchange Processes for the Treatment of Radioactive Waste and Management of Spent Ion Exchangers. (Technical report series no. 408). Vienna: International Atomic Energy Agency.

[87] Lawless T, Grime T, J R. Investigation into the interaction of zinc with cation and anion exchange resins under anaerobic, alkaline conditions akin to those in primary circuits.: Nuclear Department.

[88] Braz J. The effect of temperature and flow rate on the clarification of the aqueous stevia-extract in a fixed-bed column with zeolites. Brazilian Journal of Chemical Engineering. 2004 September; 21(1).

[89] Hou X, Jones B. Inductively Coupled Plasma/Optical Emission Spectrometry. In Meyers RA, editor. Encyclopeia of Analytical Chemistry. Chichester: John Wiley & Sons Ltd; 2000. p. 9468-9485

[90] Yuan G, Tian Y, Liu J, Tu H, Liao J, Yang J, et al. Schiff base anchored on metal-organic framework for Co (II) removal from aqueous solution. Chemical Engineering Journal. 2017 October; 326.

[91] Bulai, Petru & Balan, Catalin & Scripcariu, Camelia & Macoveanu, Matei. (2009). Equilibrium and Kinetic Studies of Copper (II) Removal on Purolite S930 Resin. 1103-1109.

[92] Sari A., Tuzen M., Citak D., Soylak M., (2007), Equilibrium, kinetic and thermodynamic studies of adsorption of Pb(II) from aqueous solution onto Turkish kaolinite clay, Journal of Hazardous Materials, 149, 283–291.

[93] A.O, D. (2012). Langmuir, Freundlich, Temkin and Dubinin–Radushkevich Isotherms Studies of Equilibrium Sorption of Zn 2+ Unto Phosphoric Acid Modified Rice Husk. IOSR Journal of Applied Chemistry, 3(1), pp.38-45.

[94] Simister, C., Caron, F. and Gedye, R., 2004. Determination of the thermal degradation rate of polystyrene-divinyl benzene ion exchange resins in ultra-pure water at ambient and service temperature. Journal of Radioanalytical and Nuclear Chemistry, 261(3), pp.523-531.

[95] De Decker, Jeroen. (2017). Functionalized Metal-Organic Frameworks as Selective Metal Adsorbents. [PhD Thesis], Ghent University.

[96] Bonner, O. and Smith, L., 1957. A Selectivity Scale for Some Divalent Cations on Dowex 50. *The Journal of Physical Chemistry*, 61(3), pp.326-329.

[97] EPRI, "MULTEQ Version 9.0 Desktop Application." 2018

[98] Asci, Y., Kaya, S. (2014) Removal of cobalt ions from water by ion-exchange method. *Desalination and Water Treatment*, 52 (1-3), 267-273. Available from doi:10.1080/19443994.2013.781544 [Accessed 5th May 2021]

[99] Nomngongo, P., Ngila, J., Msagati, T. and Moodley, B., 2014. Kinetics and Equilibrium Studies for the Removal of Cobalt, Manganese, and Silver in Ethanol using Dowex 50W-x8 Cation Exchange Resin. *Separation Science and Technology*, 49(12), pp.1848-1859.

[100] Lee, I., Kuan, Y. and Chern, J., 2007. Equilibrium and kinetics of heavy metal ion exchange. *Journal of the Chinese Institute of Chemical Engineers*, 38(1), pp.71-84.

[101] INGLEZAKIS, V., ZORPAS, A., LOIZIDOU, M. and GRIGOROPOULOU, H., 2005. The effect of competitive cations and anions on ion exchange of heavy metals. Separation and Purification Technology, 46(3), pp.202-207.

[102] Jain, M., Garg, V. and Kadirvelu, K., 2009. Chromium(VI) removal from aqueous system using Helianthus annuus (sunflower) stem waste. Journal of Hazardous Materials, 162(1), pp.365-372.

[103] Purolite Ltd, 1998. Capacity of Strong (Sulfonic) Acid Cation Resins. p.1.

[104] W. L. Marshall and E. U. Franck, "Ion product of water substance, 0–1000 °C, 1–10,000 bars New International Formulation and its background," J. Phys. Chem. Ref. Data, vol. 10, no. 2, pp. 295–304, Apr. 1981.

[105] IUPAC Periodic Table of the Elements and Isotopes (IPTEI) for the Education Community (IUPAC Technical Report). (2019). Chemistry International, 41(1), pp.42-42.

[106] Pomerance, H. (1952). Thermal Neutron Capture Cross Sections. Physical Review, 88(2), pp.412-413.

[107] Goldman, D. (1968). Neutron cross sections and technology. Washington: U.S. National Bureau of Standards; for sale by the Supt. of Docs., U.S. Govt. Print. Off.

[108] Ahlf, J. (1993). High flux reactor (HFR) Petten. Luxembourg: Office for Official Publications of the European Communities.

[109] Riess, R., Odar, Kysela, J. and Nordmann, 2011. PWR/VVER Primary Side Coolant Chemistry. Sweden: Advanced Nuclear Technology International, pp.5-41(5-102).

[110] Frattini P. L., Analysis Report on 1999-2001 field experience with elevated, constant pH, EPRI Report 1003153, Nov.2001.

[111] Bellir, K., Lehocine, M. and Meniai, A., 2013. Zinc removal from aqueous solutions by adsorption onto bentonite. Desalination and Water Treatment, 51(25-27), pp.5035-5048.

[112] Lyu, H., Gao, B., He, F., Zimmerman, A., Ding, C., Huang, H. and Tang, J., 2018. Effects of ball milling on the physicochemical and sorptive properties of biochar: Experimental observations and governing mechanisms. Environmental Pollution, 233, pp.54-63.

[113] Sheha, R., Moussa, S., Attia, M., Sadeek, S. and Someda, H., 2018. Development and application of carbon nanotubes reinforced hydroxyapatite composite in separation of Co(II) and Eu(III) ions from aqueous solutions. Radiochimica Acta, 107(1), pp.67-82.

[114] Rachou, J., Gagnon, C. and Sauvé, S., 2007. Use of an ion-selective electrode for free copper measurements in low salinity and low ionic strength matrices. Environmental Chemistry, 4(2), p.90.

[115] MCPA Software, "FACSIMILE - Introduction," 2014. [Online]. Available at: http://www.mcpa-software.com/styled-27/styled/. [Accessed: 11-Apr-2020].

[116] J. C. (John C. Butcher, Numerical methods for ordinary differential equations. J. Wiley, 2003.

[117] J. H. Alexander and L. Luu, "MULTEQ: Equilibrium of an electrolytic solution with vapor-liquid partitioning and precipitation: Volume 1: User's manual, Revision 1." 01-May-1989.

[118] Uk.mathworks.com. 2020. MATLAB GUI. [online] Available at: https://uk.mathworks.com/discovery/matlab-gui.html. [Accessed: 11-Apr-2020].

[119] 17) Rafique, M., Mirza, N. and Mirza, S., 2008. Numerical simulations of corrosion product activity in the purification system of a typical PWR under nonlinearly rising corrosion and flow rate perturbations. International Journal of Nuclear Energy Science and Technology, 4(2), p.132.

[120] Rafique, M., Mirza, N., Mirza, S., Kearfott, K., Abbasi, S. and Naeem, S., 2015. Parametric Study of Time-Dependent Corrosion Product Activity due to56Mn,58Co, and60Co in the Primary Coolant Circuit of a Typical Pressurized Water Reactor. Journal of Chemistry, 2015, pp.1-10.

[121] Sarkar, S., SenGupta, A. and Prakash, P., 2010. The Donnan Membrane Principle: Opportunities for Sustainable Engineered Processes and Materials. *Environmental Science & Technology*, 44(4), pp.1161-1166.

[122] Inamuddin, M. and Luqman, M. (2012). Ion Exchange Technology I. New York: Springer.

[123] Aniceto, J., Cardoso, S., Faria, T., Lito, P. and Silva, C. (2012). Modeling ion exchange equilibrium: Analysis of exchanger phase non-ideality. Desalination, 290, pp.43-53.

[124] Dranoff, J. and Lapidus, L. (1957). Equilibrium in Ternary Ion Exchange Systems.Industrial & Engineering Chemistry, 49(8), pp.1297-1302.

[125] Walton, H. (1962). Ion Exchange. F. G. Helfferich. McGraw-Hill, New York, 1962. ix + 624 pp. Illus. $16. Science, 138(3537), pp.133-133.

[126] Valverde, J., de Lucas, A. and Rodríguez, J. (1999). Comparison between Heterogeneous and Homogeneous MASS Action Models in the Prediction of Ternary Ion Exchange Equilibria. Industrial & Engineering Chemistry Research, 38(1), pp.251-259.

[127] Kester, D. R.; Pytkowicz, R. M. Theoretical model for the formation of ion pairs in seawater. Marine Chem. 1975, 3, 365.

8 APPENDIX

8.1 Chapter 3 Supplementary

8.1.1 Metal Salt Comparison Graphs

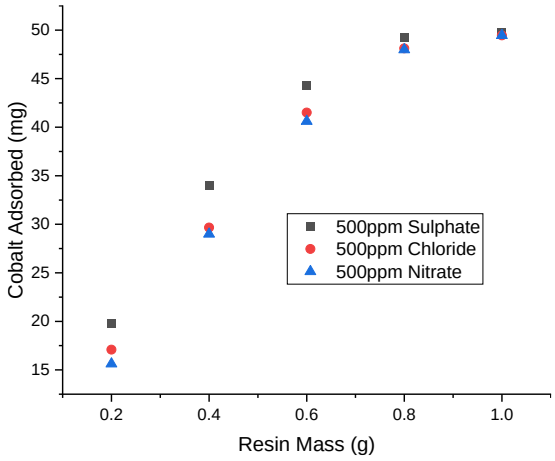

Figure 8.1.1 Effect of Metal Salts on Adsorption (1)

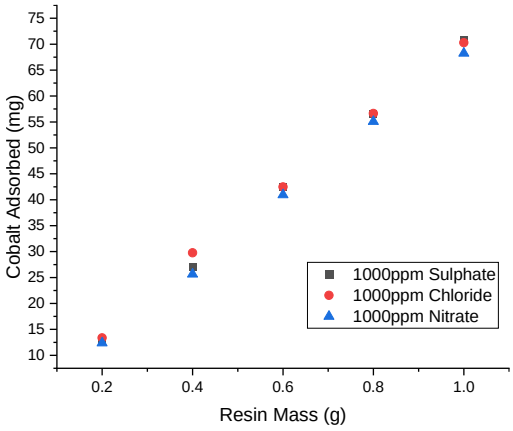

Figure 8.1.2 Effect of Metal Salts on Adsorption (2)

8.1.2 ICP-OES Calibration Plots

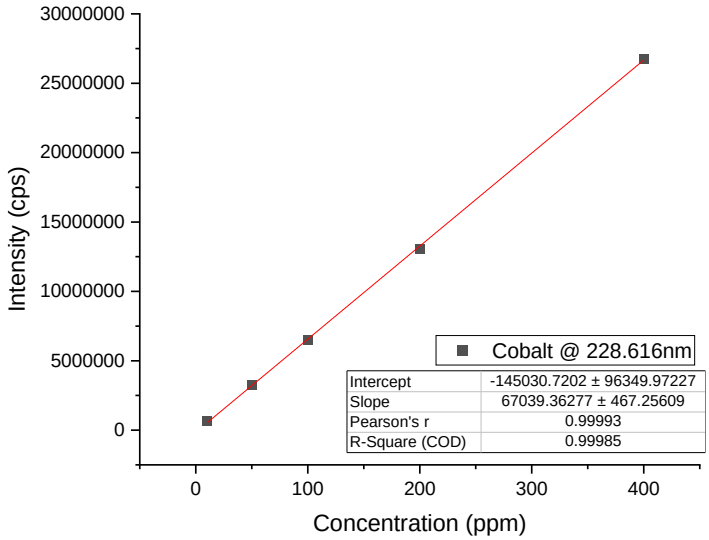

Figure 8.1.3 ICP-OES Calibration Plot for Cobalt

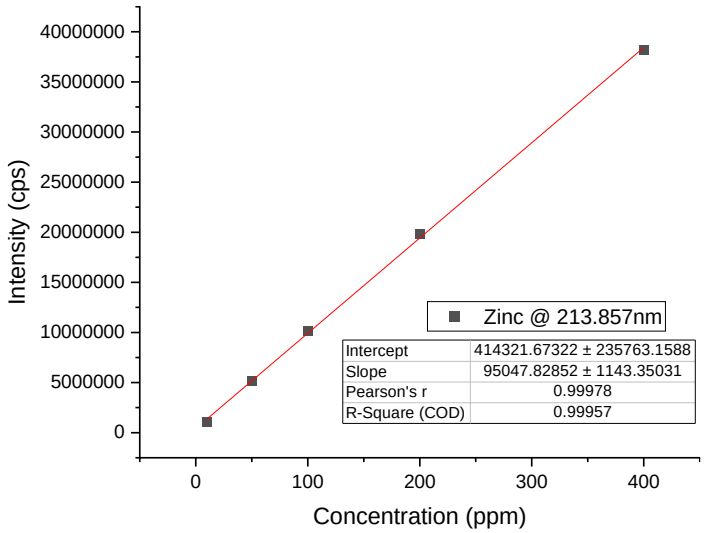

Figure 8.1.4 ICP-OES Calibration Plot for Zinc

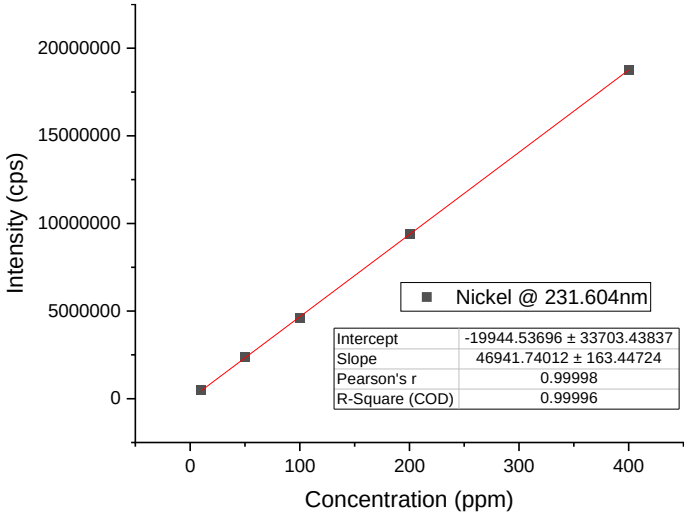

Figure 8.1.5 ICP-OES Calibration Plot for Nickel

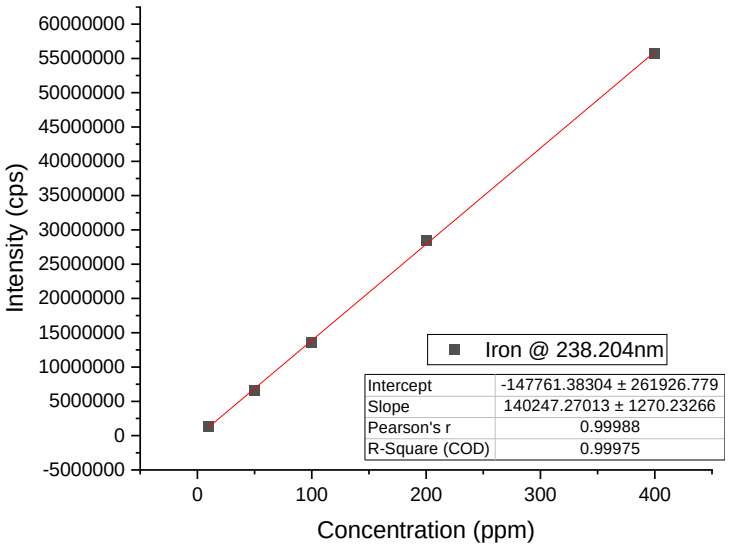

Figure 8.1.6 ICP-OES Calibration Plot for Iron

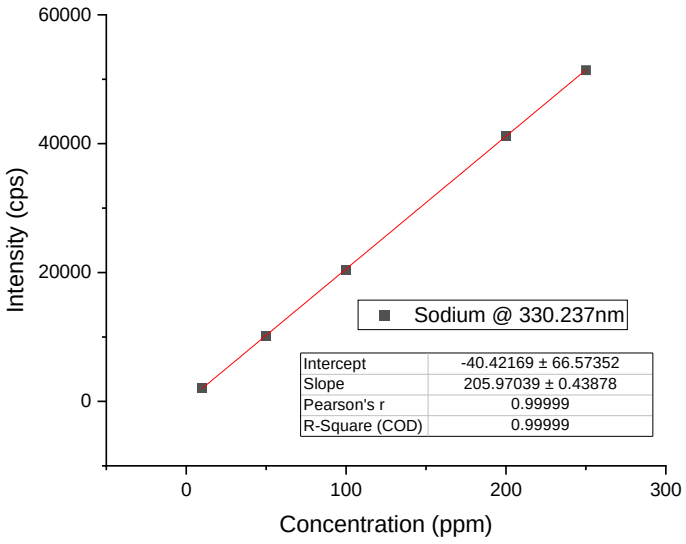

Figure 8.1.7 ICP-OES Calibration Plot for Sodium

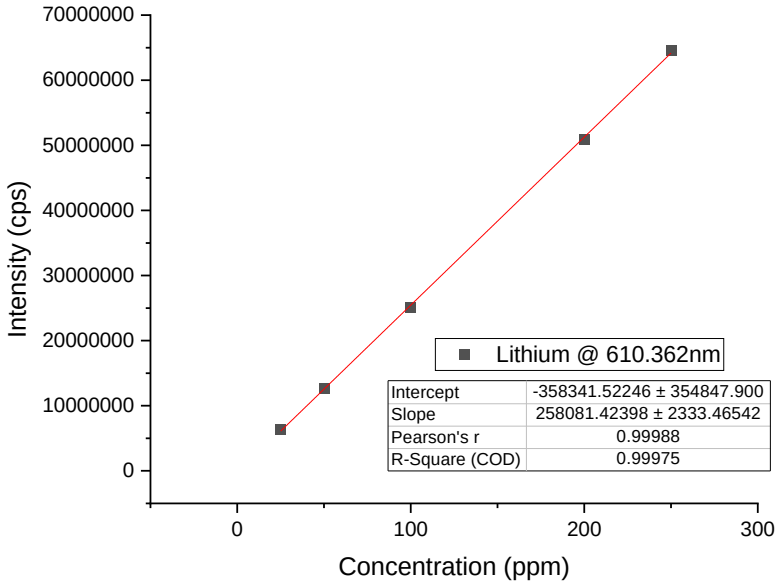

Figure 8.1.8 ICP-OES Calibration Plot for Lithium

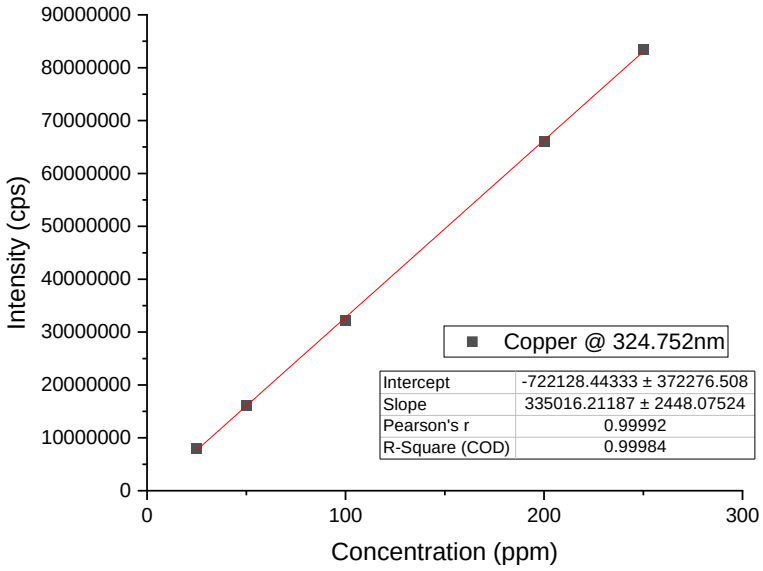

Figure 8.1.9 ICP-OES Calibration Plot for Copper

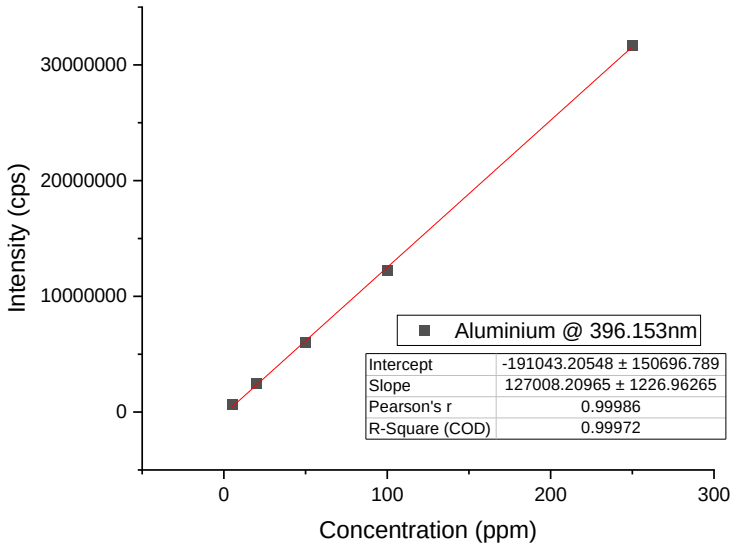

Figure 8.1.10 ICP-OES Calibration Plot for Aluminum

8.2 Chapter 4 Supplementary

8.2.1 Linear Plots from Second Order Rate Equation

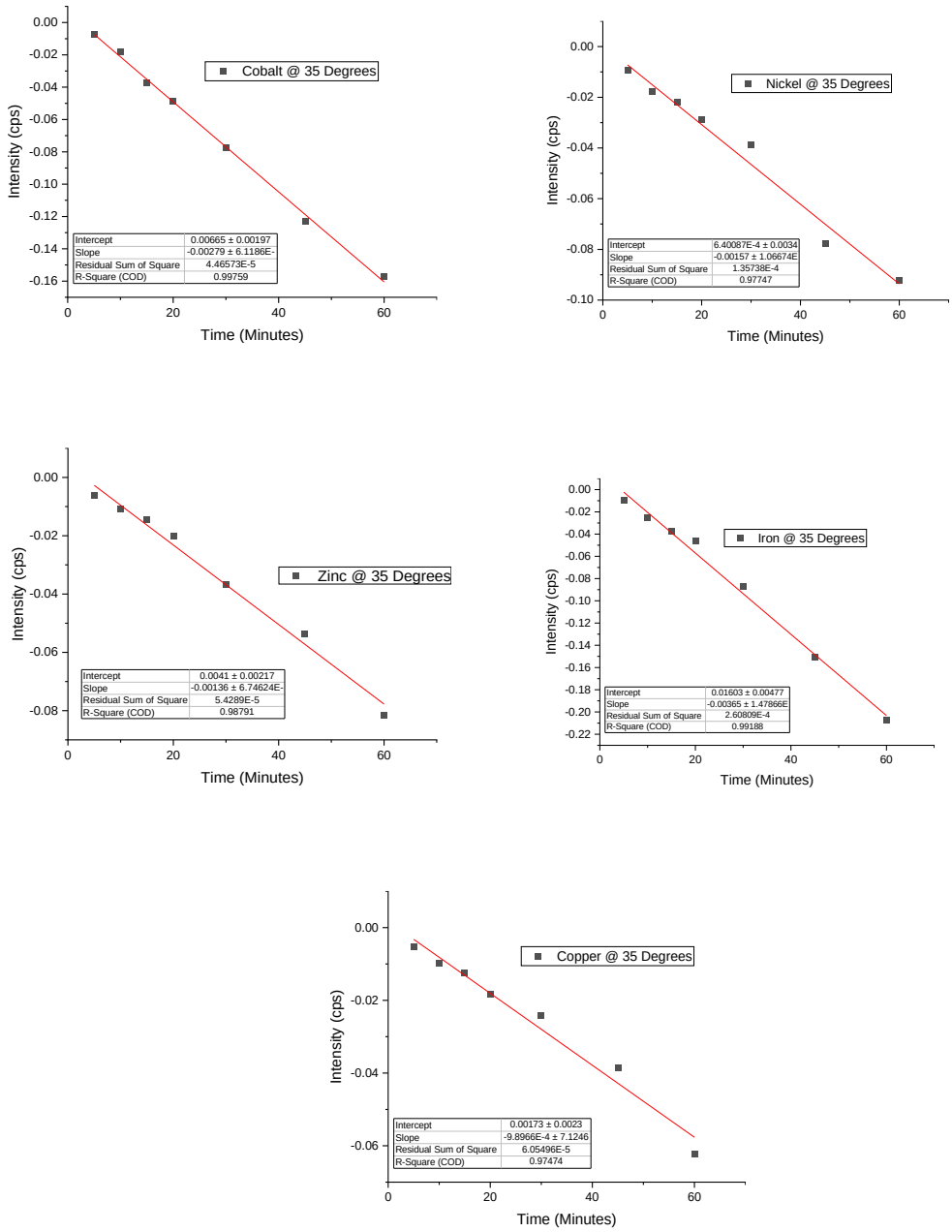

Figure 8.2.1 Linear Plots of Eq 4.1 to determine second order rate constant, k for (A)Cobalt, (B)Nickel, (C)Zinc, (D)Iron and (E)Copper at 35°C.

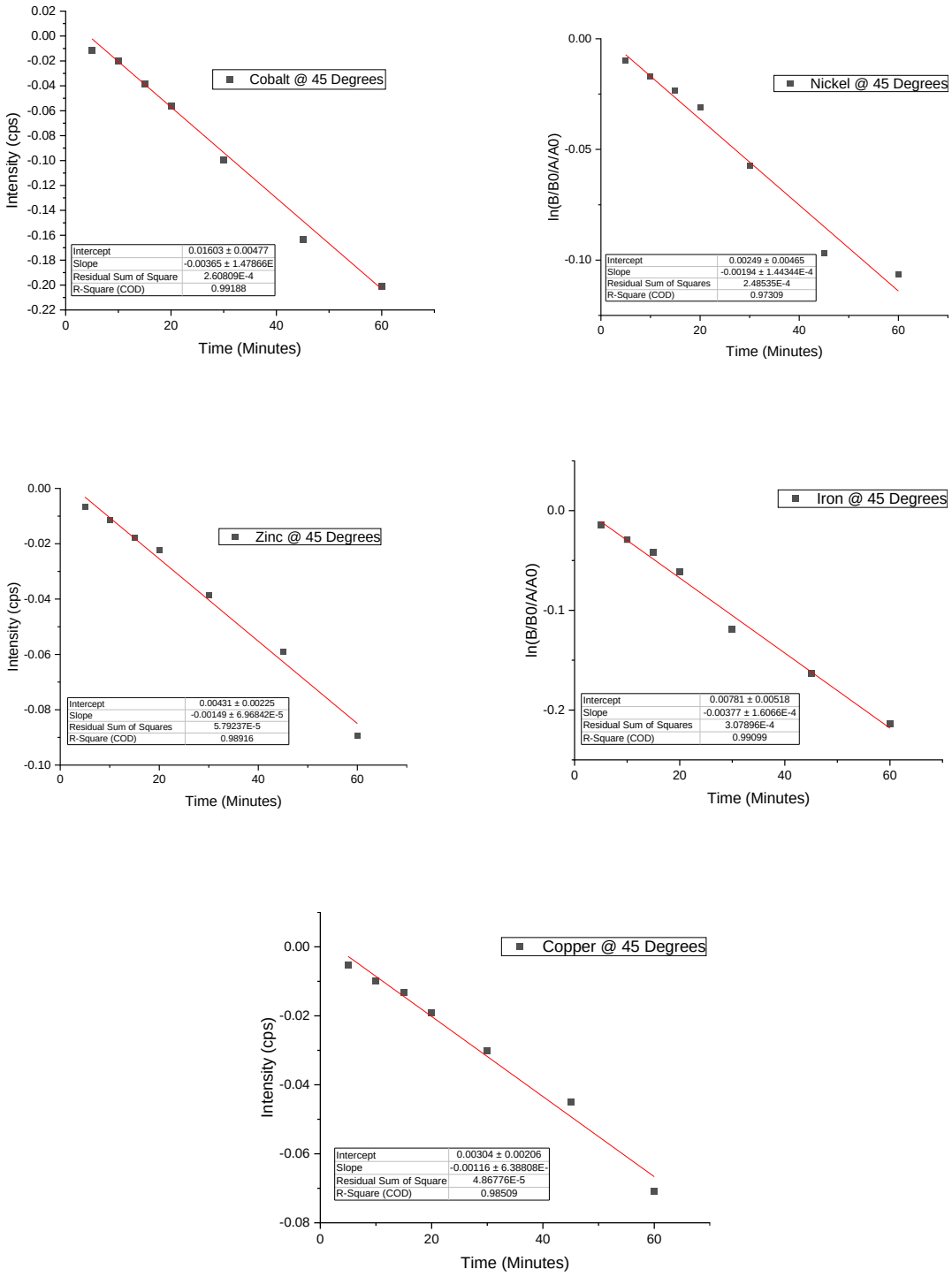

Figure 8.2.2 Linear Plots of Eq 4.1 to determine second order rate constant, k for (A)Cobalt, (B)Nickel, (C)Zinc, (D)Iron and (E)Copper at 45°C.

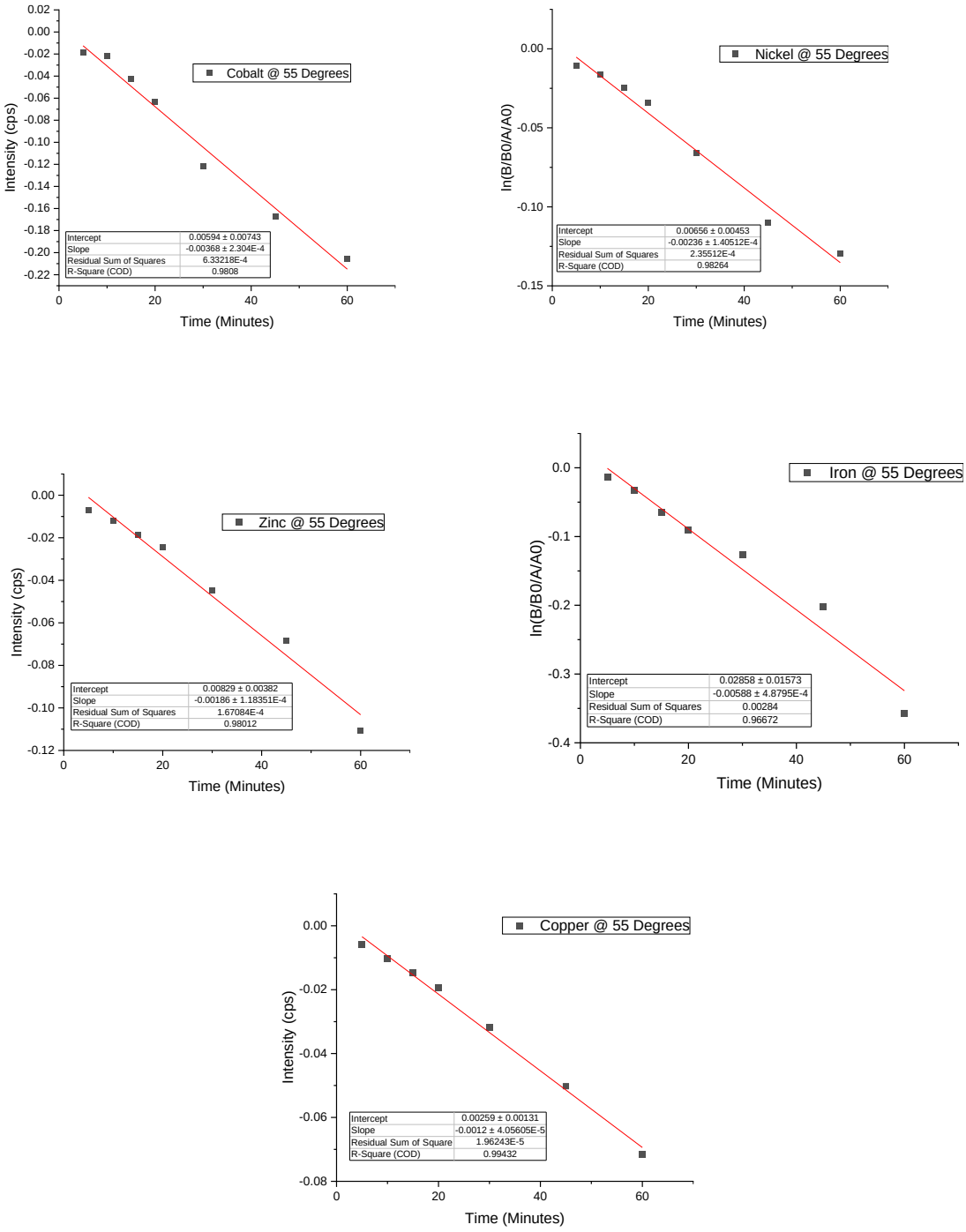

Figure 8.2.3 Linear Plots of Eq 4.1 to determine second order rate constant, k for (A)Cobalt, (B)Nickel, (C)Zinc, (D)Iron and (E)Copper at 55°C.

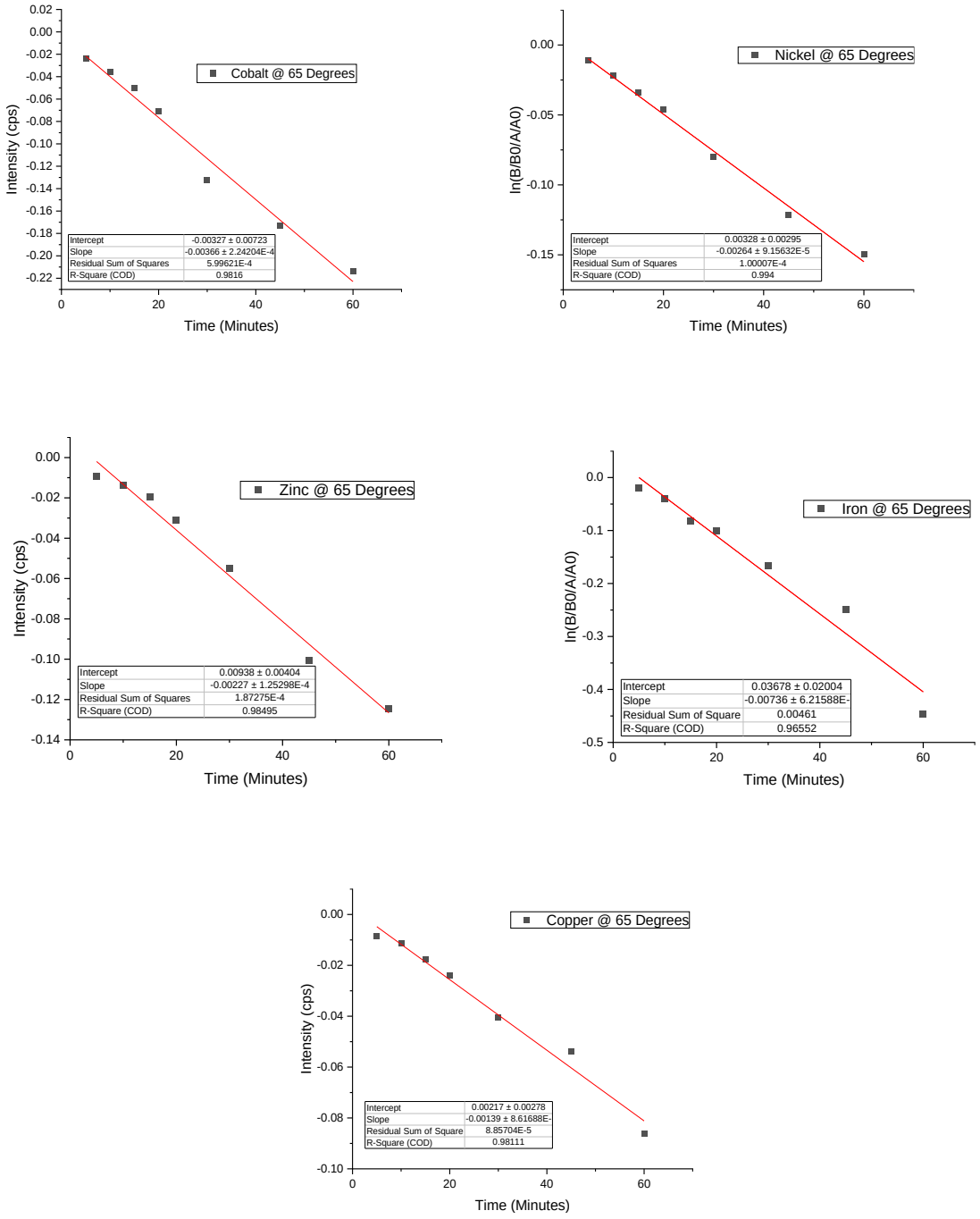

Figure 8.2.4 Linear Plots of Eq 4.1 to determine second order rate constant, k for (A)Cobalt, (B)Nickel, (C)Zinc, (D)Iron and (E)Copper at 65°C.

8.2.2 Transient Experiments Results (Concentration vs Time)

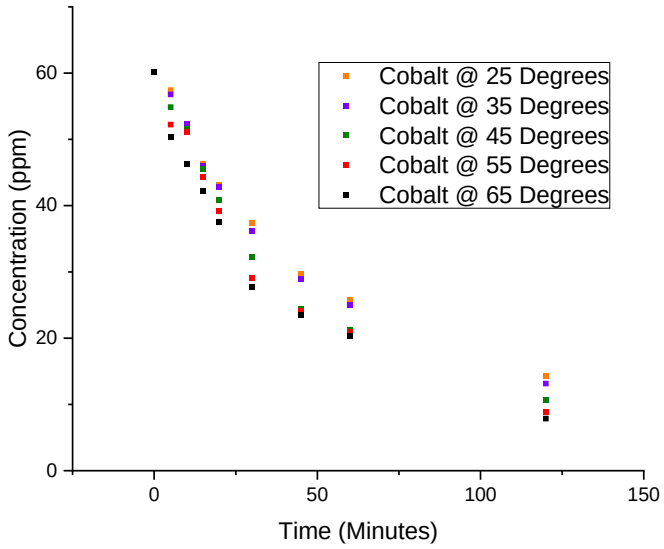

Figure 8.2.5 Cobalt Concentration against Time at 25°C, 35°C, 45°C, 55°C and 65°C.

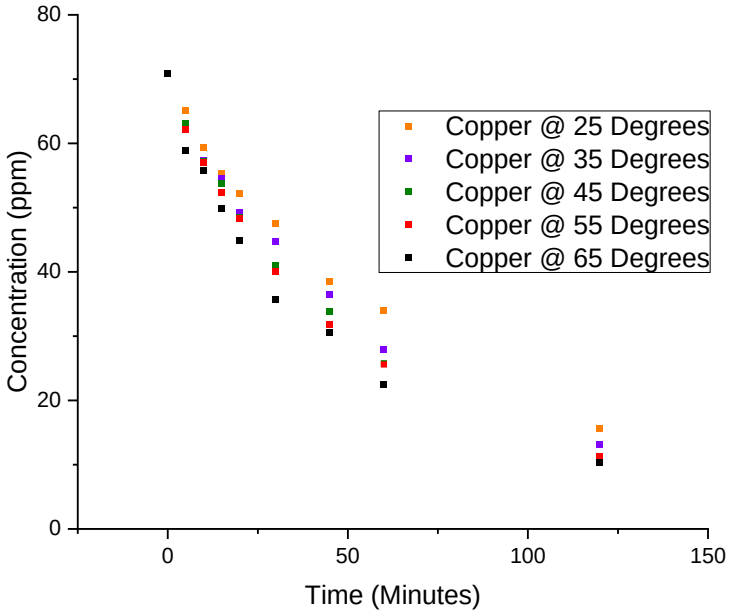

Figure 8.2.6 Copper Concentration against Time at 25°C, 35°C, 45°C, 55°C and 65°C.

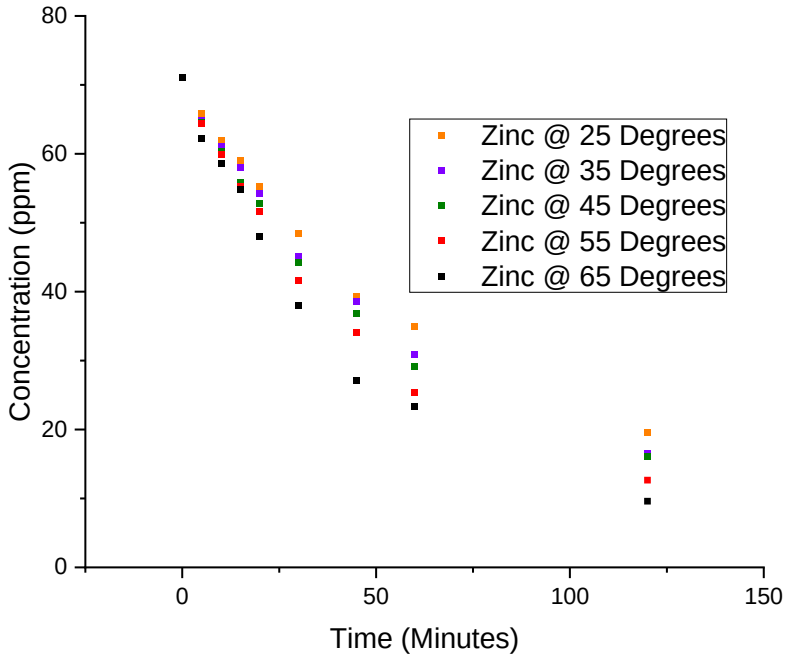

Figure 8.2.7 Zinc Concentration against Time at 25°C, 35°C, 45°C, 55°C and 65°C.

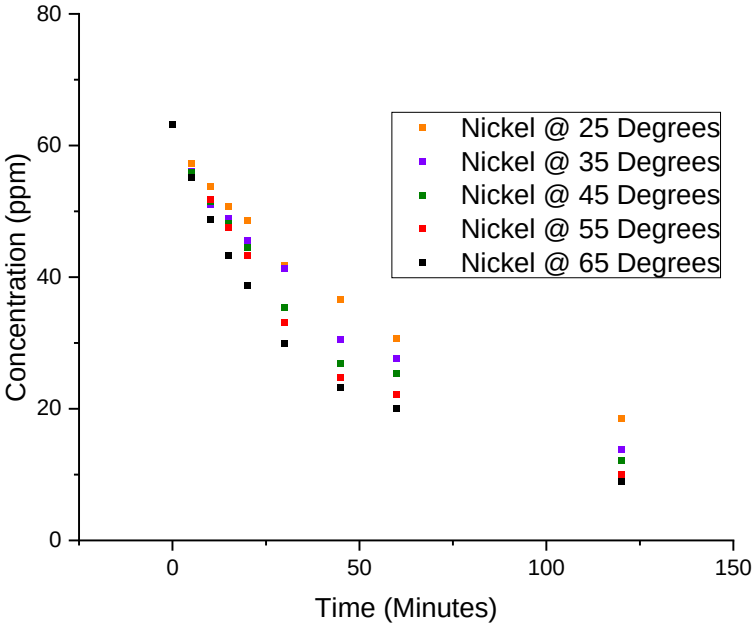

Figure 8.2.8 Nickel Concentration against Time at 25°C, 35°C, 45°C, 55°C and 65°C.

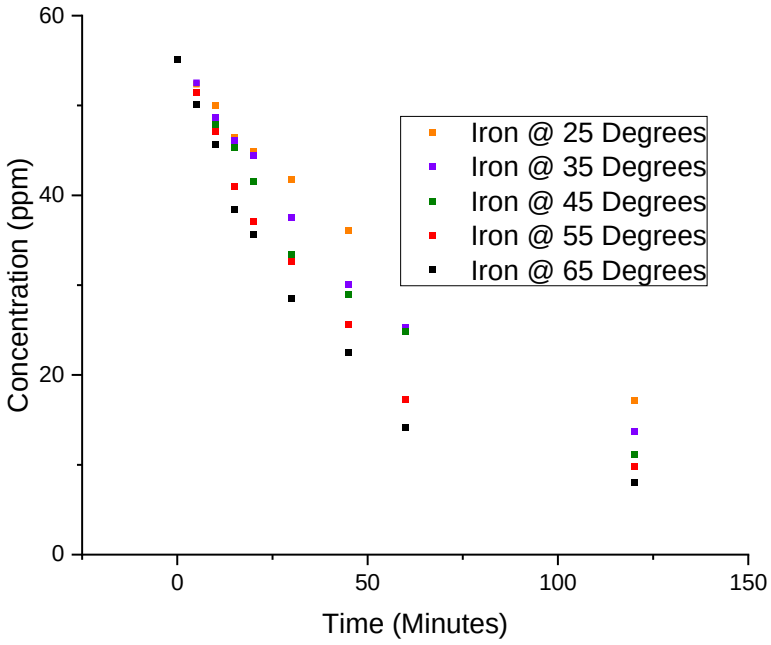

Figure 8.2.9 Iron Concentration against Time at 25℃, 35℃, 45℃, 55℃ and 65℃.

8.2.3 Transient Experiments Results (Flow Rate)

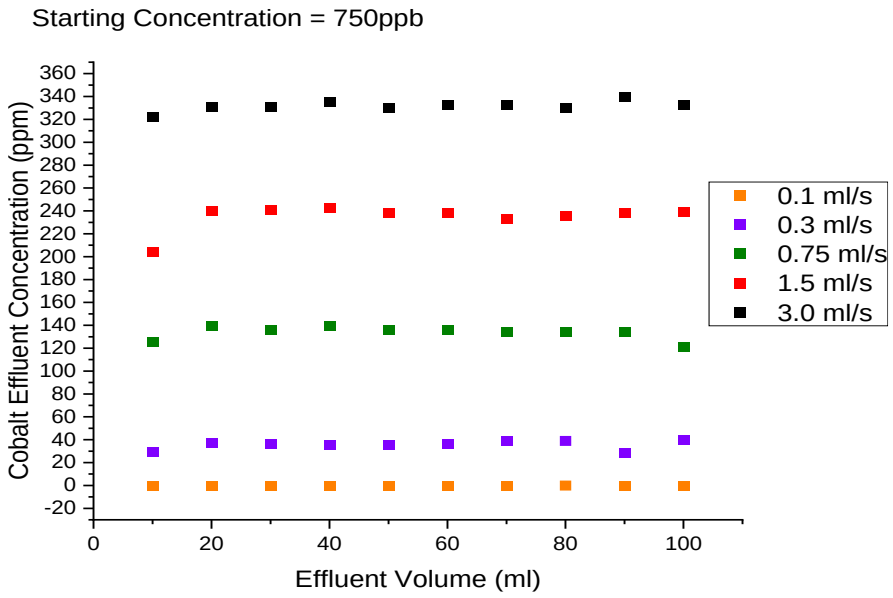

Figure 8.2.10 Cobalt effluent concentration against effluent volume at different flow rates. (Starting Concentration = 750ppb)

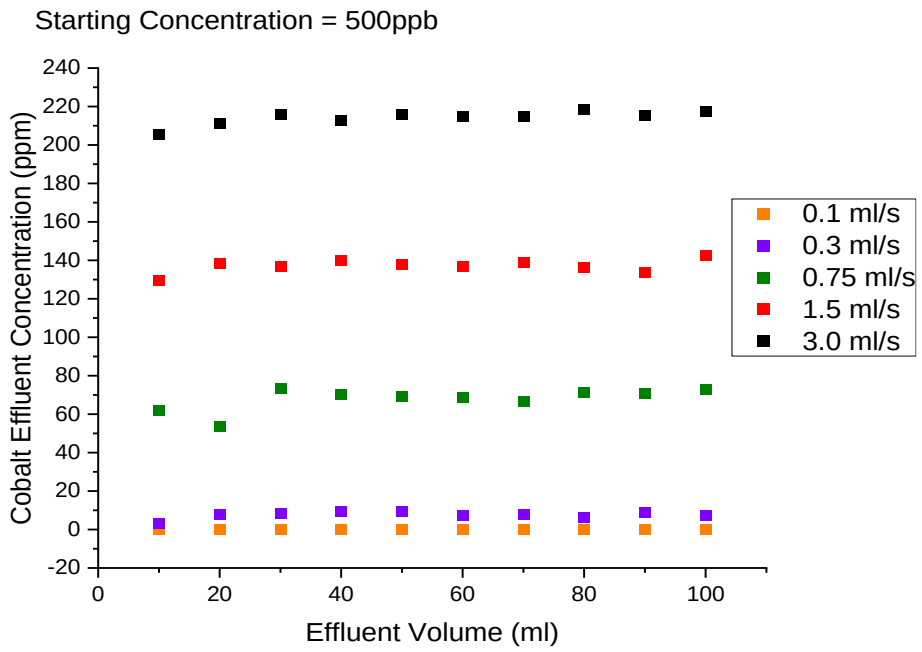

Figure 8.2.11 Cobalt effluent concentration against effluent volume at different flow rates. (Starting Concentration = 500ppb)

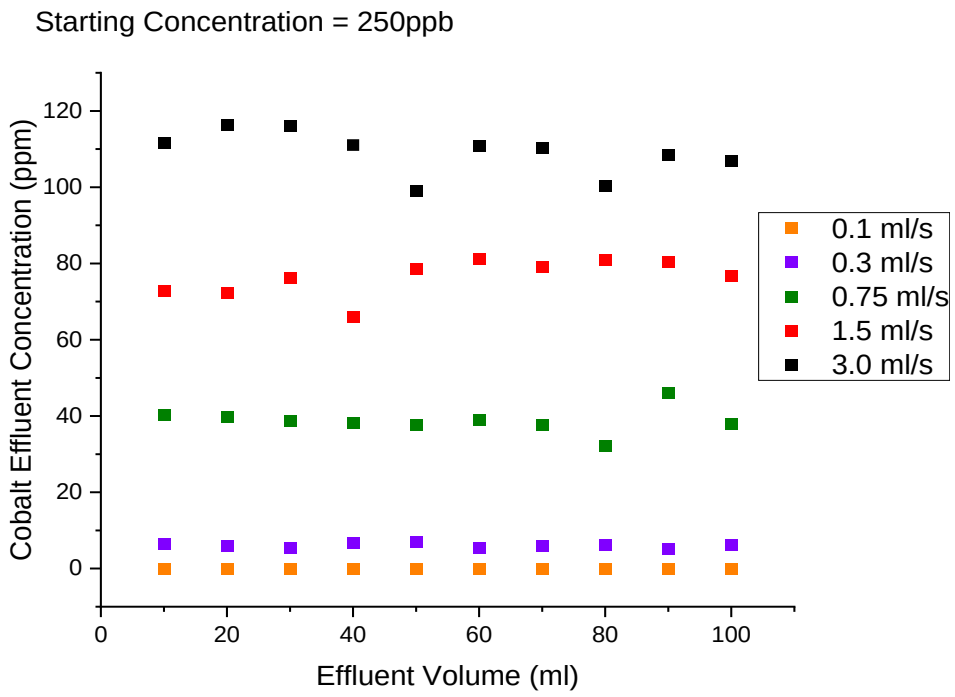

Figure 8.2.12 Cobalt effluent concentration against effluent volume at different flow rates. (Starting Concentration = 250ppb)

8.3 Chapter 5 Supplementary

8.3.1 Ion Exchange Model Walkthrough.

Opening the Model

To operate the model, the user is required to have the programs FACSIMILE4 and MATLAB installed on their personal computer. The user must also have a FACSIMILE dongle inserted into the USB slot on their personal computer.

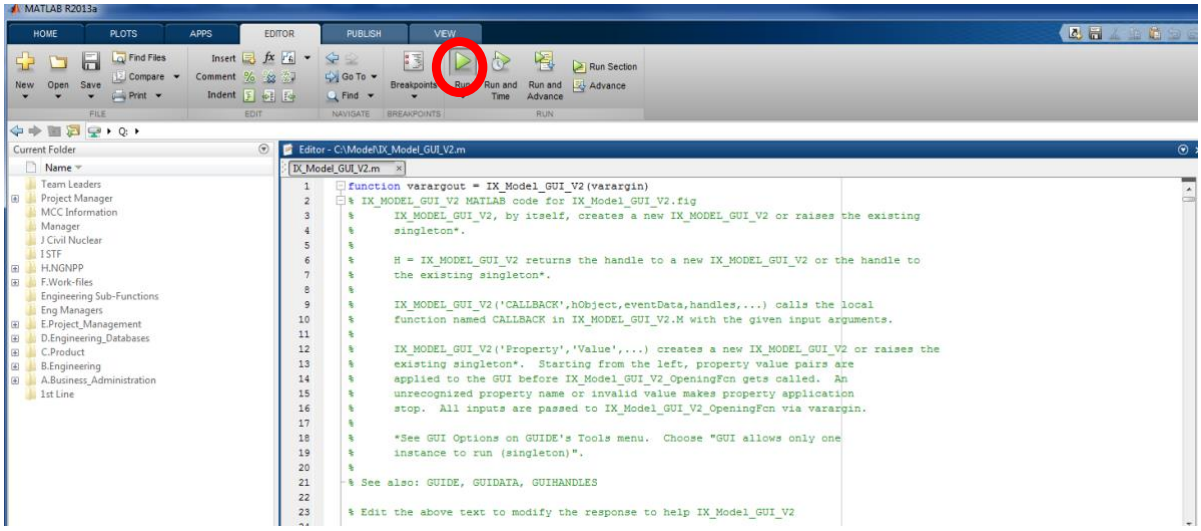

Figure 8.3.1 Open Ion Exchange Model

Pressing the highlighted green button in Figure 8.3.1 in the Ion exchange model (IXM) opens to the GUI. Here you will find the majority of inputs the user can alter. The GUI screen size cannot currently be changed by the user. The GUI should appear as shown in Figure 8.3.2.

Within the GUI the user can use the drop down menus, as shown in Figure 8.3.2, to input values for the corresponding parameter.

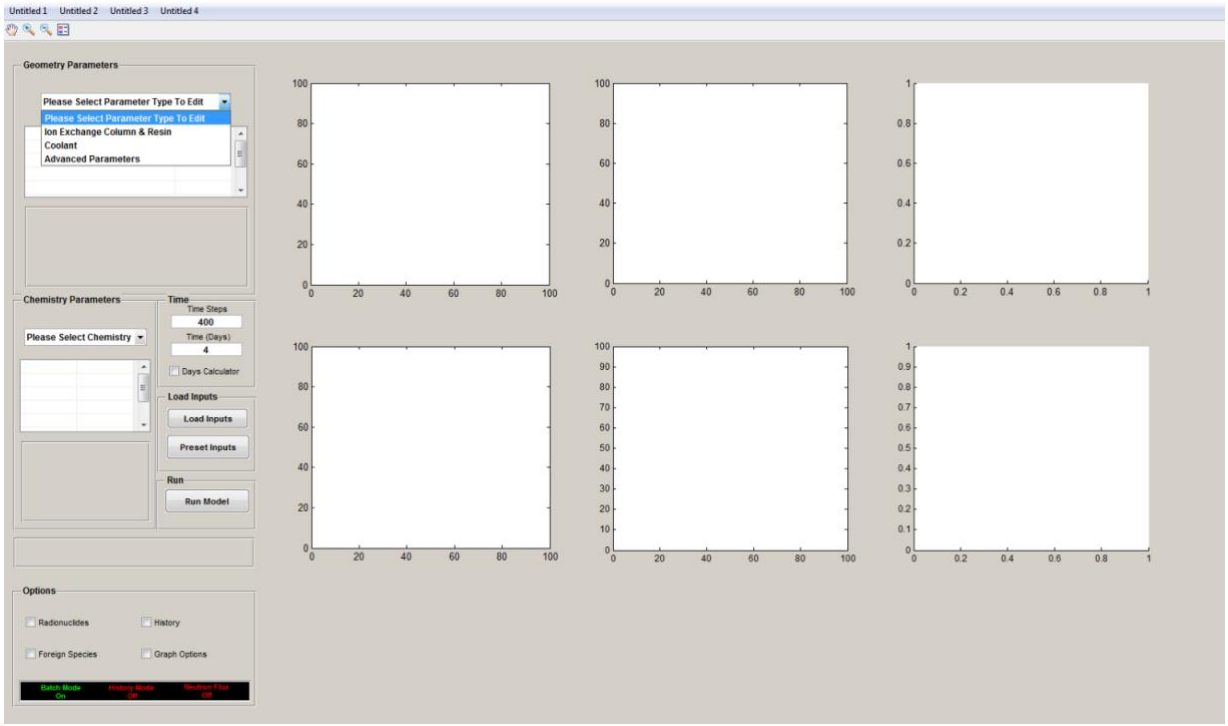

Figure 8.3.2 Ion Exchange Model Graphical User Interface Drop Down Menu

The table within the drop down menu gives details as to what each parameter does and gives details of some of the limitations the user faces when it comes to inputting values, as shown in Figure 8.3.3. The units for each of the inputs are also listed within the drop down table.

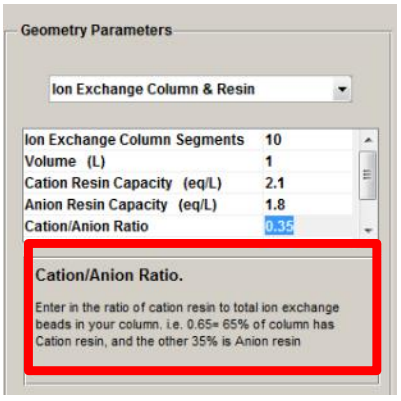

Figure 8.3.3 GUI Input Description Example

Running the Model

In order to run the model, the user must populate all batch mode inputs. The history input table must also be populated even if the model is to be run in batch mode. The user can do this manually or they can press the 'Load' button as this will populate the table with the previously saved data, as highlighted in Figure 8.3.4. Despite this requirement, the values in the table will have no impact on a calculation if the "On/Off" checkbox in the history input table are unclicked.

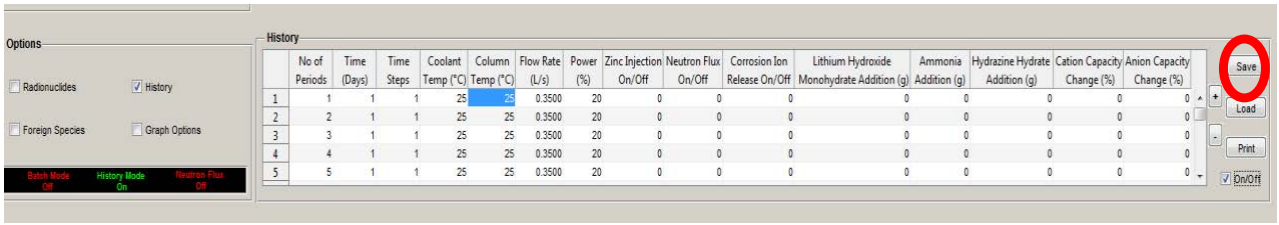

	No of Periods	Time (Days)	Time Steps	Coolant Temp (°C)	Column Temp (°C)	Flow Rate (L/s)	Power (%)	Zinc Injection On/Off	Neutron Flux On/Off	Corrosion Ion Release On/Off	Lithium Hydroxide Monohydrate Addition (g)	Ammonia Addition (g)	Hydrazine Hydrate Addition (g)	Cation Capacity Change (%)	Anion Capacity Change (%)
1	1	1	1	25	25	0.3500	20	0	0	0	0	0	0	0	0
2	2	1	1	25	25	0.3500	20	0	0	0	0	0	0	0	0
3	3	1	1	25	25	0.3500	20	0	0	0	0	0	0	0	0
4	4	1	1	25	25	0.3500	20	0	0	0	0	0	0	0	0
5	5	1	1	25	25	0.3500	20	0	0	0	0	0	0	0	0

Figure 8.3.4 Model Run Prerequisite

To auto populate values used for Batch Mode the user can press the 'Preset Inputs' button as shown in Figure 8.3.5. In this model version, this button is only to be used as to ensure all required inputs are filled; these inputs do not represent the NSRP geometry, operation or chemistry.

The 'Load Inputs' button shown in Figure 8.3.5 writes all the geometry, chemistry and time inputs for Batch Mode to the text file 'datainputs'.This is commonly used a test to ensure that the model is able to write data as the 'Run Model' button has the same functionality built in.

Once the user is confident with all the inputs, they can press the button 'Run Model'. This button will write all the inputs to text files, and use these inputs to run the FACSIMILE

model. The FACSIMILE model will then output various .txt and .out files which the GUI can read and produce a visual output.

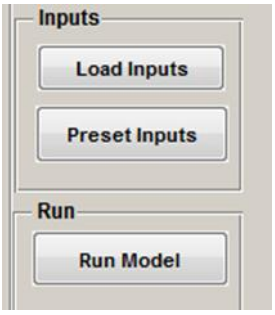

Figure 8.3.5 GUI Inputs Description

The GUI has a text display which informs the user of the progress of the model run as shown in Figure 8.3.6. Upon Pressing 'Run model' the IXM will inform the user when inputs have been loaded, when the previous run data has been cleared, when the FACSIMILE section of the model is running, and when the model has run to completion.

If the FACSIMILE model is unable to run the IXM's text display will show as seen in Figure 8.3.7. Furthermore the visual outputs in the GUI will remain blank as to not confuse the user.

The model failing to run would typically be due to the inputs being entered incorrectly. This may include leaving an input blank, or using a character as opposed to a number. The model will also fail to run, or end a run early if all reactions are in equilibrium.

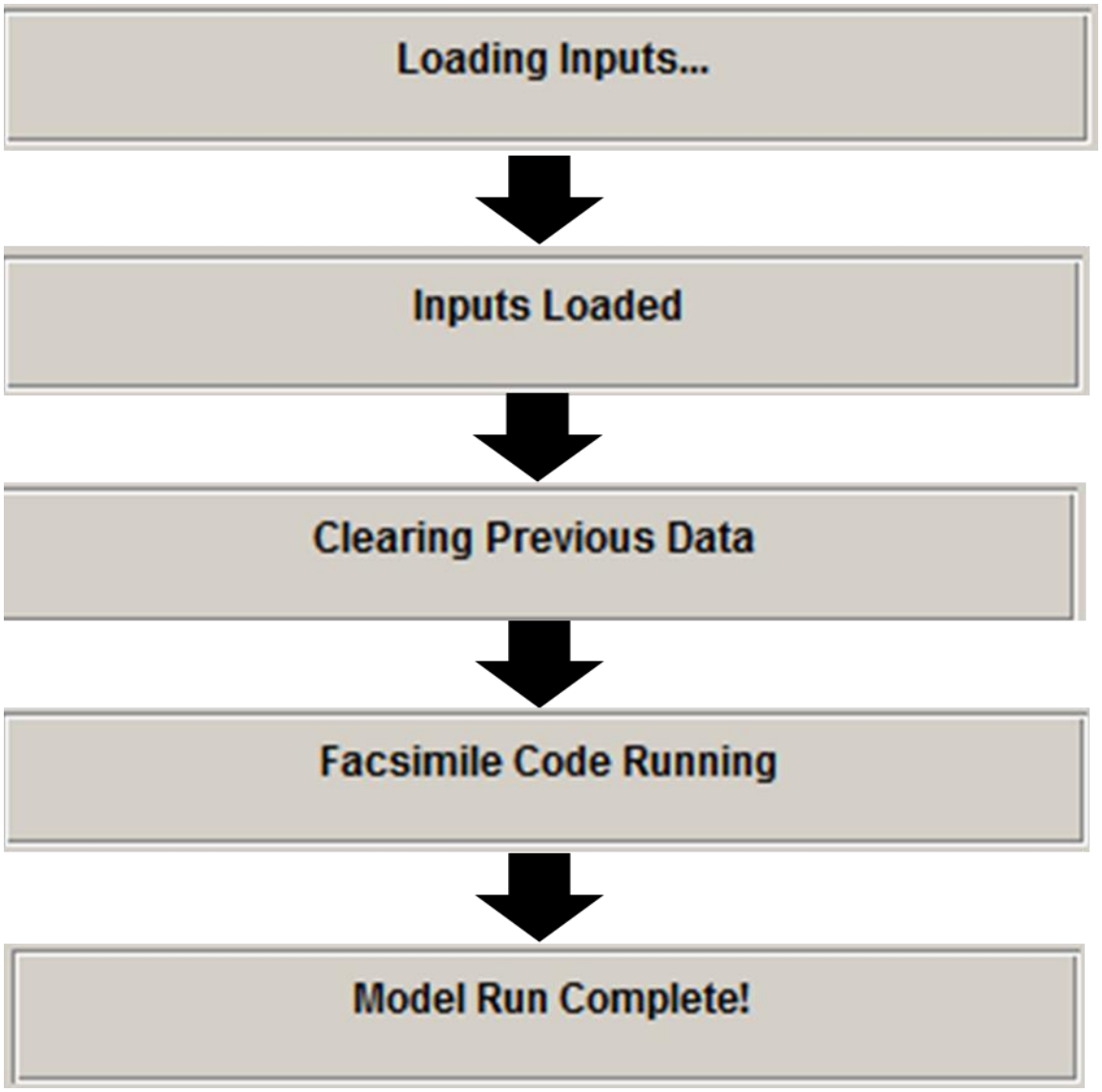

Figure 8.3.6 IXM Model Run Display

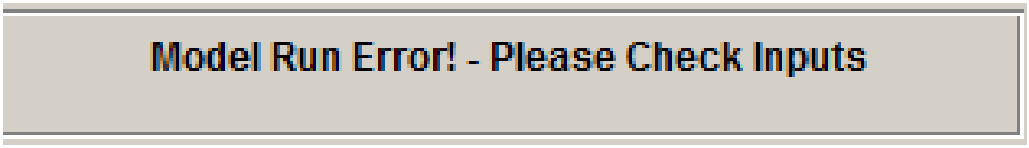

Figure 8.3.7 IXM Model Error Text Display

Interpreting Results

Once the model has run the IXM will output six visual graphs, as shown in Figure 8.3.8. The graphs are titled with what they display, and in what units, and the legends display what species are shown in the graphs.

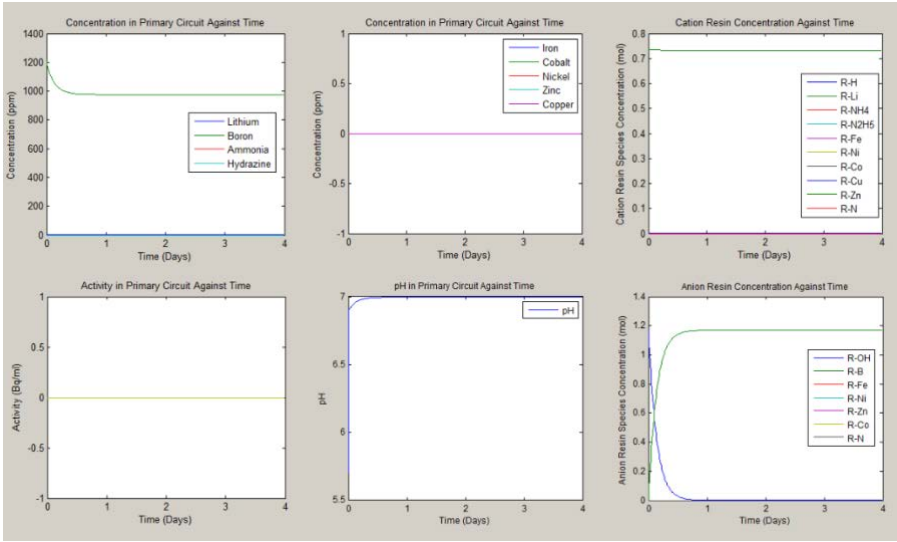

Figure 8.3.8 Ion Exchange Model Graphical User Interface Drop Down Menu

The user can further manipulate these graphs by clicking the 'Graph Options' checkbox. Within graph options, shown in Figure 8.3.9, the user can click on the 'Graph' button which corresponds to the position of the graph displayed on the GUI. Within this the user can select which species or output parameter they wish to appear on the graph. The user must click 'Display Results' once they have selected their options.

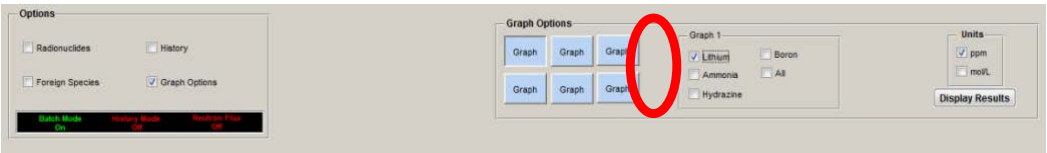

Figure 8.3.9 Graph Display Options

The two graph options for the cation and anion resin graphs, highlighted in Figure 8.3.9, are not in use for this version of IXM.

As previously mentioned, once the model runs a plethora of input and output .txt and .out files are generated. Some of these files are input files which should not be modified by the user. They are also in a format that is not easily interpreted by the user. The others are output files which can be used by the user.

The user can open these files, which contain additional data that is not displayed in the interface, and use the results to perform data manipulation in programs such as Microsoft Excel. Table 1 details which are input and output files and describes what each output file contains.

Table 8.3.1 Table of Input and Output Descriptions

Input Files	
datainputs.txt	Input file for all parameters running in Batch Mode.
foreigninputs.txt	Input file for all parameters pertaining to foreign species.
historyinputs.txt	Input file for all parameters running in History Mode.
historyinputs2.txt	A second input file for further parameters running in History Mode.

RNuclidesinputs.txt	Input file for all parameters pertaining to Radionuclides.
Output Files	
dataout_bulk.txt	This output files contains concentrations for species in the bulk coolant for every time step. Outputs have units of both ppm and mol/kg. Elemental concentrations are the total concentration of that element summed over all species. This also contains an output for pH of the bulk coolant at the inputted temperature.
Boron_Species.txt	This output files contains concentrations for specific boron species in the bulk coolant as well as potassium for every time step. Outputs have units of both ppm and mol/kg.
Foreign_Species.txt	This output files contains concentrations for all Foreign species in the bulk coolant for every time step. Outputs have units of mol/kg.
Foreign_Resin.txt	This output files contains concentrations for all Foreign species on the resin. These include concentrations for every IXC segment inputted for every time step. Outputs have units of mol, indicating the total moles on the resin.
BIXAIX.txt	This output files contains BIX and After-Ion Exchange (AIX) activities for all radionuclides for every time step. BIX activity is calculated as the sum of the activity of all

	radionuclides in the bulk. AIX activity is calculated as the sum of the activity of all radionuclides in the last element of the IXC. Outputs have units of Bq/ml. This output also contains the power, as a percentage, at every time step. **Note:** BIX and AIX values will not be directly comparable with Degassed Gross Activity values reported by submarines as not all radionuclides are included in this model.
Activity.txt	This output files contains activity for the majority of radionuclides for every time step. Outputs have units of Bq/ml.
Activity2.txt	This output files contains activity for the remaining radionuclides for every time step. Outputs have units of Bq/ml.
AIX.out	This output files contains AIX values for individual radionuclides for every time step. This file is for activated products. Outputs have units of Bq/ml.
AIX2.out	This output files contains AIX values for individual radionuclides for every time step. This file is for fission products. Outputs have units of Bq/ml.

AnionResin_mol.out	This output files contains concentrations for all species on the anion resin. These include the total concentrations for every IXC segment inputted for every time step. For species 'R-X', 'R' denotes the resin phase and 'X' denotes the species on the resin. For all 'X' species, it refers to the anion part of their speciation (i.e. R-Fe results in $FeOH_3^-$ on the resin). Outputs have units of mol.
CationResin_mol.out	This output files contains concentrations for all cationic species on the cation resin. These include the total concentrations for every IXC segment inputted for every time step. For species 'R-X', 'R' denotes the resin phase and 'X' denotes the species on the resin. For all 'X' species, it refers to the cation part of their speciation (i.e. R-Fe results in $FeOH^+$ and/or Fe^{2+} on the resin). R-N refers to sites which potentially have been damaged due to a radionuclide decays whilst adsorbed on the resin. Outputs have units of mol.

Hydrolysis_species_All.out	This output files contains concentrations for all Hydrolysis species in the coolant. These also include concentrations for the coolant in every IXC segment inputted for every time step. For each time step the first line presents the concentration in the bulk with the following lines presenting concentration for each cell through the IXC ordered in the direction of coolant flow. Outputs have units of mol.
Hydrolysis_Species_Bulk.out	This output files contains concentrations for hydrolysis species in the bulk coolant for every time step. Outputs have units of mol/kg.
IX_Resin_Species.out	This output files contains concentrations for all species on the resin. These include concentrations for every IXC segment inputted for every time step. For each time step the first line presents concentrations for the first cell in the IXC, following lines give results for cells in the order of flow. Outputs have units of mol.
RadioNucl_Conc.out	This output files contains concentrations for a number of radionuclides in the bulk coolant for every time step. Outputs have units of both ppm.
RadioNucl_Conc2.out	This output files contains concentrations for further radionuclides in the bulk coolant for every time step. Outputs have units of both ppm.

8.3.2 Effect of Time Steps on the Model.

Time steps is an important input parameter for the model. A low number for time steps will allow the model to run quickly, but the resolution of results will be poor as shown in Figure 8.3.10

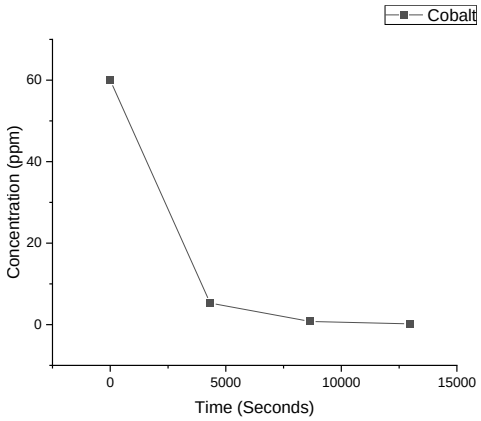

Figure 8.3.10 Basic Model Run with Low Time Steps

Figure 8.3.10 was a simple model run with a cobalt concentration, but with only 4 time steps. This will produce 4 data points at equal times until the defined run time. However when a larger number is used for time steps, it causes the model to run slower but the resolution of results is superior, as seen in Figure 8.3.11.

Figure 8.3.11 used 40 time steps and as shown the resolution is far superior. The number of time steps the user should enter depends on the length of the run and how well the user wants the results defined.

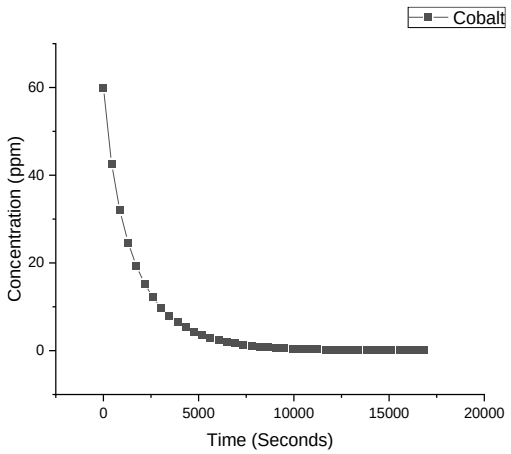

Figure 8.3.11 Basic Model Run with High Time Steps

8.3.3 FACSIMILE Ion Exchange Code*.

*Sensitive information has been blacked out.

The code used for the io exchange model begins on the next page.

```
*=======================Data Input Files=====================;
EXECUTE OPEN 16 "datainputs.txt";
EXECUTE OPEN 22 "historyinputs.txt";
EXECUTE OPEN 29 "historyinputs2.txt";
EXECUTE OPEN 25 "RNuclidesinputs.txt";
*====================================================;
*=======================Data Output Files=====================;
EXECUTE OPEN 11 "Hydrolysis_Species_Bulk.out";
EXECUTE OPEN 13 "IX_ParameterCheck.out"; 'pH Output'
EXECUTE OPEN 14 "Activity.txt"; 'Activity Conc'
EXECUTE OPEN 15 "dataout_bulk.txt"; 'Species conc in bulk'
EXECUTE OPEN 18 "IX_Resin_Species.out";
EXECUTE OPEN 19 "Hydrolysis_species_All.out";
EXECUTE OPEN 21 "RadioNucl_Conc.out";
EXECUTE OPEN 23 "IX_RadioHydrol.out";
EXECUTE OPEN 26 "Activity2.txt"; 'Activity Conc prt 2'
*====================================================;
permit +-;
*====================================================;
* time steps and number of cells in IX and circuit wkspace ;
* and time in hours - converted to secs later. ;
*time steps TIME1=time in days TIMETOT=time in seconds ;
*TINCR=Time per time step ;
*====================================================;
INTEGER
#NSTEP
#NCELL1 1
#NCELL2
#NCELL
#NWK
#NPERIODS 1
#NPOINTS
#NSWITCH 1
#READHIST
```

#NPER 0

;

PARAMETER

TIMEDAY

TIMESEC

TIMETOT

IMAXCAT

IMAXAN

VOLBULK

VOLCOL

CATCAP

ANCAP

CATRATIO

ANRATIO

Q

LiInj 0

pHInitial

FH

FLi

FNH4

FN2H5

FCo

FNi

FCu

FZn

FFe

PriCirArea

PrimCircArea

COOLANTTEMPC

COLUMNTEMPC

H0

LI0

NH30

Co0

Cu0

Ni0

Fe0

Zn0

N2H40

KOX

KDecomp1

KDecomp2

H3BO30 0

Co600 0

Co580 0

Fe590 0

```
Mn540 0
ZnInj0
ZnLB
ZnCheck
FluxCheck
CorrosionCheck
KCrCo0
KCrNi0
KCrFe0
dt
;

COMPILE INSTANT;

read 16 #NCELL2;
read 16 VOLCOL;
read 16 CATCAP;
read 16 ANCAP;
read 16 CATRATIO;
read 16 VOLBULK;
read 16 COOLANTTEMPC;
read 16 COLUMNTEMPC;
read 16 pHInitial;
read 16 Q;
read 16 TimeDay;
read 16 #NSTEP;
read 16 FH;
read 16 FLi;
read 16 FNH4;
read 16 FN2H5;
read 16 FFe;
read 16 FZn;
read 16 FNi;
read 16 FCO;
read 16 FCu;
read 16 H0;
read 16 Li0;
read 16 NH30;
read 16 N2H40;
read 16 Fe0;
read 16 Zn0;
read 16 Ni0;
read 16 Co0;
read 16 Cu0;
read 16 PriCirArea;
read 16 ZnLB;
```

```
read 16 ZnInj0;
read 16 ZnCheck;
read 16 FluxCheck;
read 16 CorrosionCheck;
read 16 KCrCo0;
read 16 KCrNi0;
read 16 KCrFe0;
read 16 #READHIST;
#NPOINTS = #NSTEP;
IMAXCAT=CATCAP*CATRATIO*VOLCOL;
ANRATIO=1 - CATRATIO;
IMAXAN=ANCAP*ANRATIO*VOLCOL;
TIMESEC=TIMEDAY*3600*24;
TIMETOT=TIMESEC;
**;
*====================================
==========================;
* Radionuclides Parameters                    ;
*====================================
==========================;
PARAMETER
POWER
PRODRATE
YI131
YI132
YI133
YI134
YI135
YCs134
YCs137
YCs138
YXe133
YXe135
YXe138
YTe131
YTe132
YTe133
YTe134
YTe135
RNRATE
;
COMPILE INSTANT;
READ 25 POWER;
READ 25 PRODRATE;
READ 25 YI131;
READ 25 YI132;
```

```
READ 25 YI133;
READ 25 YI134;
READ 25 YI135;
READ 25 YCs134;
READ 25 YCs137;
READ 25 YCs138;
READ 25 YXe133;
READ 25 YXe135;
READ 25 YXe138;
READ 25 YTe131;
READ 25 YTe132;
READ 25 YTe133;
READ 25 YTe134;
READ 25 YTe135;
**;


*===================================
==========================;
* History Parameters                    ;
*===================================
==========================;
COMPILE INSTANT;
if <#READHIST - 1> 90 90 *;
read 22 #NPERIODS;
read 22 #NPOINTS;
#NSWITCH = #NPERIODS;
label 90;
**;
PARAMETER <#NPOINTS> settime powtime
settime2 powtime2;
PARAMETER <#NSWITCH> switch;
PARAMETER <#NPERIODS> Hpower FlowRate
CoolTemp ColmnTemp
ZincInjCk FluxCk CorrosionCk ;
PARAMETER pow;
COMPILE INSTANT;
if <#READHIST - 1> 93 93 *;
read 22 settime;
read 22 powtime;
read 22 switch;
read 22 Hpower;
read 22 flowrate;
read 22 CoolTemp;
read 22 ColmnTemp;
read 22 ZincInjCk;
```

```
read 22 FluxCk;

read 22 CorrosionCk;

pow = Hpower<0>;

label 93;

if <#READHIST - 1> 91 * 91;

pow = POWER;

switch<0> = 0;

read 29 settime;

read 29 powtime;

Write 1=28,"swtich", ((E14,3)) switch;

Write 1=28,"settime", ((E14,3)) settime;

label 91;

**;

*====================================
==========================;

* calculate total number of cells                ;

*====================================
==========================;

compile instant;

#NCELL=#NCELL1 + #NCELL2;

#NWK=30000*#NCELL;

**;

*====================================
==========================;

* calculated  parameters                         ;

*====================================
==========================;

PARAMETER TINCR;

PARAMETER<#NSTEP> OUTT1;

PARAMETER ENDRUN;

*====================================
==========================;

* define chemical species                        ;

*====================================
==========================;

VARIABLE<#NCELL> H+ H2 OH- Li+ NH4+ NH3
N2H4 N2H5+ LiOH

RH ROH RLi RNH4 RN2H5

Cu+2 CuOH+ CuOH2 CuOH3-

RRCu RCuOH RCuOH3

Fe+2 FeOH+ FeOH2 FeOH3-

RRFe RFeOH RFeOH3 FeTot

Co+2 CoOH+ CoOH2

RRCo  RCoOH

Ni+2 NiOH+ NiOH2 NiOH3-

RRNi RNIOH  RNiOH3 NiTot

Zn+2 ZnOH+ ZnOH2 ZnOH3- ZnOH42-

RRZn RZnOH RZnOH3 RRZnOH4
```

H3BO3 BOH4- B2OOH5- B3O3OH4- B4O2OH8

RBOH4 RB2OOH5 RB3O3OH4

Co60 Co60OH+ Co60OH2

RRCo60 RCo60OH

Ni58 Ni58OH+ Ni58OH2 Ni58OH3-

RRNi58 RNi58OH RNi58OH3

Co58 Co58OH+ Co58OH2

RRCo58 RCo58OH RCo58OH3

Fe58 Fe58OH+ Fe58OH2 Fe58OH3-

RRFe58 RFe58OH RFe58OH3

Fe54 Fe54OH+ Fe54OH2 Fe54OH3-

RRFe54 RFe54OH RFe54OH3

Fe59 Fe59OH+ Fe59OH2 Fe59OH3-

RRFe59 RFe59OH RFe59OH3

Mn54 Mn54OH+ Mn54OH2 Mn54OH3-

Cr54 Cr54OH+ Cr54OH2 Cr54OH3-

RRMn54 RMn54OH RMn54OH3

RRCr54 RCr54OH RCr54OH3

I131 I132 I133 I134 I135

RI131 RI132 RI133 RI134 RI135

Cs134 Cs137 Cs138

RCs134 RCs137 RCs138

Te131 Te132 Te133 Te134 Te135

RTe131 RTe132 RTe133 RTe134 RTe135

Xe133 Xe135 Xe138

RN

;

*==========

==========;

* temperatures and equilibria and rates ;

*==========

==========;

parameter<#NCELL> Kw KFe1 KFe2 KFe3 KCo1 KCo2 KCo3 KNi1 KNi2

KNi3 KZn1 KZn2 KZn3 KZn4 KCu1 KCu2 KCu3 H2O KLi KNH3 KF KF0

KMAG KMod1 KMod2 KMod3

H2O KN2H4 KBO31 KBO32 KBO33 KBO34 KLIOH KNH3 SOLH2 KFe3O4 KNi1c KNi2c

KNi3c

TEMPK DW COOLANTTEMPK COLUMNTEMPK TF Qdw Qdw1 Qdw2 Qdw3 Qdw4 Qdw5

thermalnflux fastnflux

Co60lambda Co59Xsect Co58lambda Ni58Xsect Mn54lambda Fe54Xsect

```
Fe59lambda Fe58Xsect KCoProd KNiProd
KZnProd KFeProd KCuProd KAc
kco21 kco22
I131lambda I132lambda I133lambda
I134lambda I135lambda
Cs134lambda Cs137lambda Cs138lambda
Xe133lambda Xe135lambda Xe138lambda
Te131lambda Te132lambda Te133lambda
Te134lambda Te135lambda;
*====================================
==========================;
* Corrosion Rates                    ;
*====================================
==========================;

parameter<#NCELL> KCrCo KCrNi KCrFe;

*====================================
==========================;
*molecular weights & Avagadro Constant
;
*====================================
==========================;
PARAMETER MWLi 6.9999 MWO 16 MWH 1
MwCo60 60 MwCo 59 MwCo58 58
MwNi58 58 MwNi 58.69
MwFe58 58 MwFe59 59 MwFe54 54 MwFe 55.85
MWZn 65.38 MWCu 63.546 MWNH3 17
MWN2H4 3
MWH3BO3 61.83 MWB 10.8110 MWLiOH 24
MWH2 2.01588 MWMn 54.938
MWZnOAc2 182 NAvo 6.022E23 MwFe3O4
231.55 MWNiO 74
MWNiFe2O4 235
MWI131 131 MWI132 132 MWI133 133 MWI134
134 MWI135 135
MWCs134 134 MWCs137 137 MWCs138 138
MWXe133 133 MWXe135 135 MWXe138 138
MWTe131 131 MWTe132 132 MWTe133 133
MWTe134 134 MWTe135 135
MWCr 54;

*====================================
==========================;
* work array                         ;
*====================================
==========================;
parameter<#NWK> WKSPACE;
```

```
*===================================
==========================;

* Delta S, Delta H, Arhenius Prefactor, Activation
Energy and ;

* Rate Constant Values determined
experimentally. ;

* rate KM and selectivity coefficent. ;

*===================================
==========================;

PARAMETER

FeDS 32.0571212 ZnDS 42.5876336 NiDS
39.6062332 CoDS 40.2281204

CuDS 52.1520592

FeDH 2823.8501 ZnDH 6213.0522 NiDH
3870.91526 CoDH 4724.26422

CuDH 7154.11386

RGasC 8.314

KRLI 0.68 KRNH4 1.85 KRN2H5 1.85 KRBO4 9.0


KRI 1 KRCs 1 KrTe 1

KM 1.7E-2

KRFE KRZn KRNi KRCo KRCu

FeArh 37.903 ZnArh 6.608 NiArh 12.763 CoArh
4.075 CuArh 0.752

FeEa 17432.8783 ZnEa 14923.9626 NiEa
16169.3166

CoEa 11924.6039 CuEa 9753.1534

KRES KRESLi KRESCo KRESFe KRESCu KRESZn
KRESNi;

*===================================
==========================;

* routine to Calculate Temperature based
Selectivity ;

*===================================
==========================;

Compile Selectivity;

KRCo = (CoDS/RGasC) - ((CoDH/RGasC) *
(1/(COLUMNTEMPC + 273.15)));

KRCo = EXP(KRCo);

KRCu = (CuDS/RGasC) - ((CuDH/RGasC) *
(1/(COLUMNTEMPC + 273.15)));

KRCu = EXP(KRCu);

KRZn = (ZnDS/RGasC) - ((ZnDH/RGasC) *
(1/(COLUMNTEMPC + 273.15)));

KRZn = EXP(KRZn);

KRNi = (NiDS/RGasC) - ((NiDH/RGasC) *
(1/(COLUMNTEMPC + 273.15)));

KRNi = EXP(KRNi);
```

```
KRFe = (FeDS/RGasC) - ((FeDH/RGasC) * (1/(COLUMNTEMPC + 273.15)));

KRFe = EXP(KRFe);

KRES = 1.473698E-1;

KRESLi = 1.473698E-1;

KRESCo = LOG(CoArh) - ((CoEa/RGasC) * (1/(COLUMNTEMPC + 273.15)));

KRESCo = EXP(KRESCo);

KRESFe = LOG(FeArh) - ((FeEa/RGasC) * (1/(COLUMNTEMPC + 273.15)));

KRESFe = EXP(KRESFe);

KRESCu = LOG(CuArh) - ((CuEa/RGasC) * (1/(COLUMNTEMPC + 273.15)));

KRESCu = EXP(KRESCu);

KRESZn = LOG(ZnArh) - ((ZnEa/RGasC) * (1/(COLUMNTEMPC + 273.15)));

KRESZn = EXP(KRESZn);

KRESNi = LOG(NiArh) - ((NiEa/RGasC) * (1/(COLUMNTEMPC + 273.15)));

KRESNi = EXP(KRESNi);

**;

*=================================
==========================;

* routine to calculate Temperature based array in Kelvin ;

*=================================
==========================;

compile Temperature;

array<#NCELL> WKSPACE;

COOLANTTEMPK=COOLANTTEMPC + 273.15;

TF=647.25 - COOLANTTEMPK;

COLUMNTEMPK=COLUMNTEMPC + 273.15;

TF=647.25 - COOLANTTEMPK;

TEMPK = COLUMNTEMPK;

array end;

TEMPK<0> = COOLANTTEMPK<0>;

array<#NCELL> WKSPACE;

TF=647.25 - TEMPK;

array end;

**;

*=================================
==========================;

* routine to calculate array based and initial parameters ;

*=================================
==========================;

compile Instant;

KRCo = (CoDS/RGasC) - ((CoDH/RGasC) * (1/(COLUMNTEMPC + 273.15)));
```

```
KRCo = EXP(KRCo);

KRCu = (CuDS/RGasC) - ((CuDH/RGasC) * (1/(COLUMNTEMPC + 273.15)));

KRCu = EXP(KRCu);

KRZn = (ZnDS/RGasC) - ((ZnDH/RGasC) * (1/(COLUMNTEMPC + 273.15)));

KRZn = EXP(KRZn);

KRNi = (NiDS/RGasC) - ((NiDH/RGasC) * (1/(COLUMNTEMPC + 273.15)));

KRNi = EXP(KRNi);

KRFe = (FeDS/RGasC) - ((FeDH/RGasC) * (1/(COLUMNTEMPC + 273.15)));

KRFe = EXP(KRFe);

KRES = 1.473698E-1;

KRESLi = 1.473698E-1;

KRESCo = LOG(CoArh) - ((CoEa/RGasC) * (1/(COLUMNTEMPC + 273.15)));

KRESCo = EXP(KRESCo);

KRESFe = LOG(FeArh) - ((FeEa/RGasC) * (1/(COLUMNTEMPC + 273.15)));

KRESFe = EXP(KRESFe);

KRESCu = LOG(CuArh) - ((CuEa/RGasC) * (1/(COLUMNTEMPC + 273.15)));

KRESCu = EXP(KRESCu);

KRESZn = LOG(ZnArh) - ((ZnEa/RGasC) * (1/(COLUMNTEMPC + 273.15)));

KRESZn = EXP(KRESZn);

KRESNi = LOG(NiArh) - ((NiEa/RGasC) * (1/(COLUMNTEMPC + 273.15)));

KRESNi = EXP(KRESNi);

array<#NCELL> WKSPACE;

COOLANTTEMPK=COOLANTTEMPC + 273.15;

TF=647.25 - COOLANTTEMPK;

COLUMNTEMPK=COLUMNTEMPC + 273.15;

TF=647.25 - COOLANTTEMPK;

TEMPK = COLUMNTEMPK;

array end;

TEMPK<0> = COOLANTTEMPK<0>;

array<#NCELL> WKSPACE;

TF=647.25 - TEMPK;

*Temperature Dependent Reaction Rates;

KF = 1E3;

KF0 = 1E7;

*==================================
==========================;

*Neutron Flux Values with Half Lives & Cross Sections ;
```

```
*===================================
==========================;
thermalnflux = 0;
fastnflux = 0;

*Half life of 5.271 years;
Co60lambda = 4.1699E-9;
Co59XSect = 37.1E-24;
*Half life of 71 Days;
Co58lambda = 1.1299E-7;
Ni58XSect = 0.1422E-24;
*Half life of 312 Days;
Mn54lambda = 2.5713E-8;
Fe54Xsect = 0.0758E-24;
*Half life of 44.5 Days;
Fe59lambda = 1.8028E-7;
Fe58Xsect = 2.5E-24;

I131lambda = 9.98E-7;
I132lambda = 8.37E-5;
I133lambda = 9.257E-6;
I134lambda = 2.196E-4;
I135lambda = 2.917E-5;
Cs134lambda = 1.098E-8;
Cs137lambda = 7.322E-10;
Cs138lambda = 3.59E-4;
Xe133lambda = 1.5301E-6;
Xe135lambda = 2.1158E-5;
Xe138lambda = 8.19E-4;
Te131lambda = 4.621E-4;
Te132lambda = 2.588E-6;
Te133lambda = 2.085E-4;
Te134lambda = 2.751E-4;
Te135lambda = 3.648E-2;

*===================================
==========================;
* routine to calculate Temperature Based Rates
;
*===================================
==========================;

RNRATE = PRODRATE * POW/100;
KOX = (-3063/COOLANTTEMPK) + 5.21;
KOX = 2.718@(KOX);
KOX = KOX/60;
*set equilibria coefficients;
```

```
H2O=1;
dw = 1 + 0.1342489*TF@(1/3) - 3.946263e-
3*TF;
dw = dw/(3.1975 - 0.3151548*(TF@(1/3)) -
(1.203374e-3)*TF
   + (7.489081e-13)*TF@4);
kw = 10@(-4.098 - 3245.2/TEMPK +
2.2362e5/TEMPK**2 -
    3.984e7/TEMPK**3 + (13.957 -
1262.3/TEMPK +
    8.5641e5/TEMPK**2)*log10(dw));
*====================================
==========================;
* Temp Dependent Equilibrium constants from
MULTEQ Manual    ;
*====================================
==========================;
KLIOH =
KNH3 =
KN2H4 =
KBO31
KBO32
KBO33 =
KBO34 =
KFe1=
KFe2=
```

KFe3 =

KCo1=

KCo2=

KNi1=

KNi2=

KNi3=

KZn1=

KZn2=

KZn3=

KZn4=

KCu1=

KCu2=

KCu3=

ARRAY END;

```
**;

*====================================
==========================;
* routine to calculate Temperature Based Rates
;
*====================================
==========================;
Compile Rates;

array<#NCELL> WKSPACE;
RNRATE = PRODRATE * POW/100;

*set equilibria coefficients;

H2O=1;

dw = 1 + 0.1342489*TF@(1/3) - 3.946263e-
3*TF;

dw = dw/(3.1975 - 0.3151548*(TF@(1/3)) -
(1.203374e-3)*TF
    + (7.489081e-13)*TF@4);

kw = 10@(-4.098 - 3245.2/TEMPK +
2.2362e5/TEMPK**2 -
    3.984e7/TEMPK**3 + (13.957 -
1262.3/TEMPK +
    8.5641e5/TEMPK**2)*log10(dw));

*====================================
==========================;
* Temp Dependent Equilibrium constants from
MULTEQ Manual  ;
*====================================
==========================;

KLIOH = [redacted]

KNH3 = [redacted]
```

KN2H4 =

KBO31

KBO32

KBO33 =

KBO34 =

KFe1=

KFe2=

KFe3 =

KCo1=

KCo2=

KNi1=

KNi2=

KNi3=

KZn1=

KZn2=

[redacted]

KZn3= [redacted]

[redacted]

KZn4= [redacted]

[redacted]

[redacted]

KCu1= [redacted]

[redacted]

[redacted]

KCu2= [redacted]

[redacted]

[redacted]

[redacted]

KCu3= [redacted]

[redacted]

[redacted]

[redacted]

array end;

**;

*==========

==========;

*calculate mol/kg (Molality) ;

*==========

==========;

Compile Instant;

array<#NCELL> WKSPACE;

H+<0> = H0;

Li+=0;

LiOH=(LI0/((1.0E6) - LI0)*1000/MWLI);

NH3=(NH30/((1.0E6) - NH30)*1000/MWNH3);

N2H4=(N2H40/((1e6) -
N2H40)*1000/MWN2H4);

H3BO3=(H3BO30/((1e6) -
H3BO30)*1000/MWB);

CoOH2=(Co0/((1e6) - Co0)*1000/MwCo);

*Done to split into the isotope abundancies;

NiTot=((Ni0/((1e6) - Ni0)*1000/MwNi));

NiOH2=(1 - 0.68077)*NiTot;

```
Ni58OH2=0.68077*NiTot;


FeTot=(Fe0/((1e6) - Fe0)*1000/MwFe);

FeOH2=FeTot*(1 - 0.05845 - 0.00282);

Fe58OH2=FeTot*0.00282;

Fe54OH2=FeTot*0.05845;

ZnOH2=(Zn0/((1e6) - Zn0)*1000/MwZn);

CuOH2=(Cu0/((1e6) - Cu0)*1000/MwCu);

*====================================
==========================;

*Production term for metal ions. i.e. from ion release from CP ;

*====================================
==========================;

*currently set to 0, and changes if corrosion checkbox is checked;

KCrCo = 0;

KCrNi = 0;

KCrFe = 0;

array end;

**;

*====================================
============================;


* calculate time steps and cell volumes and initialise variables ;

*====================================
============================;

*define cell volume array;

parameter<#NCELL> CELLVOL TRFAC DUMMY;

COMPILE INSTANT;


* Compute time step for output;

TINCR = TIMETOT/FLOAT(#NSTEP - 1);

* fill time based arrays with output times;

DO 1 FOR #1=0(1)(#NSTEP - 1) ;

  outt1<#1> = TINCR*FLOAT(#1) ;

LABEL 1 ;

DO 2 FOR #2=(#NSTEP - 1) ;

  ENDRUN = TINCR*FLOAT(#2) ;

LABEL 2 ;

ARRAY<#NCELL> WKSPACE;

CELLVOL=(dw*VOLCOL)/FLOAT(#NCELL2);

*Conversion to Mass Flow Rate (kg/s);

Qdw = Q*dw;

TRFAC=Qdw;

KR=(1.0 - EPS)*3*KM/(EPS*RAD);
```

```
dummy=0.0;

RH=(FH*IMAXCAT)/(VOLCOL*dw<1>);

RLi=(FLi*IMAXCAT)/(VOLCOL*dw<1>);

RNH4=(FNH4*IMAXCAT)/(VOLCOL*dw<1>);

RN2H5=(FN2H5*IMAXCAT)/(VOLCOL*dw<1>);

RRCo=(FCo*IMAXCAT)/(VOLCOL*dw<1>);

RRCu=(FCu*IMAXCAT)/(VOLCOL*dw<1>);

RRFe=(FFe*IMAXCAT)/(VOLCOL*dw<1>);

RRZn=(FZn*IMAXCAT)/(VOLCOL*dw<1>);

RRNi=(FNi*IMAXCAT)/(VOLCOL*dw<1>);

ROH=IMAXAN/(VOLCOL*dw<1>);

H+ = KW@0.5;

OH- = KW@0.5;

ARRAY END;

*SETS RESIN CONC IN BULK;

DO 9 FOR #3=0(1)(#NCELL1 - 1);

CELLVOL<#3>=(dw<0>*VOLBULK)/float(#NCE
LL1);

*KR<#3>=0;

*no resin in first cells;

RN<#3>=0;

RH<#3>=0;

ROH<#3>=0;

RLi<#3>=0;

RNH4<#3>=0;

RN2H5<#3>=0;

RRFe<#3>=0;

RFeOH<#3>=0;

RFeOH3<#3>=0;

RRFe58<#3>=0;

RFe58OH<#3>=0;

RFe58OH3<#3>=0;

RRFe54<#3>=0;

RFe54OH<#3>=0;

RFe54OH3<#3>=0;

RRMn54<#3>=0;

RMn54OH<#3>=0;

RMn54OH3<#3>=0;

RRCr54<#3>=0;

RCr54OH<#3>=0;

RCr54OH3<#3>=0;

RRCo<#3>=0;

RCoOH<#3>=0;

RRCo60<#3>=0;

RCo60OH<#3>=0;

RRCo58<#3>=0;
```

```
RCo58OH<#3>=0;
RRNi<#3>=0;
RNIOH<#3>=0;
RNiOH3<#3>=0;
RRNi58<#3>=0;
RNi58OH<#3>=0;
RNi58OH3<#3>=0;
RRZn<#3>=0;
RZnOH<#3>=0;
RZnOH3<#3>=0;
RRZnOH4<#3>=0;
RRCu<#3>=0;
RCuOH<#3>=0;
RCuOH3<#3>=0;
RBOH4<#3>=0;
RB2OOH5<#3>=0;
RB3O3OH4<#3>=0;
LABEL 9;
*Sets species in column to 0;
DO 10 FOR #9=1(1)(#NCELL - 1);
* H+<#9>=0;
* H2<#9>=0;
* OH-<#9>=0;
Li+<#9>=0;
LiOH<#9>=0;
NH3<#9>=0;
NH4+<#9>=0;
N2H4<#9>=0;
N2H5+<#9>=0;
Fe+2<#9>=0;
FeOH+<#9>=0;
FeOH2<#9>=0;
FeOH3-<#9>=0;
Fe58<#9>=0;
Fe58OH+<#9>=0;
Fe58OH2<#9>=0;
Fe58OH3-<#9>=0;
Fe54<#9>=0;
Fe54OH+<#9>=0;
Fe54OH2<#9>=0;
Fe54OH3-<#9>=0;
Mn54<#9>=0;
Mn54OH+<#9>=0;
Mn54OH2<#9>=0;
Mn54OH3-<#9>=0;
Cr54<#9>=0;
```

```
Cr54OH+<#9>=0;
Cr54OH2<#9>=0;
Cr54OH3-<#9>=0;
Co+2<#9>=0;
CoOH+<#9>=0;
CoOH2<#9>=0;
Co60<#9>=0;
Co60OH+<#9>=0;
Co60OH2<#9>=0;
Co58<#9>=0;
Co58OH+<#9>=0;
Co58OH2<#9>=0;
Ni+2<#9>=0;
NIOH+<#9>=0;
NiOH2<#9>=0;
NiOH3-<#9>=0;
Ni58<#9>=0;
NI58OH+<#9>=0;
Ni58OH2<#9>=0;
Ni58OH3-<#9>=0;
Zn+2<#9>=0;
ZnOH+<#9>=0;
ZnOH2<#9>=0;
ZnOH3-<#9>=0;
ZnOH42-<#9>=0;
Cu+2<#9>=0;
CuOH+<#9>=0;
CuOH2<#9>=0;
CuOH3-<#9>=0;
ZnOAc2<#9>=0;
LABEL 10;
**;
COMPILE EQUATIONS;
ARRAY<#NCELL> WKSPACE;
*====================================
==========================;
*Water and Acid/Base Equilibrium Chemistry
;
*====================================
==========================;
%kf0 %kf0/Kw   : H2O = H+ + OH-;
%kf %kf/KLIOH : LiOH = Li+ + OH-;
%kf %kf/KNH3  : NH3 + H+ = NH4+;
*====================================
==========================;
*Boric Acid Equilibrium Chemistry                ;
```

*==========
==========;

%kf %kf/KBO31 : H3BO3 + OH- = BOH4-;

%kf %kf/KBO32 : H3BO3 + H3BO3 + OH- = B2OOH5- + H2O;

%kf %kf/KBO33 : H3BO3 + H3BO3 + H3BO3 + OH- =B3O3OH4- + H2O + H2O + H2O;

%kf %kf/KBO34 : H3BO3 + H3BO3 + H3BO3 + H3BO3 = B4O2OH8 + H2O + H2O;

*==========
==========;

*Metal Hydrolysis Equilibrium Chemistry ;

*==========
==========;

%kf %kf/KFe1 : Fe+2 + H2O = FeOH+ + H+;

%kf %kf/KFe2 : Fe+2 + H2O + H2O = FeOH2 + H+ + H+;

%kf %kf/KFe3 : Fe+2 + OH- + H2O + H2O = FeOH3- + H+ + H+;

%kf %kf/KFe1 : Fe54 + H2O = Fe54OH+ + H+;

%kf %kf/KFe2 : Fe54 + H2O + H2O = Fe54OH2 + H+ + H+;

%kf %kf/KFe3 : Fe54 + OH- + H2O + H2O = Fe54OH3- + H+ + H+;

%kf %kf/KFe1 : Fe58 + H2O = Fe58OH+ + H+;

%kf %kf/KFe2 : Fe58 + H2O + H2O = Fe58OH2 + H+ + H+;

%kf %kf/KFe3 : Fe58 + OH- + H2O + H2O = Fe58OH3- + H+ + H+;

%kf %kf/KFe1 : Fe59 + H2O = Fe59OH+ + H+;

%kf %kf/KFe2 : Fe59 + H2O + H2O = Fe59OH2 + H+ + H+;

%kf %kf/KFe3 : Fe59 + OH- + H2O + H2O = Fe59OH3- + H+ + H+;

%kf %kf/KFe1 : Mn54 + H2O = Mn54OH+ + H+;

%kf %kf/KFe2 : Mn54 + H2O + H2O = Mn54OH2 + H+ + H+;

%kf %kf/KFe3 : Mn54 + OH- + H2O + H2O = Mn54OH3- + H+ + H+;

%kf %kf/KCo1 : Co+2 + H2O = CoOH+ + H+;

%kf %kf/KCo2 : Co+2 + H2O + H2O = CoOH2 + H+ + H+;

%kf %kf/KCo1 : Co60 + H2O = Co60OH+ + H+;

%kf %kf/KCo2 : Co60 + H2O + H2O = Co60OH2 + H+ + H+;

%kf %kf/KNi1 : Ni+2 + H2O = NiOH+ + H+ ;

%kf %kf/KNi2 : Ni+2 + H2O + H2O = NiOH2 + H+ + H+;

%kf %kf/KNi3 : Ni+2 + H2O + H2O + H2O = NiOH3- + H+ + H+ + H+;

%kf %kf/KNi1 : Ni58 + H2O = Ni58OH+ + H+;

%kf %kf/KNi2 : Ni58 + H2O + H2O = Ni58OH2 + H+ + H+;

%kf %kf/KNi3 : Ni58 + H2O + H2O + H2O = Ni58OH3- + H+ + H+ + H+;

%kf %kf/KCo1 : Co58 + H2O = Co58OH+ + H+;

%kf %kf/KCo2 : Co58 + H2O + H2O = Co58OH2 + H+ + H+;

%kf %kf/KZn1 : Zn+2 + H2O = ZnOH+ + H+;

%kf %kf/KZn2 : Zn+2 + H2O + H2O = ZnOH2 + H+ + H+;

%kf %kf/KZn3 : Zn+2 + H2O + H2O + H2O = ZnOH3- + H+ + H+ + H+;

%kf %kf/KZn4 : Zn+2 + H2O + H2O + H2O + H2O = ZnOH42- + H+

+ H+ + H+ + H+;

%kf %kf/KCu1 : Cu+2 + H2O = CuOH+ + H+;

%kf %kf/KCu2 : CuOH+ + CuOH+ + H2O + H2O = CuOH2 + CuOH2 + H+ + H+;

%kf %kf/KCu3 : CuOH+ + H2O + H2O = CuOH3- + H+ + H+;

*==========;

* Activated Products ;

*==========;

%thermalnflux*Co59Xsect : Co+2<0> = Co60<0>;

%thermalnflux*Co59Xsect : CoOH+<0> = Co60OH+<0>;

%thermalnflux*Co59Xsect : CoOH2<0> = Co60OH2<0>;

%fastnflux*Ni58Xsect : Ni58<0> = Co58<0>;

%fastnflux*Ni58Xsect : Ni58OH+<0> = Co58OH+<0>;

%fastnflux*Ni58Xsect : Ni58OH2<0> = Co58OH2<0>;

%thermalnflux*Fe58Xsect : Fe58<0> = Fe59<0>;

%thermalnflux*Fe58Xsect : Fe58OH+<0> = Fe59OH+<0>;

%thermalnflux*Fe58Xsect : Fe58OH2<0> = Fe59OH2<0>;

%thermalnflux*Fe58Xsect : Fe58OH3-<0> = Fe59OH3-<0>;

%fastnflux*Fe54Xsect : Fe54<0> = Mn54<0>;

%fastnflux*Fe54Xsect : Fe54OH+<0> = Mn54OH+<0>;

%fastnflux*Fe54Xsect : Fe54OH2<0> = Mn54OH2<0>;

%fastnflux*Fe54Xsect : Fe54OH3-<0> = Mn54OH3-<0>;

*==========;

* Metal Species Production ;

*==========;

%KCrCo : =CoOH2;

%(KCrNi *(0.68077)) : =Ni58OH2;

%(KCrNi *(1 - 0.68077)) : =NiOH2;

%(KCrFe *(1 - 0.05845 - 0.00282)) : =FeOH2;

%(KCrFe *(0.00282)): =Fe58OH2;

%(KCrFe *(0.05845)): =Fe54OH2;

*==========;

* Cation column selectivity ;

*==========;

% Kres %kres/KRLi : RH + Li+ = RLi + H+;

% kres %kres/KRNH4 : RH + NH4+ = RNH4 + H+;

% kres %kres/(KRNH4/KRLi) : RLi + NH4+ = RNH4 + Li+;

% kres %kres/KRN2H5 : RH + N2H5+ = RN2H5 + H+;

% kres %kres/(KRN2H5/KRLi) : RLi + N2H5+ = RN2H5 + Li+;

% KRESFe % KRESFe/KRFe : RH + RH + Fe+2 = RRFe + H+ + H+;

% KRESFe % KRESFe/KRFe : RH + FeOH+ = RFeOH + H+;

% KRESFe % KRESFe/KRFe : RH + RH + Fe58 = RRFe58 + H+ + H+;

% KRESFe % KRESFe/KRFe : RH + Fe58OH+ = RFe58OH + H+;

% KRESFe % KRESFe/KRFe : RH + RH + Fe59 = RRFe59 + H+ + H+;

% KRESFe % KRESFe/KRFe : RH + Fe59OH+ = RFe59OH + H+;

% KRESFe % KRESFe/KRFe : RH + RH + Fe54 = RRFe54 + H+ + H+;

% KRESFe % KRESFe/KRFe : RH + Fe54OH+ = RFe54OH + H+;

% KRESFe % KRESFe/KRFe : RH + RH + Mn54 = RRMn54 + H+ + H+;

% KRESFe % KRESFe/KRFe : RH + RH + Cr54 = RRCr54 + H+ + H+;

% KRESFe % KRESFe/KRFe : RH + Mn54OH+ = RMn54OH + H+;

% KRESFe % KRESFe/KRFe : RH + Cr54OH+ = RCr54OH + H+;

% KRESNi % KRESNi/KRNi : RH + RH + Ni+2 = RRNi + H+ + H+;

% KRESNi % KRESNi/KRNi : RH + NiOH+ = RNiOH + H+;

% KRESNi % KRESNi/KRNi : RH + RH + Ni58 = RRNi58 + H+ + H+;

% KRESNi % KRESNi/KRNi : RH + Ni58OH+ = RNi58OH + H+;

% KRESCo % KRESCo/KRCo : RH + RH + Co+2 = RRCo + H+ + H+;

% KRESCo % KRESCo/KRCo : RH + CoOH+ = RCoOH + H+;

% KRESCo % KRESCo/KRCo : RH + RH + Co60 = RRCo60 + H+ + H+;

% KRESCo % KRESCo/KRCo : RH + Co60OH+ = RCo60OH + H+;

% KRESCo % KRESCo/KRCo : RH + RH + Co58 = RRCo58 + H+ + H+;

% KRESCo % KRESCo/KRCo : RH + Co58OH+ = RCo58OH + H+;

% KRESZn % KRESZn/KRZn : RH + RH + Zn+2 = RRZn + H+ + H+;

% KRESZn % KRESZn/KR : RH + ZnOH+ = RZnOH + H+;

% KRESCu % KRESCu/KRCu : RH + RH + Cu+2 = RRCu + H+ + H+;

% KRESCu % KRESCu/KRCu : RH + CuOH+ = RCuOH + H+;

% KRES % KRES/KRTe : RH + RH + Te131 = RTe131 + H+ + H+;

% KRES % KRES/KRTe : RH + RH + Te132 = RTe132 + H+ + H+;

% KRES % KRES/KRTe : RH + RH + Te133 = RTe133 + H+ + H+;

% KRES % KRES/KRTe : RH + RH + Te134 = RTe134 + H+ + H+;

% KRES % KRES/KRTe : RH + RH + Te135 = RTe135 + H+ + H+;

% KRES % KRES/KRCs : RH + Cs134 = RCs134 + H+;

% KRES % KRES/KRCs : RH + Cs137 = RCs137 + H+;

% KRES % KRES/KRCs : RH + Cs138 = RCs138 + H+;

%KRESFe/KRLi %kres/(KRFe) : RLi + RLi + Fe+2 = RRFe + Li+ + Li+;

%KRESFe/KRLi %kres/(KRFe) : RLi + FeOH+ = RFeOH + Li+;

%KRESFe/KRLi %kres/(KRFe) : RLi + RLi + Fe58 = RRFe58 + Li+ + Li+;

%KRESFe/KRLi %kres/(KRFe) : RLi + Fe58OH+ = RFe58OH + Li+;

%KRESFe/KRLi %kres/(KRFe) : RLi + RLi + Fe59 = RRFe59 + Li+ + Li+;

%KRESFe/KRLi %kres/(KRFe) : RLi + Fe59OH+ = RFe59OH + Li+;

%KRESFe/KRLi %kres/(KRFe) : RLi + RLi + Fe54 = RRFe54 + Li+ + Li+;

%KRESFe/KRLi %kres/(KRFe) : RLi + Fe54OH+ = RFe54OH + Li+;

%KRESFe/KRLi %kres/(KRFe) : RLi + RLi + Mn54 = RRMn54 + Li+ + Li+;

%KRESFe/KRLi %kres/(KRFe) : RLi + RLi + Cr54 = RRCr54 + Li+ + Li+;

%KRESFe/KRLi %kres/(KRFe) : RLi + Mn54OH+ = RMn54OH + Li+;

%KRESFe/KRLi %kres/(KRFe) : RLi + Cr54OH+ = RCr54OH + Li+;

%KRESNi/KRLi %kres/(KRNi) : RLi + RLi + Ni+2 = RRNi + Li+ + Li+;

%KRESNi/KRLi %kres/(KRNi) : RLi + NiOH+ = RNiOH + Li+;

%KRESNi/KRLi %kres/(KRNi) : RLi + RLi + Ni58 = RRNi58 + Li+ + Li+;

%KRESNi/KRLi %kres/(KRNi) : RLi + Ni58OH+ = RNi58OH + Li+;

%KRESCo/KRLi %kres/(KRCo) : RLi + RLi + Co+2 = RRCo + Li+ + Li+;

%KRESCo/KRLi %kres/(KRCo) : RLi + CoOH+ = RCoOH + Li+;

%KRESCo/KRLi %kres/(KRCo) : RLi + RLi + Co60 = RRCo60 + Li+ + Li+;

%KRESCo/KRLi %kres/(KRCo) : RLi + Co60OH+ = RCo60OH + Li+;

%KRESCo/KRLi %kres/(KRCo) : RLi + RLi + Co58 = RRCo58 + Li+ + Li+;

%KRESCo/KRLi %kres/(KRCo) : RLi + Co58OH+ = RCo58OH + Li+;

%(KRESZn)/KRLi %kres/(KRZn) : RLi + RLi + Zn+2 = RRZn + Li+ + Li+;

%(KRESZn)/KRLi %kres/(KRZn) : RLi + ZnOH+ = RZnOH + Li+;

%KRESCu/KRLi %kres/(KRCu) : RLi + RLi + Cu+2 = RRCu + Li+ + Li+;

%KRESCu/KRLi %kres/(KRCu) : RLi + CuOH+ = RCuOH + Li+;

% KRES/KRLi % KRES/(KRTe) : RLi + RLi + Te131 = RTe131 + Li+ + Li+;

% KRES/KRLi % KRES/(KRTe) : RLi + RLi + Te132 = RTe132 + Li+ + Li+;

% KRES/KRLi % KRES/(KRTe) : RLi + RLi + Te133 = RTe133 + Li+ + Li+;

% KRES/KRLi % KRES/(KRTe) : RLi + RLi + Te134 = RTe134 + Li+ + Li+;

% KRES/KRLi % KRES/(KRTe) : RLi + RLi + Te135 = RTe135 + Li+ + Li+;

% KRES/KRLi % KRES/(KRCs) : RLi + Cs134 = RCs134 + Li+;

% KRES/KRLi % KRES/(KRCs) : RLi + Cs137 = RCs137 + Li+;

% KRES/KRLi % KRES/(KRCs) : RLi + Cs138 = RCs138 + Li+;

% kres %kres/(KRFe/KRNH4) : RNH4 + RNH4 + Fe+2 = RRFe + NH4+ + NH4+;

% kres %kres/(KRFe/KRNH4) : RNH4 + FeOH+ = RFeOH + NH4+;

% kres %kres/(KRFe/KRNH4) : RNH4 + RNH4 + Fe58 = RRFe58 + NH4+ + NH4+;

% kres %kres/(KRFe/KRNH4) : RNH4 + Fe58OH+ = RFe58OH + NH4+;

% kres %kres/(KRFe/KRNH4) : RNH4 + RNH4 + Fe59 = RRFe59 + NH4+ + NH4+;

% kres %kres/(KRFe/KRNH4) : RNH4 + Fe59OH+ = RFe59OH + NH4+;

% kres %kres/(KRFe/KRNH4) : RNH4 + RNH4 + Fe54 = RRFe54 + NH4+ + NH4+;

% kres %kres/(KRFe/KRNH4) : RNH4 + Fe54OH+ = RFe54OH + NH4+;

% kres %kres/(KRFe/KRNH4) : RNH4 + RNH4 + Mn54 = RRMn54 + NH4+ + NH4+;

% kres %kres/(KRFe/KRNH4) : RNH4 + RNH4 + Cr54 = RRCr54 + NH4+ + NH4+;

% kres %kres/(KRFe/KRNH4) : RNH4 + Mn54OH+ = RMn54OH + NH4+;

% kres %kres/(KRFe/KRNH4) : RNH4 + Cr54OH+ = RCr54OH + NH4+;

% kres %kres/(KRNi/KRNH4) : RNH4 + RNH4 + Ni+2 = RRNi + NH4+ + NH4+;

% kres %kres/(KRNi/KRNH4) : RNH4 + NiOH+ = RNiOH + NH4+;

% kres %kres/(KRNi/KRNH4) : RNH4 + RNH4 + Ni58 = RRNi58 + NH4+ + NH4+;

% kres %kres/(KRNi/KRNH4) : RNH4 + Ni58OH+ = RNi58OH + NH4+;

% kres %kres/(KRCo/KRNH4) : RNH4 + RNH4 + Co+2 = RRCo + NH4+ + NH4+;

% kres %kres/(KRCo/KRNH4) : RNH4 + CoOH+ = RCoOH + NH4+;

% kres %kres/(KRCo/KRNH4) : RNH4 + RNH4 + Co60 = RRCo60 + NH4+ + NH4+;

% kres %kres/(KRCo/KRNH4) : RNH4 + Co60OH+ = RCo60OH + NH4+;

% kres %kres/(KRCo/KRNH4) : RNH4 + RNH4 + Co58 = RRCo58 + NH4+ + NH4+;

% kres %kres/(KRCo/KRNH4) : RNH4 + Co58OH+ = RCo58OH + NH4+;

% kres %kres/(KRZn/KRNH4) : RNH4 + RNH4 + Zn+2 = RRZn + NH4+ + NH4+;

% kres %kres/(KRZn/KRNH4) : RNH4 + ZnOH+ = RZnOH + NH4+;

% kres %kres/(KRCu/KRNH4) : RNH4 + RNH4 + Cu+2 = RRCu + NH4+ + NH4+;

% kres %kres/(KRCu/KRNH4) : RNH4 + CuOH+ = RCuOH + NH4+;

% KRES % KRES/(KRTe/KRNH4) : RNH4 + RNH4 + Te131 = RTe131 + NH4+ + NH4+;

% KRES % KRES/(KRTe/KRNH4) : RNH4 + RNH4 + Te132 = RTe132 + NH4+ + NH4+;

% KRES % KRES/(KRTe/KRNH4) : RNH4 + RNH4 + Te133 = RTe133 + NH4+ + NH4+;

% KRES % KRES/(KRTe/KRNH4) : RNH4 + RNH4 + Te134 = RTe134 + NH4+ + NH4+;

% KRES % KRES/(KRTe/KRNH4) : RNH4 + RNH4 + Te135 = RTe135 + NH4+ + NH4+;

% KRES % KRES/(KRCs/KRNH4) : RNH4 + Cs134 = RCs134 + NH4+;

% KRES % KRES/(KRCs/KRNH4) : RNH4 + Cs137 = RCs137 + NH4+;

% KRES % KRES/(KRCs/KRNH4) : RNH4 + Cs138 = RCs138 + NH4+;

*==========;

* Anion column selectivity ;

*==========;

% kres % kres/KRFe : ROH + FeOH3- = RFeOH3 + OH-;

% kres % kres/KRFe : ROH + Fe58OH3- = RFe58OH3 + OH-;

% kres % kres/KRFe : ROH + Fe59OH3- = RFe59OH3 + OH-;

% kres % kres/KRFe : ROH + Fe54OH3- = RFe54OH3 + OH-;

% kres % kres/KRFe : ROH + Mn54OH3- = RMn54OH3 + OH-;

% kres % kres/KRFe : ROH + Cr54OH3- = RCr54OH3 + OH-;

% kres % kres/KRNi : ROH + NiOH3- = RNiOH3 + OH-;

% kres % kres/KRNi : ROH + Ni58OH3- = RNi58OH3 + OH-;

% kres % kres/KRZn : ROH + ZnOH3- = RZnOH3 + OH-;

% kres % kres/KRZn : ROH + ROH + ZnOH42- = RRZnOH4 + OH- + OH-;

% kres % kres/KRCu : ROH + CuOH3- = RCuOH3 + OH-;

% kres % kres/KRBO4 : ROH + BOH4- = RBOH4 + OH-;

% kres % kres/KRBO4 : ROH + B2OOH5- = RB2OOH5 + OH-;

% kres % kres/KRBO4 : ROH + B3O3OH4- = RB3O3OH4 + OH-;

% kres % kres/KRBO4 : ROH + OAc- = ROAc + OH-;

% KRES % KRES/KRI : ROH + I131 = RI131 + OH-;

% KRES % KRES/KRI : ROH + I132 = RI132 + OH-;

% KRES % KRES/KRI : ROH + I133 = RI133 + OH-;

% KRES % KRES/KRI : ROH + I134 = RI134 + OH-;

% KRES % KRES/KRI : ROH + I135 = RI135 + OH-;

*==========;

* Activated Products Decay ;

*==========;

'Co60 = 'Co60 - (Co60lambda*Co60);

'Ni+2 = 'Ni+2 + (Co60lambda*Co60) + (Co60lambda*RRCo60);

'Co60OH+ = 'Co60OH+ - (Co60lambda*Co60OH+);

'NiOH+ = 'NiOH+ + (Co60lambda*Co60OH+) + (Co60lambda*RCo60OH);

'Co60OH2 = 'Co60OH2 - (Co60lambda*Co60OH2);

'NiOH2 = 'NiOH2 + (Co60lambda*Co60OH2);

'Co58 = 'Co58 - (Co58lambda*Co58);

'Fe58 = 'Fe58 + (Co58lambda*Co58) + (Co58lambda*RRCo58);

'Co58OH+ = 'Co58OH+ - (Co58lambda*Co58OH+);

```
'Fe58OH+ = 'Fe58OH+ + (Co58lambda*Co58OH+) + (Co58lambda*RCo58OH);

'Co58OH2 = 'Co58OH2 - (Co58lambda*Co58OH2);

'Fe58OH2 = 'Fe58OH2 + (Co58lambda*Co58OH2);

'Mn54 = 'Mn54 - (Mn54lambda*Mn54);

'Cr54 = 'Cr54 + (Mn54lambda*Mn54) + (Mn54lambda*RRMn54);

'Mn54OH+ = 'Mn54OH+ - (Mn54lambda*Mn54OH+);

'Cr54OH+ = 'Cr54OH+ + (Mn54lambda*Mn54OH+) + (Mn54lambda*RMn54OH);

'Mn54OH2 = 'Mn54OH2 - (Mn54lambda*Mn54OH2);

'Cr54OH2 = 'Cr54OH2 + (Mn54lambda*Mn54OH2);

'Mn54OH3- = 'Mn54OH3- - (Mn54lambda*Mn54OH3-);

'Cr54OH3- = 'Cr54OH3- + (Mn54lambda*Mn54OH3-) + (Mn54lambda*RMn54OH3);


'Fe59 = 'Fe59 - (Fe59lambda*Fe59);

'Co+2 = 'Co+2 + (Fe59lambda*Fe59) + (Fe59lambda*RRFe59);

'Fe59OH+ = 'Fe59OH+ - (Fe59lambda*Fe59OH+);

'CoOH+ = 'CoOH+ + (Fe59lambda*Fe59OH+) + (Fe59lambda*RFe59OH);

'Fe59OH2 = 'Fe59OH2 - (Fe59lambda*Fe59OH2);

'CoOH2 = 'CoOH2 + (Fe59lambda*Fe59OH2);

'Fe59OH3- = 'Fe59OH3- - (Fe59lambda*Fe59OH3-);

'CoOH2 = 'CoOH2 + (Fe59lambda*Fe59OH3-) + (Fe59lambda*RFe59OH3);

*==================================
==============================;

*Fission Products Forming Radionuclides and Decaying. ;

*==================================
==============================;

'I131<0> = 'I131<0> + (RNRate*YI131);

'I132<0> = 'I132<0> + (RNRate*YI132);

'I133<0> = 'I133<0> + (RNRate*YI133);

'I134<0> = 'I134<0> + (RNRate*YI134);

'I135<0> = 'I135<0> + (RNRate*YI135);

'Cs134<0> = 'Cs134<0> + (RNRate*YCs134);

'Cs137<0> = 'Cs137<0> + (RNRate*YCs137);
```

```
'Cs138<0> = 'Cs138<0> + (RNRate*YCs138);
'Xe133<0> = 'Xe133<0> + (RNRate*YXe133);
'Xe135<0> = 'Xe135<0> + (RNRate*YXe135);
'Xe138<0> = 'Xe138<0> + (RNRate*YXe138);
'Te131<0> = 'Te131<0> + (RNRate*YTe131);
'Te132<0> = 'Te132<0> + (RNRate*YTe132);
'Te133<0> = 'Te133<0> + (RNRate*YTe133);
'Te134<0> = 'Te134<0> + (RNRate*YTe134);
'Te135<0> = 'Te135<0> + (RNRate*YTe135);
'I131 = 'I131 - (I131Lambda*I131);
'I132 = 'I132 - (I132Lambda*I132);
'I133 = 'I133 - (I133Lambda*I133);
'I134 = 'I134 - (I134Lambda*I134);
'I135 = 'I135 - (I135Lambda*I135);
'Cs134 = 'Cs134 - (Cs134Lambda*Cs134);
'Cs137 = 'Cs137 - (Cs137Lambda*Cs137);
'Cs138 = 'Cs138 - (Cs138Lambda*Cs138);
'Xe133 = 'Xe133 - (Xe133Lambda*Xe133);
'Xe135 = 'Xe135 - (Xe135Lambda*Xe135);
'Xe138 = 'Xe138 - (Xe138Lambda*Xe138);
'Te131 = 'Te131 - (Te131Lambda*Te131);
'Te132 = 'Te132 - (Te132Lambda*Te132);
'Te133 = 'Te133 - (Te133Lambda*Te133);
'Te134 = 'Te134 - (Te134Lambda*Te134);
'Te135 = 'Te135 - (Te135Lambda*Te135);
'I131 = 'I131 + (Te131Lambda*Te131) +
(Te131Lambda*RTe131);
'I132 = 'I132 + (Te132Lambda*Te132) +
(Te131Lambda*RTe132);
'I133 = 'I133 + (Te133Lambda*Te133) +
(Te131Lambda*RTe133);
'I134 = 'I134 + (Te134Lambda*Te134) +
(Te131Lambda*RTe134);
'I135 = 'I135 + (Te135Lambda*Te135) +
(Te131Lambda*RTe135);
'Xe133 = 'Xe133 + (I133Lambda*I133) +
(I133Lambda*RI133);
'Xe135 = 'Xe135 + (I135Lambda*I135) +
(I133Lambda*RI135);
'Cs138 = 'Cs138 + (Xe138Lambda*Xe138);
*===================================
==========================;
*Resin Species Decaying                    ;
*===================================
==========================;
'RRCo60 = 'RRCo60 - (Co60Lambda*RRCo60);
'RCo60OH = 'RCo60OH -
(Co60Lambda*RCo60OH);
```

```
'RRCo58 = 'RRCo58 - (Co58Lambda*RRCo58);
'RCo58OH = 'RCo58OH - (Co58Lambda*RCo58OH);
'RRMn54 = 'RRMn54 - (Mn54Lambda*RRMn54);
'RMn54OH = 'RMn54OH - (Mn54Lambda*RMn54OH);
'RMn54OH3 = 'RMn54OH3 - (Mn54Lambda*RMn54OH3);
'RRFe59 = 'RRFe59 - (Fe59Lambda*RRFe59);
'RFe59OH = 'RFe59OH - (Fe59Lambda*RFe59OH);
'RFe59OH3 = 'RFe59OH3 - (Fe59Lambda*RFe59OH3);
'RI131 = 'RI131 - (I131Lambda*RI131);
'RI132 = 'RI132 - (I132Lambda*RI132);
'RI133 = 'RI133 - (I133Lambda*RI133);
'RI134 = 'RI134 - (I134Lambda*RI134);
'RI135 = 'RI135 - (I135Lambda*RI135);
'RTe131 = 'RTe131 - (Te131Lambda*RTe131);
'RTe132 = 'RTe132 - (Te132Lambda*RTe132);
'RTe133 = 'RTe133 - (Te133Lambda*RTe133);
'RTe134 = 'RTe134 - (Te134Lambda*RTe134);
'RTe135 = 'RTe135 - (Te135Lambda*RTe135);
'RCs134 = 'RCs134 - (Cs134Lambda*RCs134);
'RCs137 = 'RCs137 - (Cs137Lambda*RCs137);
'RCs138 = 'RCs138 - (Cs138Lambda*RCs138);
'RN = 'RN + ((Co60Lambda*RRCo60) + (Co60Lambda*RCo60OH)
+ (Co58Lambda*RRCo58) + (Co58Lambda*RCo58OH)
+ (Mn54Lambda*RRMn54) + (Mn54Lambda*RMn54OH)
+ (Mn54Lambda*RMn54OH3) + (Fe59Lambda*RRFe59) +
(Fe59Lambda*RFe59OH)
+ (Fe59Lambda*RFe59OH3) + (I131Lambda*RI131) + (I132Lambda*RI132)
+ (I133Lambda*RI133) + (I134Lambda*RI134) + (I135Lambda*RI135)
+ (Te131Lambda*RTe131) + (Te132Lambda*RTe132) +
(Te132Lambda*RTe133)
+ (Te132Lambda*RTe134) + (Te132Lambda*RTe135) +
(Cs134Lambda*RCs134)
+ (Cs137Lambda*RCs137) + (Cs137Lambda*RCs138));
```

ARRAY END;

*==========

==========;

*transport statements ;

*==========

==========;

TRANSPORT<#ncell> (CELLVOL) Li+ TRFAC DUMMY;

TRANSPORT<#ncell> (CELLVOL) LiOH TRFAC DUMMY;

TRANSPORT<#ncell> (CELLVOL) H+ TRFAC DUMMY;

TRANSPORT<#ncell> (CELLVOL) H2 TRFAC DUMMY;

TRANSPORT<#ncell> (CELLVOL) OH- TRFAC DUMMY;

TRANSPORT<#ncell> (CELLVOL) Zn+2 TRFAC DUMMY;

TRANSPORT<#ncell> (CELLVOL) ZnOH+ TRFAC DUMMY;

TRANSPORT<#ncell> (CELLVOL) ZnOH2 TRFAC DUMMY;

TRANSPORT<#ncell> (CELLVOL) ZnOH3- TRFAC DUMMY;

TRANSPORT<#ncell> (CELLVOL) ZnOH42- TRFAC DUMMY;

TRANSPORT<#ncell> (CELLVOL) Fe+2 TRFAC DUMMY;

TRANSPORT<#ncell> (CELLVOL) FeOH+ TRFAC DUMMY;

TRANSPORT<#ncell> (CELLVOL) FeOH2 TRFAC DUMMY;

TRANSPORT<#ncell> (CELLVOL) FeOH3- TRFAC DUMMY;

TRANSPORT<#ncell> (CELLVOL) Fe58 TRFAC DUMMY;

TRANSPORT<#ncell> (CELLVOL) Fe58OH+ TRFAC DUMMY;

TRANSPORT<#ncell> (CELLVOL) Fe58OH2 TRFAC DUMMY;

TRANSPORT<#ncell> (CELLVOL) Fe58OH3- TRFAC DUMMY;

TRANSPORT<#ncell> (CELLVOL) Fe59 TRFAC DUMMY;

TRANSPORT<#ncell> (CELLVOL) Fe59OH+ TRFAC DUMMY;

TRANSPORT<#ncell> (CELLVOL) Fe59OH2 TRFAC DUMMY;

TRANSPORT<#ncell> (CELLVOL) Fe59OH3- TRFAC DUMMY;

TRANSPORT<#ncell> (CELLVOL) Fe54 TRFAC DUMMY;

TRANSPORT<#ncell> (CELLVOL) Fe54OH+ TRFAC DUMMY;

TRANSPORT<#ncell> (CELLVOL) Fe54OH2 TRFAC DUMMY;

TRANSPORT<#ncell> (CELLVOL) Fe54OH3- TRFAC DUMMY;

TRANSPORT<#ncell> (CELLVOL) Fe3O4s TRFAC DUMMY;

TRANSPORT<#ncell> (CELLVOL) Mn54 TRFAC DUMMY;

TRANSPORT<#ncell> (CELLVOL) Mn54OH+ TRFAC DUMMY;

TRANSPORT<#ncell> (CELLVOL) Mn54OH2 TRFAC DUMMY;

TRANSPORT<#ncell> (CELLVOL) Mn54OH3- TRFAC DUMMY;

TRANSPORT<#ncell> (CELLVOL) Cr54 TRFAC DUMMY;

TRANSPORT<#ncell> (CELLVOL) Cr54OH+ TRFAC DUMMY;

TRANSPORT<#ncell> (CELLVOL) Cr54OH2 TRFAC DUMMY;

TRANSPORT<#ncell> (CELLVOL) Cr54OH3- TRFAC DUMMY;

TRANSPORT<#ncell> (CELLVOL) Ni+2 TRFAC DUMMY;

TRANSPORT<#ncell> (CELLVOL) NiOH+ TRFAC DUMMY;

TRANSPORT<#ncell> (CELLVOL) NiOH2 TRFAC DUMMY;

TRANSPORT<#ncell> (CELLVOL) NiOH3- TRFAC DUMMY;

TRANSPORT<#ncell> (CELLVOL) Ni58 TRFAC DUMMY;

TRANSPORT<#ncell> (CELLVOL) Ni58OH+ TRFAC DUMMY;

TRANSPORT<#ncell> (CELLVOL) Ni58OH2 TRFAC DUMMY;

TRANSPORT<#ncell> (CELLVOL) Ni58OH3- TRFAC DUMMY;

TRANSPORT<#ncell> (CELLVOL) Co+2 TRFAC DUMMY;

TRANSPORT<#ncell> (CELLVOL) Co60 TRFAC DUMMY;

TRANSPORT<#ncell> (CELLVOL) Co58 TRFAC DUMMY;

TRANSPORT<#ncell> (CELLVOL) CoOH+ TRFAC DUMMY;

TRANSPORT<#ncell> (CELLVOL) CoOH2 TRFAC DUMMY;

TRANSPORT<#ncell> (CELLVOL) Co6OOH+ TRFAC DUMMY;

TRANSPORT<#ncell> (CELLVOL) Co6OOH2 TRFAC DUMMY;

TRANSPORT<#ncell> (CELLVOL) Co58OH+ TRFAC DUMMY;

TRANSPORT<#ncell> (CELLVOL) Co58OH2 TRFAC DUMMY;

TRANSPORT<#ncell> (CELLVOL) Cu+2 TRFAC DUMMY;

TRANSPORT<#ncell> (CELLVOL) CuOH+ TRFAC DUMMY;

TRANSPORT<#ncell> (CELLVOL) CuOH2 TRFAC DUMMY;

TRANSPORT<#ncell> (CELLVOL) CuOH3- TRFAC DUMMY;

TRANSPORT<#ncell> (CELLVOL) NH4+ TRFAC DUMMY;

TRANSPORT<#ncell> (CELLVOL) NH3 TRFAC DUMMY;

TRANSPORT<#ncell> (CELLVOL) N2H4 TRFAC DUMMY;

TRANSPORT<#ncell> (CELLVOL) N2H5+ TRFAC DUMMY;

TRANSPORT<#ncell> (CELLVOL) H3BO3 TRFAC DUMMY;

TRANSPORT<#ncell> (CELLVOL) BOH4- TRFAC DUMMY;

TRANSPORT<#ncell> (CELLVOL) B2OOH5- TRFAC DUMMY;

TRANSPORT<#ncell> (CELLVOL) B3O3OH4- TRFAC DUMMY;

TRANSPORT<#ncell> (CELLVOL) B4O2OH8 TRFAC DUMMY;

TRANSPORT<#ncell> (CELLVOL) ZnOAc2 TRFAC DUMMY;

TRANSPORT<#ncell> (CELLVOL) ACOH TRFAC DUMMY;

TRANSPORT<#ncell> (CELLVOL) OAc- TRFAC DUMMY;

TRANSPORT<#ncell> (CELLVOL) CO2 TRFAC DUMMY;

TRANSPORT<#ncell> (CELLVOL) HCO3- TRFAC DUMMY;

TRANSPORT<#ncell> (CELLVOL) CO32- TRFAC DUMMY;

TRANSPORT<#ncell> (CELLVOL) CH4 TRFAC DUMMY;

TRANSPORT<#ncell> (CELLVOL) I131 TRFAC DUMMY;

TRANSPORT<#ncell> (CELLVOL) I132 TRFAC DUMMY;

```
TRANSPORT<#ncell> (CELLVOL) I133 TRFAC
DUMMY;

TRANSPORT<#ncell> (CELLVOL) I134 TRFAC
DUMMY;

TRANSPORT<#ncell> (CELLVOL) I135 TRFAC
DUMMY;

TRANSPORT<#ncell> (CELLVOL) Te131 TRFAC
DUMMY;

TRANSPORT<#ncell> (CELLVOL) Te132 TRFAC
DUMMY;

TRANSPORT<#ncell> (CELLVOL) Te133 TRFAC
DUMMY;

TRANSPORT<#ncell> (CELLVOL) Te134 TRFAC
DUMMY;

TRANSPORT<#ncell> (CELLVOL) Te135 TRFAC
DUMMY;

TRANSPORT<#ncell> (CELLVOL) Cs134 TRFAC
DUMMY;

TRANSPORT<#ncell> (CELLVOL) Cs137 TRFAC
DUMMY;

TRANSPORT<#ncell> (CELLVOL) Cs138 TRFAC
DUMMY;

TRANSPORT<#ncell> (CELLVOL) Xe133 TRFAC
DUMMY;

TRANSPORT<#ncell> (CELLVOL) Xe135 TRFAC
DUMMY;

TRANSPORT<#ncell> (CELLVOL) Xe138 TRFAC
DUMMY;

*==================================
==========================;

* inlet boundary conditions                ;

* This moves species from bulk into the first cell
on the col ;

*==================================
==========================;

FOR #14 = 1;

% Li+<0>*TRFAC<#14>/CELLVOL<#14>      :
=Li+<#14>;

% LiOH<0>*TRFAC<#14>/CELLVOL<#14>     :
=LiOH<#14>;

% H+<0>*TRFAC<#14>/CELLVOL<#14>       :
=H+<#14>;

% H2<0>*TRFAC<#14>/CELLVOL<#14>       :
=H2<#14>;

% OH-<0>*TRFAC<#14>/CELLVOL<#14>      :
=OH-<#14>;

% Zn+2<0>*TRFAC<#14>/CELLVOL<#14>     :
=Zn+2<#14>;

% ZnOH+<0>*TRFAC<#14>/CELLVOL<#14>    :
=ZnOH+<#14>;
```

% ZnOH2<0>*TRFAC<#14>/CELLVOL<#14> : =ZnOH2<#14>;

% ZnOH3-<0>*TRFAC<#14>/CELLVOL<#14> : =ZnOH3-<#14>;

% ZnOH42-<0>*TRFAC<#14>/CELLVOL<#14> : =ZnOH42-<#14>;

% Fe+2<0>*TRFAC<#14>/CELLVOL<#14> : =Fe+2<#14>;

% FeOH+<0>*TRFAC<#14>/CELLVOL<#14> : =FeOH+<#14>;

% FeOH2<0>*TRFAC<#14>/CELLVOL<#14> : =FeOH2<#14>;

% FeOH3-<0>*TRFAC<#14>/CELLVOL<#14> : =FeOH3-<#14>;

% Fe58<0>*TRFAC<#14>/CELLVOL<#14> : =Fe58<#14>;

% Fe58OH+<0>*TRFAC<#14>/CELLVOL<#14> : =Fe58OH+<#14>;

% Fe58OH2<0>*TRFAC<#14>/CELLVOL<#14> : =Fe58OH2<#14>;

% Fe58OH3-<0>*TRFAC<#14>/CELLVOL<#14> : =Fe58OH3-<#14>;

% Fe59<0>*TRFAC<#14>/CELLVOL<#14> : =Fe59<#14>;

% Fe59OH+<0>*TRFAC<#14>/CELLVOL<#14> : =Fe59OH+<#14>;

% Fe59OH2<0>*TRFAC<#14>/CELLVOL<#14> : =Fe59OH2<#14>;

% Fe59OH3-<0>*TRFAC<#14>/CELLVOL<#14> : =Fe59OH3-<#14>;

% Fe54<0>*TRFAC<#14>/CELLVOL<#14> : =Fe54<#14>;

% Fe54OH+<0>*TRFAC<#14>/CELLVOL<#14> : =Fe54OH+<#14>;

% Fe54OH2<0>*TRFAC<#14>/CELLVOL<#14> : =Fe54OH2<#14>;

% Fe54OH3-<0>*TRFAC<#14>/CELLVOL<#14> : =Fe54OH3-<#14>;

% Mn54<0>*TRFAC<#14>/CELLVOL<#14> : =Mn54<#14>;

% Mn54OH+<0>*TRFAC<#14>/CELLVOL<#14> : =Mn54OH+<#14>;

% Mn54OH2<0>*TRFAC<#14>/CELLVOL<#14> : =Mn54OH2<#14>;

% Mn54OH3-<0>*TRFAC<#14>/CELLVOL<#14> : =Mn54OH3-<#14>;

% Cr54<0>*TRFAC<#14>/CELLVOL<#14> : =Cr54<#14>;

% Cr54OH+<0>*TRFAC<#14>/CELLVOL<#14> : =Cr54OH+<#14>;

% Cr54OH2<0>*TRFAC<#14>/CELLVOL<#14> : =Cr54OH2<#14>;

% Cr54OH3-<0>*TRFAC<#14>/CELLVOL<#14> : =Cr54OH3-<#14>;

% Ni+2<0>*TRFAC<#14>/CELLVOL<#14> : =Ni+2<#14>;

% NiOH+<0>*TRFAC<#14>/CELLVOL<#14> : =NiOH+<#14>;

% NiOH2<0>*TRFAC<#14>/CELLVOL<#14> : =NiOH2<#14>;

% NiOH3-<0>*TRFAC<#14>/CELLVOL<#14> : =NiOH3-<#14>;

% Ni58<0>*TRFAC<#14>/CELLVOL<#14> : =Ni58<#14>;

% Ni58OH+<0>*TRFAC<#14>/CELLVOL<#14> : =Ni58OH+<#14>;

% Ni58OH2<0>*TRFAC<#14>/CELLVOL<#14> : =Ni58OH2<#14>;

% Ni58OH3-<0>*TRFAC<#14>/CELLVOL<#14> : =Ni58OH3-<#14>;

% Co+2<0>*TRFAC<#14>/CELLVOL<#14> : =Co+2<#14>;

% Co60<0>*TRFAC<#14>/CELLVOL<#14> : =Co60<#14>;

% CoOH+<0>*TRFAC<#14>/CELLVOL<#14> : =CoOH+<#14>;

% CoOH2<0>*TRFAC<#14>/CELLVOL<#14> : =CoOH2<#14>;

% Co60OH+<0>*TRFAC<#14>/CELLVOL<#14> : =Co60OH+<#14>;

% Co60OH2<0>*TRFAC<#14>/CELLVOL<#14> : =Co60OH2<#14>;

% Co58<0>*TRFAC<#14>/CELLVOL<#14> : =Co58<#14>;

% Co58OH+<0>*TRFAC<#14>/CELLVOL<#14> : =Co58OH+<#14>;

% Co58OH2<0>*TRFAC<#14>/CELLVOL<#14> : =Co58OH2<#14>;

% Cu+2<0>*TRFAC<#14>/CELLVOL<#14> : =Cu+2<#14>;

% CuOH+<0>*TRFAC<#14>/CELLVOL<#14> : =CuOH+<#14>;

% CuOH2<0>*TRFAC<#14>/CELLVOL<#14> : =CuOH2<#14>;

% CuOH3-<0>*TRFAC<#14>/CELLVOL<#14> : =CuOH3-<#14>;

% NH4+<0>*TRFAC<#14>/CELLVOL<#14> : =NH4+<#14>;

% NH3<0>*TRFAC<#14>/CELLVOL<#14> : =NH3<#14>;

% N2H4<0>*TRFAC<#14>/CELLVOL<#14> : =N2H4<#14>;

% N2H5+<0>*TRFAC<#14>/CELLVOL<#14> : =N2H5+<#14>;

% H3BO3<0>*TRFAC<#14>/CELLVOL<#14> : =H3BO3<#14>;

% BOH4-<0>*TRFAC<#14>/CELLVOL<#14> : =BOH4-<#14>;

% B2OOH5-<0>*TRFAC<#14>/CELLVOL<#14> : =B2OOH5-<#14>;

% B3O3OH4-<0>*TRFAC<#14>/CELLVOL<#14> : =B3O3OH4-<#14>;

% B4O2OH8<0>*TRFAC<#14>/CELLVOL<#14> : =B4O2OH8<#14>;

% Fe3O4s<0>*TRFAC<#14>/CELLVOL<#14> : =Fe3O4s<#14>;

% ZnOAc2<0>*TRFAC<#14>/CELLVOL<#14> : =ZnOAc2<#14>;

% ACOH<0>*TRFAC<#14>/CELLVOL<#14> : =ACOH<#14>;

% OAc-<0>*TRFAC<#14>/CELLVOL<#14> : =OAc- <#14>;

% CO2<0>*TRFAC<#14>/CELLVOL<#14> : =CO2<#14>;

% HCO3-<0>*TRFAC<#14>/CELLVOL<#14> : =HCO3-<#14>;

% CO32-<0>*TRFAC<#14>/CELLVOL<#14> : =CO32-<#14>;

% CH4<0>*TRFAC<#14>/CELLVOL<#14> : =CH4<#14>;

% I131<0>*TRFAC<#14>/CELLVOL<#14> : =I131<#14>;

% I132<0>*TRFAC<#14>/CELLVOL<#14> : =I132<#14>;

% I133<0>*TRFAC<#14>/CELLVOL<#14> : =I133<#14>;

% I134<0>*TRFAC<#14>/CELLVOL<#14> : =I134<#14>;

% I135<0>*TRFAC<#14>/CELLVOL<#14> : =I135<#14>;

% Te131<0>*TRFAC<#14>/CELLVOL<#14> : =Te131<#14>;

% Te132<0>*TRFAC<#14>/CELLVOL<#14> : =Te132<#14>;

% Te133<0>*TRFAC<#14>/CELLVOL<#14> : =Te133<#14>;

% Te134<0>*TRFAC<#14>/CELLVOL<#14> : =Te134<#14>;

% Te135<0>*TRFAC<#14>/CELLVOL<#14> : =Te135<#14>;

% Cs134<0>*TRFAC<#14>/CELLVOL<#14> : =Cs134<#14>;

% Cs137<0>*TRFAC<#14>/CELLVOL<#14> : =Cs137<#14>;

% Cs138<0>*TRFAC<#14>/CELLVOL<#14> : =Cs138<#14>;

% Xe133<0>*TRFAC<#14>/CELLVOL<#14> : =Xe133<#14>;

% Xe135<0>*TRFAC<#14>/CELLVOL<#14> : =Xe135<#14>;

% Xe138<0>*TRFAC<#14>/CELLVOL<#14> : =Xe138<#14>;

*==========

==========;

*outlet boundary problem ;

*This removes the species from the Bulk taking into account dw ;

*==========

==========;

%TRFAC<#14>/CELLVOL<0> : Li+<0>=;

%TRFAC<#14>/CELLVOL<0> : LiOH<0>=;

%TRFAC<#14>/CELLVOL<0> : H+<0>=;

%TRFAC<#14>/CELLVOL<0> : H2<0>=;

%TRFAC<#14>/CELLVOL<0> : OH-<0>=;

%TRFAC<#14>/CELLVOL<0> : Zn+2<0>=;

%TRFAC<#14>/CELLVOL<0> : ZnOH+<0>=;

%TRFAC<#14>/CELLVOL<0> : ZnOH2<0>=;

%TRFAC<#14>/CELLVOL<0> : ZnOH3-<0>=;

%TRFAC<#14>/CELLVOL<0> : ZnOH42-<0>=;

%TRFAC<#14>/CELLVOL<0> : Fe+2<0>=;

%TRFAC<#14>/CELLVOL<0> : FeOH+<0>=;

%TRFAC<#14>/CELLVOL<0> : FeOH2<0>=;

%TRFAC<#14>/CELLVOL<0> : FeOH3-<0>=;

%TRFAC<#14>/CELLVOL<0> : Fe58<0>=;

%TRFAC<#14>/CELLVOL<0> : Fe58OH+<0>=;

%TRFAC<#14>/CELLVOL<0> : Fe58OH2<0>=;

%TRFAC<#14>/CELLVOL<0> : Fe58OH3-<0>=;

%TRFAC<#14>/CELLVOL<0> : Fe59<0>=;

%TRFAC<#14>/CELLVOL<0> : Fe59OH+<0>=;

%TRFAC<#14>/CELLVOL<0> : Fe59OH2<0>=;

%TRFAC<#14>/CELLVOL<0> : Fe59OH3-<0>=;

%TRFAC<#14>/CELLVOL<0> : Fe54<0>=;

%TRFAC<#14>/CELLVOL<0> : Fe54OH+<0>=;

%TRFAC<#14>/CELLVOL<0> : Fe54OH2<0>=;

%TRFAC<#14>/CELLVOL<0> : Fe54OH3-<0>=;

%TRFAC<#14>/CELLVOL<0> : Mn54<0>=;

%TRFAC<#14>/CELLVOL<0> : Mn54OH+<0>=;

%TRFAC<#14>/CELLVOL<0> : Mn54OH2<0>=;

%TRFAC<#14>/CELLVOL<0> : Mn54OH3-<0>=;

%TRFAC<#14>/CELLVOL<0> : Cr54<0>=;

%TRFAC<#14>/CELLVOL<0> : Cr54OH+<0>=;

%TRFAC<#14>/CELLVOL<0> : Cr54OH2<0>=;

%TRFAC<#14>/CELLVOL<0> : Cr54OH3-<0>=;

%TRFAC<#14>/CELLVOL<0> : Ni+2<0>=;

%TRFAC<#14>/CELLVOL<0> : NiOH+<0>=;

%TRFAC<#14>/CELLVOL<0> : NiOH2<0>=;

%TRFAC<#14>/CELLVOL<0> : NiOH3-<0>=;

%TRFAC<#14>/CELLVOL<0> : Ni58<0>=;

%TRFAC<#14>/CELLVOL<0> : Ni58OH+<0>=;

%TRFAC<#14>/CELLVOL<0> : Ni58OH2<0>=;

%TRFAC<#14>/CELLVOL<0> : Ni58OH3-<0>=;

%TRFAC<#14>/CELLVOL<0> :Co+2<0>=;

%TRFAC<#14>/CELLVOL<0> : CoOH+<0>=;

%TRFAC<#14>/CELLVOL<0> : CoOH2<0>=;

%TRFAC<#14>/CELLVOL<0> :Co60<0>=;

%TRFAC<#14>/CELLVOL<0> : Co60OH+<0>=;

%TRFAC<#14>/CELLVOL<0> : Co60OH2<0>=;

%TRFAC<#14>/CELLVOL<0> :Co58<0>=;

%TRFAC<#14>/CELLVOL<0> : Co58OH+<0>=;

%TRFAC<#14>/CELLVOL<0> : Co58OH2<0>=;

%TRFAC<#14>/CELLVOL<0> : Cu+2<0>=;

%TRFAC<#14>/CELLVOL<0> : CuOH+<0>=;

%TRFAC<#14>/CELLVOL<0> : CuOH2<0>=;

%TRFAC<#14>/CELLVOL<0> : CuOH3-<0>=;

%TRFAC<#14>/CELLVOL<0> : NH3<0>=;

%TRFAC<#14>/CELLVOL<0> : NH4+<0>=;

%TRFAC<#14>/CELLVOL<0> : N2H4<0>=;

%TRFAC<#14>/CELLVOL<0> : N2H5+<0>=;

%TRFAC<#14>/CELLVOL<0> : H3BO3<0>=;

%TRFAC<#14>/CELLVOL<0> : BOH4-<0>=;

%TRFAC<#14>/CELLVOL<0> : B2OOH5-<0>=;

%TRFAC<#14>/CELLVOL<0> : B3O3OH4-<0>=;

%TRFAC<#14>/CELLVOL<0> : B4O2OH8<0>=;

%TRFAC<#14>/CELLVOL<0> : Fe3O4s<0>=;

%TRFAC<#14>/CELLVOL<0> : ZnOAc2<0>=;

%TRFAC<#14>/CELLVOL<0> : AcOH<0>=;

%TRFAC<#14>/CELLVOL<0> : OAc-<0>=;

%TRFAC<#14>/CELLVOL<0> : CO2<0>=;

%TRFAC<#14>/CELLVOL<0> : HCO3-<0>=;

%TRFAC<#14>/CELLVOL<0> : CO32-<0>=;

%TRFAC<#14>/CELLVOL<0> : CH4<0>=;

%TRFAC<#14>/CELLVOL<0> : I131<0>=;

%TRFAC<#14>/CELLVOL<0> : I132<0>=;

%TRFAC<#14>/CELLVOL<0> : I133<0>=;

%TRFAC<#14>/CELLVOL<0> : I134<0>=;

%TRFAC<#14>/CELLVOL<0> : I135<0>=;

%TRFAC<#14>/CELLVOL<0> : Te131<0>=;

%TRFAC<#14>/CELLVOL<0> : Te132<0>=;

%TRFAC<#14>/CELLVOL<0> : Te133<0>=;

%TRFAC<#14>/CELLVOL<0> : Te134<0>=;

%TRFAC<#14>/CELLVOL<0> : Te135<0>=;

%TRFAC<#14>/CELLVOL<0> : Cs134<0>=;

%TRFAC<#14>/CELLVOL<0> : Cs137<0>=;

%TRFAC<#14>/CELLVOL<0> : Cs138<0>=;

%TRFAC<#14>/CELLVOL<0> : Xe133<0>=;

%TRFAC<#14>/CELLVOL<0> : Xe135<0>=;

%TRFAC<#14>/CELLVOL<0> : Xe138<0>=;

*==========

==========;

* inlet boundary conditions ;

* This moves species from final cell in column back in the bulk;

*==========

==========;

FOR #5 = #NCELL - 1;

% Li+<#5>*TRFAC<0>/CELLVOL<0> : =Li+<0>;

% LiOH<#5>*TRFAC<0>/CELLVOL<0> : =LiOH<0>;

% H+<#5>*TRFAC<0>/CELLVOL<0> : =H+<0>;

% H2<#5>*TRFAC<0>/CELLVOL<0> : =H2<0>;

% OH-<#5>*TRFAC<0>/CELLVOL<0> : =OH-<0>;

% Zn+2<#5>*TRFAC<0>/CELLVOL<0> : =Zn+2<0>;

% ZnOH+<#5>*TRFAC<0>/CELLVOL<0> : =ZnOH+<0>;

% ZnOH2<#5>*TRFAC<0>/CELLVOL<0> : =ZnOH2<0>;

% ZnOH3-<#5>*TRFAC<0>/CELLVOL<0> : =ZnOH3-<0>;

% ZnOH42-<#5>*TRFAC<0>/CELLVOL<0> : =ZnOH42-<0>;

% Fe+2<#5>*TRFAC<0>/CELLVOL<0> : =Fe+2<0>;

% FeOH+<#5>*TRFAC<0>/CELLVOL<0> : =FeOH+<0>;

% FeOH2<#5>*TRFAC<0>/CELLVOL<0> : =FeOH2<0>;

% FeOH3-<#5>*TRFAC<0>/CELLVOL<0> : =FeOH3-<0>;

% Fe58<#5>*TRFAC<0>/CELLVOL<0> : =Fe58<0>;

% Fe58OH+<#5>*TRFAC<0>/CELLVOL<0> : =Fe58OH+<0>;

% Fe58OH2<#5>*TRFAC<0>/CELLVOL<0> : =Fe58OH2<0>;

% Fe58OH3-<#5>*TRFAC<0>/CELLVOL<0> : =Fe58OH3-<0>;

% Fe59<#5>*TRFAC<0>/CELLVOL<0> : =Fe59<0>;

% Fe59OH+<#5>*TRFAC<0>/CELLVOL<0> : =Fe59OH+<0>;

% Fe59OH2<#5>*TRFAC<0>/CELLVOL<0> : =Fe59OH2<0>;

% Fe59OH3-<#5>*TRFAC<0>/CELLVOL<0> : =Fe59OH3-<0>;

% Fe54<#5>*TRFAC<0>/CELLVOL<0> : =Fe54<0>;

% Fe54OH+<#5>*TRFAC<0>/CELLVOL<0> : =Fe54OH+<0>;

% Fe54OH2<#5>*TRFAC<0>/CELLVOL<0> : =Fe54OH2<0>;

% Fe54OH3-<#5>*TRFAC<0>/CELLVOL<0> : =Fe54OH3-<0>;

% Mn54<#5>*TRFAC<0>/CELLVOL<0> : =Mn54<0>;

% Mn54OH+<#5>*TRFAC<0>/CELLVOL<0> : =Mn54OH+<0>;

% Mn54OH2<#5>*TRFAC<0>/CELLVOL<0> : =Mn54OH2<0>;

% Mn54OH3-<#5>*TRFAC<0>/CELLVOL<0> : =Mn54OH3-<0>;

% Mn54<#5>*TRFAC<0>/CELLVOL<0> : =Cr54<0>;

% Mn54OH+<#5>*TRFAC<0>/CELLVOL<0> : =Cr54OH+<0>;

% Mn54OH2<#5>*TRFAC<0>/CELLVOL<0> : =Cr54OH2<0>;

% Mn54OH3-<#5>*TRFAC<0>/CELLVOL<0> : =Cr54OH3-<0>;

% Ni+2<#5>*TRFAC<0>/CELLVOL<0> : =Ni+2<0>;

% NiOH+<#5>*TRFAC<0>/CELLVOL<0> : =NiOH+<0>;

% NiOH2<#5>*TRFAC<0>/CELLVOL<0> : =NiOH2<0>;

% NiOH3-<#5>*TRFAC<0>/CELLVOL<0> : =NiOH3-<0>;

% Ni58<#5>*TRFAC<0>/CELLVOL<0> : =Ni58<0>;

% Ni58OH+<#5>*TRFAC<0>/CELLVOL<0> : =Ni58OH+<0>;

% Ni58OH2<#5>*TRFAC<0>/CELLVOL<0> : =Ni58OH2<0>;

% Ni58OH3-<#5>*TRFAC<0>/CELLVOL<0> : =Ni58OH3-<0>;

% Co+2<#5>*TRFAC<0>/CELLVOL<0> : =Co+2<0>;

```
% Co60<#5>*TRFAC<0>/CELLVOL<0>  :
=Co60<0>;

% CoOH+<#5>*TRFAC<0>/CELLVOL<0>  :
=CoOH+<0>;

% CoOH2<#5>*TRFAC<0>/CELLVOL<0>  :
=CoOH2<0>;

% Co60OH+<#5>*TRFAC<0>/CELLVOL<0>  :
=Co60OH+<0>;

% Co60OH2<#5>*TRFAC<0>/CELLVOL<0>  :
=Co60OH2<0>;

% Co58<#5>*TRFAC<0>/CELLVOL<0>  :
=Co58<0>;

% Co58OH+<#5>*TRFAC<0>/CELLVOL<0>  :
=Co58OH+<0>;

% Co58OH2<#5>*TRFAC<0>/CELLVOL<0>  :
=Co58OH2<0>;

% Cu+2<#5>*TRFAC<0>/CELLVOL<0>  :
=Cu+2<0>;

% CuOH+<#5>*TRFAC<0>/CELLVOL<0>  :
=CuOH+<0>;

% CuOH2<#5>*TRFAC<0>/CELLVOL<0>  :
=CuOH2<0>;

% CuOH3-<#5>*TRFAC<0>/CELLVOL<0>  :
=CuOH3-<0>;

% NH4+<#5>*TRFAC<0>/CELLVOL<0>  :
=NH4+<0>;

% NH3<#5>*TRFAC<0>/CELLVOL<0>  :
=NH3<0>;

% N2H4<#5>*TRFAC<0>/CELLVOL<0>  :
=N2H4<0>;

% N2H5+<#5>*TRFAC<0>/CELLVOL<0>  :
=N2H5+<0>;

% H3BO3<#5>*TRFAC<0>/CELLVOL<0>  :
=H3BO3<0>;

% BOH4-<#5>*TRFAC<0>/CELLVOL<0>  :
=BOH4-<0>;

% B2OOH5-<#5>*TRFAC<0>/CELLVOL<0>  :
=B2OOH5-<0>;

% B3O3OH4-<#5>*TRFAC<0>/CELLVOL<0>  :
=B3O3OH4-<0>;

% B4O2OH8<#5>*TRFAC<0>/CELLVOL<0>  :
=B4O2OH8<0>;

% Fe3O4s<#5>*TRFAC<0>/CELLVOL<0>  :
=Fe3O4s<0>;

% ZnOAc2<#5>*TRFAC<0>/CELLVOL<0>  :
=ZnOAc2<0>;

% I131<#5>*TRFAC<0>/CELLVOL<0>  :
=I131<0>;

% I132<#5>*TRFAC<0>/CELLVOL<0>  :
=I132<0>;

% I133<#5>*TRFAC<0>/CELLVOL<0>  :
=I133<0>;
```

% I134<#5>*TRFAC<0>/CELLVOL<0> : =I134<0>;

% I135<#5>*TRFAC<0>/CELLVOL<0> : =I135<0>;

% Te131<#5>*TRFAC<0>/CELLVOL<0> : =Te131<0>;

% Te132<#5>*TRFAC<0>/CELLVOL<0> : =Te132<0>;

% Te133<#5>*TRFAC<0>/CELLVOL<0> : =Te133<0>;

% Te134<#5>*TRFAC<0>/CELLVOL<0> : =Te134<0>;

% Te135<#5>*TRFAC<0>/CELLVOL<0> : =Te135<0>;

% Cs134<#5>*TRFAC<0>/CELLVOL<0> : =Cs134<0>;

% Cs137<#5>*TRFAC<0>/CELLVOL<0> : =Cs137<0>;

% Cs138<#5>*TRFAC<0>/CELLVOL<0> : =Cs138<0>;

% Xe133<#5>*TRFAC<0>/CELLVOL<0> : =Xe133<0>;

% Xe135<#5>*TRFAC<0>/CELLVOL<0> : =Xe135<0>;

% Xe138<#5>*TRFAC<0>/CELLVOL<0> : =Xe138<0>;

*==========;

*outlet boundary problem ;

*This removes the species from the final cell in the column. ;

*This stops species building up in the end of the column. ;

*==========;

%TRFAC<0>/CELLVOL<#5> : Li+<#5>=;

%TRFAC<0>/CELLVOL<#5> : LiOH<#5>=;

%TRFAC<0>/CELLVOL<#5> : H+<#5>=;

%TRFAC<0>/CELLVOL<#5> : H2<#5>=;

%TRFAC<0>/CELLVOL<#5> : OH-<#5>=;

%TRFAC<0>/CELLVOL<#5> : Zn+2<#5>=;

%TRFAC<0>/CELLVOL<#5> : ZnOH+<#5>=;

%TRFAC<0>/CELLVOL<#5> : ZnOH2<#5>=;

%TRFAC<0>/CELLVOL<#5> : ZnOH3-<#5>=;

%TRFAC<0>/CELLVOL<#5> : ZnOH42-<#5>=;

%TRFAC<0>/CELLVOL<#5> : Fe+2<#5>=;

%TRFAC<0>/CELLVOL<#5> : FeOH+<#5>=;

%TRFAC<0>/CELLVOL<#5> : FeOH2<#5>=;

%TRFAC<0>/CELLVOL<#5> : FeOH3-<#5>=;

%TRFAC<0>/CELLVOL<#5> : Fe58<#5>=;

%TRFAC<0>/CELLVOL<#5> : Fe58OH+<#5>=;

%TRFAC<0>/CELLVOL<#5> : Fe58OH2<#5>=;

%TRFAC<0>/CELLVOL<#5> : Fe58OH3-<#5>=;

%TRFAC<0>/CELLVOL<#5> : Fe59<#5>=;

%TRFAC<0>/CELLVOL<#5> : Fe59OH+<#5>=;

%TRFAC<0>/CELLVOL<#5> : Fe59OH2<#5>=;

%TRFAC<0>/CELLVOL<#5> : Fe59OH3-<#5>=;

%TRFAC<0>/CELLVOL<#5> : Fe54<#5>=;

%TRFAC<0>/CELLVOL<#5> : Fe54OH+<#5>=;

%TRFAC<0>/CELLVOL<#5> : Fe54OH2<#5>=;

%TRFAC<0>/CELLVOL<#5> : Fe54OH3-<#5>=;

%TRFAC<0>/CELLVOL<#5> : Mn54<#5>=;

%TRFAC<0>/CELLVOL<#5> : Mn54OH+<#5>=;

%TRFAC<0>/CELLVOL<#5> : Mn54OH2<#5>=;

%TRFAC<0>/CELLVOL<#5> : Mn54OH3-<#5>=;

%TRFAC<0>/CELLVOL<#5> : Cr54<#5>=;

%TRFAC<0>/CELLVOL<#5> : Cr54OH+<#5>=;

%TRFAC<0>/CELLVOL<#5> : Cr54OH2<#5>=;

%TRFAC<0>/CELLVOL<#5> : Cr54OH3-<#5>=;

%TRFAC<0>/CELLVOL<#5> : Ni+2<#5>=;

%TRFAC<0>/CELLVOL<#5> : NiOH+<#5>=;

%TRFAC<0>/CELLVOL<#5> : NiOH2<#5>=;

%TRFAC<0>/CELLVOL<#5> : NiOH3-<#5>=;

%TRFAC<0>/CELLVOL<#5> : Ni58<#5>=;

%TRFAC<0>/CELLVOL<#5> : Ni58OH+<#5>=;

%TRFAC<0>/CELLVOL<#5> : Ni58OH2<#5>=;

%TRFAC<0>/CELLVOL<#5> : Ni58OH3-<#5>=;

%TRFAC<0>/CELLVOL<#5> :Co+2<#5>=;

%TRFAC<0>/CELLVOL<#5> : CoOH+<#5>=;

%TRFAC<0>/CELLVOL<#5> : CoOH2<#5>=;

%TRFAC<0>/CELLVOL<#5> :Co60<#5>=;

%TRFAC<0>/CELLVOL<#5> : Co60OH+<#5>=;

%TRFAC<0>/CELLVOL<#5> : Co60OH2<#5>=;

%TRFAC<0>/CELLVOL<#5> :Co58<#5>=;

%TRFAC<0>/CELLVOL<#5> : Co58OH+<#5>=;

%TRFAC<0>/CELLVOL<#5> : Co58OH2<#5>=;

%TRFAC<0>/CELLVOL<#5> : Cu+2<#5>=;

%TRFAC<0>/CELLVOL<#5> : CuOH+<#5>=;

%TRFAC<0>/CELLVOL<#5> : CuOH2<#5>=;

%TRFAC<0>/CELLVOL<#5> : CuOH3-<#5>=;

%TRFAC<0>/CELLVOL<#5> : NH3<#5>=;

%TRFAC<0>/CELLVOL<#5> : NH4+<#5>=;

%TRFAC<0>/CELLVOL<#5> : N2H4<#5>=;

%TRFAC<0>/CELLVOL<#5> : N2H5+<#5>=;

%TRFAC<0>/CELLVOL<#5> : H3BO3<#5>=;

%TRFAC<0>/CELLVOL<#5> : BOH4-<#5>=;

%TRFAC<0>/CELLVOL<#5> : B2OOH5-<#5>=;

%TRFAC<0>/CELLVOL<#5> : B3O3OH4-<#5>=;

%TRFAC<0>/CELLVOL<#5> : B4O2OH8<#5>=;

%TRFAC<0>/CELLVOL<#5> : Fe3O4s<#5>=;

%TRFAC<0>/CELLVOL<#5> : ZnOAc2<#5>=;

%TRFAC<0>/CELLVOL<#5> : AcOH<#5>=;

%TRFAC<0>/CELLVOL<#5> : OAc-<#5>=;

%TRFAC<0>/CELLVOL<#5> : CO2<#5>=;

%TRFAC<0>/CELLVOL<#5> : HCO3-<#5>=;

%TRFAC<0>/CELLVOL<#5> : CO32-<#5>=;

%TRFAC<0>/CELLVOL<#5> : CH4<#5>=;

%TRFAC<0>/CELLVOL<#5> : I131<#5>=;

%TRFAC<0>/CELLVOL<#5> : I132<#5>=;

%TRFAC<0>/CELLVOL<#5> : I133<#5>=;

%TRFAC<0>/CELLVOL<#5> : I134<#5>=;

%TRFAC<0>/CELLVOL<#5> : I135<#5>=;

%TRFAC<0>/CELLVOL<#5> : Te131<#5>=;

%TRFAC<0>/CELLVOL<#5> : Te132<#5>=;

%TRFAC<0>/CELLVOL<#5> : Te133<#5>=;

%TRFAC<0>/CELLVOL<#5> : Te134<#5>=;

%TRFAC<0>/CELLVOL<#5> : Te135<#5>=;

%TRFAC<0>/CELLVOL<#5> : Cs134<#5>=;

%TRFAC<0>/CELLVOL<#5> : Cs137<#5>=;

%TRFAC<0>/CELLVOL<#5> : Cs138<#5>=;

%TRFAC<0>/CELLVOL<#5> : Xe133<#5>=;

%TRFAC<0>/CELLVOL<#5> : Xe135<#5>=;

%TRFAC<0>/CELLVOL<#5> : Xe138<#5>=;

**;

parameter

pH0

OHmol

feppm fecolppm

coppm cocolppm

Co+2ppm

Co60ppm Co59ppm Co58ppm

Ni58ppm TotNippm

Fe58ppm Fe54ppm Fe59ppm TotFeppm

TotCoppm

Mn54ppm

Co60Activity

Co58Activity

Fe59Activity

Mn54Activity

I131Activity

I132Activity

I133Activity

I134Activity

I135Activity

Te131Activity

Te132Activity

Te133Activity

Te134Activity

Te135Activity

Cs134Activity

Cs137Activity

Cs138Activity

Xe133Activity

Xe135Activity

Xe138Activity

TotalActivity

Fe54Abun

Fe58Abun

Ni58Abun

CO60OHppm

Co60OH2ppm

Co60OH3ppm

nippm nicolppm

znppm zncolppm

cuppm cucolppm

femol fecolmol

comol cocolmol

nimol nicolmol

znmol zncolmol

cumol cucolmol

hmol limol nh3mol LiOHmol

hppm lippm nh3ppm

n2h4ppm n2h4mol

Licumu NH3cumu Fecumu

Nicumu Zncumu Cocumu

N2H4Tot

Cucumu

FeOHppm FeOH2ppm FeOH3ppm

NiOHppm NiOH2ppm NiOH3ppm

ZnOHppm ZnOH2ppm ZnOH3ppm

CoOHppm CoOH2ppm CoOH3ppm

CuOHppm CuOH2ppm CuOH3ppm

FeOHmol FeOH2mol FeOH3mol

NiOHmol NiOH2mol NiOH3mol

ZnOHmol ZnOH2mol ZnOH3mol

CoOHmol CoOH2mol CoOH3mol

CuOHmol CuOH2mol CuOH3mol

RLimol RNH4mol RHmol

RN2H5mol

RRFemol RFeOHmol

RRNimol RNiOHmol

RRZnmol RZnOHmol

RRComol RCoOHmol

RRCumol RCuOHmol

RNmol

LiKcalc NH4Kcalc FeKcalc

NiKcalc ZnKcalc CoKcalc CuKcalc

FeOHKcalc CuOHKcalc CoOHKcalc

NiOHKcalc ZnOHKcalc

RCoOH3ppm

RLiTot HTot RHTot LiTot

TestNH3 TestNH4 TestNi TestNiOH TestNiOH2 TestNiOH3

TestFe TestFeOH TestFeOH2 TestFeOH3

TestLi TestLiOH TestZn TestZnOH

TestZnOH2 TestZnOH3 TestZnOH4

TestCo TestCoOH TestCoOH2

CoolantTemp

Power

Co60t Co58t Mn54t Fe59t I131t I132t I133t I134t I135t

Te131t Te132t Te133t Te134t Te135t Cs134t Cs137t Cs138t

Xe133t Xe135t Xe138t

;

*==========

==========;

* Outputs for Hydrolysis Species in bulk section

;

*==========

==========;

SETPSTREAM 4 11 20;

TIME

FeOHppm FeOH2ppm FeOH3ppm

NiOHppm NiOH2ppm NiOH3ppm

ZnOHppm ZnOH2ppm ZnOH3ppm

CoOHppm CoOH2ppm CoOH3ppm

CuOHppm CuOH2ppm CuOH3ppm

;

**;

```
*====================================
==========================;
* Outputs for Activity from Radioactive species
;
*====================================
==========================;
SETPSTREAM 5 14 20;
TIME
Co60Activity Co58Activity Fe59Activity
Mn54Activity
I131Activity I132Activity I133Activity
I134Activity I135Activity Te131Activity
Te132Activity
Te133Activity Te134Activity Te135Activity;
**;


*====================================
==========================;
* Outputs for Activity from Radioactive species
part 2 ;
*====================================
==========================;
SETPSTREAM 14 26 20;
TIME
Cs134Activity Cs137Activity Cs138Activity
Xe133Activity
Xe135Activity Xe138Activity;
**;


*====================================
==========================;
* Outputs for Bulk Concentrations against time in
Mol/L & ppm ;
*====================================
==========================;
SETPSTREAM 6 15 20;
TIME hppm lippm nh3ppm n2h4ppm
feppm coppm nippm
znppm cuppm hmol limol
nh3mol n2h4mol femol comol
nimol znmol cumol
pH0 ;
**;


*====================================
==========================;
```

```
* Outputs for Resin species across all times
;
*==================================
==========================;
SETPSTREAM 8 18 20;
TIME
RLimol  RNH4mol RHmol
RRFemol RFeOHmol RN2H5mol
RRNimol RNiOHmol
RRZnmol RZnOHmol
RRComol RCoOHmol
RRCumol RCuOHmol
RNmol;
**;


*==================================
==========================;
* Outputs for Hydrolysis Species at all positions
;
*==================================
==========================;
SETPSTREAM 9 19 20;
TIME
Limol
FeOHmol FeOH2mol FeOH3mol
NiOHmol NiOH2mol NiOH3mol
ZnOHmol ZnOH2mol ZnOH3mol
CoOHmol CoOH2mol CoOH3mol
CuOHmol CuOH2mol CuOH3mol;
**;
integer #nn8;


*==================================
==========================;
* Outputs for radioactive species ;
*==================================
==========================;
SETPSTREAM 11 21 20;
TIME Co60ppm Co59ppm Co58ppm TotCoppm
Ni58ppm TotNippm Fe58ppm
Fe54ppm Fe59ppm TotFeppm Mn54ppm
Fe54Abun Fe58Abun
Ni58Abun;
**;


*==================================
==========================;
* Outputs for Hydrolysis species ;
```

```
*====================================
==========================;
SETPSTREAM 13 23 20;
TIME Co+2ppm CoOHppm CoOH2ppm
CoOH3ppm Co60ppm Co60OHppm
Co60OH2ppm Co60OH3ppm RCoOH3ppm;
**;



*====================================
==========================;
*Compiles out 1 which is species for all cells at all
times ;
*====================================
==========================;
compile out1;


LiTot = 0;


do 20 for #4=0(1)#NCELL - 1;
pH0 = 14 - (-log10((Li+<#4>) + (H+<#4>)));
Limol =(Li+<#4> + LiOH<#4>)*CELLVOL<#4>;
femol=(fe+2<#4> + feoh+<#4> + feoh2<#4> +
feoh3-<#4>)*CELLVOL<#4>;
fecolmol=(rrfe<#4> +
rfeoh<#4>)*CELLVOL<#4>;
nimol=(ni+2<#4> + nioh+<#4> + nioh2<#4> +
nioh3-<#4>)*CELLVOL<#4>;
nicolmol=(rrni<#4> +
rnioh<#4>)*CELLVOL<#4>;
comol=(co+2<#4> + cooh+<#4> +
cooh2<#4>)*1000*MWCo;
cocolmol=(rrco<#4> +
rcooh<#4>)*CELLVOL<#4>;


znmol=(zn+2<#4> + znoh+<#4> + znoh2<#4> +
znoh3-<#4>
 + znoh42-<#4>)*CELLVOL<#4>;
zncolmol=(rrzn<#4> + rznoh<#4> + rznoh3<#4>
+ rrznoh4<#4>)*CELLVOL<#4>;
cumol=(cu+2<#4> + cuoh+<#4> + cuoh2<#4> +
cuoh3-<#4>)*CELLVOL<#4>;
cucolmol=(rrcu<#4> +
rcuoh<#4>)*CELLVOL<#4>;
RRFemol=(rrfe<#4>)*CELLVOL<#4>;
RFeOHmol=(rfeoh<#4>)*CELLVOL<#4>;
RRNimol=(rrni<#4>)*CELLVOL<#4>;
RNiOHmol=(rnioh<#4>)*CELLVOL<#4>;
```

```
RRZnmol=(rrzn<#4>)*CELLVOL<#4>;
RZnOHmol=(rznoh<#4>)*CELLVOL<#4>;
RRComol=(rrco<#4>)*CELLVOL<#4>;
RCoOHmol=(rcooh<#4>)*CELLVOL<#4>;
RRCumol =(rrcu<#4>)*CELLVOL<#4>;
RCuOHmol=(rcuoh<#4>)*CELLVOL<#4>;
RLimol=(RLi<#4>)*CELLVOL<#4>;
RNH4mol=(RNH4<#4>)*CELLVOL<#4>;
RN2H5mol=(RN2H5<#4>)*CELLVOL<#4>;
RHmol=(RH<#4>)*CELLVOL<#4>;
RNmol=(RN<#4>)*CELLVOL<#4>;
FeOHmol=(feoh+<#4>)*CELLVOL<#4>;
FeOH2mol=(feoh2<#4>)*CELLVOL<#4>;
FeOH3mol=(feoh3-<#4>)*CELLVOL<#4>;
NiOHmol=(nioh+<#4>)*CELLVOL<#4>;
NiOH2mol=(nioh2<#4>)*CELLVOL<#4>;
NiOH3mol=(nioh3-<#4>)*CELLVOL<#4>;
ZnOHmol=(znoh+<#4>)*CELLVOL<#4>;
ZnOH2mol=(znoh2<#4>)*CELLVOL<#4>;
ZnOH3mol=(znoh3-<#4>)*CELLVOL<#4>;
CoOHmol=(cooh+<#4>)*CELLVOL<#4>;
CoOH2mol=(cooh2<#4>)*CELLVOL<#4>;
CuOHmol=(cuoh+<#4>)*CELLVOL<#4>;
CuOH2mol=(cuoh2<#4>)*CELLVOL<#4>;
CuOH3mol=(cuoh3-<#4>)*CELLVOL<#4>;
pstream 8;
pstream 9;
label 20;
Call Out2;
Call Out3;
Call Out4;
Call Out5;
Call Out6;
Call Out7;
**;
*====================================
==========================;
*  Compiles out2 which is species for bulk cell at
all times  ;
*====================================
==========================;
compile out2;
do 21 for #6=0(1)#NCELL1 - 1;
pH0=(-log10(H+<#6>));
* pH0=14 - (-log10(Li+<#6>));
*  pH0  =(14  -  (-log10(Li+<#6>)))  +  (-
log10(H+<#6>));
```

* pH0=14 - (-log10((Li+<#6>) + (H+<#6>)));

coppm=((co+2<#6> + cooh+<#6> + cooh2<#6>)*1000*MWCo)

+ ((co60<#6> + co60oh+<#6> + co60oh2<#6>)*1000*MWCo60)

+ ((co58<#6> + co58oh+<#6> + co58oh2<#6>)*1000*MWCo58);

co59ppm=(co+2<#6> + cooh+<#6> + cooh2<#6>)*1000*MWCo;

co60ppm=(co60<#6> + co60oh+<#6> + co60oh2<#6>)*1000*MWCo60;

co58ppm=(co58<#6> + co58oh+<#6> + co58oh2<#6>)*1000*MWCo58;

*Total Nickel;

nippm=((ni+2<#6> + nioh+<#6> + nioh2<#6> + nioh3-<#6>)*1000*MwNi)

+ ((ni58<#6> + ni58oh+<#6> + ni58oh2<#6> + ni58oh3-<#6>)*1000*MWNi58);

ni58ppm=(ni58<#6> + ni58oh+<#6> + ni58oh2<#6> +

ni58oh3-<#6>)*1000*MWNi58;

*Total Iron;

feppm=((fe+2<#6> + feoh+<#6> + feoh2<#6> + feoh3-<#6>)*1000*MWFe)

+ ((Fe58<#6> + Fe58oh+<#6> + Fe58oh2<#6> + Fe58oh3-<#6>)*1000*MWFe58)

+ ((Fe59<#6> + Fe59oh+<#6> + Fe59oh2<#6> + Fe59oh3-<#6>)*1000*MWFe59)

+ ((Fe54<#6> + Fe54oh+<#6> + Fe54oh2<#6> + Fe54oh3-<#6>)*1000*MWFe54);

Fe58ppm=(Fe58<#6> + Fe58oh+<#6> + Fe58oh2<#6> +

Fe58oh3-<#6>)*1000*MWFe58;

Fe59ppm=(Fe59<#6> + Fe59oh+<#6> + Fe59oh2<#6> +

Fe59oh3-<#6>)*1000*MWFe59;

Fe54ppm=(Fe54<#6> + Fe54oh+<#6> + Fe54oh2<#6> +

Fe54oh3-<#6>)*1000*MWFe54;

TotFeppm= feppm;

Mn54ppm=(Mn54<#6> + Mn54oh+<#6> + Mn54oh2<#6> +

Mn54oh3-<#6>)*1000*MWMn;

znppm=(zn+2<#6> + znoh+<#6> + znoh2<#6> + znoh3-<#6>

+ ZnOH42-<#6> + ZnOAc2<#6>)*1000*MWZn;

cuppm=(cu+2<#6> + cuoh+<#6> + cuoh2<#6> + cuoh3-<#6>)*1000*MWCu;

hppm=(H+<#6>)*1000;

```
lippm=(Li+<#6> + LiOH<#6>)*1000*MWLi;
Nh3ppm=(NH3<#6> + NH4+<#6>)*1000*MWNH3;
N2H4ppm=(N2H4<#6> + N2H5+<#6>)*1000*MWN2H4;
FeOHppm=(feoh+<#6>)*1000*MWFe;
FeOH2ppm=(feoh2<#6>)*1000*MWFe;
FeOH3ppm=(feoh3-<#6>)*1000*MWFe;
NiOHppm=(nioh+<#6>)*1000*MWNi;
NiOH2ppm=(nioh2<#6>)*1000*MWNi;
NiOH3ppm=(nioh3-<#6>)*1000*MWNi;
ZnOHppm=(znoh+<#6>)*1000*MWZn;
ZnOH2ppm=(znoh2<#6>)*1000*MWZn;
ZnOH3ppm=(znoh3-<#6>)*1000*MWZn;
Co+2ppm=co+2<#6> *1000*MWCo;
CoOHppm=(cooh+<#6>)*1000*MWCo;
CoOH2ppm=(cooh2<#6>)*1000*MWCo;
Co60OHppm=(co60oh+<#6>)*1000*MWCo;
Co60OH2ppm=(co60oh2<#6>)*1000*MWCo;
CuOHppm=(cuoh+<#6>)*1000*MWCu;
CuOH2ppm=(cuoh2<#6>)*1000*MWCu;
CuOH3ppm=(cuoh3-<#6>)*1000*MWCu;

femol=(fe+2<#6> + feoh+<#6> + feoh2<#6> + feoh3-<#6>)*CELLVOL<#6>;
nimol=(ni+2<#6> + nioh+<#6> + nioh2<#6> + nioh3-<#6>)*CELLVOL<#6>;
comol=(co+2<#6> + cooh+<#6> + cooh2<#6>)*CELLVOL<#6>;
znmol=(zn+2<#6> + znoh+<#6> + znoh2<#6> + znoh3-<#6> + znoh42-<#6>)
*CELLVOL<#6>;
cumol=(cu+2<#6> + cuoh+<#6> + cuoh2<#6> + cuoh3-<#6>)*CELLVOL<#6>;
hmol=(H+<#6>)*CELLVOL<#6>;
limol=(Li+<#6> + LiOH<#6>)*CELLVOL<#6>;
Nh3mol=(NH3<#6> + NH4+<#6>)*CELLVOL<#6>;
n2h4mol=(N2H4<#6> + N2H5+<#6>)*CELLVOL<#6>;
Co60t=((Co60<#6> + Co60OH+<#6> + Co60OH2<#6>) * 1000 * MwCo60);
Co58t=((Co58<#6> + Co58OH+<#6> + Co58OH2<#6>) * 1000 * MwCo58);
```

```
Mn54t=((Mn54<#6> + Mn54OH+<#6> + Mn54OH2<#6> + Mn54OH3-<#6>) * 1000 * MwMn);

Fe59t=((Fe59<#6> + Fe59OH+<#6> + Fe59OH2<#6> + Fe59OH3-<#6>) * 1000 * MwFe59);

I131t=(I131<#6> * 1000 * MwI131);

I132t=(I132<#6> * 1000 * MwI132);

I133t=(I133<#6> * 1000 * MwI133);

I134t=(I134<#6> * 1000 * MwI134);

I135t=(I135<#6> * 1000 * MwI135);

Te131t=(Te131<#6> * 1000 * MwTe131);

Te132t=(Te132<#6> * 1000 * MwTe132);

Te133t=(Te133<#6> * 1000 * MwTe133);

Te134t=(Te134<#6> * 1000 * MwTe134);

Te135t=(Te135<#6> * 1000 * MwTe135);

Cs134t=(Cs134<#6> * 1000 * MwCs134);

Cs137t=(Cs137<#6> * 1000 * MwCs137);

Cs138t=(Cs138<#6> * 1000 * MwCs138);

Xe133t=(Xe133<#6> * 1000 * MwXe133);

Xe135t=(Xe135<#6> * 1000 * MwXe135);

Xe138t=(Xe138<#6> * 1000 * MwXe138);

pstream 6;

pstream 4;

pstream 11;

pstream 13;

pstream 16;

pstream 17;

label 21;

**;

*====================================
==========================;

* Compiles Out4 which is for Activity from Radioactive species ;

*====================================
==========================;

Compile OUT4;

do 30 for #8=0(1)#NCELL1 - 1;

Co60Activity = dw<#8>*NAvo*((co60<#8> + co60oh+<#8> + co60oh2<#8>)

Co58Activity = dw<#8>*NAvo*((co58<#8> + co58oh+<#8> + co58oh2<#8>)

Fe59Activity = dw<#8>*NAvo*((Fe59<#8> + Fe59oh+<#8> + Fe59oh2<#8> +

Fe59oh3-<#8>)*Fe59lambda<#8>)/1E3;

Mn54Activity = dw<#8>*NAvo*((Mn54<#8> + Mn54oh+<#8> + Mn54oh2<#8> +

Mn54oh3-<#8>)*Mn54lambda<#8>)/1E3;
```

```
I131Activity = dw<#8>*NAvo*(I131<#8> * I131Lambda<#8>)/1E3;

I132Activity = dw<#8>*NAvo*(I132<#8> * I132Lambda<#8>)/1E3;

I133Activity = dw<#8>*NAvo*(I133<#8> * I133Lambda<#8>)/1E3;

I134Activity = dw<#8>*NAvo*(I134<#8> * I134Lambda<#8>)/1E3;

I135Activity = dw<#8>*NAvo*(I135<#8> * I135Lambda<#8>)/1E3;

Te131Activity = dw<#8>*NAvo*(Te131<#8> * Te131Lambda<#8>)/1E3;

Te132Activity = dw<#8>*NAvo*(Te132<#8> * Te132Lambda<#8>)/1E3;

Te133Activity = dw<#8>*NAvo*(Te133<#8> * Te133Lambda<#8>)/1E3;

Te134Activity = dw<#8>*NAvo*(Te134<#8> * Te134Lambda<#8>)/1E3;

Te135Activity = dw<#8>*NAvo*(Te135<#8> * Te135Lambda<#8>)/1E3;

Cs134Activity = dw<#8>*NAvo*(Cs134<#8> * Cs134Lambda<#8>)/1E3;

Cs137Activity = dw<#8>*NAvo*(Cs137<#8> * Cs137Lambda<#8>)/1E3;

Cs138Activity = dw<#8>*NAvo*(Cs138<#8> * Cs138Lambda<#8>)/1E3;

Xe133Activity = dw<#8>*NAvo*(Xe133<#8> * Xe133Lambda<#8>)/1E3;

Xe135Activity = dw<#8>*NAvo*(Xe135<#8> * Xe135Lambda<#8>)/1E3;

Xe138Activity = dw<#8>*NAvo*(Xe138<#8> * Xe138Lambda<#8>)/1E3;

pstream 5;

pstream 14;

label 30;

**;

SETERRORTOL 1.0e-10;

*====================================
==========================;

* Whenever Statements.                    ;

*====================================
==========================;

WHENEVER


*====================================
============================;

* When Time equals input Show Various Outputs.
;
```

```
*===================================
============================;
TIME = SETTIME % CALL OUT1;
TIME = 0 % CALL FluxOnOff RESTART;
TIME = 0 % CALL CorrosionRelease RESTART;
TIME = SWITCH CALL NEWPERIOD RESTART;
**;
*===================================
=========================;
* Compile New Periods                    ;
*===================================
=========================;
Compile NewPeriod;
IF <#READHIST - 1> 99 99 *;
FOR #88 = (#NPER);
Q = flowrate<#88>;
COOLANTTEMPC = CoolTemp<#88>;
COLUMNTEMPC = ColmnTemp<#88>;
POW = Hpower<#88>;
ZnCheck = ZincInjCk<#88>;
FluxCheck = FluxCk<#88>;
CorrosionCheck = CorrosionCk<#88>;
#NPER = #NPER + 1;
Call Temperature;
Call Selectivity;
Call Rates;
ARRAY<#NCELL> WKSPACE;
Qdw = Q*dw;
TRFAC=Qdw;
ARRAY END;
If (CorrosionCheck - 0.9) 69 69 *;
ARRAY<#NCELL> WKSPACE;
KCrCo = KCrCo0;
* release rate units of mol/kg/sec;
KCrCo                                  =
KCrCo/MwCo*PrimCircArea/(VOLBULK*dw<0>
);
KCrNi = KCrNi0;
* release rate units of mol/kg/sec;
KCrNi                                  =
KCrNi/MwNi*PrimCircArea/(VOLBULK*dw<0>)
;
KCrFe = KCrFe0;
* release rate units of mol/kg/sec;
KCrFe                                  =
KCrFe/MwFe*PrimCircArea/(VOLBULK*dw<0>)
;
```

```
ARRAY END;

label 69;

If (CorrosionCheck - 0.9) * * 79;

ARRAY<#NCELL> WKSPACE;

KCrCo = 0;

* release rate units of mol/kg/sec;

KCrCo = 0;

KCrNi = KCrNi0;

* release rate units of mol/kg/sec;

KCrNi = 0;

KCrFe = KCrFe0;

* release rate units of mol/kg/sec;

KCrFe = 0;

ARRAY END;

label 79;

If (FluxCheck - 0.9) * * 65 ;

ARRAY<#NCELL> WKSPACE;

thermalnflux<0> = 0;

fastnflux<0> = 0;

RNRate = 0;

ARRAY END;

label 65;

If (FluxCheck - 0.9) 75 75 * ;

ARRAY<#NCELL> WKSPACE;

thermalnflux<0> = 1.14E14;

fastnflux<0> = 1.03E14;

RNRATE = PRODRATE * POW/100;

ARRAY END;

label 75;

LABEL 99;

**;

*==================================
==========================;

* Compile Corrosion Release Mechanism
(Options) ;

*==================================
==========================;

COMPILE CorrosionRelease;

If (CorrosionCheck - 0.9) 69 69 *;

ARRAY<#NCELL> WKSPACE;

KCrCo = KCrCo0;

* release rate units of mol/kg/sec;

KCrCo =
KCrCo/MwCo*PrimCircArea/(VOLBULK*dw<0>
);

KCrNi = KCrNi0;

* release rate units of mol/kg/sec;
```

```
KCrNi                                   =
KCrNi/MwNi*PrimCircArea/(VOLBULK*dw<0>)
;
KCrFe = KCrFe0;
* release rate units of mol/kg/sec;
KCrFe                                   =
KCrFe/MwFe*PrimCircArea/(VOLBULK*dw<0>)
;
ARRAY END;
label 69;
**;
COMPILE CROff;
ARRAY<#NCELL> WKSPACE;
KCrCo = 0;
KCrNi = 0;
KCrFe = 0;
ARRAY END;
**;
*====================================
==========================;
* Compile Neutron Flux Changes (Options)
;
*====================================
==========================;
Compile FluxOnOff;
If (FluxCheck - 0.9) 65 65 * ;
ARRAY<#NCELL> WKSPACE;
thermalnflux<0> = 1.14E14;
fastnflux<0> = 1.03E14;
RNRATE = PRODRATE * POW/100;
ARRAY END;
label 65;
**;
Compile FluxChange;
ARRAY<#NCELL> WKSPACE;
RNRate = 0;
thermalnflux<0> = 0;
fastnflux<0> = 0;
ARRAY END;
**;
*====================================
==========================;
*                   END
;
*====================================
==========================;
BEGIN;
```

```
STOP;
```